The Host/Guest Clathrate System

$[(ZnI_2)_6(ZnQ)]/[Pn_4Q_x]$ (Pn = P, As ; Q = S, Se)

A qualitative approach to structures, identification and synthesis

Dissertation

zur Erlangung des Doktorgrades
der Naturwissenschaften (Dr. rer. nat.)
der Fakultät für Chemie und Pharmazie
der Universität Regensburg

vorgelegt von

Msc. Jung Hoon Hong

aus Kyungki / Süd Korea

Regensburg, Januar 2004

The Host/Guest Clathrate System

$[(ZnI_2)_6(ZnQ)]/[Pn_4Q_x]$ (Pn = P, As ; Q = S, Se)

A qualitative approach to structures, identification and synthesis

Dissertation

zur Erlangung des Doktorgrades
der Naturwissenschaften (Dr. rer. nat.)
der Fakultät für Chemie und Pharmazie
der Universität Regensburg

vorgelegt von

Msc. Jung Hoon Hong

aus Kyungki / Süd Korea

Regensburg, Januar 2004

Promotionsgesuch eingereicht am:	14. Jan 2004
Tag des Kolloquiums:	30. Jan 2004
Die Arbeit wurde angeleitet von:	Prof. Dr. A. Pfitzner
Prüfungsausschuß:	
Vorsitzender	Prof. Dr. H. Krienke
Erster Prüfer	Prof. Dr. A. Pfitzner
Zweiter Prüfer	Prof. Dr. H. Brunner
Dritter Prüfer	Prof. Dr. T. Troll

dedicate this thesis to
my wife, *Kyung Ho Yoon* and
my son, *Yoon Ha Hong*.

Danksagung

Diese Arbeit entstand in der Zeit von Januar 2000 bis Januar 2004 unter der Anleitung von Herrn Prof. Dr. A. Pfitzner am Lehrstuhl für Anorganische Chemie der naturwissenschaftlichen Fakultät für Chemie und Pharmazie der Universität Regensburg.

Mein ganz besonderer Dank gilt meinen Doktorvater Herrn Prof. Dr. Arno Pfitzner für die Möglichkeit zur Promotion und die Bereitstellung des ausgezeichneten Forschungsumfeldes. Sein stets fördernde Interesse am Fortgang meiner Arbeit sowie seine verständisvolle und engagierte Betreuung war mir eine wertvolle Hilfe.

Für die Sammlung der Messdaten am STOE IPDS Diffraktometer danke ich Frau Dr. M. Andratschke und Herrn Dr. T. Nielges. Insbesondere für die vielen weiterführenden Hilfen bei experimentellen Fragen bedanke ich mich bei Herrn K. G. Lange und Herrn F. Rau.

Ebenfalls zu Dank verpflichtet bin ich Herrn Prof. Dr. H. Eckert und Herrn Prof. Dr. H. Haeuseler für die Aufnahmen von NMR und ir/Raman Proben.

Allen meinen Lehrstuhl-Kollegen, T. Bernert, M. Bräu, D. Feil, M. Jablonska, F. v. Krziwanek, S. Lange, M. Leitl, C. Preitschaft, A. Roduch, U. Schiessl, K. Schneider, F. Truksa, Dr. R. Weihrich, Dr. D. Kurowski und S. Nielges, danke ich für das stets gute und harmonische Arbeitsklima und ihre Hilfsbereitschaft.

Nicht zuletzt gilt mein besonders herzlicher Dank meiner Familie in Korea, meiner Mutter, den Brüdern, den Schwestern, und insbesondere meiner Schwiegermutter und der ganzen Familie in Busan.

Contents **page**

Tables **page**

Figures **page**

1. Introduction

1. 1. A comprehensive synthetic strategy using metal halides

1. 1. 1. CuI with main group 15 and/or 16 adducts

A concept for synthetic strategy using metal halides as a synthetic tool has been investigated by Pfitzner[1, 2] during the last decade. According to his recent paper[2] concerning '*the use of Cu (I) halides as a preparative tool*', he pointed out that the design of new copper ion-conducting materials requires both structural and chemical prerequisites. From a chemical viewpoint, weakly bonded and/or highly polarizable bonding partners for the mobile ions are necessary to provide easy jumps from one site to another. This reveals the most important structural prerequisite, namely a large number of positions which energetically are almost equal. In addition, these positions have to be separated only by small energy barriers, for example, by common faces of the coordination polyhedra of the mobile ions. Under this comprehensive concept, new polymers or monomers of main group elements (some of which have been predicted by theoretical investigation) can be obtained in a crystalline state and are accessible for a basic structural characterization. This synthetic route for hybrid materials or those crystalline compounds of ionic metal halides and main group elements may be illustrated by following experimental evidences. $(CuI)_8P_{12}$ was the first compound of a *formally neutral phosphorous polymer* embedded in a copper halide matrix[3]. $(CuI)_3P_{12}$ and $(CuI)_2P_{14}$ could also be prepared by using copper iodide as solid solvent for phosphorus[4, 5]. The notable aspect of these compounds is that they consist of neutral phosphorus strands embedded in copper iodide. Also the copper halide matrix can be used to form adduct compounds not only with neutral selenium or tellurium chains, but also with six-member selenium rings like in the structures of $(CuBr)_2Se_6$ and $(CuI)_2Se_6$. In both compounds two-thirds of the chalcogen atoms are bonded to copper and further chalcogen atoms, whereas one-third exhibits only covalent bonds to further selenium atoms. A series of crystals using heteroatomic chalcogen analogues was reported[6, 7], i.e., $(CuI)_3Cu_2TeS_3$ and $CuClCu_2TeS_3$, respectively, by Pfitzner *et al.* [2].

Also, neutral phosphorus chalcogenide molecules can be obtained in a copper halide matrix. These molecules form polymers in $(CuI)_5P_{16}Q$ and in $(CuI)_2P_{4-y}Q_x$ (Q = S, Se)[8, 9]. A first example of a well-characterized phosphorus chalcogenide cage molecule in a copper halide matrix was recently obtained by a high temperature reaction of *catena*-$(P_4Se_4)_x$[10] with copper iodide. At a reaction temperature of 400 °*C* the polymeric *catena*-$(P_4Se_4)_x$ decomposed and at least one of the four possible P_4Se_4 cage molecules could be isolated in a matrix of copper iodide. A so-called α-cage (comparable to As_4S_4), a β-cage, and two different P_4Se_3 cages with an additional exo-Se atom have to be distinguished. The resulting compound was $(CuI)_3P_4Se_4$[11]. Thus the β-P_4Se_4 cage which has been controversially discussed during the past three decades[12, 13, 14] was accessible for a complete structural characterization. $(CuI)_3P_4Se_4$ can be transferred to $(CuI)P_4Se_4$ by chemical transport reaction using elemental iodine as the transporting agent[15]. In this compound polymeric P_4Se_4 chain molecules are found which closely resemble the corresponding chains in *catena*-$(P_4Se_4)_x$. However, the polymers have a mirror plane perpendicular to the chain axis when they are embedded in CuI. By contrast these polymers are chiral in the pure phosphorus selenide.

1. 1. 2. The cage molecule candidates from main group 15 and 16 elements

In terms of valence electrons, a group 15 atom is iso-electronic with a {CR}-unit. Thus, white phosphorus, P_4, is related to the tetrahedrane C_4-*t*-Bu_4. Several phosphorus-containing clusters are also well known for which a parent poly-cyclic-hydrocarbon molecule is easily recognized. The unit white phosphorus provides a huge synthetic utilization. In a parallel, the cluster structures of the well known homo-atomic anions $[P_{16}]^{2-}$, $[P_{21}]^{3-}$, $[P_{26}]^{4-}$ as a series of alkali metal phosphides was reported and recently ${}^{1}_{\infty}([P8]P4(4)[])^{0}$ in $(CuI)_8P_{12}$, ${}^{1}_{\infty}([P10]P2[])^{0}$ in $(CuI)_3P_{12}$, and ${}^{1}_{\infty}([P12]P2[])^{0}$ in $(CuI)_2P_{14}$ are isolated[2] in a copper halide matrix which can be comparable with Hittorf's phosphorus based on $[P_7]^{3-}$. One characteristic structural motif of former anions is exhibited by $[P_7]^{5-}$ (see **Fig. 1-1**), the simplest cage of this type. Also, a large number of phosphorus-containing clusters may be formally derived from the $[P_7]^{3-}$ ion[16]. Three basic cluster shapes or derivatives thereof occur amongst such spieces and the relationship of each to the adamantane-cage is apparent. For instance, group **(b)** in **Fig. 1-1** is rather poorly represented compared with others. No doubt new examples will be added to the groups; in group **(c)**, the structure of $[P_4N_{10}]^{10-}$ was elucidated in 1991.

There are many compounds which lie in between those given in **Fig. 1-1**. Examples included P_4S_4 and P_4S_5, P_4S_7, P_4S_9, and $P_4O_3S_6$; a third isomer of P_4S_4 has one exo-cyclic sulfur atom. In 1991, P_4S_6 was isolated and structurally characterized; it is not iso-structural with P_4O_6 but is derived instead from β-P_4S_5. Phosphorus selenides included P_4Se_5 (iso-structural with α-P_4S_5) and P_4Se_4 (possessing one exo-cyclic selenium atom). Unlike the phosphorus oxides where 'phosphorus pentaoxide' is synonymous with P_4O_{10}, the selenides P_2Se_5 and P_4Se_{10} both have separate identities. Also with an another approach, the ability of phosphorus to stabilize clusters by functioning as a Lewis base has already been mentioned, for example in the cubane $[RAlPR']_4$ and in the cubane-like $[t\text{-BuPB(Cl)CH}_2\text{B(Cl)P}t\text{-Bu}]_2$. $[MeNPF_3]_4$ also possesses a cubic cage but, unlike the two previous examples, the phosphorus atoms in $[MeNPF_3]_4$ are 6-coordinate.

Pn_4

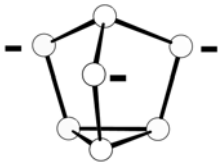

$[Pn_7]^{3-}$

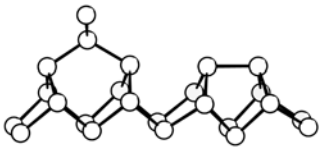

Hittorf's phosphorus

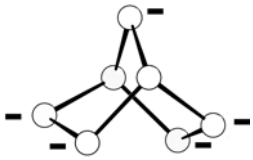

$[Pn_7]^{5-}$

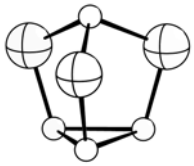

α-Pn_4Q_3

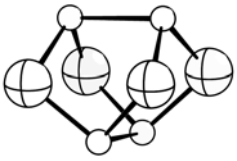

α-Pn_4Q_4

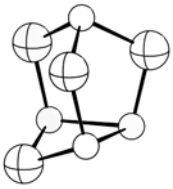

β-Pn_4Q_4

(a)

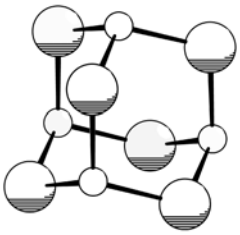

(b)

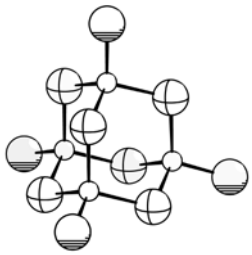

(c)

Fig. 1-1. Important classes of Group 15 compounds which are structurally related to the adamantane-type of cage [where open = P or iso-electonic atom or group, cross = PR, [P]-, or iso-electronic atom (S, Se) or group, shadow = O, S, Se, or iso-electronic atom or group].

And the presumed $[As_7]^{3-}$ and $[Sb_7]^{3-}$, are both iso-electrical with $[P_7]^{3-}$. Structural analogous hetero-atomic clusters in group 15 atoms occupy the 3-coordinate sites and group 16 atoms the 2-coordinate sites include As_4S_3, As_4Se_3, As_3PSe_3, $As_2P_2S_3$, and $As_2P_2Se_3$.

Those kinds of adamantane-like cluster molecules using Group 15 and 16 elements have been revealed by M. E. Jason *et al.*[17(a)] with respect to oxidation mechanism, especially at low temperature, and J. Wachter[17(b)] with respect to mixed ligand topology. Especially for the case of P_4Q_x (Q = S, Se; x = 3 or 4) [see **(a)** in **Fig. 1-1**], there were so many arguments world-widely concerning those theoretical calculations, those spectroscopic assignments and thermal behaviors[18] also.
Adducts to similar neutral molecules are limited to a few examples[19, 20] such as $(PdCl_2)Se_6$, $(NbCl_5)_2P_4S_4$ and recently $(P_4Se_3)\cdot(BI_3)$[21] and $[(triphos)Re(CO)_2\{\eta^1\text{-}P_{\textit{apical}}\text{-}P_4Q_3\}]^+$ (Q = S, Se) and $[(triphos)Re\text{-}(CO)_2\{\eta^1\text{-}P_{\textit{basal}}\text{-}P_4Q_3\}]^+$ (Q = S, Se)[22] are reported.

In our work group, the exploration of adduct compounds based on copper halides and neutral or low-charged molecules of group 15 and 16 elements (see **Fig. 1-1**) led to new insight into the coordination chemistry of these elements. The resulting compounds may be regarded as a combination of the incorporated elements. However, attempts to separate the matrix from the polymers which has always resulted in amorphous products to date. Thus, the goal of preparing these modifications, especially of phosphorus, in crystalline solids has yet to be achieved. However, this synthetic approach gives access to polymers or cage molecules that have been calculated to be thermodynamically stable. In the case of the P_4Se_4 cage molecule numerous former attempts to obtain it as a well-defined material failed when mixtures of phosphorus and selenium were combined at various temperatures. It can be concluded that the addition of copper halides to the reaction mixture just helps to transfer the reaction products to a crystalline state.

1. 1. 3. Expansion from Cu halides to Zn halides

Structural characteristics of group 12 halides change non-monotonically down the group, especially those of their crystal structures. While Zn has tetrahedral coordination in the crystals of its di-halides, cadmium di-halides form octahedral layers, and mercury di-halides are more or less molecular crystals, with two-coordination of mercury. In contrast to that of divalent cadmium and mercury, *very little work has been carried out into the coordination chemistry of Zn with Group 15 and/or 16 molecules*. Zn halides is based upon 4-coordination of the metal atoms and those of the cadmium halides upon 6-coordination. Complex halides of the type $MZnX_3$ and M_2ZnX_4 are known (M = M^+, X = F, Cl and Br). Iodo-complexes of Zn have low stability constants, and seldom solid species have yet been isolated for instance $Li_2M^{II}X_4$ such as Li_2ZnI_4,[1] Li_2FeCl_4,[23] $M^I_2ZnX_4$ (M^I = Li, Na, X = Cl, Br),[24] Li_6FeCl_8 and LiI-$M^{II}I_2$ (M^{II} = Mn, Cd, Pb)[25, 26].

In addition, two very interesting cases are reported[27, 28] and shown in **Fig. 1-2**.

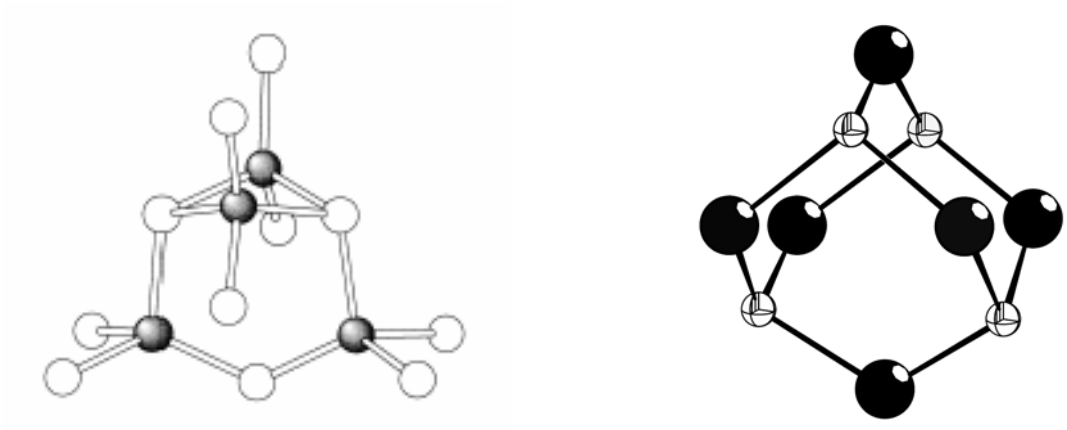

adamantane-like $CuCl_4$ tetramer adamantane-like ZnI_4 unit

Fig. 1-2. Adamantane-like structure of Cu and Zn halide tetrahedral unit.

On the contrary to show to former reported trigonal ZnI_2 structure[$P\bar{3}c1$ (No.165)][29], those adamantane-like tetragonal structure of ZnI_2[$I4_1/acd$ (No.142)] give an extension of concept of *templating a three-dimensional anionic or neutral framework with bulky cations or molecules not only to the copper halide system, but also to zinc halide system*.

To add to this, a general concept[30], so called '*a building block approach to the rational synthesis of solid-state materials*' with respect to metal halide analogues of chalcogenides was reported and described through a comparison of binary MX_n (M = *d*-block elements, X = halogen and chalcogen) salts. According to their successive concept from 'solid-state inorganic enzymes', designs with structural features known for oxide materials that are constructed utilizing reactive and polarizable metal halides can be envisioned. Actually, the concept is focused primarily on the structural and bonding relationships of chlorides and bromides to the oxides and sulfides. These halides and chalcogenides are chosen because their similarity in size and electronegativity results in the greatest commonality of structure. The electronegativities of Cl (3.0) and Br (2.8) are intermediate between O (3.5) and S (2.5), whereas F (4.0) is outside the range of chalcogenides. With respect to size, the covalent radius of O (0.74 Å) is close to that of F (0.72 Å), S (1.04 Å) is similar to Cl (0.99 Å), and Br (1.14 Å) is close to Se (1.17 Å). For instance, between the polymorphs of $ZnCl_2$ (α- and δ-phase) and SiO_2 (high cristobalite and $Pna2_1$-cristobalite) have a structural similarity (see **Fig. 1-3**).

There are four crystallographically characterized phases of $ZnCl_2$, but only α-$ZnCl_2$, which is iso-structural to high cristobalite (see **Fig. 1-3**), adopts a structure that is a direct analogue of SiO_2. The structure of δ-$ZnCl_2$ (or orthorhombic $ZnCl_2$) adopts an analogous structure to the $Pna2_1$-cristobalite structure observed for several ternary phases such as α-$NaGaSiO_2$. δ-$ZnCl_2$ is the first binary compound of this structure, however, this structure has been predicted for SiO_2 by simulated annealing techniques. A comparison of the oxide and chloride structures, as shown in **Fig. 1-3**, clearly indicates that these MX_2 salts exhibit a common crystal structure (tetragonal, $I\bar{4}2d$, and $Pna2_1$, respectively), however, the anions are ordered into layers in $ZnCl_2$, whereas in SiO_2 the anion layers are quite puckered. This is a result of the difference in the T-X-T bond angle (T = tetrahedral cation) dictated by the T-X bond distance. The longer Zn-Cl bonds, 2.31 Å, allow for a more acute T-X-T angle, 108.3°, without unfavorable T-T repulsion, than is possible for a silicate where the short Si-O bonds, 1.62 Å, favor the expanded Si-O-Si of approximately 140°.

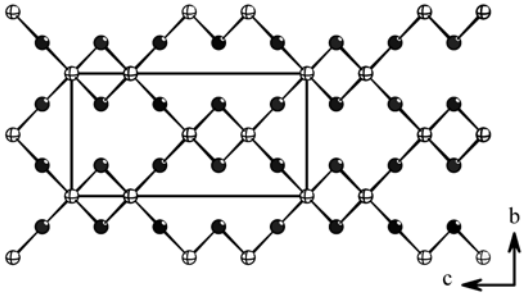

α-$ZnCl_2$

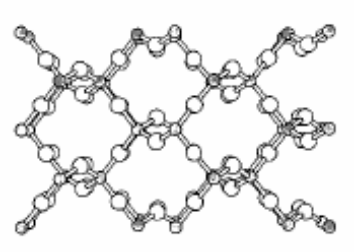

SiO_2 (high cristobalite)

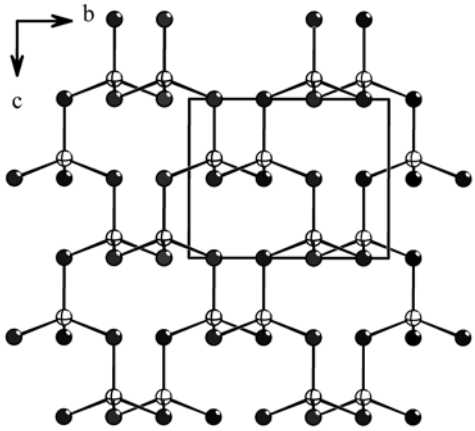

δ-$ZnCl_2$

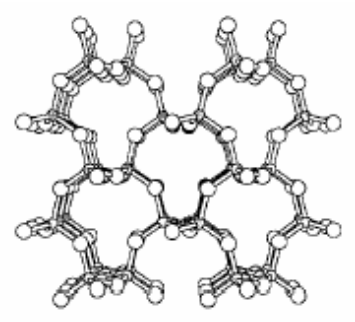

SiO_2 ($Pna2_1$ cristobalite)

Fig. 1-3. Similarity between the polymorphs[30] of $ZnCl_2$ and SiO_2.

Both the BeF_2 (Be-F = 1.35 ~ 1.57 Å) and $[PN_2]^-$ (P-N = 1.65 ~ 1.72 Å) structures have metrical parameters much more similar to the silicates than to the zinc chlorides. This bond length influence on bond angles raises the possibility of framework flexibility resulting from a variation in the T-X-T angle. A maximal expansion to 180° gives the C9-diamondoid connectivity. Interestingly, the contraction of the T-X-T angle to approximately 109° brings the anions into a closest packed arrangement in which the metal cations fill one-fourth of the tetrahedral holes. A (112) section of the α-$ZnCl_2$ structure contains the closest packed layers which are stacked in a cubic closest packed fashion. The δ-phase of $ZnCl_2$ contains the same

closest packed layers but they are stacked in a hexagonal closest packed pattern. The limit to this T-X-T angle is imposed largely by the minimization of cation-cation repulsion. Thus, long T-X bonds will favor more acute T-X-T angles.

In a parallel with above sense, according to a recent report from A. Grzechnik, *et al.*[31], they urged that there is a tendency for disulfides and diselenides to adopt the three-dimensional GeS_2, $GeSe_2$ and SiS_2 ($I\bar{4}2d$) or two-dimensional HgI_2 ($P4_2/nmc$) structures at high pressures. Both types have a common Me_4X_{10} (where Me = Si, Ge and X = S, Se) unit consisting of four corner-sharing tetrahedra. They evaluated the structural transformations in $GeSe_2$ at high pressures (2 ~ 6 GPa) and high temperatures using angle-dispersion X-ray diffraction in a large volume Paris-Edinburgh cell. The results of Rietveld refinement indicated that the compound transformed from $I\bar{4}$, Z = 4 at 2 GPa and 698 K to $P\bar{4}$, Z = 4 at 6 GPa and 773K.

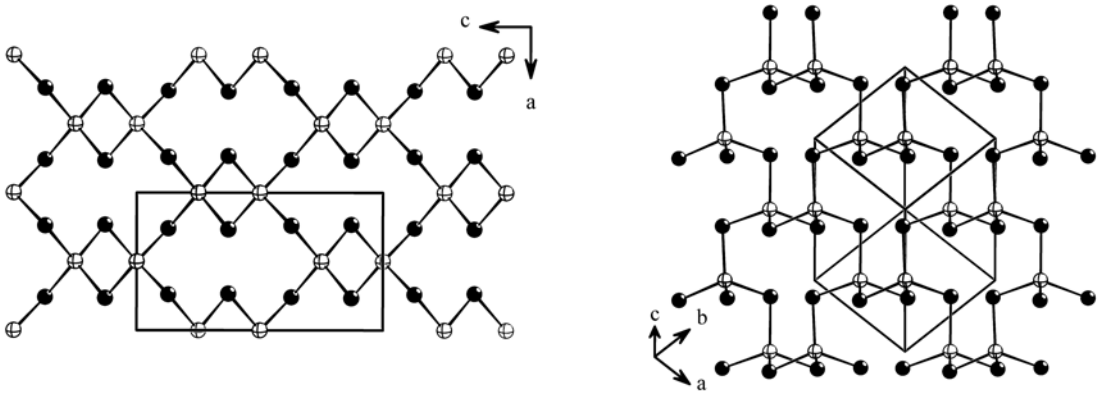

Fig. 1-4. Polymorph of $GeSe_2$ ($I\bar{4}$) with Z = 4 at 2 GPa and 689K.

They concluded that in analogy to crystalline polymorphism, above behavior in a glass would be called an '*amorphous polymorphism*'. However, they measurements were limited to the pressure range up to 6 GPa, so, based on the presented data, it possible to infer whether the anomalous expansion of the $I\bar{4}$ lattice, with a subsequent symmetry descent to the $P\bar{4}$ one, can be discussed as a prelude to a phase transition into another denser, possibly six-fold coordinated, phase. One of the examples for such a *four-to-six transformation* in the compounds with MeX_2 stoichiometry is the crystoballite → stishovite transition in SiO_2. Anyway, the

polymorph of $GeSe_2$ with respect to views from two different directions (see **Fig. 1-4**) showed a similarity with either polymorph of α-$ZnCl_2$ or one of δ-$ZnCl_2$.

To add to above synthetic utilization, the well-known crystalline phases using mixed metal halides, mixed metal chalcogenides and mixed metal chalco-halides were reviewed by J. R. Long, *et al.*[32] under their *dimensional reduction concept*, so called 'A practical formalism for manipulating solid structure' using dimensional reducing agents for instance alkali halides from $MnCl_2$ (2-D) to Na_2MnCl_4 (1-D)[33] or alkali oxides from IrO_2 (3-D) through $CaIrO_3$ (2-D)[34] to Ca_2IrO_4 (1-D)[35] and from SiO_2 (3-D) through $Li_2Si_2O_5$ (2-D)[36] to Li_4SiO_4 (0-D)[37], finally *d*-block metal halides from $Re_6Se_8Cl_2$ (2-D)[38] through $Tl_2Re_6Se_8Cl_4$ (1-D) to $Tl_5Re_6Se_8Cl_7$ (0-D)[39]. Such a dimensional reduction concept was already confirmed by our work group using LiI. The adamantane-like ZnI_4 unit (3-D) was dimensionally reduced into layered Li_2ZnI_4 (2-D)[1] compound. On the contrary to such a concept of dimensional reduction, however, the final goal of our synthetic strategy is to achieve an enhanced dimensionality not only using well-developed series of globular molecules, but also using continuously being developed 3-dimensional metal halide frameworks. At the initial stage, we discussed how something should was done concerning following points,

(i) from the ICDS data base, the metal halide-chalcogen ternary system have been seldom reported.

(ii) instead of that, metal halide-phosphorus chalcogenide quasi-ternary system was suggested.

(iii) for the initial stage, ZnI_2-Q (Q = Se, S) system for analogues of $Re_6Q_8X_2$ (Q = S, Se and X = Cl, Br)[40] and ZnI_2-P(As)-Se(S) system for analogues of boracite family [$M_3B_7O_{13}X$ (M = Fe, Mg, Mn and Cu ; X = Cl, Br and I) were suggested.

Conclusively speaking, in the point of boracite analogues or those related materials, the two different types of coordination by B_xO_y units and metal halides can be replaced by the quasi-ternary CuX-Pn-Q system (where X = halogen, Pn = P, As and Q = S, Se) or by the regular tetrahedral ZnX_2-Pn-Q system, which was recently suggested by our work group as following reasons,

(i) CuX-Pn-Q system has been well developed by our work group, and the polymeric units, also neutral molecules by Pn and /or Q also (see **Fig. 1-1**).

(ii) recently reported $CuCl_4$ tetramer unit built 3-D open framework, instead of that, adamantane-like ZnI_4 unit was suggested for replacement (see **Fig. 1-2**), and the similarity between the polymorph of $ZnCl_2$ and one of SiO_2 was reported also (see **Fig. 1-3**).

(iii) from the consideration of the well-known 3-D framework analogues of group 15 , 16 elements and ZnX_2, the mineral boracite family was suggested with respect to synthetic point of view. And based on the chemical vapor transport method, the cases of $x_{ZnX2} > 0.5$ and Q/Pn = 1 (for Pn_4Q_4) were suggested for the purpose of initial investigation (see **Fig. 1-5**).

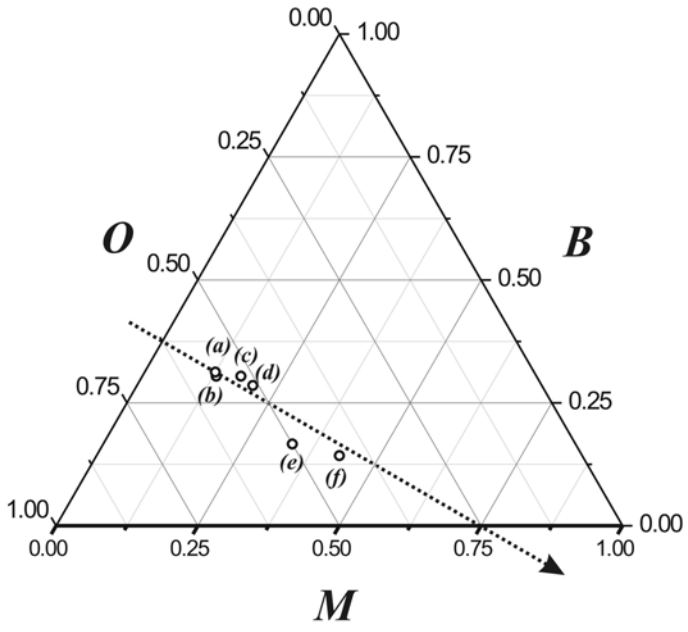

Fig. 1-5. The triangular phase diagram of reported boracite with respect to quasi-ternary system (where M = M^{2+} or M^{+} and the arrow indicates tendency which can be made). (a) $Eu_2B_5O_9X$[41] ; x_M = 0.125, (b) $M^{II}_3B_7O_{13}X$[42] ; x_M = 0.13, (c) $Li_4B_7O_{12}X$[43] ; x_M = 0.17, (d) $Li_5B_7O_{12.5}X$[44] ; x_M = 0.204, (e) $Zn_2(BO_3)[(OH)_{0.75}F_{0.25}]$[45] ; x_M = 0.33 and (f) $M^{II}_3BO_3X_3$ [46] ; x_M = 0.43.

(iv) due to inducing Zn atom, a minimized structural deformation, i.e., no Jahn-Teller effect was expected from the consideration of various boracite structures (see **Fig. 1-6**).

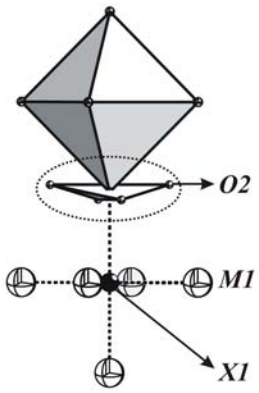

Environment of the metal ions in cubic boracite

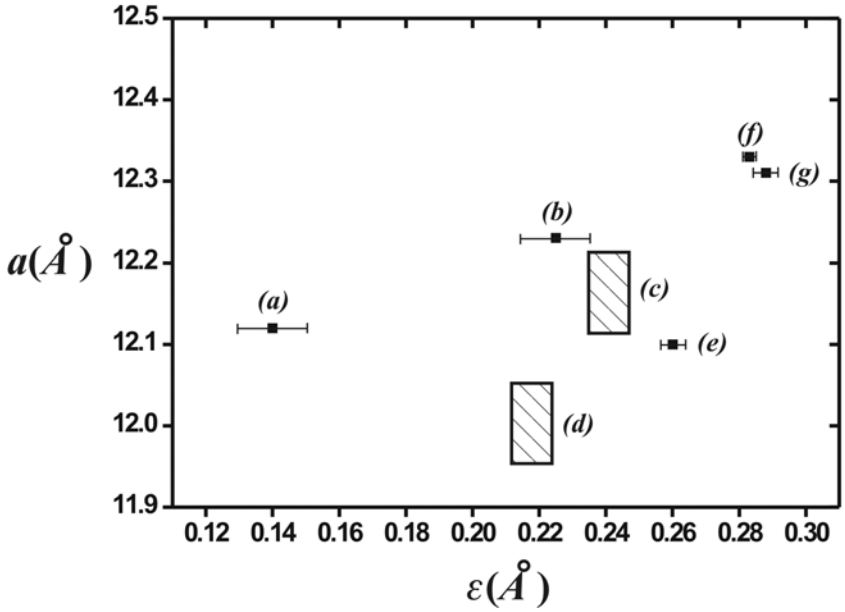

Fig. 1-6. Deviation from planarity, ε [where ε defined as ε (Å) = x(O1) × a (Å) by Nelmes[47]], of the O-atom environment around the metal atoms (site symmetry of metal atoms $\bar{4}$) in cubic boracites as a function of cubic cell parameter, a

[where with general fomular $M^{II}_3B_7O_{13}X$ (a) Zn-Cl (773K) (b) Fe-I (373K) (c) Cr-Cl, Cr-Br (113 and 293K), Cr-I, and Co-I (d) Ni-I (77 and 293K), Cu-Cl (390K), Cu-Br and Cu-I (e) Mg-Cl (673K) (f) Mn-I(421K) and (g) Mn-Br (570K)] [42(e)].

2. Preparation

2. 1. Thermodynamic aspects

2. 1. 1. A non-aqueous solvent

The reason why the thermodynamic considerations about starting materials should be induced in this section can be focused to following points,

(i) the possibility of a gas phase reaction can be ignored at a moderate synthetic temperature under the absence of definite reaction medium, i.e., a solvent, since with respect to Born-Haber cycle, it is too difficult to be dissociated from neutral metal halide to hypothetical gaseous metal ion and halide ion.

(ii) how metal halides can be effectively dispersed for forming a transient complex, i.e., how the homogeneity of eutectic mixture can be embodied, and consequently,

(iii) how the energy relationship between hypothetical gaseous ion and solvated ion can be approximated in closely accordance with the nature of various solvents. Also we can consider the application of an enthalpy cycle to the reaction of complex formation (*AB*) between solvated acid and base in an equilibrium with respect to generalized acid – base interaction in a solvent[48],

$$A(solv) + B(solv) \Leftrightarrow AB(solv)$$

The value of ΔH for this reaction will depend upon four enthalpy changes

(a)	$A(solv) \rightarrow A(g) + solvent$	$-\Delta H[(a)]$
(b)	$B(solv) \rightarrow B(g) + solvent$	$-\Delta H[(b)]$
(c)	$A(g) + B(g) \rightarrow AB(g)$	$\Delta H[(c)]$
(d)	$AB(g) + solvent \rightarrow AB(solv)$	$\Delta H[(d)]$

$$A(solv) + B(solv) \Leftrightarrow AB(solv) \qquad \Delta H[(c)] + \Delta H[(d)] - \Delta H[(a)] - \Delta H[(b)]$$

Clearly $\Delta H[(c)]$ (where it is the enthalpy of the reaction between A and B in the gas phase), its value will be similar to the overall enthalpy of the reaction in solution if the terms, $\Delta H[(d)] - \Delta H[(a)] - \Delta H[(b)]$ are negligible. It is unrealistic to consider that the generalized acid – base interaction in a solvent will be unaffected by the nature of that solvent and the enthalpies of solvation may well be disparate.

(iv) Conclusively first of all, a design of non - aqueous solvent system should be considered for retaining the initial structure of starting materials as the complete fragmentation be minimized for instance the synthesis of $(CuI)_3P_{12}$ or $(CuI)_2P_{14}$ from CuI and P as a non – aqueous medium. For simplicity, assuming a qualitative introduction of ion – solvent interaction by Born equation roughly with respect to Gibbs free energy of solvation, the dielectric constant (ε_r) should be minimized with the last respect. However, the condition which the terms, $\Delta H[(d)] - \Delta H[(a)] - \Delta H[(b)]$ are negligible can be found out from only experimental way as ΔS of complex increases by temperature, since such a theoretical thermodynamic calculation of solvation still too much costs.

$$\Delta G_s^o = -\frac{N_A z^2 e^2}{8\pi\varepsilon_o r}\left(1 - \frac{1}{\varepsilon_r}\right)$$

where N_A is the Avogadro constant, z is the charges number, e is the elementary charge and ε_o, ε_r are dielectric constants in vacuum and solvent, respectively.

As above reason, the inorganic synthesis using metal halides as a starting material should be mainly governed by adopting either the non-aqueous solvent or the molten salt method for obtaining new crystalline materials. For instance, cryolte (Na_3AlF_6) melts at 1003^oC, whilst the eutectic mixture, $AlCl_3$ + NaCl + KCl, melts at only 89^oC. The solubility of metal in metal – metal halide system is in close accordance with structure definition of molten salts, actually with four factors, (1) the type of entities present for instance ions, molecules, complex ion, etc., (2) the nature and effect of holes or vacancies present, (3) distribution

functions relating to the relative positions of structural entities and holes and (4) the nature of the bonds or inter-ionic forces between the entities in the melt. The considerable variety of salts and salt mixtures available leads to a potential class of solvents operative over a temperature range of more than 1000 ^{o}C [49].

Table 2-1. Metal (group IIb) solubility data.

system	m.p. (salt) (^{o}C)	m.p. (metal) (^{o}C)	solubility of metal in metal halide		ref.
			temp. (^{o}C)	mol. %	
Zn + ZnI_2	446	419.47	500	0.28	50
Cd + CdI_2	568	40 (vac.)	400	2.50	51
			600	6.07	
			700	15.0	
			900	25.0	
Hg + HgI_2	259	-38.87	230	25.0	52
			280	35.0	
			350	33.6	

Under the molten salts, the solubility of Cd in CdI_2 at 700 ^{o}C has been given as 15.0 mol.% The diamagnetic nature of the solution indicates that the mechanism of metal solubility is either through the formation of Cd_2^{2+} or a true solution of molecules or atoms. And the presence of KCl, i.e., $CdCl_2$ + KCl system, strongly suppresses the solubility of Cd in molten $CdCl_2$ over a wide composition range, thus suggesting the removal of Cd^{2+} from $CdCl_2$ solutions in the form of complex ions, such as $CdCl_4^{2-}$. To the contrary to this, the metal solubility in the Zn + ZnX_2 (where X = Cl and I) is only of the order of 1 mol. %. By analogue with the Cd systems we could attribute low solubility to the lack of free Zn^{2+} ions in molten ZnI_2 which most probably exists in the form of complex ions. The smaller solubility of metal in this system relative to the Cd system is in accordance with the view that the smaller Zn^{2+} ion is more capable of forming stable complex ions than Cd^{2+}. Since the complexes formed are of the type MX_n, any factors that enhance the central cation's ability to

attract anions will promote complex formation. It is not surprising, therefore, that the tendency of M to form complex anions increases in the order,

$$Hg^{2+} < Cd^{2+} < Zn^{2+} < Mg^{2+}$$

This is also the order of charge density.

The evaluation of molten salt system Zn + ZnI_2 suggests that under ZnI_2 or analogues which have similar dielectric constant (ε_r). The mixture can form stable complex ion, since the complex ion ZnI_4^{-2} is stable over the wide range of temperature and composition. Inducing CuI, CuI has been successively used in the systems like $(CuI)_3P_{12}$ and $(CuI)_2P_{14}$. In this stage, we have to reveal the dielectric constants of pnictogen halides compared with conventional '*good*' solvents like H_2O and NH_3 (see **Table 2-2**). According to the definition of ionic atmosphere, the Coulomb potential at a distance r from an ion of charge $z_i e$ is given by follows,

$$\phi_i = \left(\frac{z_i e}{4\pi\varepsilon_0}\right)\left(\frac{1}{r}\right)$$

This is the potential due to an isolated ion in vacuum. In solution two modifications are needed. In the first place, the solvent decrease the strength of the potential and if the electric permittivity is ε the potential at r is given by follows,

$$\phi_i = \left(\frac{z_i e}{4\pi\varepsilon}\right)\left(\frac{1}{r}\right)$$

Finally the permittivity is usually expressed in terms of the *relative permittivity* (or *dielectric constant* ; ε_r), through $\varepsilon = \varepsilon_r \times \varepsilon_0$. Since $\varepsilon_r > 1$ the potential is reduced from its vacuum value. This reduction is very important in many solvents. For example, ε_r = 78.5 for water

(H_2O) at 25 ^oC, and so at a given distance the Coulombic potential is reduced from the vacuum value by near two order of magnitude, i.e., $\sim\frac{1}{100}$. This is one reason why water (H_2O) is such a '*successful or good*' solvent. Therefore, the Coulombic interactions are so strongly reduced by the solvent that the ions interact only weakly with each other and do not aggregate into a crystal like follows,

$$nZnI_2(s) \rightarrow nZn^{2+}(aq) + 2nI^-(aq).$$

Table 2-2. Dielectric constant of Pnictogen halides compared with conventional solvents.

solvent	dielectric constant (ε_r)	temp. (^oC)	ref.	solvent	dielectric constant (ε_r)	temp. (^oC)	ref.
H_2O	78.54	25	49	PI_3	3.66 (s)	20	53
NH_3	16.9	25	49		4.12 (l)	65	
	22.4	-33		AsI_3	5.38 (s)	20	53
CCl_4	2.18	17	49		7.0 (l)	150	
P_4	4.02 (l)	20	53	SbI_3	9.1 (s)	20	53
	3.85 (l)	45			13.9 (l)	175	

However, we need to obtain stable complex ion of ZnI_2 like a $ZnI_4^{-2}(solv)$ instead of almost perfectly fragmented species like both $Zn^{2+}(aq)$ and $I^-(aq)$ during the reaction steps, which means that it is necessary to choose a '*non-successful or bad*' solvents which can lead the reaction to very mild condition and also which can minimize the bond cleavages of metal halide like follows, i.e., with similarity of auto-complex formation of CdI_2 in concentrated aqueous solution which is strongly supported by Raman spectra of CdI_4^{2-} and $CdBr_4^{2-}$.

$$nZnI_2(s) \leftrightarrow \frac{n}{2}ZnI_4^{2-}(solv) + \frac{n}{2}Zn^{2+}(solv).$$

With above respect, most of the pnictogen or those halides showed a '*bad*' solvent characteristic (see **Table 2-2**).

To add to this, recently reactions of P_4 and I_2 with Ag^+ in suitable ratios to prepare naked polyphosphorus cations were carried out and were fully accounted for by thermo-chemical Born-Haber cycles based on (RI-)MP2/TZVPP *ab initio*, COSMO solvation and lattice enthalpy calculations[54]. According to this report, a postulated general cycle for elusive formation of polyphosphorus cations is the following Fig 2-1 as a closed loop,

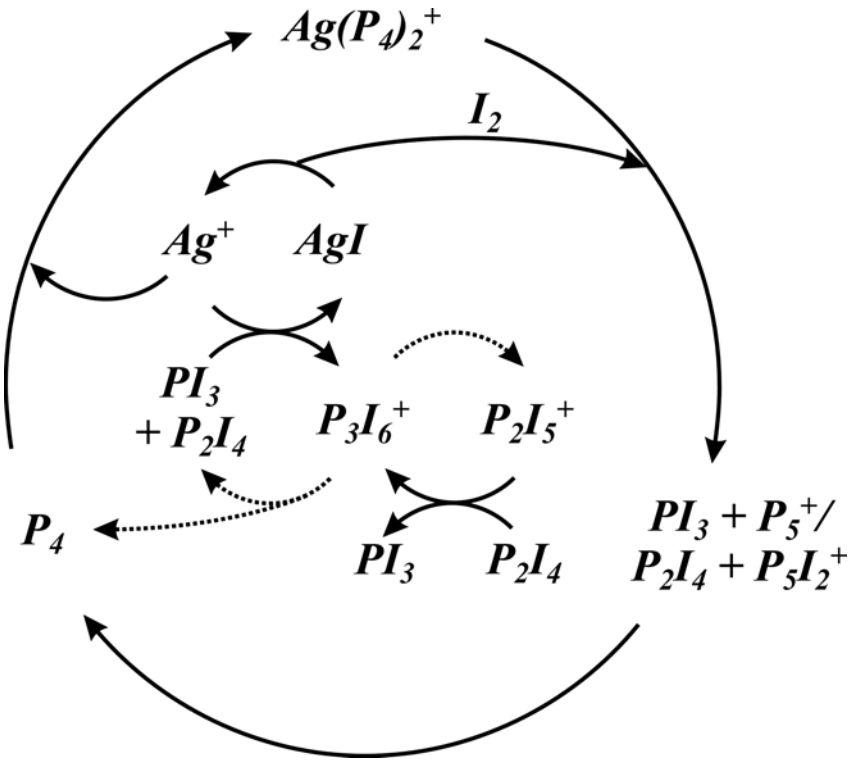

Fig. 2-1. The closed loop reaction of $Ag(P_4)_2^+$ with I_2 (where the solid line indicates the reaction pathways with $\Delta G < 0$ and the dotted line with $\Delta G > 0$).

Conclusively speaking, though above reaction mechanism was suggested by a theoretical thermodynamic calculation, the existence of postulated intermediates were well supported by ^{31}P-NMR spectra and we should point out the consequences for ZnI_2 + P system as follows,

(i) the reaction pathways in **Fig. 2-1** are constructed by the main body cycle (clockwise direction) which is believed as a closed loop. And the main closed loop can be supported by the thermodynamically stable sub-reactions.

(ii) the species like Cu^{+} and Zn^{2+} can be easily stabilized by forming a type of adduct like $Ag(P_4)_2^{+}$. And,

(iii) in the AgI + P reaction system, a series of reaction was performed that finally led to salts of the $P_5I_2^{+}$ as a binary phosphorus rich P – X cation (where X = halogen) and $P_3I_6^{+}$ as a sub-valent phosphorus P – X cation (where X = halogen). The later was suggested that is only marginally stable in solid state.

As a conclusion, in the solid state reaction of ZnI_2 containing P and Se for obtaining new crystalline compounds, the following consequences are expected,

(i) the possibility of gas phase reaction except a structural rearrangement of ZnI_2 can be ignored due to the thermodynamic obstacle of the dissociation of ZnI_2.

(ii) the embodiment of homogeneity in the solid state reaction using ZnI_2, P and Se can be evaluated by means of quasi-binary and ternary molten salt approaches for instance ZnI_2 + P, ZnI_2 + Se and ZnI_2 + P + Se, which can be paralleled with a non-aqueous solvent approach.

(iii) from the molten salt approach of Zn + ZnI_2 system, the solubility data indicate that ZnI_2 have a tetrahedral species like ZnI_4^{2-} over the wide range of temperature and composition which is believed a very stable species compared with CuI_4^{2-} from monovalent CuI.

(iv) the rough thermodynamic approximation about solvation of ZnI_2 into P or Se allows that we can estimate initial reaction condition of quasi-binary system ZnI_2 + P or ZnI_2 + Se using Gibbs free energy change through quasi-equilibrium treatment.

(v) the AgI + P system has been well reported and also the CuI + P system has been well developed by our work group, therefore the first investigation will be limited on the case of quasi-binary ZnI_2 + Se system based on *red-ox* reaction.

2. 1. 2. Approach by Gibbs free energy change of formation

In this section, I allow the pages for illustration through the thermo-chemical approach in order to obtain the ZnI_2 based crystalline solids with following reasons,

(i) the comprehensive inorganic synthetic route for CuI + P, probably including closed loop cycle of AgI + P reaction, has been well developed and reported.

(ii) instead of CuI, ZnI_2 has a regular tetrahedra as a halogen complex under the various non-aqueous solvent conditions.

But the main difficulty for estimating reaction conditions using pnictogens and chalcogens is lying on the allotropes of solid pnictogens and chalcogens which can be divided into very complicate phase transition including polymerization steps or amorphous phases.

Now we have to pay our attention to less complicate liquid phase of S and Se than gaseous phase, since the thermodynamic tracing in gas phase reaction should be supported by additional reaction conditions, i.e., pressures of such complicate species or composition in an equilibrium. Even though such a successful approximation in liquid phase, it leads to slight error for estimating Gibbs free energy change. The heat capacity (C_p) of liquid sulfur (see **Fig. 2-2** above) cannot readily be presented in the form of a T dependent equation, for around 428 K there is an abrupt increase in C_p, with a maximum around 432.3 K. There are appreciable differences between the results of various workers for C_p value above 423 K. The order – disorder transformation (second – order transformations) like liquid S produce an increase of C_p to a peak value over a range of temperature. This in turn results in an increase in heat content and the enthalpy associated with this type of transition may be calculated by determining the area associated with the 'bump' in the C_p - T curve, by projecting the C_p curve for pre – and post – transition periods. For instance, the heat content data of Gattow and Heinrich are out of line for liquid selenium (see **Fig. 2-2** down) and have been disregarded.

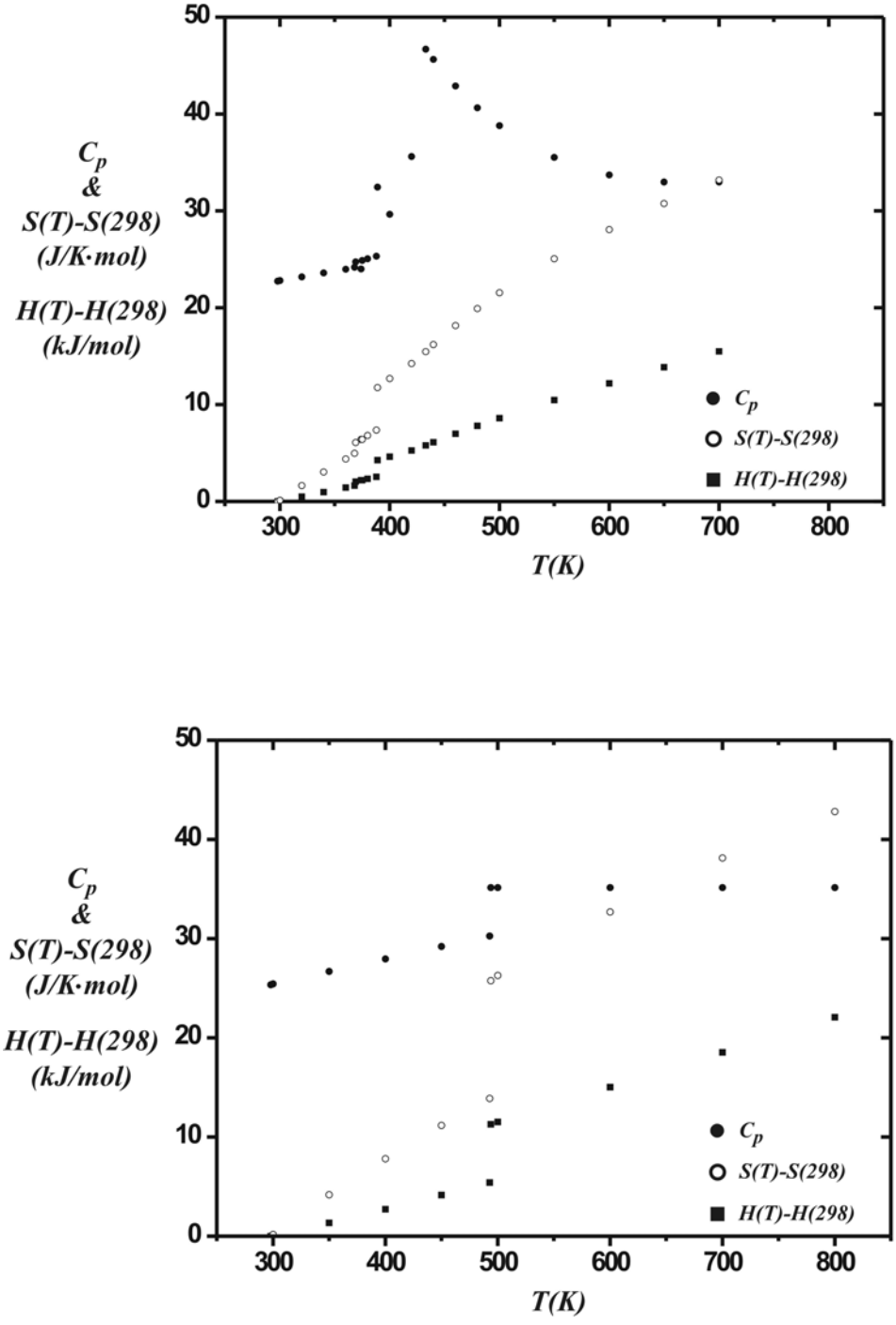

Fig. 2-2. Thermodynamic data for solid – liquid transition of S (above) and Se (down)[55].

Upon this reason, the thermodynamic calculation for finding out reaction condition and proper stoichiometry is adopted by the data of selenium as a standard, since the data of C_p is almost constant (see **Fig. 2-2** down) above the *m.p.* = 493 K (for hexagonal selenium). Comparing with the allotropes of S and Se, the halogens show a gaseous phase over the wide temperature range, which means the entropy term (including Giauque function) should be at constant and the free energy change directly depend on the ΔH^o_{298} .

To add to this, recently I choosed following **Table 2-4** which has an advantage for predicting proper reaction conditions, because chalcogens were directly measured in those liquid phase instead of gaseous phase.

The reactions of metal with halogen have the highest enthalpy of formation per metal atoms (so that highly exothermic) compared with both metal pnictogenides and metal chalcogenides (see **Table 2-3**) which means the metal halide itself as a starting material can not easily thermally decomposed, even at 1000 K.

Table 2-3. Standard enthalpies of formation of zinc related compounds at 298.15 K (kJ/mol).

comp.	$\Delta_f H^o$	ref.	comp.	$\Delta_f H^o$	ref.	comp.	$\Delta_f H^o$	ref.
Zn_3N_2	-28.9	55	ZnO	-348.0	55	ZnF_2 [57]	-736.4	57
Zn_3P_2	-147.1	55	ZnS	-204.6	56	$ZnCl_2$ [57]	-416.7	57
Zn_3As_2	(-103)	55	ZnSe	-177.6	56	$ZnBr_2$ [57]	-358.6	57
Zn_3Sb_2	-213.4	55	ZnTe	-119.0	56	ZnI_2 [57]	-270.7	57

Cf. bracketed value showed an uncertainty.

To the contrary, both the enthalpy of formation (per halogen atom or chalcogen atom) of metal halides and one of metal chalcogenides show similarity as a order of electronegativity of the halogens and chalcogens for instance ZnS (χ_S = 2.58 with Pauling scale) $\Delta_f H^o$ = -204.6kJ/S atom and ½$ZnCl_2$ (χ_{Cl} = 3.16) $\Delta_f H^o$ = -208.4kJ/Cl atom or ZnSe (χ_{Se} = 2.55) $\Delta_f H^o$ = -177.6kJ/Se atom and ½$ZnBr_2$ (χ_{Br} = 2.96) $\Delta_f H^o$ = -179.3kJ/Br atom. This

means that the oxidation of metal halides using chalcogenide should be performed by the upward combination of periodic table for instance ZnI_2 with Se, S or O, $ZnBr_2$ with S or O and $ZnCl_2$ with O as treating with an equi-atomic stoichiometry. Clearly the oxidation route by using pnictogens is rather less effective than one by using chalcogens. According to J. D. Martin *et al.*[30] suggested the possibility of substitution based on ionic radii of halogen and chalcogen, which was introduced in first chapter, for instance I^- (216 pm) with Te^{2-} (221 pm), Br^- (195 pm) with Se^{2-} (198 pm) and Cl^- (181 pm) with S^{2-} (184 pm).

Therefore, for first evaluation, we should approximate the reaction condition with an equi-molar stoichiometry approach as a standard, and then, on the interpretation of thermodynamic approximation, the detailed sub-reaction can be discussed.

Table 2-4. The Gibbs free energy change of Group 12 and those related materials.

reaction			$\Delta_r G^o(J/mol)$	ref.
$ZnI_2(s)$[1]	→	$Zn(s) + I_2(g)$	$278980 - 187.58T + 0.0617T^2 (\pm 2000)$ $(289.1 < T < 1000)$	57
$Zn(s) + Se(l)$	→	$ZnSe(s)$	$-185720 + 28.31T(\pm 370)$ $(640 < T < 693)$	56
$Zn(l) + Se(l)$	→	$ZnSe(s)$	$-192590 + 38.22T(\pm 350)$ $(693 < T < 825)$	56
$Zn(s) + S(l)$	→	α-$ZnS(s)$	$-210117 + 27.70T(\pm 410)$ $(640 < T < 690)$	56
$Cd(s) + Se(l)$	→	$CdSe(s)$	$-159403 + 36.14T(\pm 320)$ $(640 < T < 825)$	56
$3Zn(l) + 2P(V)$[2]	→	α-$Zn_3P_2(s)$	$\Delta H_0^o - aT\ln T - \left(\frac{b}{2}\right)T^2 - \left(\frac{c}{2}\right)T^{-1}\cdot 10^5 + fT$	58

ref. states	temp. range	ΔH_0^o	*a*	*b*	*c*	*f*
s, red (V)	298 - 692	-144613	-1.644	-0.0574	-1.58	-29.163
l, red (V)	692 - 704	-153862	-31.779	-0.0225	0	-200.655
l, P_4 (*g*)	704 - 1180	-219348	-31.779	0	0	-99.705
g, P_4 (*g*)	1180 - 1446	-602844	0	0	0	450.06

1. the reference states, s – solid, g – gas, l – liquid.
2. an allotropic phase of red phosphorus.
3. ref. 58, the coefficients are shown in the separated table.

The Gibbs free energy changes of ZnI_2 dissociation and formations of α-Zn_3P_2, ZnSe and α-ZnS are summarized as 'Ellingham plot' compared with CuI. (see **Fig. 2-3**)

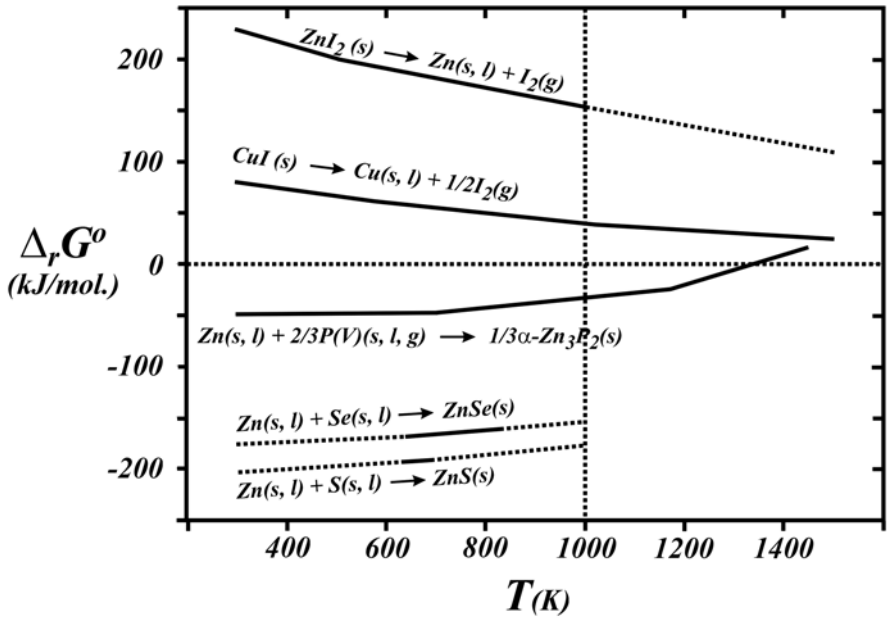

Fig. 2-3. Ellingham plot of Zn related materials.

Under above consideration of enthalpies of formation of ZnI_2, it can be oxidized by either chalcogens (after here Q) or pnictogens (after here Pn) with proper conditions, for instance with controlling stoichiometry and / or with temperature and pressure. As suggested, ZnI_2 can be oxidized by Se, S and O from following reaction equilibrium.

(a) $Zn\,(s, l) + I_2\,(g) \leftrightarrow ZnI_2\,(s)$ $\qquad \Delta_f G_m^o[(a)]$

(b) $ZnI_2\,(s) \leftrightarrow Zn\,(s, l) + I_2\,(g)$ $\qquad \Delta_d G_m^o[(b)] = -\Delta_f G_m^o[(a)]$

(c) $Zn\,(s, l) + Q\,(l) \leftrightarrow ZnQ\,(s)$ $\qquad \Delta_f G_m^o[(c)]$

(d) $ZnI_2\,(s) + Q\,(l) \leftrightarrow ZnQ\,(s) + I_2\,(g)$ $\qquad \Delta_f G_m^o[(d)] = \Delta_f G_m^o[(c)] - \Delta_f G_m^o[(a)]$

The standard Gibbs function of reaction *(a)* indicates the metal's affinity for iodine. At room temperature the contribution of reaction entropy to $\Delta_r G^o$ is dominated by the reaction enthalpy, and so the order of increasing $\Delta_r G^o$ is the same order of increasing $\Delta_r H^o$. This gives the order of values on the diagram of **Fig. 2-3** (ZnI_2 is more endothermic than CuI). The standard reaction entropy is similar for all metals, as is shown by similar slopes of the lines by ZnI_2 and CuI. The kinks at high temperatures correspond to the evaporation of the metals; less pronounced kinks occur at the melting temperatures of the metal and the halides. Oxidation of the halides depends on the competition of the chalcogen for the halogen bound to the metal. The equilibrium lies to the right if $\Delta_r G^o < 0$ under the condition of reaction *(d)* at any high temperature, since at room temperature, still ZnI_2 is not oxidized by any Zn chalcogenide reaction except oxygen (so that the reverse reaction is then spontaneous). To contrary to this, ZnI_2 does never react with elemental phosphorus, even at very high temperature.

Above reaction *(d)* is summarized and shown in **Fig. 2-4**. As a synthetic utility using oxidative elements or materials, i.e., *compensating the energetic obstacle of dissociation of Metal halides*, the synthetic strategy can be supported from well reported thermodynamic data and physical properties.

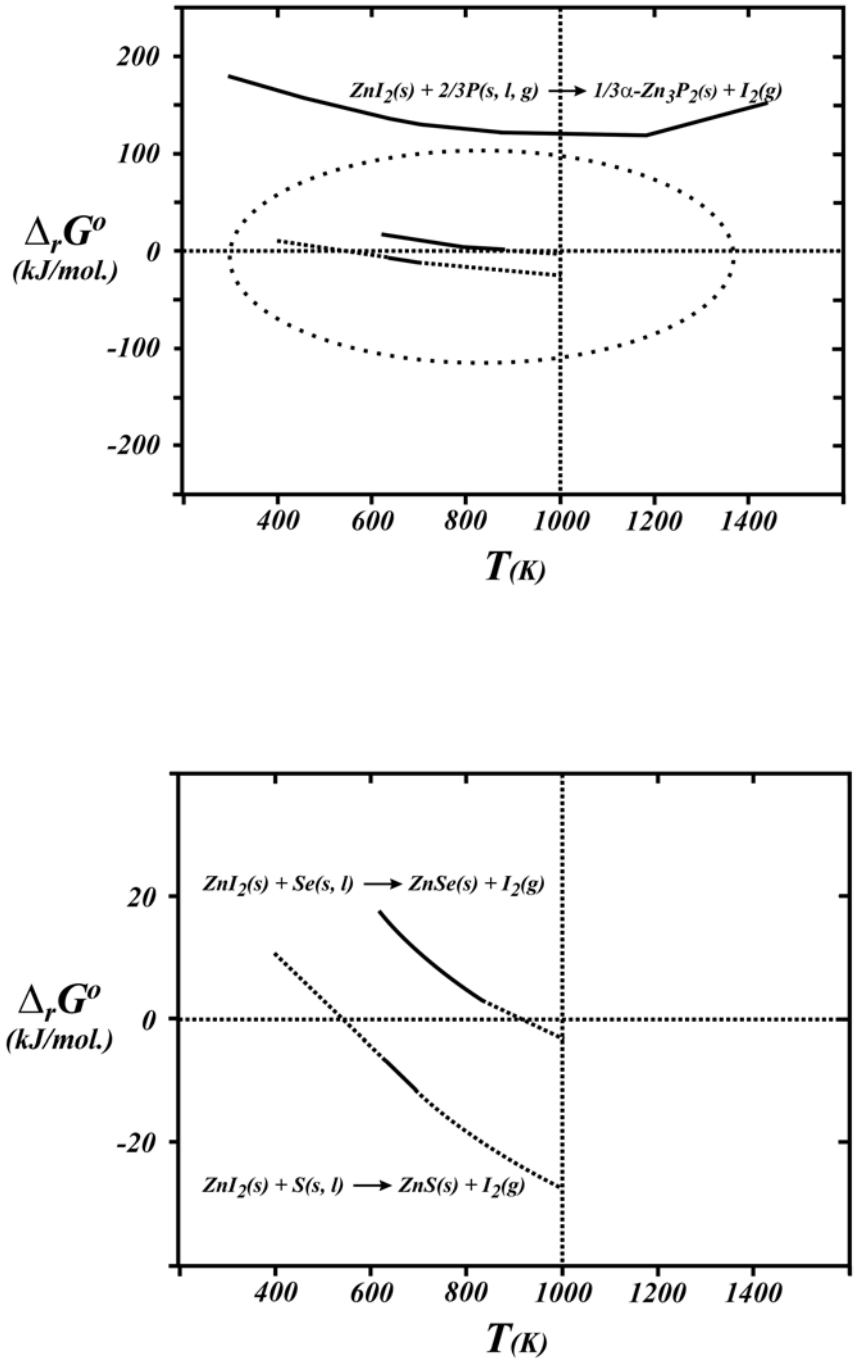

Fig. 2-4. Ellingham plot of ZnI_2 oxidation reaction by S, Se and P [(down) enlarged part of ellipsoid of above figure].

2. 2. Preliminary synthesis

2. 2. 1. ZnI_2 + Se system

First of all, the system of ZnI_2 + Se was investigated from following reasons,

(i) the ternary CuI + P system have been well reported and developed, instead of that,

(ii) the thermodynamic data concerning reaction (1) which has an advantage to use it directly to our system should be confirmed, since the data were measured by using liquid S, Se and Te.

(iii) the gas forming reaction should strongly depend on the reactor volume. Generally speaking, the temperature dependence of the standard Gibbs functions of reaction (1) depends on the reaction entropy through the following relationship (2), there is a net increase in the amount of I_2 gas, if the phase of Se is maintained as solid or liquid at given temperature, the standard reaction entropy ($\Delta_r S^o$) is large and positive, therefore, $\Delta_r G^o$ decreases sharply with increasing temperature.

$$ZnI_2(s,l) + Se(s,l) \leftrightarrow ZnSe(s) + I_2(g) \quad (1)$$

$$\left(\frac{\partial \Delta_r G^o}{\partial T}\right)_p = -\Delta_r S^o \quad (2)$$

(iv) The net *red-ox* reaction can be presented as (3) in the melt of ternary ZnI_2 + Se system.

$$2I^-(melt) + Se^0(melt) \leftrightarrow Se^{2-}(melt) + I_2(g) \quad (3)$$

(v) The equilibrium constant (4) will strongly depends on the formation of I_2 (*g*), i.e., $K \propto [I_2(g)]$.

$$K_S = \frac{[Se^{2-}(melt)][I_2(g)]}{[I^-(melt)]^2[Se^0(melt)]} \quad (4)$$

(vi) at a fixed reactor volume and at a constant temperature, however, the reaction (1) leads to constant pressure of I_2 (g) if the vapor pressures of ZnI_2 and Se can be ignored, since in accordance with ideal gas approximation of I_2 (g). Varying the reactor volume, the net increment of I_2 (g) directly depends on the reactor volume (5). But the concentration of I_2 (g) is constant with varying reactor volume at fixed temperature and pressure.

$$pV = nRT$$

$$\Delta V \propto \Delta n \tag{5}$$

$$C(concentration) = \frac{(mol.)}{(volume)} = \frac{\Delta n}{\Delta V} \propto const. \tag{6}$$

(vii) The expected molar change-time and concentration-time curve for (4) without competition with respect to reactor volume (since the reactor has a constant diameter, accordingly only the length can be varied) as follows,

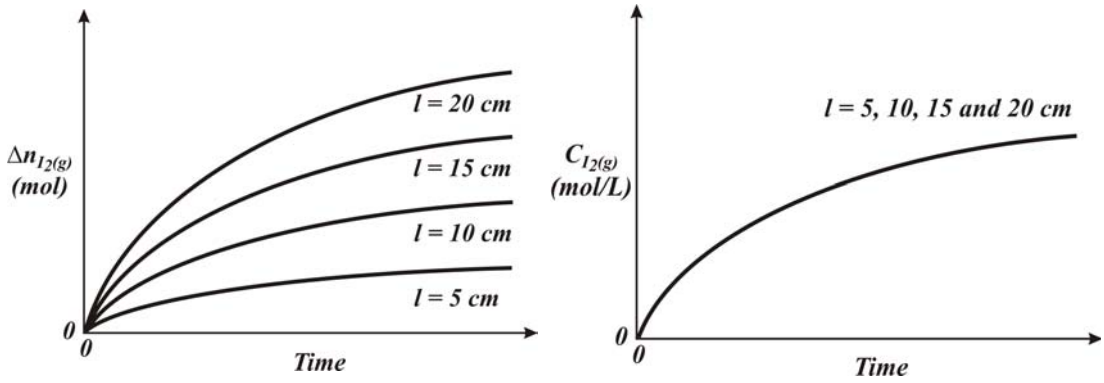

Fig. 2-5. The molar change of I_2-time curve (left) and the concentration of I_2-time curve (right) at fixed temperature and composition.

Therefore, the thermodynamic data allows calculation of the condition for $\Delta_r G^o(1) = 0$ from the standard free G^o with respect to function of temperature, of the reacting materials.

$$ZnI_2(s) \leftrightarrow Zn(s) + I_2(g)$$

$$-\Delta_f G^o = \Delta_d G^o(J/mol) = 278980 - 187.58T + 0.0617T^2 \ (289.1 < T(K) < 1000) \qquad (7)$$

Zn (s,l) + Se (l) $\leftrightarrow$ ZnSe (s)

$$\Delta_f G^o(J/mol) = -185720 + 28.31T(\pm 370) \ (640 < T(K) < 693) \text{ for Zn}(s) \qquad (8)$$

$$\Delta_f G^o(J/mol) = -192590 + 38.22T(\pm 350) \ (693 < T(K) < 825) \text{ for Zn}(l) \qquad (9)$$

The reaction temperature for $\Delta_f G^o = 0$ can be calculated from the relationship (7) and (8) as T = 898 K (625^oC) and (7) and (9) as T = 957 K (684^oC). Above 923 K (650^oC), Zn should be liquid so that the later result is preferable for initial reaction condition.

The reaction (1) was varied by the ampoule length l = 5, 10, 15 and 20 cm (inner ϕ 9 mm and outer ϕ 11 mm) which was aimed to find out the optimum length for obtaining crystalline ZnSe solids at fixed composition, specially stoichiomertic ratio ZnI_2 : Se = 1 : 1. The case of varying composition and amount of reactants was disregarded. The fairly yellow crystal (~ 1 mm) which was able to confirm with eye shot was obtained from silica ampoule l = 20 cm.

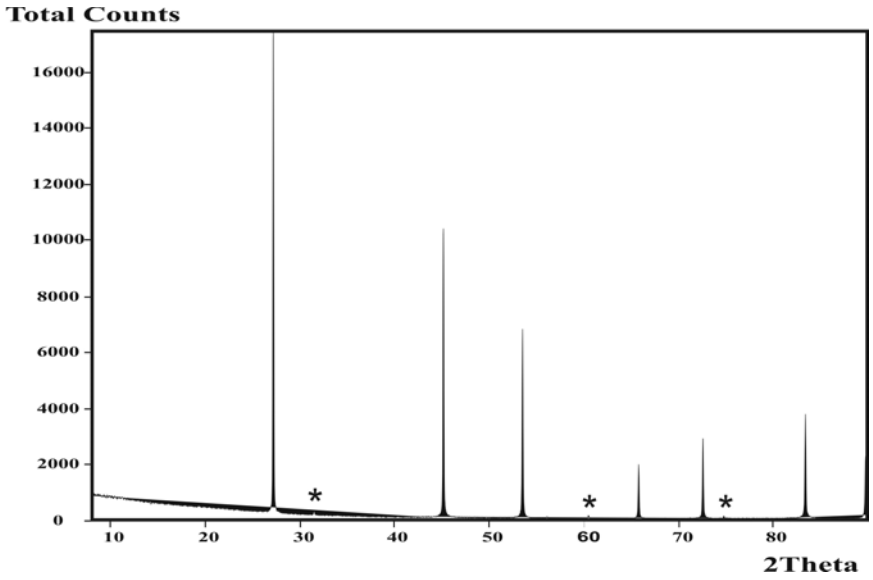

Fig. 2-6. Powder diffraction of Zinc blende type ZnSe at 923 K by ZnI_2 oxidation using Se (* indicates Se impurity).

The lattice constant of measure powder diffraction showed quite good resemblance with reported data (see **Table 2-5**).

Table 2-5. The comparison of reported ZnSe with this work.

comp.		$Zn_{1-x}Mn_xSe$	Zise81-03*
symmetry		cubic	cubic
space group		$F\bar{4}3m$ (no. 216)	$F\bar{4}3m$ (no. 216)
cell param.	a (Å)	5.67	5.672(1)
	V (Å^3)	182.28	182.46(1)
	Z	4	4
method		zinc blende for $0 \leq x \leq 0.3$ wurtzite for $0.33 \leq x \leq 0.57$	ZnI_2 + Se at 923K
ref.		59	this work

1. Synthesis : ZnI_2 [0.802 g (2.51 mmol)] + Se [0.198 g (2.51 mmol)] in silica ampoule (ϕ 9 mm × l 20 cm).
2. Measured by STOE Transmission X-ray diffraction system STADI P type [generator: 1.68kW, 2θ range : 10 ~ 90°, detector : linear PSD and measuring time : 2h] and refined by the STOE Powder Diffraction Software-*WinXPow* 1.08 package.

As a result,

(i) first of all, the volume increment approach by quasi-equilibrium without additional identification of reaction condition for instance by a tracing inner pressure or a spectroscopic tool could not give a quantitative information, since with such a small volume increment the reaction condition could be hardly confirmed. But the qualitative developments were clear as follows,

(ii) at fixed temperature and composition, the reaction (1) in 5, 10 and 15 cm ampoule sized reactors were not optimum for obtaining ZnSe single crystal with an eye shot.

(iii) in the cooler part of the inclined and long reactors like l = 10, 15 and 20 cm due to a temperature gradient of oven, the condensed Se was able to be confirmed. During the reaction, however, the color of I_2 (g) was same over all the reactors, which means the concentration of I_2 (g) is same over all the reactors and the net increment of I_2 (g) formation has a direct relationship with reactor volume.

(iv) it seems that the thermodynamic data concerning reaction (1) are quite correct. Therefore, if the possibility of gas phase reaction can be ignored, we can conclude that the solubility of Se into ZnI_2 is very low, at least under $\frac{0.251 mmol}{4} = 0.06 mmol$, which means under one fourth of initial amount of Se can react with ZnI_2, since the distinguishable ZnSe crystals were found out in the bottom of reactors among a mixture with unreacted clear ZnI_2.

(v) I guess that such a low solubility of Se is just same case with molten salt approach of Zn + ZnI_2 system.

(vi) the unreacted Se vapor was confirmed with an eye shot on cooler part of ampoule.

2. 2. 2. ZnI_2 + P + Se system

In order to induce phosphorus into the ZnI_2 + Se system,

(i) according to evaluation of ZnI_2 + Se system, the result indicated very low solubility of Se into ZnI_2, which is believed as a similar case of molten Zn + ZnI_2 system. Consequently,

(ii) we should remind the thermodynamic properties of phosporus in accordance with those allotropes, and pay our attention to a considered temperature range, i.e., 600 ~ 1000 K. Using less reactive Pn (where Pn = P and As) than chalcogens against relative stable metal halides, the quasi-ternary MX (or MX_2) + Pn + Q system should be simplified into quasi-binary MX (or MX_2) (where X = halogens) + Q system.

(iii) the I_2 gas forming reaction as a ZnI_2 + Se system was well supported by related thermodynamic data, especially around 923 K. Therefore, we can evaluate the phase transitions of phosphorus at such a given temperature. At a given temperature, the stoichiometric molar of ZnI_2 + P + Se can be deducible from the $\Delta_r G^o$ data of possible reaction pairs, for instance mainly ZnI_2 + Se system, ZnI_2 + P system and P + Se, also subsidiary P + I and Se + I system which can be considered as the minor routes from $\Delta_f H_{298}$ data.

(iv) total reaction for obtaining new crystalline solids based on ZnI_2 is targeted as follows, and qualitatively assuming the mechanistic routes, the $\Delta_f H^o_{298}$ data containing phosphorus show rather less exothermic than one containing Se. For example, the enthalpy of PI_3 ($\Delta_f H^o_{298}$ = - 46.2 kJ/I atom) is almost one third of the enthalpy of ZnI_2 ($\Delta_f H^o_{298}$ = -135.4 kJ/I atom) or ZnSe ($\Delta_f H^o_{298}$ = -177.6 kJ/Se atom). To add to this, very unstable species Se_xI_y has still not reported so that such routes may be ignoble. The enthalpy of reported $SeCl_4$ was $\Delta_f H^o_{298}$ = -48.22 kJ/Cl atom. Therefore, if the similar species like SeI_4 is stable, the value of enthalpy will be around -10 kJ/I atom, which is in the range of enthalpy of transformation of phosphorus allotropes, i.e., transformation *(e)*. Accordingly the

total reaction can be designed by thermodynamic consideration about the reactions *(d)*, *(e)* and *(f)*.

$p\mathrm{ZnI_2}\,(s) + q\mathrm{P}\,(l) + r\mathrm{Se}\,(l) \rightarrow \{\mathrm{ZnI_2}$ based crystalline solid $(s)\} + \mathrm{I_2}\,(g)$

	Main routes	
(a)	$\mathrm{Zn}\,(s, l) + \mathrm{I_2}\,(g) \leftrightarrow \mathrm{ZnI_2}\,(s)$	$\Delta_f G_m^o[(a)]$
(b)	$\mathrm{ZnI_2}\,(s) \leftrightarrow \mathrm{Zn}\,(s, l) + \mathrm{I_2}\,(g)$	$\Delta_d G_m^o[(b)] = -\Delta_f G_m^o[(a)]$
(c)	$\mathrm{Zn}\,(s, l) + \mathrm{Se}\,(l) \leftrightarrow \mathrm{ZnSe}\,(s)$	$\Delta_f G_m^o[(c)]$
(d)	$\mathrm{ZnI_2}\,(s) + \mathrm{Se}\,(l) \leftrightarrow \mathrm{ZnSe}\,(s) + \mathrm{I_2}\,(g)$	$\Delta_f G_m^o[(d)] = \Delta_f G_m^o[(b) + (c)]$
(e)	$\mathrm{P}\,(s) \leftrightarrow \mathrm{P}\,(l)$	$\Delta_t G_m^o[(e)]$
(f)	$x\mathrm{P}\,(l) + y\mathrm{Se}\,(l) \leftrightarrow \mathrm{P}_x\mathrm{Se}_y\,(s, l, g)$	?

	Subsidiary routes	
(g)	$\mathrm{P}\,(l) + 3/2\ \mathrm{I_2}\,(g) \leftrightarrow \mathrm{PI_3}\,(l, g)$, *etc.*	$\Delta_f H_m^o[(g)] >> \Delta_f H_m^o[(a)]$
(h)	$\mathrm{Zn}\,(s, l) + 2/3\ \mathrm{P}\,(l) \leftrightarrow 1/3\ \mathrm{Zn_3P_2}\,(s)$, *etc.*	$\Delta_f H_m^o[(h)] >> \Delta_f H_m^o[(c)]$

(v) the thermodynamic data of reaction (f) has not been correctly established yet. The S_{298}^o for $\mathrm{P_4S_3}$ (203.3 J/mol·K) and $\mathrm{P_4Se_3}$ (239.6 J/mol·K) were reported[58]. The cases of $\mathrm{As_xQ_y}$ have been seldom reported. On the analogy of only reported $\Delta_f G$ data of $\mathrm{P_4S_3}$, such molecules are relatively stable over very wide temperature range[55] as following **Fig. 2-7**. The stability order of $\mathrm{Pn_4Q_3}$ (where Pn = P, As and Q = S, Se) cage molecules has been reported by an evaluation of chemical ionization mass spectra [60](with respect to proton affinity) and a calorimetric

thermal analysis[18] (with respect to decomposition or polymerization) as a following order,

$$P_4S_3 > P_4Se_3 > As_4S_3 > As_4Se_3$$

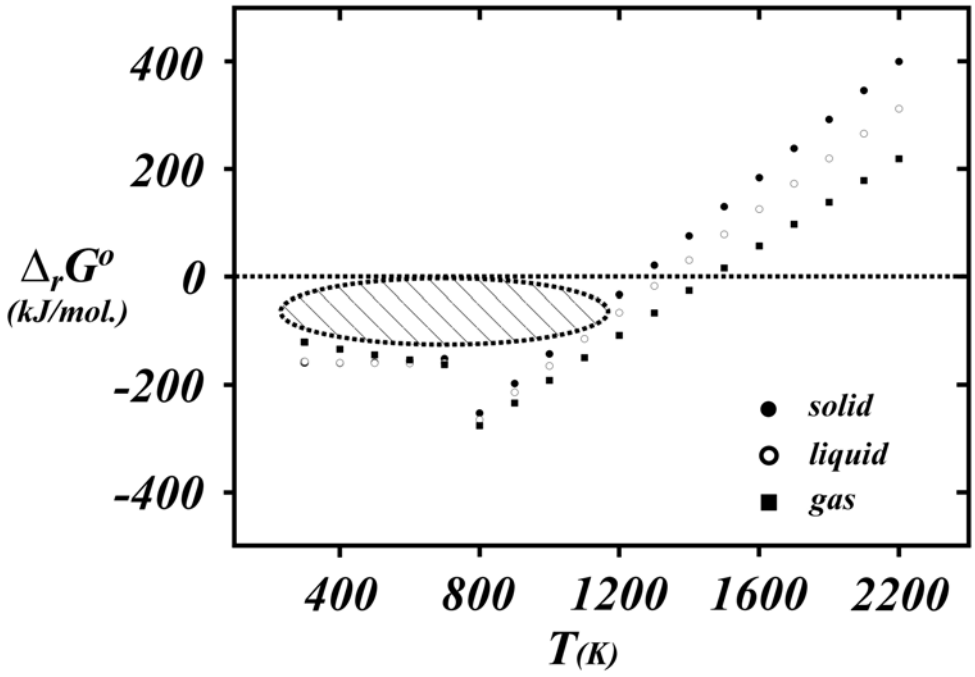

Fig. 2-7. Ellingham plot of formation of P_4S_3 with reference state[55] (the ellipsoid indicates stable region of Pn_xQ_y molecule).

(vi) therefore, the reaction and transformation *(d)*, *(e)* and the reaction *(f)* will occur independently.

(vii) the most reliable thermodynamic data concerning phosphorus related materials historically have been obtained working with white phosphorus and the meta-stable liquid.

According to above considerations, the allotropes of phosphorus as a function of free energy change to **Table 2-6**, it in turn has led to the choice of α-white/liquid phosphorus as the reference state for the element, despite experimental evidence showing the red (I), red (IV),

red (V) (where I, IV and V are stable allotropic phases of phosphorus), and both black forms are all thermodynamically stable (In fact, phosphorus is often the only chemical element for which the reference state is not the standard state). And **Table 2-6** is summarized and shown in **Fig. 2-8**.

Table 2-6. Gibbs Energy changes of transformation of phosphorus[58].

Reaction				$\Delta G^o(J/mol)$
(a)	P (red, V)	→	P (α-white)	$17201 - 15.99T - 0.00400T^2 \ (373 < T < 500)$
(b)	P (red, V)	→	P (*l*)	$19698 - 26.12T + 0.00421T^2 \ (373 < T < 500)$
(c)	P (red, V)	→	P (red, I)	$13305 - 23.25T + 0.00824T^2 \ (373 < T < 500)$
(d)	4P (meta, *l*)	→	$P_4(g)$	$52180 - 97.40T + 0.00565T^2 \ (373 < T < 500)$
(e)	4P (α-white)	→	$P_4(g)$	$62167 - 137.9T + 0.0385T^2 \ (373 < T < 500)$
(f)	4P (red, V)	→	$P_4(g)$	$130971 - 201.9T + 0.0225T^2 \ (593 < T < 833)$
(g)	4P (red, I)	→	$P_4(g)$	$77750 - 108.9T - 0.01047T^2 \ (593 < T < 833)$
(h)	P (red, V)	→	½ $P_2(g)$	$90118 - 89.10T + 0.00641T^2 \ (1073 < T < 1473)$
(i)	$2P_2(g)$	→	$P_4(g)$	$-229500 + 154.5T - 0.00313T^2 \ (1073 < T < 1473)$

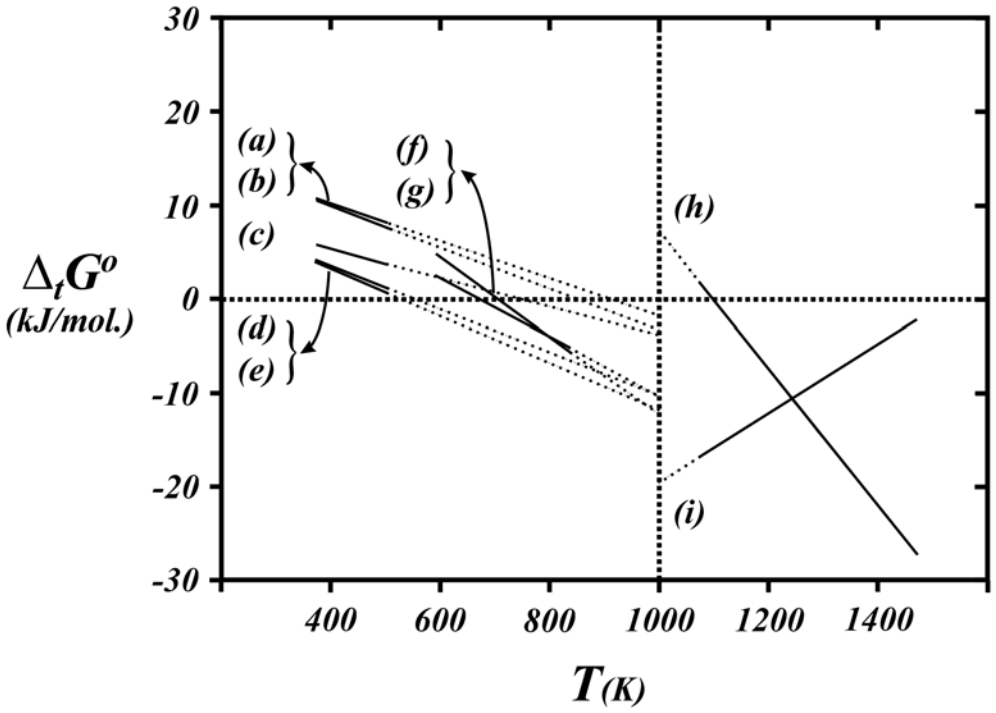

Fig. 2-8. Summarized free Gibbs energy changes of transformation of P related species (parentheses indicate reaction in **Table 2-6** and dotted lines are extrapolated).

Consequently, the most lines of extrapolated $\Delta_t G$, especially the group of transformation *(a)*, *(b)* and *(c)*, and *(d)*, *(e)*, *(f)*, and *(g)*, respectively can be converged at two points at 1000 K. It means that the transformation from P (α-white), metastable P liquid and P (red, I) to P_4 (g) is spontaneous process which can be accompanied by a very slight gap of free energy change around -10 kJ/mol. It will be very difficult to confirm a small range of meta-stable liquid phase (692 ~ 704 K with pure red phosphorus). With respect of synthetic point if any in eutectic mixture and if conformable, it also is quite good advantage to control the overall reaction. A consideration about the possible main routes of formation in ZnI_2 + P + Se system based on initial postulates including above allotropes of phosphorus gives us useful information for design of the reaction strategy in ZnI_2 + P + Se system as follows,

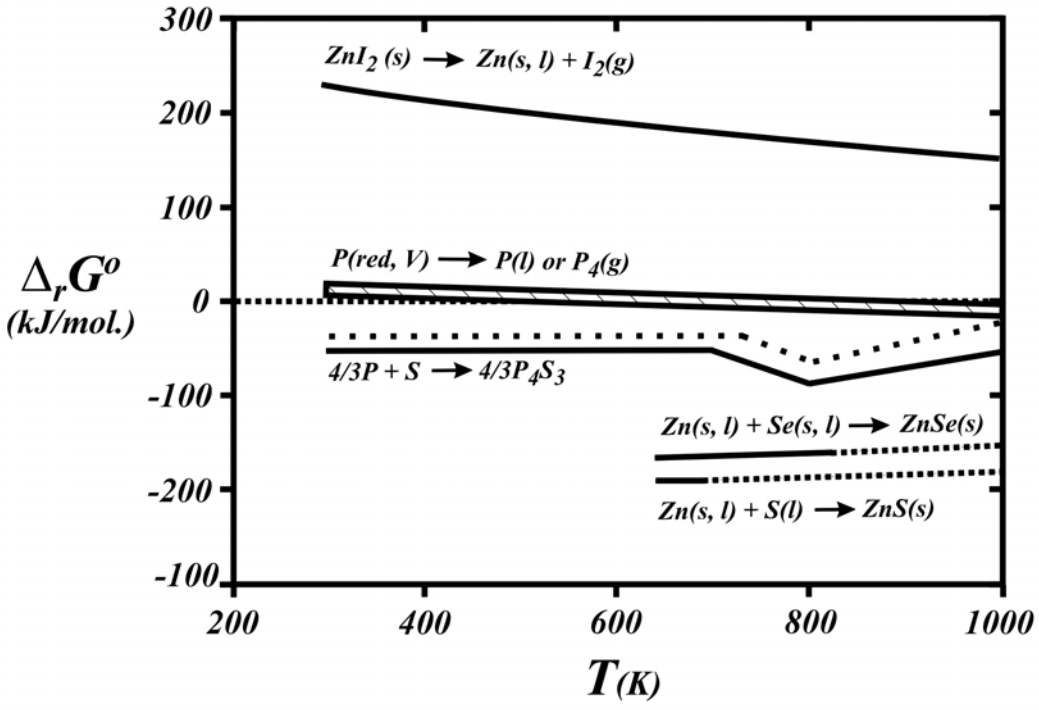

Fig. 2-9. The free Gibbs energy change of main routes in ZnI_2 + P + Se system.

(i) from thermodynamic data of main routes at 923 K, the stoichiometry of ZnI_2 + P + Se system can be deduced as follows,

(a)	$ZnI_2(s) \rightarrow Zn(s) + I_2(g)$	$\Delta_d G(923K) =$ 158407 J/mol.
(b)	$Zn(l) + Se(l) \rightarrow ZnSe(s)$	$\Delta_f G(923K) =$ -157312 J/mol.
(c)	$P(V) \rightarrow P(l)$	$\Delta_f G(923K) =$ -824 J/mol.

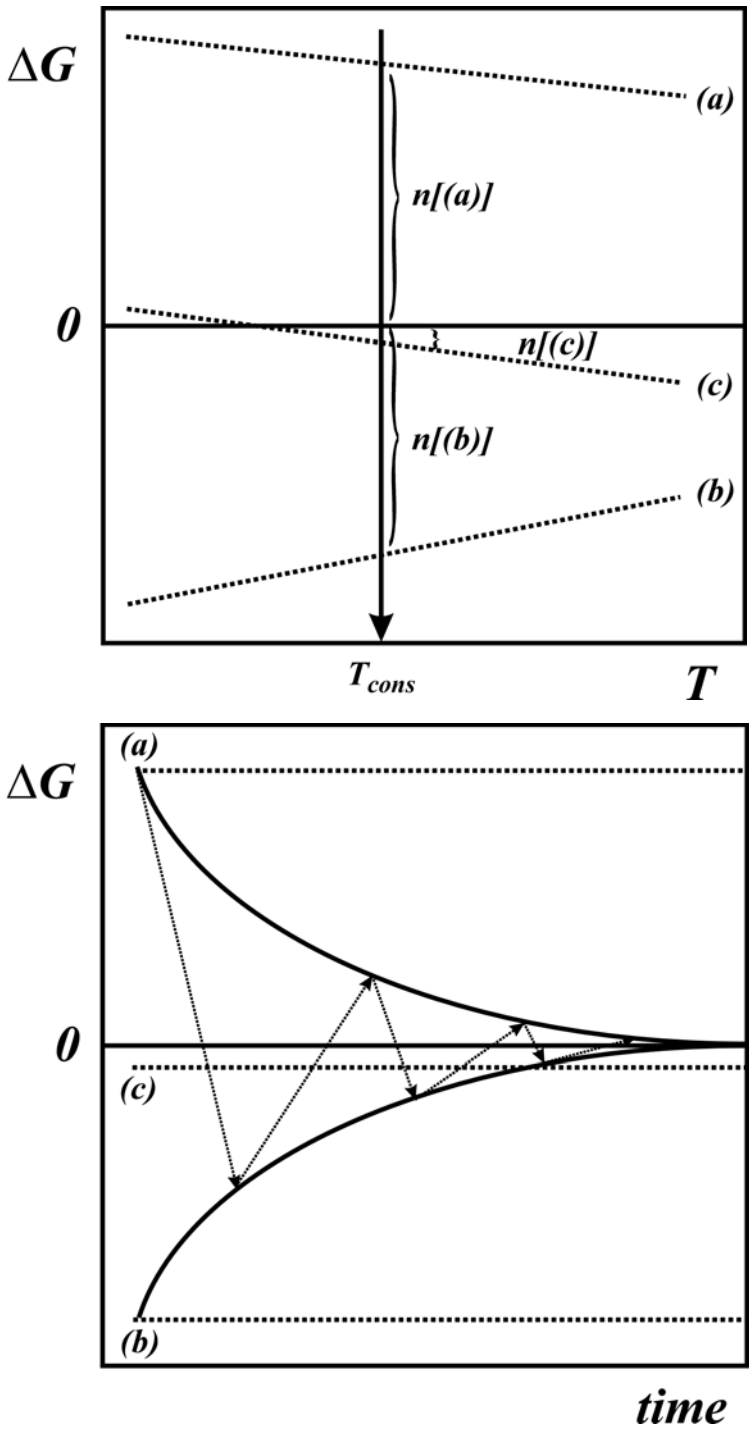

Fig. 2-10. The pictogram of a concept of the reaction strategy [*n* indicates molar amount and where (a) $\Delta G(T = T_{cons})$ for the dissociation of metal halides and T_{cons} is a considered temperature, (b) $\Delta G(T = T_{cons})$ for the formation of metal chalcogenides and (c) $\Delta G(T = T_{cons})$ for transformation of P or As from solid to liquid].

Above thermodynamic considerations (see **Table 2-2**, **2-4** and **2-5**) lead us to establish a concept for estimating composition of reactants as follows,

$$n[(a)] = n[(b)] + n[(c)] \text{ where } n[(c)] \approx 0 \text{, then } n[(a)] \approx n[(b)] \qquad (10)$$

where the condition of $n[(a)] \approx n[(b)]$ can be calculated by using thermodynamic data, since the free Gibbs energy change for physical transformation (from solid to liquid or solid to vapor) of phosphorus is almost negligible [$n[(c)] \approx 0$] compared with either the free Gibbs energy change for formation of metal chalcogenides or the free Gibbs energy change for dissociation of metal halides. The excess energy leads the reaction to consuming energy for phase transition of elemental phosphor. The result of summation is +271 J/mol which is within an estimated standard deviation of thermal measurements.

(ii) a chemical reaction should be advanced on the direction of $\Delta_r G = 0$, i.e., on an chemical equilibrium (see **Fig. 2-10** down), at considered temperature T_{cons} (where T_{cons} = 1000 K) under the existence of metal Zn, the overall reaction should be spontaneous. The subsidiary routes for formations of Zn phosphides and unstable phosphorus halides which was suggested by **Table 2-6**.

(iii) the thermodynamic properties of P + Se system is still unclear. The only reported P_4S_3, however, gives us useful information for obtaining analogue P_4Se_3 from thermodynamic consideration. The $\Delta_f G(T)$ of P_4S_3 (see **Fig. 2-7**) showed a hollow part which can be believed as a reason for formation of stable cage molecule over wide temperature range and its glassy behavior through polymerization. Comparing with Zn + Se and Zn + S pair, our attention at 1000K, especially the formation of P_4Se_3 can be roughly estimated from comparing S^o_{298} of P_4S_3 with one of P_4Se_3 [see above introduction (v)] with respect to $\Delta G = \Delta H - T\Delta S$. The estimated free Gibbs energy change (see **Fig. 2-9** dotted line) of P_4Se_3 showed also almost the same value with the one of the

phosphorus transformation. To add to this, around 700 K, P_4Q_3 cage molecules can exist with liquid – gas transformation.

From the thermodynamic consideration about the ZnI_2 + Se system and about the allotropes of phosphorus, we can conclude that we have to divide the thermal control of reaction into two stages as follows which is based on the basic idea of '*an enthalpy change of a considered transformation should be considerably smaller than one of a considered formation*'.

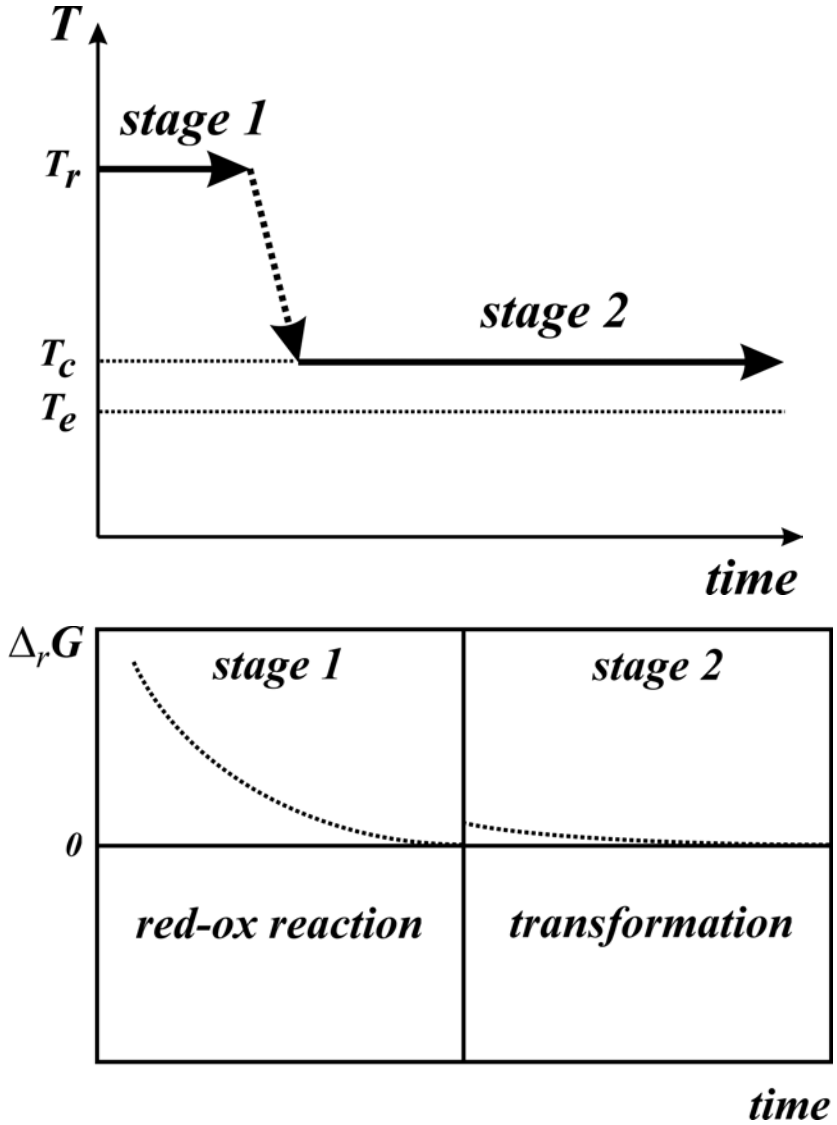

Fig. 2-11. The pictorial synthetic strategy of ZnI_2 + P + Se system by T *vs.* time for reactor control and $\Delta_r G$ *vs.* time curve (where T_r indicates the thermodynamically induced red-ox reaction temperature, T_c the crystallization temperature and T_e the eutectic temperature of unknown mixture).

2. 3. Synthesis procedure

Under the concept of thermodynamic consideration and synthetic stages, I focused the reaction condition as followings.

(i) for stage 1, the reaction temperature (T_r) for binary ZnI_2 + Se pair in quasi ternary ZnI_2 + P + Se system, should be suggested at 923 K (650 ^oC).

(ii) from the evaluation of quasi binary ZnI_2 + Se system, the ampoule length [ϕ (inner) 8 mm, ϕ (outer) 11 mm] was recommended as 6 ~ 7 cm for the purpose that the overall reaction leads to ZnI_2-based complex formation with Se, not for ZnSe (s) formation.

(iii) the overall reaction should be governed by $\Delta_r G = 0$ at 923 K, especially by $\Delta_f G$ (923 K) [$ZnSe$ (s)], since it is almost five times than the formation of Zn phosphides. Therefore, the confirmation of overall reaction equilibrium at 923 K, especially the dense color of I_2 vapor, which can be comparable with ZnI_2 : Se = 8 : 1 system, should be monitored as time goes by. To add to this, at 973 K the vaporized phosphorus species indicate that the system is in positive free Gibbs energy, i.e., $\Delta_f G > 0$, so that those species should be minimized. Instead of that, the meta-stable liquid phosphorus or phosphorus halides should be confirmed (see **Table 2-4**).

(iv) after reaction (6 ~ 7 days), the ampoule should be cooled rapidly in order to confirm whether the phosphorus vapor species appear or not on the upper and cooler side of the ampoule.

(v) the temperature for crystallization should be governed by the concept of stage 2, i.e., just above the melting point of the mixture (rf. for instance T_m of ZnI_2 is 446 ^oC). But melting and freezing points of unknown mixture are defined as those values of the variables (temperature, pressure) at which solid and liquid phase are in equilibrium. Practically, from 380 ^oC to 420 ^oC, every 10 ^oC step, the whole procedure should be repeated till a formation of distinguishable crystalline phase within eyeshot. Melting and freezing points of unknown mixture, however, are

hardly distinguishable within eyeshot, even simple binary eutectic systems. For experimental purposes, one may consider the melting point of a mixture as that temperature at which it first begins to melt upon heating and the freezing point as the initial appearance of crystals upon cooling, assuming no difficulty in nucleation. More conveniently, the freezing point may also be considered the lowest temperature at which the material is entirely molten, i.e., a homogeneity of reaction mixture. Though various thermal analysis tools have been provided solutions for solving such a problem through the evaluation of phase diagram, in case of gas forming reaction those approaches lead to errors due to slightly changed composition which can happen as soon as open the ampoules. The main interest concerning above discussion is that how I can monitor the eutectic temperature of mixture (T_e) directly. Under this consideration, after reaction step (iv), using Al foil with simple Pt-Rh thermocouple, the temperature for eutectic solidifying of considered ampoule can be confirmed for instance Zizpse6147 system showed at 375 ^oC (see **Fig. 2-6**). It is quite old method, but very effective for confirmation of T_e by means of simple way directly.

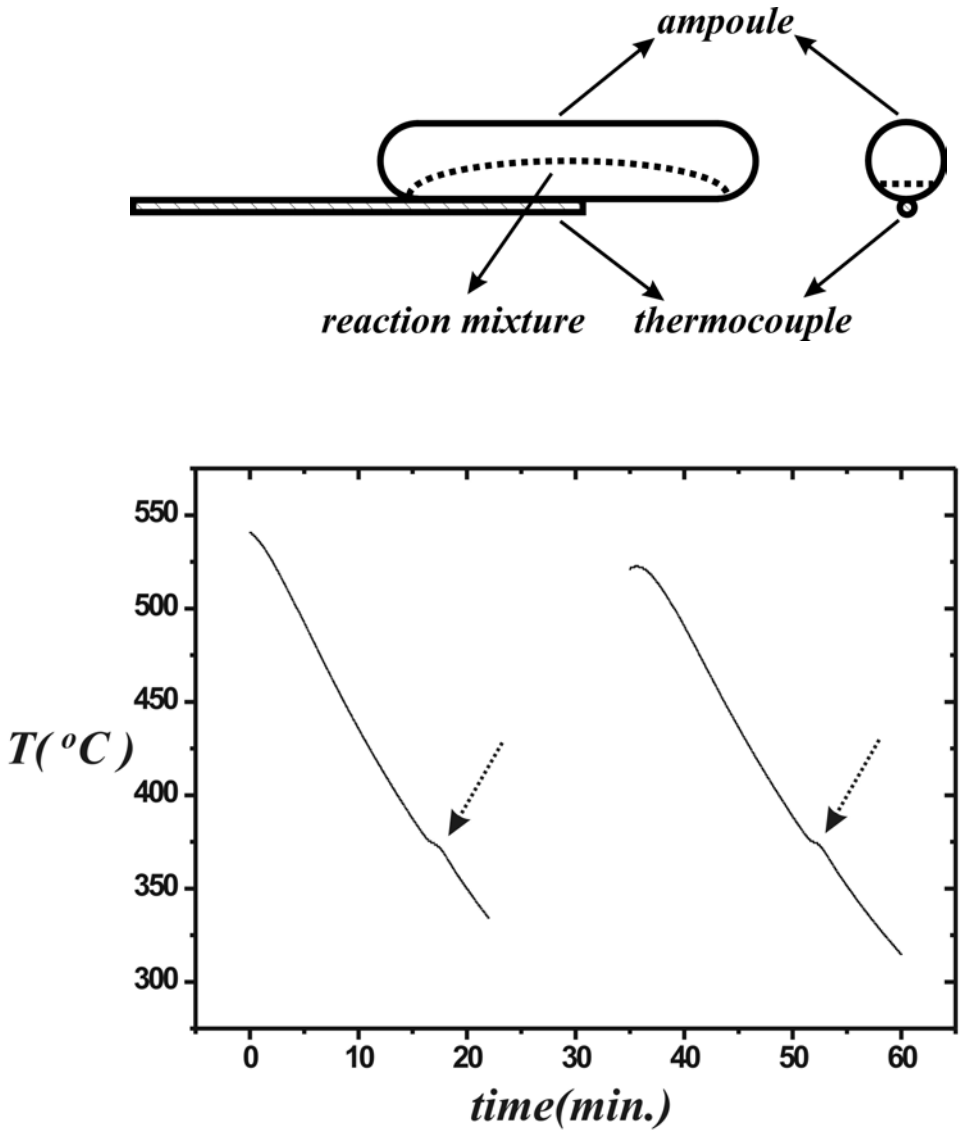

Fig. 2-12. The eutectic solidifying temperature of Zizpse6147 (down) and pictogram for bulk measurement (above) (the signals of free cooling temperature were monitored at every 0.1 sec by PICO A-D converter, running 2 times).

2. 4. Characterization of Zipse334

After the optimization for aging temperature, at 400 ^{o}C for 2 weeks,

(i) a dark brown colored crystalline compound which got single crystals (~ 5 × 5 × 3 mm) of cubic shape was obtained and was regarded as a single phase with an eyeshot due to the majority of formation of crystalline compound.

(ii) first of all, the unknown crystalline compound was characterized by powder diffraction. For determination of proper space group of unknown crystalline compound, the space group $F\bar{4}3c$ (No. 219) as an analogue of synthetic boracite was suggested and believed by an evaluation of diffraction pattern.

(iii) at the same time, single crystal measurement was performed and discussed. With respect to space group, however, the deduced refinement result coincided with the determined space group by powder diffraction by accident.

(iv) the refined value of atomic occupancy of P and Se shown very low which cause to following estimations concerning intercalated molecule(s),

(a) composition
- homo phosphorus or selenium molecule(s) due to similar scattering factor
- single or multiple occupancy by phosphorus selenides
(b) disorder
- orientational disorder by single occupancy
- dislocalization by multiple occupancy

(v) for additional characterization of intercalated molecule(s), ir / Raman and ^{31}P-MAS NMR spectroscopies were suggested, measured and discussed.

2. 4. 1. Powder diffraction pattern of Zipse334

For the purpose of initial characterization,

(i) the powder diffraction of Zipse334 was measured by high resolution Siemens D5000 diffractometer at room temperature for 30 min. and

(ii) the specimen was prepared in Ar atmosphere due to the hygroscopic nature of Zipse334. and

(iii) the indexed pattern of peaks was refined by STOE Winxpow package.

(iv) The space group of unknown crystalline compound was suggested by $F\bar{4}3c$ (no. 219) as an analogue of synthetic boracites tentatively.

Following **Fig. 2-13** and **Table 2-7** indicate initial characterization of crystalline compound Zipse334 by powder diffraction which was relative complicate, but distinguishable patterns compared with ZnI_2, P and Se or those related compounds.

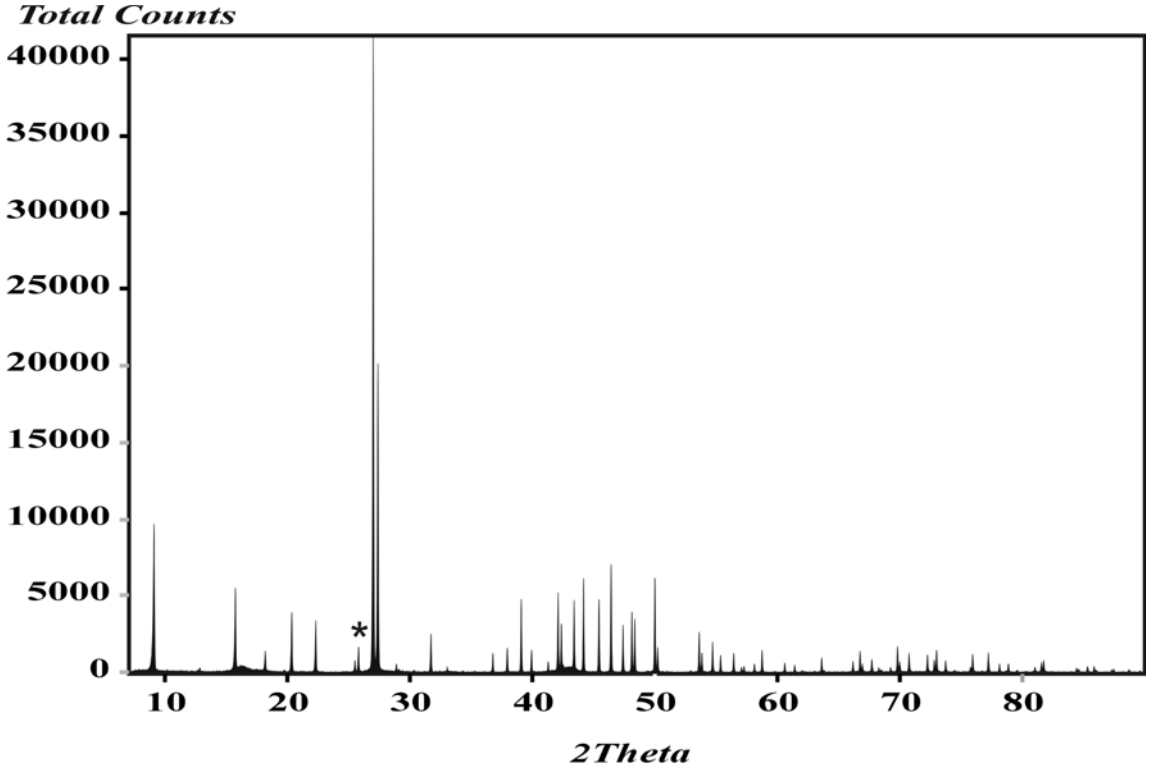

Fig. 2-13. The diffraction patterns of Zipse334 crystalline compound (* indicates an impurity of ZnI_2).

Table 2-7. The powder diffraction - Refinement Result of Zipse334.

comp.		Zipse334		
λ (Å)		1.5405 (Cu-Kα_1)		
accepted peaks (*n*)		68	single indexed lines(*n*)	68
symmetry		cubic	space group	$F\bar{4}3c$ (no. 219)
lattice parameters	*a* (Å)	19.561(1)		
	V (Å^3)	7484.4(1)		
FOM F(30)		402.0 (0.002, 38)	D	1.420

1. Synthesis: ZnI_2 [0.7008 g (2.20 mmol)] + P [0.0680 g (2.20 mmol)] + Se [0.2312 g (2.93 mmol)] in silica ampoule (ϕ 9 mm × *l* 6 cm).
2. Measured by Siemens D5000 [generator : 1.2kW, 2θ range : 8 ~ 90°, and measuring time : 0.5 h] and refined by the STOE Powder Diffraction Software-*WinXPow* 1.08 package.
3. D = Durbin-Watson serial correlation

$$D = \frac{\sum_{i=2}^{n}(\delta x_i \cdot \delta x_{i-1})}{\sum_{i=2}^{n}(\delta x_i \cdot \delta x_i)}$$

where δx_i and δx_{i-1} are the successive residuals in a series for $1.7 < D < 2.3$, with $n > 100$ distribution is random with 95% confidence interval.

The powder diffraction discussed about following points,

(i) the refinement algorithms of powder diffraction patterns for instance by Werner[62], Visser[63] and Louer[64] indicated a tetragonal cell with F.O.M[65] = 150.

(ii) the possibility of Rietveld refinement method[66] using well reported location parameters of boracite compounds was ignored due to the difficulty of refinement concerning quasi-ternary crystalline system.

(iii) with space group $F\bar{4}3c$, the refinement result showed very good F.O.M compared with other results from various algorithms.

(iv) the accepted peaks were all single indexed, but the peaks in two theta range ($60 \sim 90^{o}$), were hardly distinguishable. Consequently, the neutron diffraction was suggested.

2. 4. 2. Single crystal measurement of Zipse334

The single crystal of Zipse334 was measured by STOE IPDS and refined by SHELX[67] and Wingx[68] package as follows,

(i) the refinement result of powder diffraction showed quite unique pattern with postulated space group $F\bar{4}3c$.

(ii) the synthesized crystalline compound ; Zipse334 had $5 \times 5 \times 3$ mm dimension enough for a single crystal X-ray measurement, which was believed as a single phase.

A right-angle pole-shaped single crystal (longest edge = 0.18 mm and volume = 0.002 mm^3) was prepared in Ar atmosphere. The specimen [upper-side-closed outer glass capillary (ϕ 0.3 mm × *l* 10 mm) in which a single crystal was supported by top of inner capillary (ϕ 0.2 mm)] was closed *in vacuo*.

The measurement was performed by following condition (see **Table 2-8**).

Table 2-8. The measurement section of Zipse334 single crystal.

Exposure condition		**Initial cell**		
temp. (K)	293K	lattice		triclinic P
λ (*Å*)	0.71073	lattice parameters	*a (Å)*	19.541(1)
tube power (kW)	2.5		*b (Å)*	19.547(1)
detector distance (mm)	60		*c (Å)*	19.539(1)
irradiation/ exposure (min.)	5		α *(°)*	89.996(8)
measurement duration (h.)	55		β *(°)*	89.992(8)
Integration of reflections			γ *(°)*	89.989(8)
total number of reflections	55162		*V (Å³)*	7463.1(1.5)
$I > \sigma(I)$	11773 (21%)	**Cell transformation**		
$I > 2\sigma(I)$	9184 (17%)	lattice		cubic F
Selection of reflections		lattice parameters	*a (Å)*	19.542(1)
scan range (θ)	$1.9 < \theta < 28.15$		*V (Å³)*	7463.1(1.0)

The distance of detector was fixed at 60 mm from specimen due to a suggestion of huge cell from the result of powder diffraction. Initially the measured reflexes (number of reflections = 8000) was integrated by primitive triclinic cell within a standard deviation 2σ. The lattice parameter of selected triclinic cell indicated that the integrated data can be transformed into a cubic cell.

Fist of all, the measured data was treated by unit cell and space group analysis program XPREP and the suggested type of Bravais lattice for crystalline compound Zipse334 was a face-centered cubic system (*F*) as the highest order by analyzing lattice extinction from the measured reflections (within 3σ). After examination of reflex conditions, both XPREP and Wingx crystal solution program package indicated the structural ambiguity between a non-centrosymmetric space group $F\bar{4}3c$ (no. 219) and cetrosymmetric space group $Fm\bar{3}c$ (no. 226). The suggested probability that the structure is centrosymmetric was 77.76% for all the reflections and the Sheldrick's $|E2-1|$ criterion was 0.898 (cf. for ideal centrosymmetric is 0.968 and for ideal acentrosymmetric is 0.736). As a result, the non-centrosymmetric space group $F\bar{4}3c$ with Z = 8 was chosen tentatively based upon the centering condition and the systematic absences (0, *k*, *l*) : *k*, $l = 2n + 1$; (*h*, *h*, *l*) : *h*, $l = 2n + 1$ and (0, 0, *l*) : $l = 2n + 1$. These systematic absences also correspond to the space group $Fm\bar{3}c$. However, the crystalline compound Zipse334 obtained in the non-centrosymmetric space group gave a chemically reasonable structure with intercalated P_4Se_3 cage molecule, while the refinement in the centrosymmetric space group did not matched with P_4Se_3 cage molecule. Finally, in $F\bar{4}3c$ atomic model, the reported positions of the Se atoms in cavity structure do not allow the presence of mirror planes perpendicular to the primary axes, as required by $Fm\bar{3}c$, and therefore the choice of the non-centrosymmetric space group $F\bar{4}3c$ was confirmed. As justification of the centered cell, the (*h*, *k*, *l*) data with *h*, *k*, $l = 2n + 1$ were extraordinarily weak. If they are considered unobserved, only *h*, *k*, $l = 2n$ are observed and one must consider a primitive cubic cell with cell lengths one half of those reported for $F\bar{4}3c$. The structural models obtained from this smaller cell gave unreasonable bond distances between P and Se atoms.

The reflections were corrected for absorption by numerical method, which was supported by program STOE X-SHAPE, with an optimization of both distances and orientations. After the cycles of numerical absorption correction, the structure refinement was performed by SHELXL-97 with direct method. All along the routines of structure refinement, the atomic occupancies of intercalated molecule(s) showed very low values, then consequently twin option was used [the Flack parameter[69] against absolute structure is 0.51(7)]. Even though such a twin operation did not give us clear solution for correct decision about the nature of intercalated molecule(s), especially in the points of both (1) orientation and (2) composition.

Table 2-9. Refinement Result of Zipse334 Single crystal.

temp. (K)		293 K	λ (*Å*)	0.71073
crystal system		cubic	space group	$F\bar{4}3c$ (no. 219)
lattice parameters	*a (Å)*	19.542(1)	$d_{calc.}$ (g/cm^3)	?
	V (Å³)	7462.9(13)	diffractometer	STOE IPDS
	Z	8	μ (mm^{-1})	18.667
scan range (θ)		2.94 < θ < 24.98	measured reflections (*n*)	20957 [$I > 2\sigma(I)$]
unique reflections (R_{int})		565(0.0371)	used parameters (*n*)	46
wR_2 (for all)		0.0375	wR_2 [$I > 2\sigma(I)$]	0.0372
R_1 (for all)		0.0172	R_1 [$I > 2\sigma(I)$]	0.0164
S on *F*		1.129	residual density ($e.Å^{-3}$)	+0.429/-0.391

The refinement result (see **Table 2-9**) was illustrated by visual crystal structure information system 'Diamond (ver. 2.1b)' (see **Fig. 2-14**).

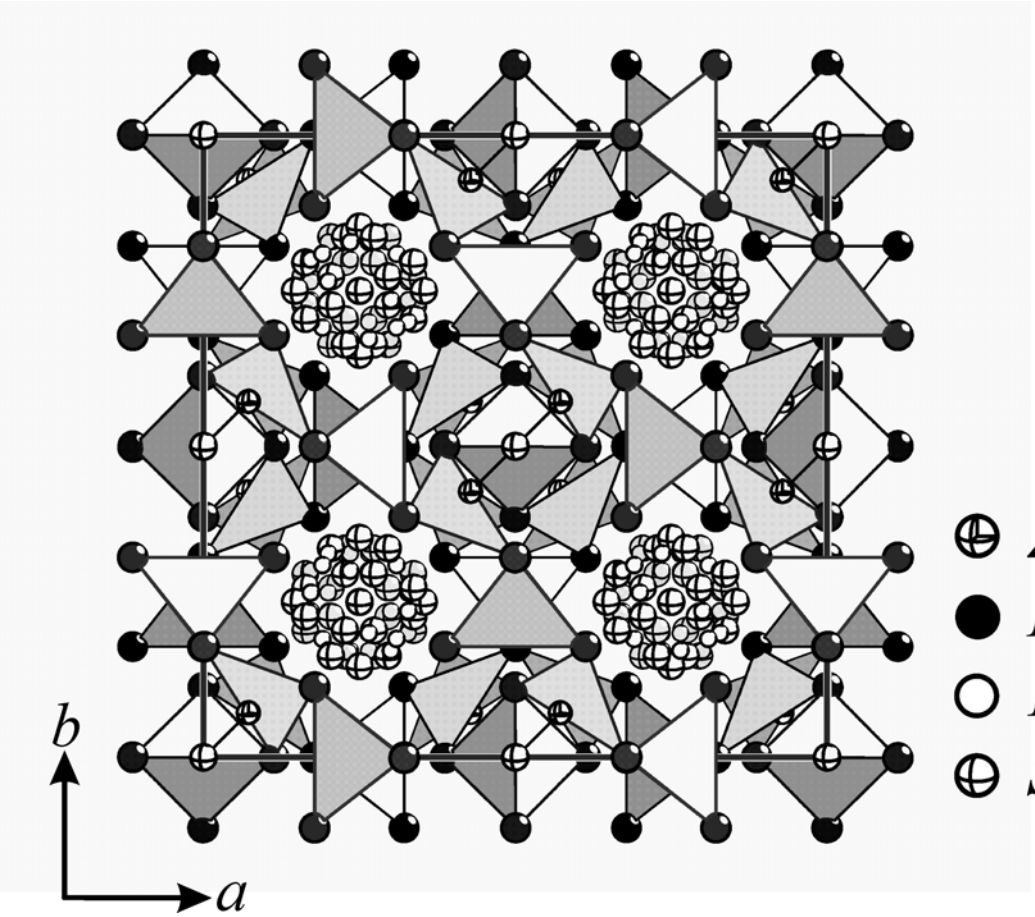

Fig. 2-14. The section of crystal structure of Zipse334 system.

Following specific characteristics of this crystalline compound were discussed,

(i) the crystallographic examinations about measured reflections indicated that the structure of Zipse334 showed the face centered $m\bar{3}m$ as the highest Laue class and intercalated molecule(s) were highly disordered. Tentatively, the space group $F\bar{4}3c$ was assigned.

(ii) all the refinement values were optimum and especially R_1 [$I > 2\sigma(I)$] showed a super-correct value ; 0.0164 (see **Table 2-9**).

(iii) the shape of Zipse334 crystalline compound by graphic illustration showed an analogue of *'host/guest clathrate system'*, since no chemical bond between host lattice and guest molecule(s) was detected by X-ray measurement (see **Fig. 2-7**) for instance the shortest distance from I (*96h*) to one atom of intercalated molecule(s) was ~ 4 Å and the shortest cavity diameter was ~ 11 Å.

(iv) the refined atomic parameters of host lattice are quite well fixed within those thermal displacement parameters, but the guest molecule(s) showed so strong disorder that we could not decide the exact orientation and composition, consequently the exact density and bond lengths also were not determined. Tentatively a cage molecule P_4Se_3 was assigned as unknown guest molecule(s) for convenience of reaffirmation concerning deduced composition from the result of structure refinement.

(v) for identification of intercalated guest molecule(s), spectroscopic tools like ^{31}P-MAS NMR and ir/Raman and for refinement of the reflection data, the technique of 'Rigid-body refinement' are suggested.

Table 2-10. Position Parameters and Equivalent Isotropic Displacement Values (Å^2) for Zipse334 at 293 K with Estimated Standard Deviations in Parentheses.

atom	Wyckoff	occup.	*x/a*	*y/b*	*z/c*	$U_{eq.}$
I1	*96h*	1	0.1132(0)	0.1783(0)	-0.0008(0)	0.0349(2)
Se1	*8a*	1	0	0	0	0.0226(3)
Zn1	*24d*	1	0	¼	0	0.0298(2)
Zn2	*32e*	0.64(1)	0.0721(1)	-0.0721(1)	0.0721(1)	0.0244(7)
Zn3	*32e*	0.36(1)	0.0719(2)	0.0719(2)	0.0719(2)	0.0328(14)
P1	*96h*	0.43(8)	0.196(4)	0.219(4)	0.172(4)	0.20(4)
P2	*96h*	0.44(9)	0.219(4)	0.260(2)	0.152(1)	0.18(3)
Se2	*32e*	0.18(5)	0.193(1)	0.193(1)	-0.193(1)	0.22(6)

Table 2-11. Anisotropic Displacement Values (Å^2) for Zipse334 at 293 K with Estimated Standard Deviations in Parentheses.

atom	U_{11}	U_{22}	U_{33}	U_{12}	U_{13}	U_{23}
I1	0.0290(2)	0.0266(2)	0.0492(2)	-0.0066(4)	-0.0028(4)	0.0016(1)
Se1	0.0226(3)	0.0226(3)	0.0226(3)	0	0	0
Zn1	0.0328(3)	0.0238(5)	0.0328(3)	0	0	0
Zn2	0.0244(7)	0.0244(7)	0.0244(7)	0.0001(8)	-0.0001(8)	0.0001(8)
Zn3	0.0328(14)	0.0328(14)	0.0328(14)	0.0017(17)	0.0017(17)	0.0017(17)
P1	0.22(6)	0.21(6)	0.18(4)	-0.04(4)	-0.15(5)	-0.01(4)
P2	0.31(7)	0.13(3)	0.09(1)	0.01(2)	-0.10(2)	0.02(2)
Se2	0.22(6)	0.22(6)	0.22(6)	0.08(3)	0.08(3)	-0.08(3)

Table 2-12. Selected interatomic distance [Å] and angle [°] for Zipse334 with Z = 1.

Atom	bond length (Å) / angle (°)
Se1 – Zn2 (× 4)	2.442(3)
Zn1 – I1 (× 4)	2.619(0)
Zn2 – I1 (× 3)	2.625(1)
Se1 – Zn2 – I1 (× 12)	109.02(6)
I1 – Zn1 – I1 (× 6) I1' – Zn1 – I1' (× 6)	106.64(1) 115.29(1)
Zn1 – I1 – Zn2 (× 6)	99.65(2)

2. 4. 3. ir/Raman Spectrum of Zipse334

According to results of X-ray measurements,

(i) the crystalline compound Zipse334 showed an analogue of clathrate system with respect to neutral framework as a cubic form and the unknown intercalated molecule(s) were embedded into octahedral hole of cubic lattice as a strongly disorder or strongly dislocalized form. Conclusively, the disordered molecule(s) could not be detected by modern tools of X-ray measurement.

(ii) comparing with other clathrate system, the cubic clathrate has a quite good advantage of investigating an/the isolated guest molecule(s), since the cubic environment provides an anisotropy for an/the isolated guest molecule(s). Therefore, it was expected that this unknown crystalline compound should show a property of regular solution owing to a relationship between the well separated column (neutral framework) as a solvent and the intercalated molecule(s) as a solute. By means of spectroscopy tool like ir/Raman, an/the isolated guest molecule act on a/the solute(s) in solution chemistry.

(iii) as a rough estimation, the vibrational characteristics of the ionic nature (Se-Zn-I bond) of host lattice and one of the covalent nature (P-Se bond) of the postulated guest molecule(s) should be quite distinguishable.

The measured solid state ir/Raman spectrum is as follows,

(i) The measured ir spectrum was almost impossible to analyze the peak tendency (see **Fig 2-15** above solid line). Instead of that the Raman scattering spectrum (see **Fig. 2-15** down) showed well arranged peaks and quite good approximation with reported data, especially with W. Bues, *et al.*[70] with respect to their solid state measurement of P_4Se_3 (the figures indicate the four A_1 modes of C_{3v} P_4Se_3) at high temperature ($300\,^oC$), but ir spectrum was far away from them (see **Fig 2-15** above dotted line). After peak assignment, however, the additional peaks could not be assigned by reported Raman scattering data of phosphorus selenide molecules.

(ii) the lattice frequencies were quite distinguishable compared with one of intercalated molecule(s), but still not identified, since the vibrational characteristics of structural unit (Se-Zn-I unit) has been never reported. In the point of qualitative views, the factor group analysis was suggested for the most intense peak at 100 cm^{-1} (not shown here and will be discussed in the section of ir/Raman spectroscopy) which is believed as one of lattice frequencies.

(iii) from the consideration about the peaks of Raman spectrum which was not assigned, the simplest cage like P_2Se_3 and phosphorus homo-cage P_7^{3-} were suggested for additional guest molecule(s) with less priority, but β-P_4Se_4 and more symmetric α-P_4Se_4 and fully saturated $P(III)_4Se_6$ were suggested.

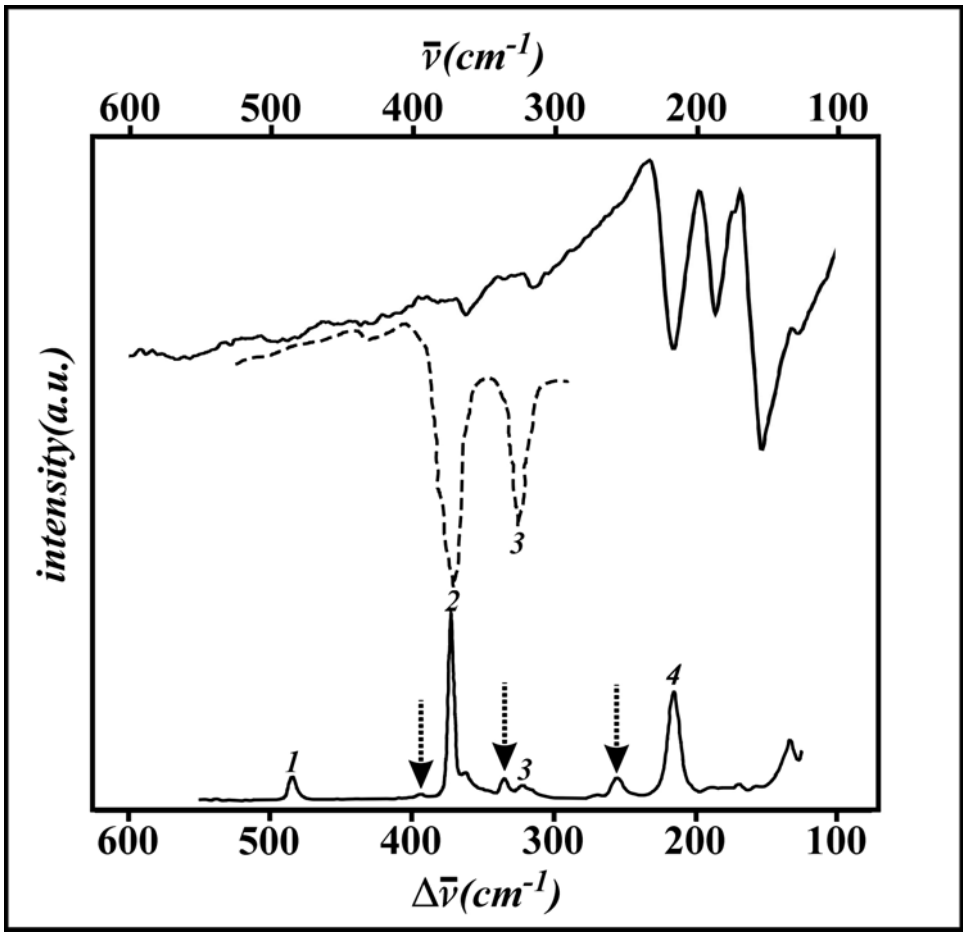

Fig. 2-15. FT-ir/Raman scattering spectrum of Zipse334 (the dotted line indicates a reported ir spectrum from P_4Se_3 molecular crystalline compound[70] and the arrows indicate that the peaks were not assigned and the figures are the symmetric normal modes of P_4Se_3 molecule).

2. 4. 4. ^{31}P MAS NMR Spectrum of Zipse334

The reason why we had to induce the additional spectroscopy for identification of intercalated molecule(s) is

(i) from former crystallographic consideration about Zipse334 system, the disordered chalcogenide molecule(s) were embedded into host framework, also observed no reasonable chemical bond between a part of host lattice and guest molecule by means of crystallographic tools. To add to this, the information about the orientation and composition of intercalated molecules(s) was lack.

(ii) the result of ir/Raman spectroscopy indicated only the rough composition of intercalated molecule(s), but still not clearly identified.

(iii) a powerful technique that avoids a structural anisotropy factors in binary phosphorus chalcogenide system P_xSe_{1-x}, i.e., solid-state NMR spectroscopy including fast magic-angle-spinning (MAS), cross polarization (CP) and recently two-dimensional technique has been well developed by our work group in cooperation with H. Eckert, *et al.*[12, 71, 72].

For identification of the intercalated molecule(s), P NMR spectroscopy was suggested and measured (see **Fig. 2-16**).

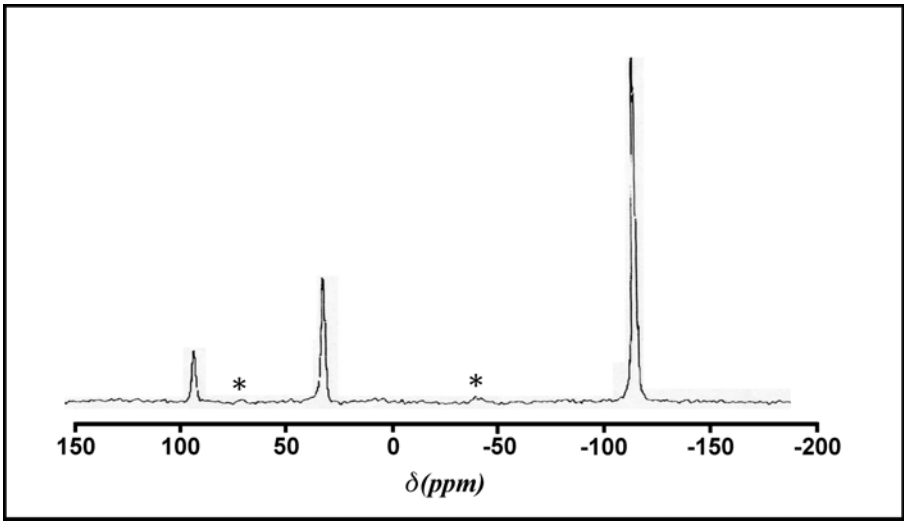

Fig. 2-16. ^{31}P MAS NMR spectrum of Zipse334 (* indicate spinning side bands).

From the spectrum, following aspects were discussed and developed,

(i) the chemical shifts of measured data showed a little bit different value from the values of already reported solid state P NMR data concerning globular binary phosphorus selenide compounds. Instead of that, under the concept of clathrate formation, a resemblance with data of solution state P NMR spectra was suggested.

(ii) the second and third peaks showed a good approximation with those of P_4Se_3, i.e., 1 : 3 with respect to those integral areas.

(iii) the first peak indicates a different kind of phosphorus molecule or one among the analogues is intercalated and not identified. Therefore, that the P_4Se_3 and P_4Se_x are alternatively occupied at the disordered lattice position was suggested (see **Fig. 2-8**).

(iv) for additional information about phosphorus selenide skeletal units for instance lower case than P_4Se_3 like P_2Se_3 or $[PSe_3]^{3-}$ and higher case than P_4Se_3 like P_4Se_4 or P_4Se_6, as a result from ir/Raman spectroscopy was suggested.

(v) the following phosphorus based selenides (see **Fig. 2-9**) are tentatively suggested, since those species are well characterized and reported from both solid state and solution chemistry with respect to a thermal stability.

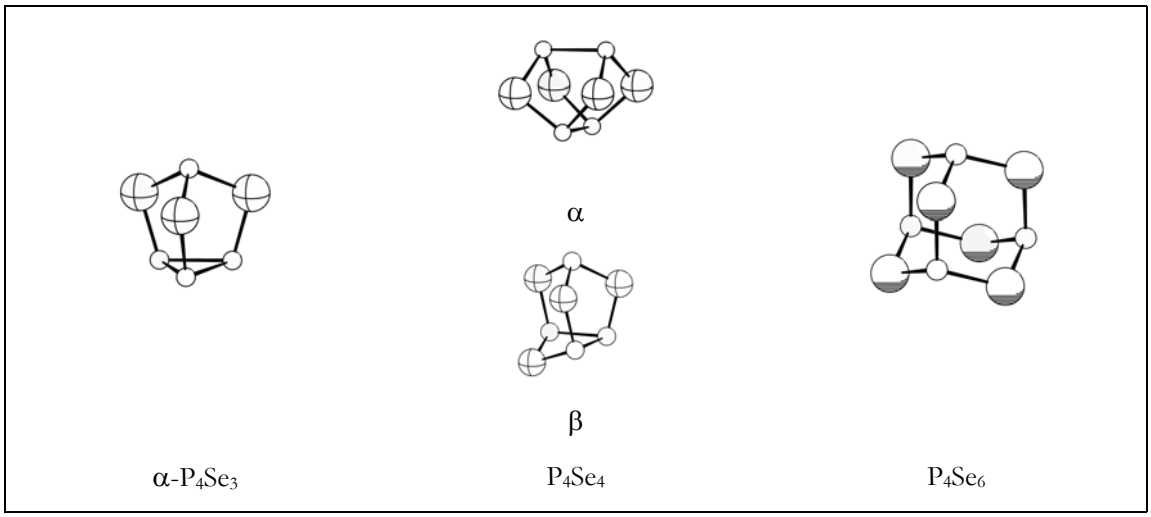

Fig. 2-17. Reported or suggested classes of globular phosphorus compounds for intercalated molecule in Zipse334 (where octant = P, cross and shadow = Se).

2. 5. Preparation for the host/guest Clathrate systems $[(ZnI_2)_6(ZnQ)]/[Pn_4Q_x]$(Pn = P, As ; Q = S, Se)

A successful interpretation about Zipse334 system by systematic approach with crystallographic tools, ir/Raman spectroscopy and ^{31}P MAS NMR spectroscopy indicates following points,

(i) the ZnI_2 based new crystalline compound showed an analogy to clathrate which was based on both the ternary Se – Zn – I host lattice and the binary P – Se cage guest molecule(s), Consequently,

(ii) it is convenient to divide the new crystalline compound into two separated parts for instance as a host part $[(ZnI_2)_6(ZnSe)]$ and a guest part $[P_4Se_3]$ or $[P_4Se_4]$.

(iii) the interpretation by various methods of characterization of Zipse334 should be reaffirmed by means of synthesis using an exact stoichiometry. For instance the crystalline compound which is Zn-Se based host lattice with P_4Se_3 cage guest molecule can be noticed as a composition ; ZnI_2 : Zn : P : Se = 6 : 1 : 4 : 4 and with P_4Se_4 cage guest molecule (for any conformers) ; ZnI_2 : Zn : P : Se = 6 : 1 : 4 : 5 .

(iv) As a point of synthetic views, the guest molecules should be separated into unique type by proper methods for instance controlling temperature or initial composition.

(v) The Se (*8a*) of host lattice can be substituted by S. In a parallel with this sense, the possibility of intercalation of guest molecules like stable P_4S_3, P_4S_4 and unstable Se richer or poorer case was suggested.

(vi) Also, some As based cage molecules like As_4Q_n (where Q = S and Se, n = 3 or 4) were reported as stable compounds which could be used as guest molecules.

All the syntheses were depicted as following **Fig. 2-18.** In all the syntheses, initially the modification of host lattice was limited on substitution of Wyckoff *8a* position with S and Se and the other positions with less priority, i.e., the substitutions of Zn (*24d* and *32e*) with Cd or Hg and the substitutions of I (*96h*) with Br and Cl were planned with less priority (the

Wyckoff symbols are based on the space group $F\bar{4}3c$), since the characteristic of formation of Zipse334 crystalline compound should be closely examined by fixing at least one reactant as a constant condition, i.e., in all syntheses the reactant ZnI_2 was fixed with varying pnictogens and chalcogens.

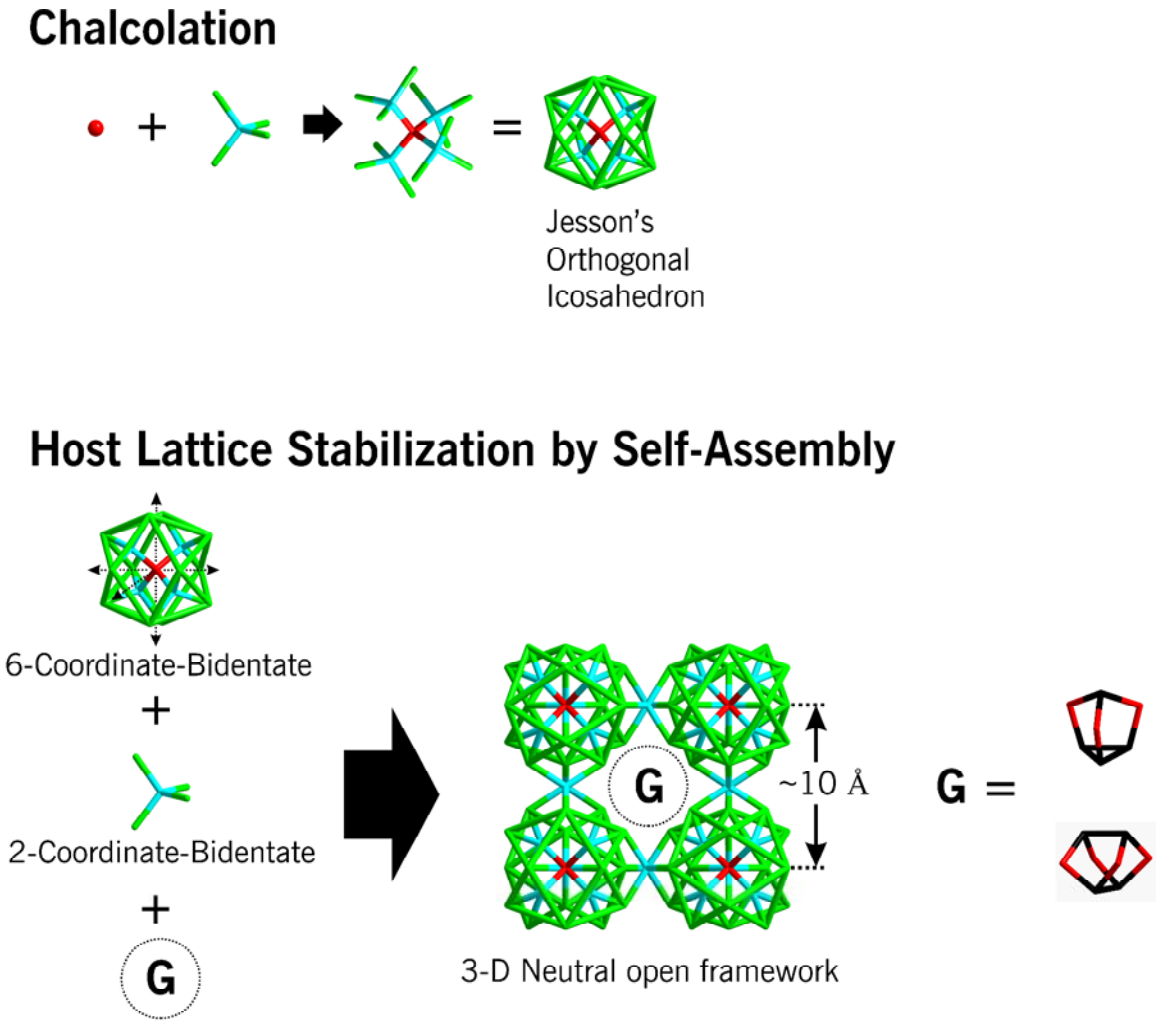

Fig. 2-18. The pictogram for preparation of host / guest clathrate $[(ZnI_2)_6(ZnQ)]/[Pn_4Q_x]$ (Pn = P, As ; Q = S, Se) system (Atoms : iodine green, zinc cyan, chalcogen red and pnictogen black).

For simplicity, summarizing this approach by means of thermodynamic factors, (1) the volume of reactor was fixed at a constant, (2) the reaction temperature (T_r) and the crystallization or aging temperature (T_c) were fixed at a constant, 650 ^oC and 400 ^oC, respectively, (3) total mole of reactants was fixed at around 4 *mmol*, and consequently (4) the partial pressures of reactants in reactor could be maintained at a constant due to the prior amount of ZnI_2. This approach has a very useful advantage for finding out the kinetic condition for a formation of clathrate analogue crystalline compounds, i.e., (5) only the remaining factor was the reaction time which was varied. The reasons why this approach adopted for all syntheses were

(i) the well investigated and reported cage molecules for guest molecules are very stable at the wide range of temperature for instance P_4S_3 is stable at ~ 1200 K (see **Fig. 2-7**) and P_4Se_3 at ~ 1000 K (see **Fig. 2-9** estimated),

(ii) we, however, had no knowledge about the thermodynamic properties of newly induced Se – Zn – I based host lattice. Also, the modification with S was quite comparable and questionable with the case of Se based host lattice.

(iii) finally, what is the sixth factor for governing the clathrate analogue formation ?

For [Zn-Se] based host lattice, all the crystal preparations were governed by the concept of stage 1 and 2 and T_r was fixed at 650 ^oC under the thermodynamic calculation and T_c at 400 ^oC, but the annealing periods for stage 2 were varied for optimization for instance [Zn-Se] based compounds for 1, 2 and 3 months and for [Zn-S] based host lattice for 2, 4 and 6 months, also [Zn-Se]/[As-Se] compounds for 4 months. For the name of compounds, Zizpse6141 which was targeted for P_4Se_0 (tetrahedral P_4), Zizpse6144 for P_4Se_3, Zizpse6145 for P_4Se_4, Zizps6144 for P_4S_3, Zizps6145 for P_4S_4 and Ziasse6144 for As_4Se_3 so on (see **Table 2-13**).

Table 2-13. The preparation of host / guest clathrate $[(ZnI_2)_6(ZnQ)]/[Pn_4Q_x]$(Pn = P, As ; Q = S, Se) system.

comp.	step.	composition of reactants (g)				total (g)	mmol.
		ZnI_2	Zn	P (As)	Se (S)		
[Zn-Se]/[P-Se] system							
Zipse334	1a step	0.7008	-	0.0680	0.2312	1.0000	7.3
Zizpse6141	1b step	0.7208	0.0246	0.0466	0.0297	0.8217	3.8
Zizpse6143	1b step	0.7208	0.0246	0.0466	0.0891	0.8811	3.8
Zizpse6144	1a step	0.8356	-	0.0463	0.1181	1.0000	3.7
	1b step	0.7208	0.0246	0.0466	0.1189	0.9109	3.8
	2 step	0.7208	0.0246	-	0.0297	0.7751	3.8
		-	-	0.1865	0.3566	0.5431	3.8
Zizpse6145	1b step	0.7208	0.0246	0.0466	0.1486	0.9406	3.8
Zizpse6147	1b step	0.7208	0.0246	0.0466	0.2080	1.0000	3.8
	1a step	0.7676	-	0.0426	0.1899	1.0000	3.4
[Zn-S]/[P-S] system							
Zizps6143	1b step	0.8223	0.0281	0.0532	0.0413	0.9449	4.3
Zizps6144	1b step	0.8223	0.0281	0.0532	0.0551	0.9587	4.3
Zizps6145	1b step	0.8223	0.0281	0.0532	0.0689	0.9725	4.3
[Zn-S]/[As-Se] system							
Zizasse6144	1b step	0.7377	0.0252	0.1154	0.1217	1.0000	3.9

After the aging period, in every one month term, the crystalline compounds were confirmed and grew up till ~ 5 × 5 × 3 mm (which was based on the calculated density of Zizpse6144; $d_{calc.} = 4.325 g/cm^3$ at room temperature. Consequently, the net weight of crystalline compound could be calculated to obtain ~ 0.3 g single crystal with the dimension of ~ 5 × 5 × 3 mm) with an eye shot and kept temperature, and the ampoules were cooled down to room temperature relatively fast (100 ^oC/hr) due to the minimization of impurity formation on surface of synthesized crystalline compounds. The following points were discussed,

(i) for the Zizpse6144 crystalline compound, three kinds of route were adopted and conclusively speaking, all the synthetic step provided same crystalline compounds with respect to those patterns of powder diffraction. The crystal growths,

however, were quite distinguishable for ~ 5 mm crystalline compound. The best case was 1b step. Even in case of 1b step, during the aging periods, the I_2 vapor was observed as a thinner color than the case of 1a step. The final sizes of crystalline compound by 1b step were similar with one by 1a step and the smallest one by 2 step.

1 step	a	$7ZnI_2$ (s) + 4P (s) + 4Se (s) → $[(ZnI_2)]_6(ZnSe)]/[P_4Se_3]$ (s) + I_2 (g)	
	b	$6ZnI_2$ (s) + Zn (s) + 4P (s) + 4Se (s) → $[(ZnI_2)]_6(ZnSe)]/[P_4Se_3]$ (s)	
2 step		$6ZnI_2$ (s) + Zn (s) + Se (s) →	$[(ZnI_2)]_6(ZnSe)]/[P_4Se_3]$ (s)
		4P (s) + 3Se (s) →	

(ii) from Zizpse6141 to Zizpse6147, the colors of final crystalline compound were quite distinguishable with an order of initial Se amount for instance Zizpse6147 was the darkest brown, and also the inner color of reactor during the reaction stage 1 (see **Fig 2-11**) showed the same tendency with above, which means that the initial stoichiometric amount of Se played the main role on the overall *red-ox* reaction and the guest formation with higher order chalcogenide.

(iii) Zizps6144 crystalline compound was prepared by the same condition with Zizpse6144 as a trial, i.e., $T_r = 650\ ^oC$ and $T_c = 400\ ^oC$ for reaction stage 1 and 2, respectively for 2 month. The calculated T_r from thermodynamic data was 273 ^oC (see **Table 2-4**). But the size of crystalline compound was ~ 1 mm. With this sense, Zizps6143 and Zizps6145 was relative long time aged for 6 months till ~ 5 mm of crystal growth at $T_c = 400\ ^oC$. These results are quite questionable with respect to a stability of S-Zn-I based host lattice including (1) thermal stability of host lattice itself and (2) relative stronger 3-dimensional hindrance of S-Zn-I unit than Se-Zn-I unit. Also, the geometric restrictions on corner-sharing octahedra owing to very close contact between neighboring octahedra was reported.

(iv) the crystalline compound Zizasse6144 was prepared by the same conditions as Zizpse6144 and Zizps6144, also as a trial, but the quality of crystalline compound

(~ 0.5 mm) was relatively bad with respect to the patterns of powder diffraction. Comparing the most intense peak of $F\bar{4}3c$ indexed crystalline compound with ZnI_2, the patterns indicated unreacted ZnI_2 as about 50 %.

2. 6. The abbreviation for the host/guest Clathrate systems $[(ZnI_2)_6(ZnQ)]/[Pn_4Q_x]$ (Pn = P, As ; Q = S, Se)

The following **Table 2-14A** and **2-14B** indicate the abbreviation of crystalline compounds which is better way to describe this clathrate compounds by means of a systematic way.

Table 2-14A. The abbreviation for crystalline compounds.

name of compounds	component ratio (initial composition of reactants)				character. methods	name of clathrate system	
	ZnI_2	Zn	P(As)	Se(S)		[Host]/[Guest]	space g.
Zizps6143	6	1	4	4	PD	$[(ZnI_2)_6(ZnS)]/[P_xS_y]$	$F\bar{4}3c$ (No.219)
Zizps6144	6	1	4	4	PD/IPDS iR/Raman NMR	$[(ZnI_2)_6(ZnS)]/[P_xSe_y]$	$F\bar{4}3c$ (No.219)
Zizps6145	6	1	4	4	PD	$[(ZnI_2)_6(ZnS)]/[P_xS_y]$	$F\bar{4}3c$ (No.219)
Zizpse6141	6	1	4	1	PD	$[(ZnI_2)_6(ZnSe)]/[P_xSe_y]$	$F\bar{4}3c$ (No.219)
Zizpse6143	6	1	4	3	PD	$[(ZnI_2)_6(ZnSe)]/[P_xSe_y]$	$F\bar{4}3c$ (No.219)
Zizpse6144	6	1	4	4	PD/IPDS iR/Raman NMR	$[(ZnI_2)_6(ZnSe)]/[\alpha\text{-}P_4Se_3]$	$F\bar{4}3c$ (No.219)
Zizpse6145	6	1	4	5	PD	$[(ZnI_2)_6(ZnSe)]/[P_xSe_y]$	$F\bar{4}3c$ (No.219)
Zipse344	3	0	3	4	PD/IPDS iR/Raman NMR	$[(ZnI_2)_6(ZnSe)]/[(\alpha\text{-}P_4Se_3) : (\alpha\text{-}P_4Se_4)] = 12 : 1$	$F\bar{4}3c$ (No.219)
Zizpse6147	6	1	4	7	PD iR/Raman NMR	$[(ZnI_2)_6(ZnSe)]/[(\alpha\text{-}P_4Se_3) : (\alpha\text{-}P_4Se_4)] = 6 : 2$	$F\bar{4}3c$ (No.219)
Zizasse6144	6	1	4	4	PD/IPDS	$[(ZnI_2)_6(ZnSe)]/[As_xSe_y]$	$F\bar{4}3c$ (No.219)

The names of compounds are based on the initial composition of reactants with atomic molar ratio (see from second row to fifth row in **Table 2-17A**) for synthesis of new crystalline compounds. In addition, the applied characterization methods (see the sixth row in **Table 2-17A**) for newly synthesized crystalline compounds indicated as a short form, for example 'PD' means the powder diffraction method, 'IPDS' means the single crystal measurement by STOE IPDS, 'ir/Raman' means the solid state ir/Raman spectroscopy and finally 'NMR' means the solid state ^{31}P NMR spectroscopy. All the tools for characterizations of newly synthesized crystalline compounds were closely related with each other.

As a result of characterization procedure, this crystal system composed of two different kinds of host lattices with respect to 'a crystal chemical isotypism' (S modification and Se modification of host lattice) and the conformers of Pn-Q cage molecules were statistically distributed into the octahedral hole of host lattice as a status of multiple occupancy. Therefore, after here the host lattices and guest chalcogenide molecules will be bracketed with general formula $[(ZnI_2)_6(ZnQ)]$-host lattice/$[\alpha$-$Pn_4Q_x]$-guest molecule (where α means a conformer of intercalated molecule, Pn = P and As, Q = S and Se and x = 3 and 4), for example, $[(ZnI_2)_6(ZnS)]$ and $[(ZnI_2)_6(ZnSe)]$, after here [Zn-S] and [Zn-Se] host lattices, or respectively. The whole system is able to be represented by a short form; clathrate [Zn-Q]/[Pn-Q] system like following description for the convenience of structural comparison with other crystalline compounds (see **Table 2-14B**).

Table 2-14B. The short form of abbreviation for this clathrate system.

<table>
<tr><td></td><td colspan="2">identified compounds</td><td colspan="2">short forms</td><td></td><td></td></tr>
<tr><td>host</td><td colspan="2">$[(ZnI_2)_6(ZnS)]$
$[(ZnI_2)_6(ZnSe)]$</td><td colspan="2">[Zn-Se]
[Zn-S]</td><td>[Zn-Q]</td><td rowspan="2">[Zn-Q]/[Pn-Q]</td></tr>
<tr><td>guest</td><td>α-P_4S_x
α-As_4S_x</td><td>α-P_4Se_x
α-As_4Se_x</td><td>[P-S]
[As-S]</td><td>[P-Se]
[As-Se]</td><td>[Pn-Q]</td></tr>
</table>

2. 7. A formalism of clathrate $[(ZnI_2)_6(ZnQ)]/[Pn_4Q_x]$ (Pn = P, As ; Q = S, Se) system

The reasons why a formalism of clathrate $[(ZnI_2)_6(ZnQ)]/[Pn_4Q_x]$ (Pn = P, As ; Q = S, Se) system should be induced in this section are as follows,

(i) in initial designing of structural composition for new crystalline compounds, the analogue of boracite family was aimed to obtain from the consideration of ICSD and CSD,

(ii) the reported structural data from well characterized crystalline compounds allow a systematic approach to solution for structural interpretation of newly synthesized crystalline compound,

(iii) the synthetic utilization or variation of newly synthesized crystalline compound is able to be supported by the comparison of structural analogues.

(iv) regarding 'a formalism of newly synthesized clathrate compounds', the definitions for isotypism and homeotypism were quoted from 'Inorganic structural chemistry' by U. Müller[73].

Therefore, the structural analogues of clathrate [Zn-Q]/[Pn-Q] system were selected (1) mainly by a resemblance of space group including sub- and super-group relationship, i.e., with respect to the isotypism including a homeotypic relationship, and (2) by a resemblance of functionality of structural units. As a result, the selected crystal structures were summarized and compared as following **Table 2-15**, **2-16** and **Fig. 2-19**,

Table 2-15. The selected analogues of clathrate [Zn-Se]/[Pn-Se] system.

	comp.	structure formula	space group	lattice constant (a/Å)	ref.
structural analogues	Zizpse6144	$[(ZnI_2)_6(ZnSe)]/[P_4Se_3]$	$F\bar{4}3c$, Z = 8	19.5	this work
	Alkaliiodoindate	$KInI_4$	$F\bar{4}3c$, Z = 24	19.9	74
	Werner complex	$[Cu_8Sb_3S_{13}]/[Fe(NH_3)_6]$	$F\bar{4}3c$, Z = 8	17.8	75
	Boracite	$Mg_3B_7O_{13}Cl$	$F\bar{4}3c$, Z = 8	12.0	42
functional analogues	Polymetal halides	Ge_6Cl_{16}	$F\bar{4}3c$, Z = 8	17.4	76
	Sodalite	$Zn_8Se_2(BO_2)_{12}$	$I\bar{4}3m$, Z = 1	7.7	77

Table 2-16. The comparison of atomic coordinates of selected clathrate analogues.

clathrate $[(ZnI_2)_6(ZnSe)]/[P_4Se_3]$ $F\bar{4}3c$ (Z = 8)						boracite $Mg_3B_7O_{13}Cl$ $F\bar{4}3c$ (Z = 8)						alkaliiodoindate $KInI_4$ $F\bar{4}3c$ (Z = 24)					
at.	*W.*	*x*	*y*	*z*	*oc.*	*at.*	*W.*	*x*	*y*	*z*	*oc.*	*at.*	*W.*	*x*	*y*	*z*	*oc.*
host part																	
Se1	*8a*	0	0	0	1	O1	*8a*	0	0	0	1	K1	*8a*	0	0	0	1
Zn1	*24d*	0	¼	0	1	B1	*24d*	0	¼	0	1	In1	*24d*	0	¼	0	1
Zn2	*32e*	~ 0.1	~ -0.1	~ 0.1	0.5	B2	*32e*	~ 0.1	~ 0.1	~ 0.1	1	-					
Zn3	*32e*	~ 0.1	~ 0.1	~ 0.1	0.5												
I1	*96h*	0.1	0.2	~ 0	1	O2	*96h*	0.1	0.2	~ 0	1	I1	*96h*	0.1	0.2	~ 0	1
guest part																	
P1 P2 Se2	~ *8b*	~ ¼	~ ¼	~ ¼	-	Cl1	*8b*	¼	¼	¼	1	K2	32e	~ 0.3	~ 0.3	~ 0.3	0.5
						M1	*24c*	¼	0	¼	1						

sodalite $Zn_8Se_2(BO_2)_{12}$ $I\bar{4}3m$ (Z = 1)					
at.	*W.*	*x*	*y*	*z*	*Oc.*
Se1	*2a*	0	0	0	1
B1	*12d*	¼	½	0	1
Zn1	*8c*	~ 0.2	~ 0.2	~ 0.2	1
O1	*24g*	~ 0.1	~ 0.1	~ 0.4	1

Where at. = atom, W = Wyckoff symbol and oc. = occupancy, also *x*, *y* and *z* are *x*/*a*, *y*/*b* and *z*/*c*, respectively.

The following **Fig. 2-19** shows the section of host /guest [Zn-Q]/[Pn-Q] (Pn = P, As ; Q = S, Se) clathrate system, space group $F\bar{4}3c$ and compared with one of boracite, alkaliiodoindate and sodalite. In addition, the guest molecule was removed for the purpose of clear views.

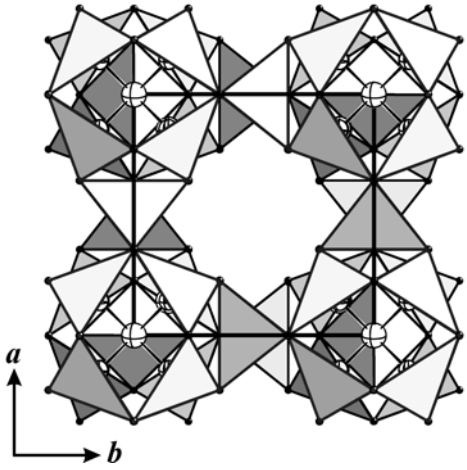

clathrate

$[(ZnI_2)_6(ZnQ)]/[Pn_4Q_x]$

cross = Q and tetrahedra = $QZnI_3$ and ZnI_4

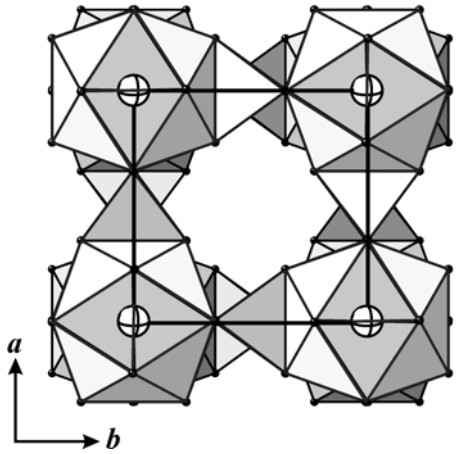

alkaliiodoindate

$KInI_4$

cross = K and tetrahedra = InI_4

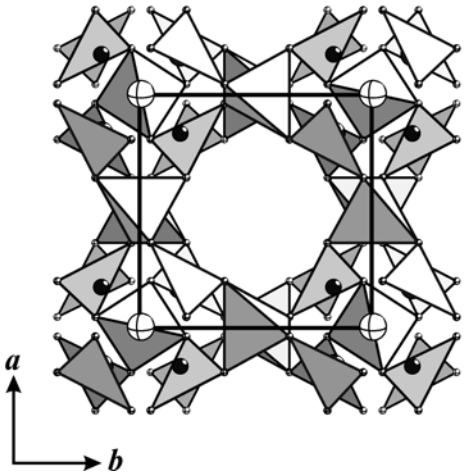

boracite

$Mg_3B_7O_{13}X$

Cross = O and tetrahedra = BO_3 and BO_4

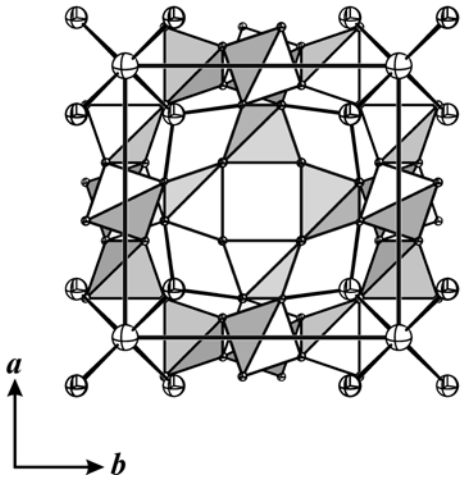

sodalite

$Zn_8Se_2(BO_2)_{12}$

Cross = Se, octant = Zn and tetrahedra = BO_4

Fig. 2-19. The comparison of crystal sections of this clathrate with boracite, sodalite and alkaliiodoindate (for clear views guest molecule in clathrate, Mg and X in boracite, $SeZn_4$ in sodalite and K2 in alkaliiodoindate were removed).

- Alkaliiodoindate type

As an example of molten salt method, the alkaliiodoindates which can be expressed with general formula M(I)In(III)I_4 (where M = Li, K, Rb and Cs) have been obtained form mixtures of the binary components by slow cooling by melts. The $LiInI_4$ is isotypic with $LiAlCl_4$, $CsInI_4$ with $CsTlI_4$ and both have a monoclinic form ($P2_1/c$ with Z = 4). In addition, $RbInI_4$ crystallized with the β-$GaBr_2$ type, which has a trigonal form ($R3c$ with Z =18). The structural interpretation concerning $LiInI_4$, $CsInI_4$ and $RbInI_4$ was discussed in elsewhere[74] and will not be focused here. Especially, $KInI_4$ which belongs to the $MTl(III)X_4 \cdot 2H_2O$ [M = NH_4, K and Rb ; X = Br and I ; as a host / guest relationship - KTl_3Br_{12} / $K_2(H_2O)_6$, $RbTl_3Br_{12}$ / $Rb_2(H_2O)_6$ and $(NH_4)Tl_3Br_{12}$ / $(NH_4)_2(H_2O)_6$][78] type of structure has a cubic form [$F\bar{4}3c$ with Z = 8, a = 19.91(1)] will be focused for comparison of formalism with [Zn-Q]/[Pn-Q] clathrate system, since in all structures of alkaliiodoindates, almost regular tetrahedra $[InI_4]^-$ occurred and the coordination numbers of alkali cations covered the wide range from 6 (Li^+) via 9 (Rb^+) and 11 (Cs^+) to 12 (K^+) in $KInI_4$ crystalline compound. In addition, regarding the crystalline structure of a host / guest relationship - KTl_3Br_{12} / $K_2(H_2O)_6$, two different atomic models have been reported, centrosymmetric $Fm\bar{3}c$ [78(a)] and non-centrosymmetric $F\bar{4}3c$ [78(b)] due to an ambiguous location of solvent water molecules in cavity structure. This ambiguity in atomic model provides a comprehensive concept for preparation of [Zn-Q]/[Pn-Q] clathrate crystalline compounds with respect to a solvent incorporation into the quasi-octahedral cavity structure during the self-assembly process. According to a structural interpretation about cubic $KInI_4$ crystalline compound,

(i) the anionic structural unit can be divided into a huge icosahedron [K1 (*8a*) – I (*96h*)$_{12}$] (after here anionic unit 'A') with 3-D orthogonal stack and tetrahedron sharing an edge with the huge icosahedra [In (*24d*) – I (*96h*)$_4$] (after here anionic unit 'B') (see **Fig. 2-20**). Consequently,

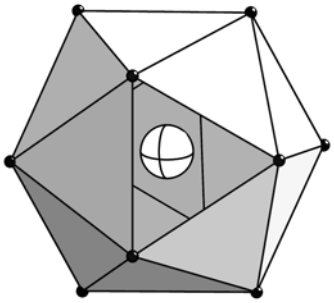

KI_{12} (= A)

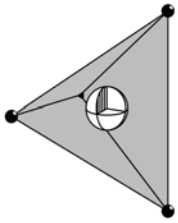

InI_4 (=B)

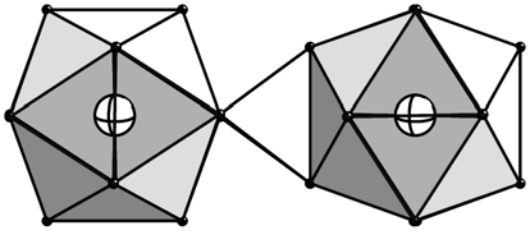

A-B-A' unit in $KInI_4$

Fig. 2-20. The schematic description of A-B-A' unit in $KInI_4$ (A and A' are orthogonal).

(ii) the composition of $KInI_4$ can be expressed by the complex term of $[K1(InI_4)_3]^{2-}$, which has a 'self-stabilized 3-D framework' like the ReO_3 structure type, i.e, as a 3-D AB_3 type structure.

Comparing the structural interpretation of $KInI_4$ with $[(ZnI_2)_6(ZnQ)]/[Pn_4Q_3]$, the anionic $[K1(InI_4)_3]^{2-}$ is able to be corresponded with $[(Q\text{-}Zn_4)(ZnI_4)_3]$, in more detail, K1 with (Q-Zn_4) and (InI_4) with (ZnI_4). In addition, a huge icosahedron [K1 (*8a*) – I (*96h*)$_{12}$] (= A) in $KInI_4$ corresponds with [Q (*8a*) – Zn (*32e*) – I (*96h*)$_{12}$] (= A) in $[(ZnI_2)_6(ZnQ)]/[Pn_4Q_3]$ and a

edge sharing tetrahedron [InI_4] in $KInI_4$ with a tetrahedron [ZnI_4] in [$(ZnI_2)_6(ZnQ)$]/[Pn_4Q_3]. A huge icosahedron by a 12 coordinated K cation showed 3-D orthogonal stack, which is believed a main reason for indexing $KInI_4$ crystal structure into a tetrahedral space group $F\bar{4}3c$ (T_d^5).

The location for K2 (*32e*) in a huge cavity (the crystallographic center of cavity: *8b*) was statistically half occupied and showed double thermal displacement parameter compared with K1 (*8a*). The reported shortest K2 – K2 distance was 3.82(1) Å, which is comparable with the measured thermal displacement parameter and occupancy factor of Se2, and the size of intercalated molecule(s) in [$(ZnI_2)_6(ZnQ)$]/[Pn_4Q_3] clathrate system.

Conclusively speaking,

(i) a series of newly synthesized [$(ZnI_2)_6(ZnQ)$]/[Pn_4Q_3] crystalline compounds showed an homeotypic structure with one of the alkaliiodoindates; $KInI_4$. Therefore, the structure of $KInI_4$ is able to be categorized into one of clathrate family as a host/guest relationship [K-I_{12}-In]/[K_2], with Z = 24 for actual composition.

Table 2-17. The comparison of structural units of clathrate [$(ZnI_2)_6(ZnQ)$]/[Pn_4Q_3] with [K-I_{12}-In]/[K_2].

		alkaiiodoindate [K-I_{12}-In_3]/[K_2]	clathrate [$(ZnI_2)_6(ZnQ)$]/[Pn_4Q_3]
host	icosahedron (= A)	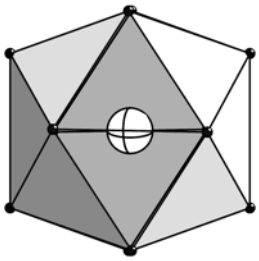 KI_{12}	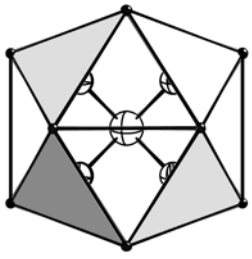 Q-Zn_4-I_{12}
	tetrahedron (= B)	InI_4	ZnI_4
guest		K_2	Pn_4Q_3

(ii) the anionic structural units of icosahedra and tetrahedra which composed the host and disordered K_2 being the guest in alkaliiodoindate $KInI_4$ correspond with host and guest in clathrate $[(ZnI_2)_6(ZnQ)]/[Pn_4Q_3]$ as shown in **Table 2-17**.

(iii) the tetrahedral Q-Zn_4 unit in $[(ZnI_2)_6(ZnQ)]/[Pn_4Q_3]$ showed a similar size (distance Q-I : 8.2 Å with distance K-I) with 12 coordinated K^+ in $[K\text{-}I_{12}\text{-}In_3]/[K_2]$, which might be utilized as a synthetic modification.

(iv) according to structural interpretation of $KInI_4$ with respect to 3-D self stabilized framework roughly like ReO_3 structure type, the clathrate $[(ZnI_2)_6(ZnQ)]/ [Pn_4Q_3]$ should be interpreted as a AB_3 type host / guest $\{[Q - Zn_4 - I_{12} (= A)] - [Zn (= B)]_3\}/[Pn_4Q_3]$ relationship which is shown in **Fig. 2-21**.

Therefore, the structural unit A of (b) can be regarded as a 6-coordination-bifuctional (bi-dentate) synthon with corner sharing octahedron, the unit B as a 2-coordiantion bi-functional (bi-dentate) synthon with edge sharing tetrahedron and the intercalated molecule (Pn_4Q_3). An orthogonality of entire host lattice, A and A', can be satisfied by a bridging tetrahedron.

(v) comparing the thermal displacement parameters of K1 (*8a*) and K2 (*32e*), host part and guest part in $KInI_4$ crystalline compound, respectively with Se (*8a*) and Se (*32e*) in Zipse334 crystalline compound, the results are as following **Table 2-18**. The disordered atom position in both crystalline compounds showed relative high value of displacement parameters compared with one in the host lattice. The atom distance of guest molecule imposes a relationship between the size of intercalated molecule and the lattice constant. This relationship will be discussed in more detailed in followed chapters.

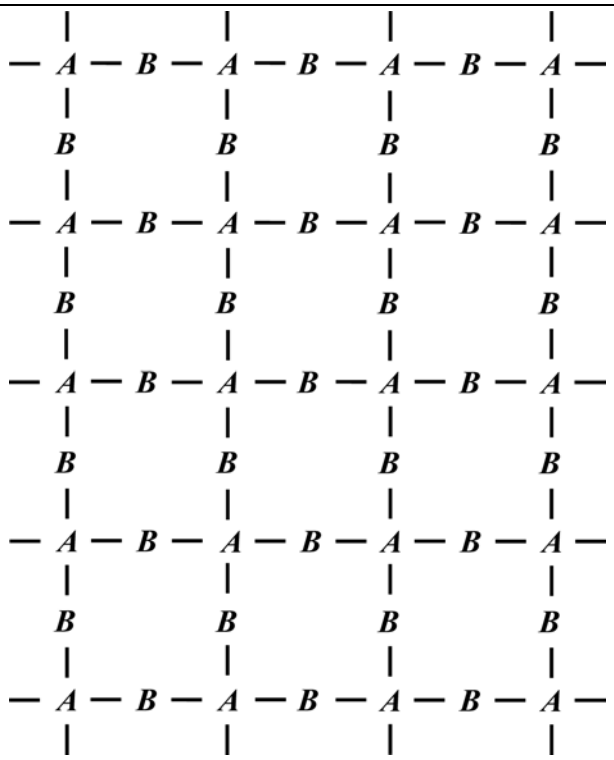

(a) 2-D AB_2 structure type

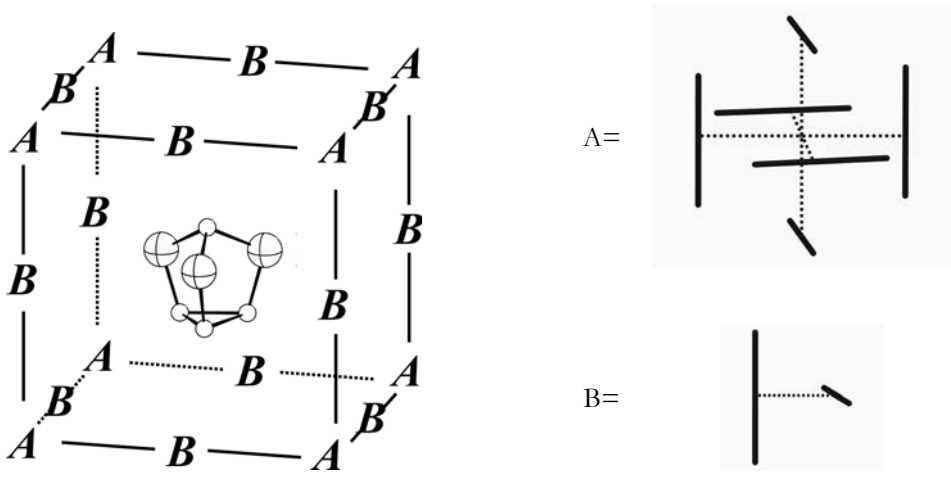

(b) $[(ZnI_2)_6(ZnQ)]/[Pn_4Q_3]$ represents as $\{[Q\text{-}Zn_4\text{-}I_{12}\ (=A)]\text{-}[Zn\ (=B)]_3\}_{oct.}/[Pn_4Q_3]_{oct.}$

Fig. 2-21. The schematic description of 3-D AB_3 type crystalline structure.

Table 2-18. The direct comparison of thermal parameters of K1 and K2 in $KInI_4$ with Se1 and Se2 in Zipse334.

alkaiiodoindate [K-I_{12}-In_3]/[K_2] a ~ 19.9 Å							clathrate Zipse334 a ~ 19.5 Å						
at.	W	oc.	*x*	*y*	*z*	$U_{eq.}$	at.	W	oc.	*x*	*y*	*z*	$U_{eq.}$
host							host						
K1	*8a*	1.	0	0	0	0.14	Se1	*8a*	1.	0	0	0	0.02
guest							guest						
K2	*32e*	0.5	0.3	0.3	-0.3	0.27	Se2	*32e*	0.18	0.2	0.2	-0.2	0.22
K2-K2 distance			~ 3.8 Å				Se2-Se2 distance			~ 3.2 Å			

Where at. = atom, W = Wyckoff symbol and oc. = occupancy, also *x*, *y* and *z* are *x*/*a*, *y*/*b* and *z*/*c*, respectively and $U_{eq.}$(the isotropic displacement parameter) in $Å^2$.

- Boracite type

Both naturally-occurring and synthetic homeotypes of boracites are well known. Synthetic boracites $M_3B_7O_{13}X$ (M = Mg, Cr, Mn, Fe, Co, Ni, Cu, Zn, or Cd ; X = F, Cl, Br, or I) form a large crystal family with more than 20 isomorphous compounds[42]. In some cases of synthetic boracites, X can be OH, S, Se, or Te, and M mono-valent Li. The chemical vapor transport method is currently used technique for the synthesis of boracites in single crystal form[79, 80] and permits the preparation of a large number of boracites. And recently the method has been improved by using N_2 protecting atmosphere instead of H_2 to prepare $M_3B_7O_{13}Cl$ (M = Fe, Co and Ni) boracite[81]. Also recently, $M_3(BO_3)F_3$ (M = Fe, Co, Ni) was prepared by using a hydrothermal synthesis[82]. And using rare earth metal for instance Eu^{2+} instead of first period *d*-block elements, needle-like single crystal $Eu_2B_5O_9Br$ which is iso-structural with Ca-boracite analogues was obtained from raw materials for instance EuB_2O_4, $EuBr_2$ and B_2O_3 by using metal halide flux method[41]. The structure consists of a 3-D infinite $[B_5O_9]$ network, in which B_5O_{12} group of three BO_4 tetrahedra and two BO_3 triangles are linked together by sharing vertex oxygen.

In a parallel with this sense, recently $Cr_3Si_2O_7 \cdot {}^1/_4MX$ (MX = NaCl, NaBr, KCl, KBr) [$I4/mmm$ (No. 139), $a \sim 10.3$ and $c \sim 12.97$ Å with Z = 8][83] cage structures as analogues of boracites $Cr_3B_7O_{13}X$ (X = Cl, Br and I) were built from $[Cr^{II}O_4]$ and $[Si_2O_7]$ anion units which were successive series of their halide disilicates $Cr_4(Si_2O_7)X_2$ (X = Cl and Br)[84]. They urged that the framework consists of two crystallographically independent Cr^{II} in square planar oxygen coordination. Three of those squares form a bent trimer $[Cr_3O_4O_{4/2}]$. Four trimers are connected through vertices forming a $[Cr_{12}O_{24}]$ cage wherein the halide ion is sited. By the linking of individual $[Cr_{12}O_{24}]$ units, disilicate groups form a second type of cage which is occupied by Na^+ or K^+. The disilicate groups are in eclipsed conformation with a bridging angle (Si-O1-Si) = 125°. Following **Table 2-19** indicates the potentially important metal halide boracites.

Table 2-19. The reported metal halide boracites (metal cations are removed for the purpose of clear views).

compound	space group	unit cell dimensions (Å)	Z	crystal section	ref.
$Cu_3B_7O_{13}I$ $Mg_3B_7O_{13}Cl$ $Mn_3B_7O_{13}Br$	F-*43c* (no.219)	a = 12.020(0) a = 12.100(0) a = 12.310(0)	8	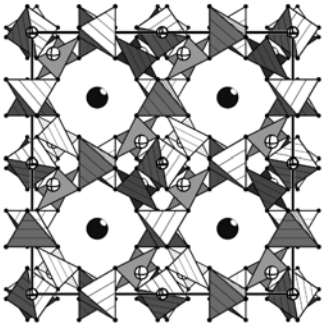	42
$Eu_2B_5O_9Br$	P*nn2* (no. 34)	a = 11.503(3) b = 11.382(3) c = 6.484(2)	4	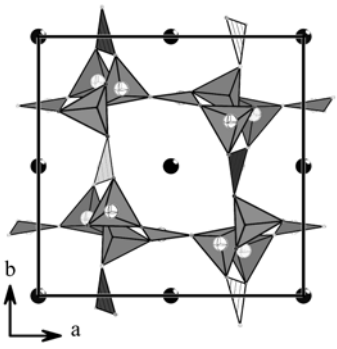	41
$Cr_3Si_2O_7$ $\cdot{}^1/_4MX$ (MX = NaCl, NaBr, KCl, KBr)	I*4/mmm* (no. 139)	a ~ 10.3 c ~ 12.97	8	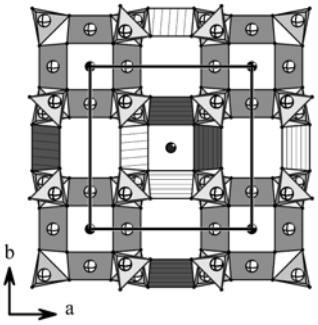	83

B_7O_{13} unit in $Mg_6B_{14}O_{26}Cl_2$ is a quite similar with an umbrella form and O1 locates on the special position *8a* in space group $F\bar{4}3c$.

According to the structural interpretation of boracite,

(i) boracites of general chemical composition $M_3B_7O_{13}X$ (here after M-X, where M stands for a bivalent metal ion and X for a halide ion) tend to undergo first order structural phase transitions from a high-temperature cubic structure (point group $\bar{4}3m$, non-centrosymmetric space group $F\bar{4}3c$ to non-cubic low-temperature structure ($mm2, m, 3m, \bar{4}2m$). In order to examine the structural resemblance with cubic clathrate, structural data of cubic boracites are required (see **Table 2-18**, **2-19** and **Fig. 2-19**).

(ii) the anionic structural unit was also able to divide into icosahedral form ; O1 (*8a*) – B2 (*32e*) – O2 (*96h*) ; B_4O_{13} (= A), which is constructed by four BO_3 planar polyhedra around O1 (*8a*) atom, and B1 (*24d*) – O2 $(96h)_4$ tetrahedra ; BO_4 (= B). The unit A corresponds with Q1 (*8a*) – Zn2, 3 $(32e)_4$ – I1 $(96h)_{12}$ (= A) with manner of half occupation of Zn2 and Zn3 and the unit B with Zn (*24d*) – I $(96h)_4$ in clathrate [Zn-Q]/[Pn-Q] system (see **Fig. 2-22**).

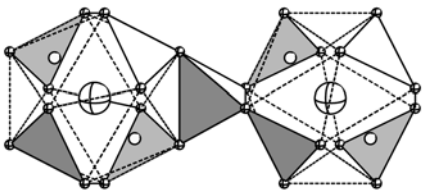

A-B-A' unit in boracite $Mg_3B_7O_{13}Cl$

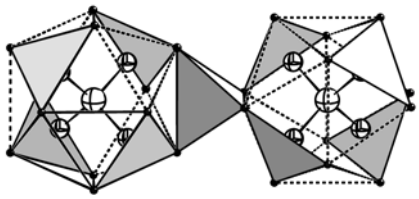

A-B-A' unit in clathrate [Zn-Q]/[Pn-Q]

Fig. 2-22. The comparison of A-B-A' unit of boracite with clathrate (atoms: for boracites, cross = O and open = B and for clathrate cross = Q, octant = Zn and closed = iodine).

(iii) with respect to guest position (~ *8b*), the chemical environment of metal and halide ions which are occupied as an alternative manner in the octahedral hole of cubic boracites lattice is shown in **Fig. 2-23**.

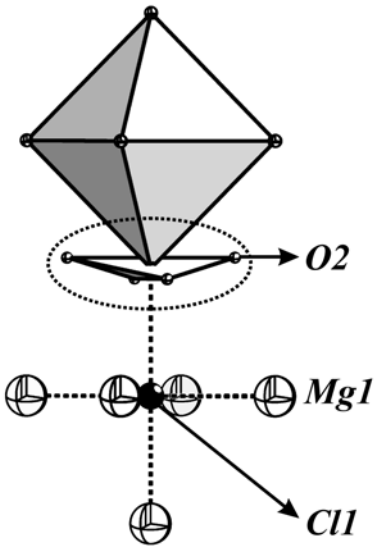

Fig. 2-23. Environment of the metal ions in cubic boracite (an ellipse indicates four nearby oxygen atoms).

The metal atoms are surrounded by four nearby oxygen atoms (O2) which are nearby coplanar and two more distant halogen atoms located on an axis perpendicular to the ideal metal-O2 plane.

(iv) So far the cubic phase has been characterized for boracites with Mg, Cr, Fe, Co, Ni, and Zn as the M^{2+} ion. Except for Mg^{2+} and Zn^{2+}, all these ions may present a Jahn-Teller effect, either in octahedral or in tetrahedral coordination, which may make the understanding of the deformation difficult. The Jahn-Teller *per se*, however, does not predict which type of distortion will take place other than the center of symmetry will remain.

Conclusively speaking,

(i) a series of newly synthesized $[(ZnI_2)_6(ZnQ)]/[Pn_4Q_3]$ showed an isotypic structure with one of the boracites ; $MgB_7O_{13}Cl$. Therefore, the structure of $MgB_7O_{13}Cl$ is

able to be categorized into one of clathrate family as a host/guest relationship [O-B_4-O_{12} (= A) - BO_4 (= B)]/[Cl].

(ii) the anionic structural units of icosahedra and tetrahedra composing of host and disordered Mg/Cl composing of guest in boracite $MgB_7O_{13}Cl$ correspond with host and guest in clathrate $[(ZnI_2)_6(ZnQ)]/[Pn_4Q_3]$ as following **Table 2-20**.

Table 2-20. The comparison of structural units of clathrate $[(ZnI_2)_6(ZnQ)]/[Pn_4Q_3]$ with $MgB_7O_{13}Cl$.

		boracites $MgB_7O_{13}Cl$	clathrate $[(ZnI_2)_6(ZnQ)]/[Pn_4Q_3]$
host	icosahedron (= A)	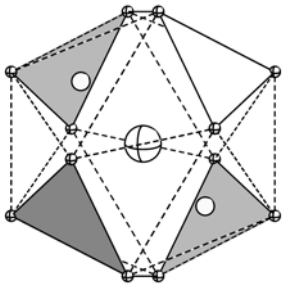 B_4O_{13}	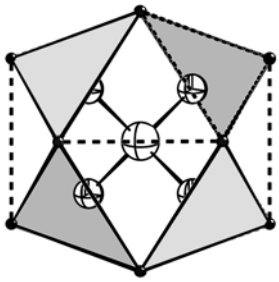 Q-Zn_4-I_{12}
	tetrahedron (= B)	BO_4	ZnI_4
guest		Cl	Pn_4Q_3

(iii) the intercalation of halide ions into the octahedral hole of boracite cubic lattice directly depends on the nature of metal atom, i.e., Jahn-Teller effect.

- Sodalite type

In the $I\bar{4}3m$ (no. 217) atomic model of sodalite; the general chemical composition $M_8T_2(BO_2)_{12}$ [Both naturally-occurring and synthetic isotypes are known for a myriad of compositions[85] (M = Li, Na, K, Ag, Ca, Sr, Zn, Cd, etc.; X = Br, Cl, OH, P, As, O, S, Se, Te, SO_4, WO_4, etc.; T = Be, B, Al, Ga, Si, Ge, etc.)]. Synthetically, a starting material of stoichiometry the intermediate ZnB_2O_4 was able to be prepared from ZnO and boric acid thermally-controlled, consequently the hydrothermal method using the intermediate and the bulk ZnSe can be synthesized for obtaining sodalite $Zn_8Se_2(BO_2)_{12}$ crystalline compound[77]. The topological details of general formula $M_8X_2(TO_2)_{12}$ sodalite structure are fully described elsewhere[86], not will be discussed here due to those complexity.

According to the structural interpretation about sodalite $Zn_8Se_2(BO_2)_{12}$ crystalline compound,

(i) there are four distinct sites ; one tetrahedral framework boron atom, one 'framework' oxygen atom, one tetrahedral (three oxygen atom neighbors + one extra-framework anion) guest cation (M), and one tetrahedral (four guest-cation neighbors) guest anion site (X). Boron occupies the (¼, ½, 0) special positions (crystallographic site symmetry ($4\,..$), oxygen (x, x, z) with $x \approx 0.15$ and $z \approx 0.43$ (symmetry $..m$), M (x, x, x) with $x \approx 0.17$ (symmetry $.3m$), and X (0, 0, 0) (symmetry $43m$).

(ii) the sodalite structure consists of a 3-dimensinal array of face-sharing B_{24} cuboctahedral 'cages' (see **Fig. 2-25** left) supported by intracage tetrahedra (where $SeZn_4$), a schematic of which is shown in **Fig. 2-25**. The general composition of the cubic sodalite unit cell is $M_8X_2[TO_2]_{12}$. The T (where T is boron) atoms are represented by vertices of the cuboctahedral cages and are connected *via* bridging oxygens which are not shown. The central anion X is represented by the large crossed circle at the centers of cages, surrounded by four M cations in a tetrahedral arrangement; the cations are directed toward alternating 6-ring faces.

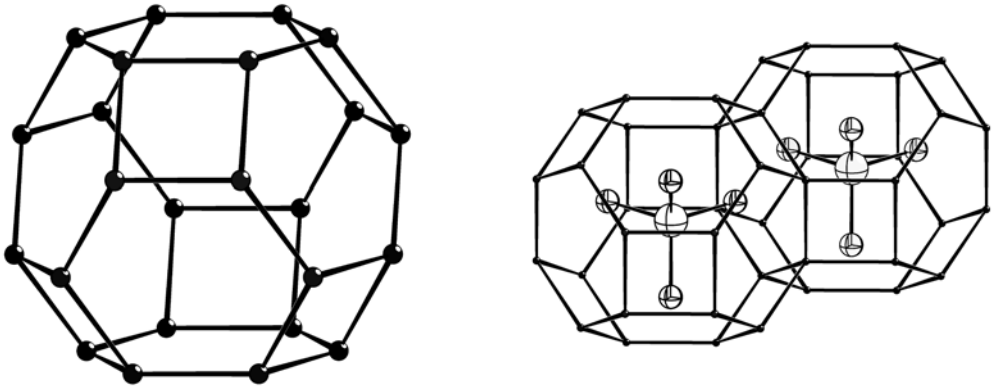

B_{24} cubocahedral cage edge-shared cages

Fig. 2-24. A schematic diagram[77] of the sodalite structure with composition $M_8X_2[TO_2]_{12}$.

(iii) the tetrahedral atoms, T (where TO_4 is BO_4), linked by bridging oxygen atoms form the anionic framework that encloses charge-balancing M_4X tetrahedra (where M_4X is Zn_4Se).

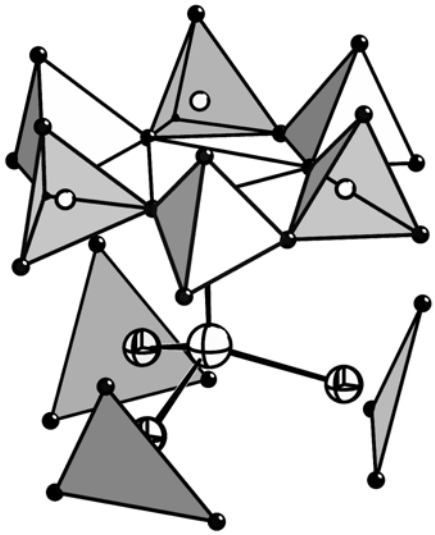

Fig. 2-25. The environment of Se in sodalite $Zn_8Se_2[BO_2]_{12}$ (Atoms: cross = Se, Octant = Zn, small black circle = O and small open circle = B).

(iv) as a result, the borate sodalite framework has a net charge of -6 which is compensated by a $[Zn_4Se]^{6+}$ tetrahedron inside each cage. Substitution of isovalent GaP for ZnSe is possible due to the size similarities of the atoms ; the covalent radii of Ga, Zn, P, and Se are 1.26, 1.25, 1.06, and 1.16 Å, respectively

Conclusively speaking,

(i) the sodalite $Zn_8Se_2[BO_2]_{12}$ crystallizes in the body-centered cubic space group $I\bar{4}3m$, characteristic of sodalite with one type of framework tetrahedral atom, which is comparable with clathrate [Zn-Q]/[Pn-Q] system with respect to a functionality of Se-Zn_4 cationic structure.

(ii) the long-range ordered Se-Zn_4 structural unit in sodalite, in which suggested as +6 cation, exactly corresponds with Se-Zn_4 unit in clathrate.

(iii) the truncated octahedron in soldalite where B_{24} cage showed hexagon the face sharing with adjacent cells is comparable with the cuboctahedron in boracite where B_{12} cage and additional boron atoms can be described as just the idealized (3,4)-connected net. The basic unit consists of an octahedron of 4-connected vertices (B) with 3-connected vertices (A) centering four of the octahedron faces to form an A_4B_6 cluster. In contrast, as well as the large holes at the centers of the snub cube (filled by Na in $NaZn_{13}$) with symmetry 432, there are holes surrounded by 12 equidistant spheres forming almost regular icosahedra. A snub cubes sharing triangular faces with eight icosahedra in $NaZn_{13}$ is closely comparable with snub cube I_{24} in clathrate [Zn-Q]/[Pn-Q] system (see **Fig. 2-24** and **Fig. 2-26**)[87].

(iv) Frameworks of corner-connected (regular) tetrahedral such as *T* structure are 6-coordinated sphere packings, in which the tetrahedron centers remain in the same positions (also labeled *12d*) but the vertices are in the positions *24g*. This type of anionic framework structure which is formed by bridging oxygen atoms in sodalite is very similar with [O – B_4O_{12} (= A) – BO_4 (= B)] (= A+B) structural unit in boracite

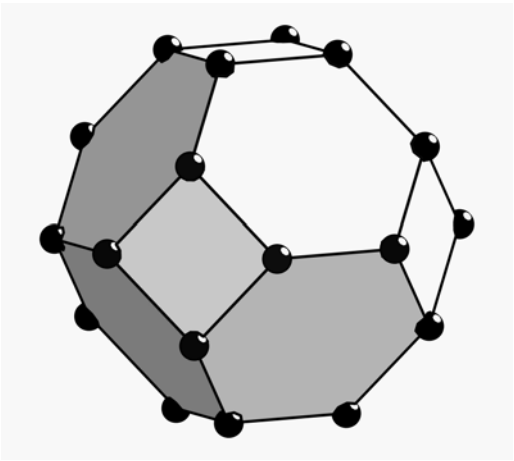

truncated octahedron (4.6^2)
of B_{24} in sodalite

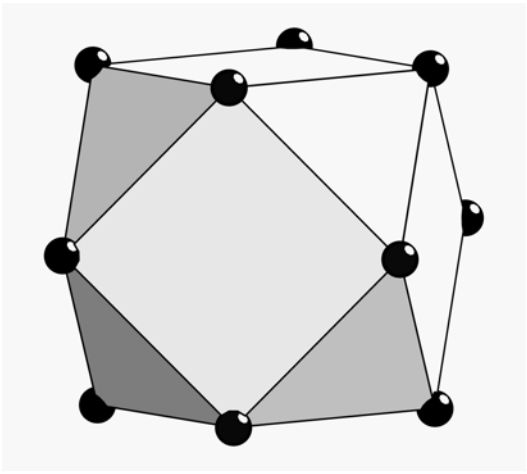

cuboctahedron (3.4.3.4)
of B_{12} in boracite

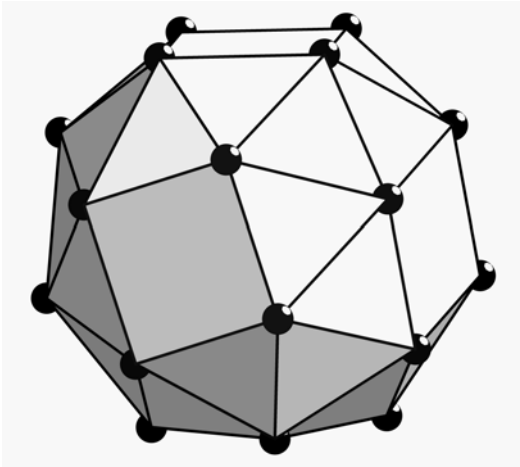

snub cube ($3^4.4$) of I_{24} in clathrate

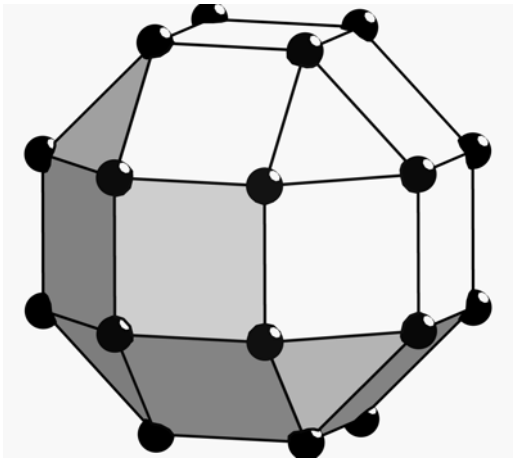

rhombicuboctahedron (3.4^3)

Fig. 2-26. An interpretation by Archimedian polyhedra of structural and functional analogues of clathrate [Zn-Q]/[Pn-Q] system[87].

Closing the **section 2** with an introduction of structural and functional formalism for the purpose of structural interpretation of newly characterized [Zn-Q]/[Pn-Q] clathrate system, the comparison of structure of alkaliiodoindate $KInI_4$, boracite $Mg_3B_7O_{13}Cl$, and soldalite $Zn_8Se_2[BO_2]_{12}$ was shown with respect to the comparison of coordination environments. Namely, the 8-coordinated metal atoms and halide ions in boracite are comparable with 4-coordinated Zn and iodine atoms in [Zn-Q]/[Pn-Q] clathrate system. Also, as the bonding partner with halogen atoms, alkali metals have been reported various coordination numbers like $M(I)In(III)I_4$ structural type. In addition, the chalcogen atoms in the modified zinc chalcogenide structural unit QZn_4 in both [Zn-Q]/[Pn-Q] clathrate system and sodalite had 3 coordination number and 6 coodination number, respectively against those bonding partners like iodine atom with a definitive oxidation state (-1) and B_xO_y structural units with mixed coordination conditions. Astonishingly, in a general formula $Ge_{38}Pn_8I_8$ (Pn = P, As, Sb)[88], and recently $Sn_{24}Pn_{19.3}I_8$ (Pn = P, As)[89] so called Clathrate-I type, where 4-coordinated Ge and pnictogen atoms compose a 3-D net, the oxidation states of atoms except for iodine are uncertain, that is reflect by the host /guest formulation $[Ge_{38}Pn_8]^{8+}/[I^-]_8$, which is comparable with boracite, sodalite and clathrate [Zn-Q]/[Pn-Q] also.

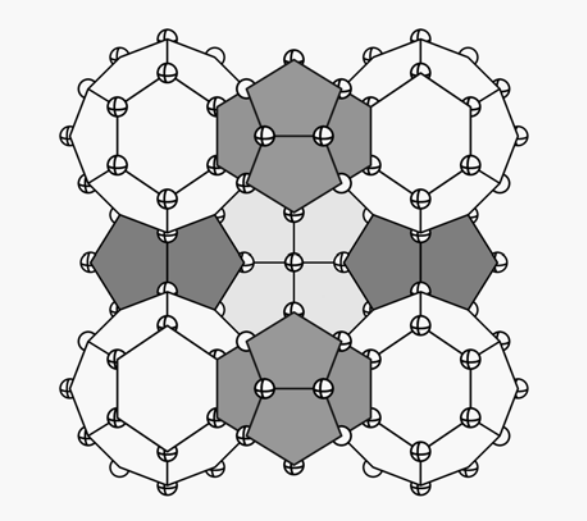

Fig. 2-27. A fragment of the Type I hydrate structure viewed down [001]. (Dodecahedra are shown with heavily shaded faces. Tetrakaidekahedra shared hexagonal faces to form rod along <100>. Atoms : Ge atoms cross circle, Pn atoms open circle and I atoms are not shown here).

In this stage, (1) the coordination of neutral phosphorus chalcogenides in cavity structure is quite questionable and (2) what is the best way to describe this newly synthesized neutral clathrate system. As a summary and definition for structure comparison, the following **Table 2-21** indicates a systematic comparison procedure.

Table 2-21. The definition for structural and functional comparison.

structural analogues				
		alkaiiodoindate $[K\text{-}I_{12}\text{-}In_3]/[K_2]$	boracites $MgB_7O_{13}Cl$	clathrate $[(ZnI_2)_6(ZnQ)]/[Pn_4Q_3]$
host	icosahedron (= A)	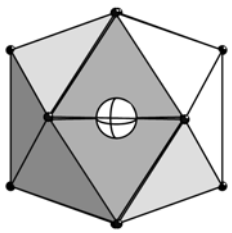 KI_{12}	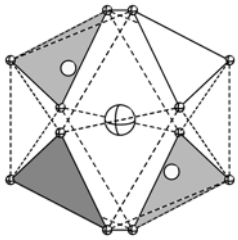 $O\text{-}B_4\text{-}O_{12}$	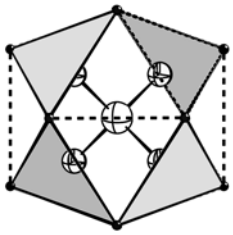 $Q\text{-}Zn_4\text{-}I_{12}$
	tetrahedron (= B)	InI_4	BO_4	ZnI_4
guest		K_2	Cl	Pn_4Q_3
functional analogues				
		Ge, Si halides Ge_6Cl_{16}	sodalite $Zn_8Se_2[BO_2]_{12}$	clatharte $[(ZnI_2)_6(ZnQ)]/[Pn_4Q_3]$
neopentyl-like		Ge_5Cl_{12}	$Se\text{-}Zn_4$	$Se\text{-}Zn_4$
planar		$Ge\text{-}Cl_3$	$Zn\text{-}O_3$	$Zn\text{-}I_3$

The detailed structural comparison of clathrate [Zn-Q]/[Pn-Q] system will be based on following definitions regarding various separated structural units.

(i) the structural analogues with clathrate for instance alkaliiodoindate $KInI_4$ and boracite $MgB_7O_{13}Cl$ will be handled by the concept of host / guest. Therefore,

(ii) the one unit of host framework, the icosahedral analogues of KI_{12} for instance $O\text{-}B_4\text{-}O_{12}$ in boracite and $Q\text{-}Zn_4\text{-}I_{12}$ in clathrate will be compared with respect to

bond length of Metal (for boracite O1) – I (for boracite O2), i.e., with respect to the size of icosahedral analogues. In addition,

(iii) the other unit of host unit, the tetrahedral analogues are directly comparable.

(iv) the detailed bond lengths and bond angles of icosahedral analogues will be compared with various homeotype structures including functional analogues for instance sodalite and polymetal halide.

3. The characterization by X-ray measurements

First of all, the characterization of newly synthesized crystalline compounds using X-ray measurements was sequentially performed by the powder diffraction for the purpose of initial confirmation of formation, consequently rough crystallinity, of this clathrate system. Then, the undistinguishable space group was closely examined by refinement results from X-ray single crystal measurement. The disordered guest molecule(s), however, was characterized by means of ir/Raman spectroscopy and mainly the exact composition(s) of guest molecule(s) were determined by solid state ^{31}P MAS NMR spectroscopy for binary phosphorus chalcogenides, but not for arsenic selenide. The exact composition of As based guest molecule(s) was still not identified. Therefore, the structural interpretation of this clathrate system will be allowed by following points,

(i) the main structural interpretation was based on the Zizpse6144 crystalline compound, since the newly synthesized crystalline compound showed a single occupancy with intercalated molecule P_4Se_3 within error range of infrared and NMR time scale. This approach gives us following advantage, revealing from the **Section 2.4.**,

(a)	Composition
	- phosphorus or selenium homo-molecule(s) due to similar scattering factor
	- single or multiple occupancy by phosphorus selenides
(b)	Disorder
	- orientational disorder by single occupancy
	- dislocalization by multiple occupancy

we can remove every one factor with respect to multiple occupancies from both composition and disorder factor, respectively.

(ii) to add to above, the order of the scattering factors of the present elements were summarized by following host / guest term and **Fig. 3-1** with $f = \frac{A_{atom}}{A_{electron}}$ term (where A_{atom} = amplitude of the wave scattered by an atom and $A_{electron}$ = amplitude of the wave scattered by one electron). Consequently, the factor in above (a) of (ii) can be solved.

[Zn-Se]/[P-Se] system > [Zn-Se]/[As-Se] system > [Zn-S]/[S-P] system

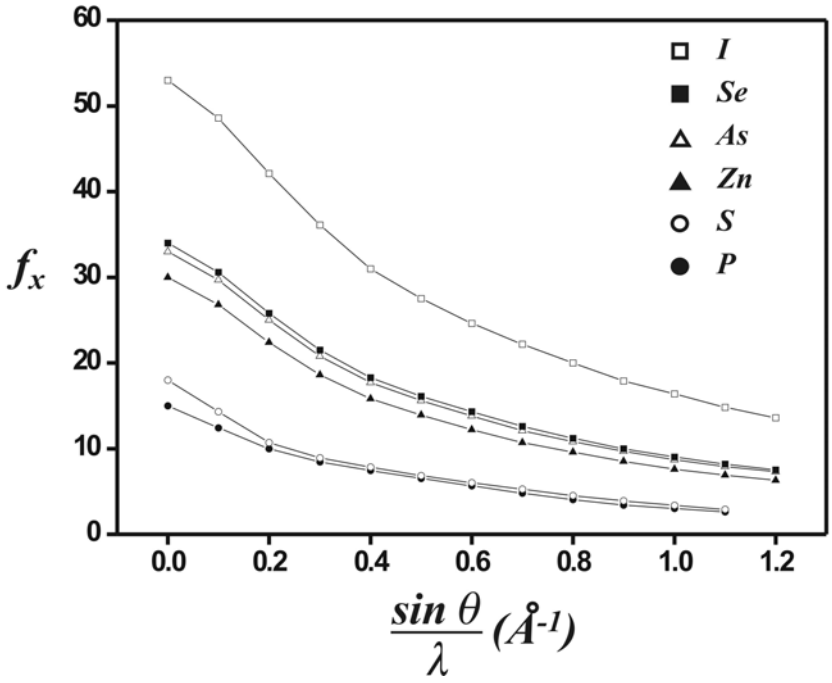

Fig. 3-1. The atomic scattering factors of the present elements[90].

(iii) the crystallographic structural interpretation will be simultaneously discussed by comparison of the structure of a representative of synthetic boracite family [mainly with $Mg_3B_7O_{13}Cl$] and a representative of sodalite family [mainly with $Zn_8Se_2(BO_2)_{12}$] with this clathrate system due to mutual structural and functional resemblances.

(iv) according to deduced lattice constants of newly synthesized crystalline compounds from the powder diffraction data, the measured lattice constant had a relationship

with the initial composition Q (where Q = S and Se) amount. In this sense, the host lattice framework should show a structural elasticity (i.e., lattice elasticity), upon which could be reflected by the structural interpretation from the refinement of X-ray single crystal measurement. In a parallel with this sense, the X-ray single crystal measurement for crystalline compound Zizpse6144 was performed at a wide temperature range 15 ~ 473 K to confirm of a threshold values of lattice elasticity and of atomic displacement parameters of disordered guest molecule(s), but for the other crystalline compounds mainly at 123 and 298 K.

(v) the interpretation of the results from temperature dependent X-ray measurement was closely related with the energy relationship between host lattice and guest molecule. Therefore, the detailed interpretation will be discussed in the separated **Section 6**.

3. 1. Powder diffraction

In the first stage of X-ray measurement as a preliminary evaluation, the phase purity of newly synthesized microcrystalline samples was analyzed at room temperature by powder X-ray diffraction, as following reasons,

(i) a confirmation was needed for a formation of this clathrate system with relatively easy and fast way. Consequently,

(ii) first of all, the rough crystallinity should be checked and compared with ZnI_2 powder diffraction pattern for successive characterization methods.

All the newly synthesized crystalline compounds were grown up till ~ 5 × 5 × 3 mm size within an eyeshot, which were believed as a single phase. One third (~ 0.1 g) of ~ 5 × 5 × 3 mm sized crystalline compound (~ 0.3 g) was powdered for the preparation of a powder diffraction specimen and at same time a specimen for ir/Raman spectroscopy in Ar atmosphere, and especially the specimens for powder diffraction were prepared by 'Scotch Film' due to the hygroscopic nature of all crystalline compounds. All the synthesized crystalline compounds from listed composition (see **Table 2-17**) showed a same powder diffraction pattern (For a representative, I showed the powder diffraction pattern of crystalline compound Zizpse6144 which was compared with calculated pattern using the atomic parameters from single crystal structure. The asterisks indicate the diffraction pattern by 'Scotch Film'). All the refinement results could be indexed assuming the space group $F\bar{4}3c$. Except Zizasse6144, it was not so difficult to select the diffraction patterns by newly synthesized crystalline compound from measured powder diffraction patterns. Actually, the mutual patterns between newly synthesized crystalline compounds ($F\bar{4}3c$; a ~ 19.5 Å) and ZnI_2 (Tetragonal a = 4.34 and c = 11.79 Å; matched with PDF No. 10-72) (The pre-dried ZnI_2 at 623 K for 1 week *in vacuo* was characterized by powder X-ray diffraction) were quite distinguishable with minor ZnI_2 impurity.

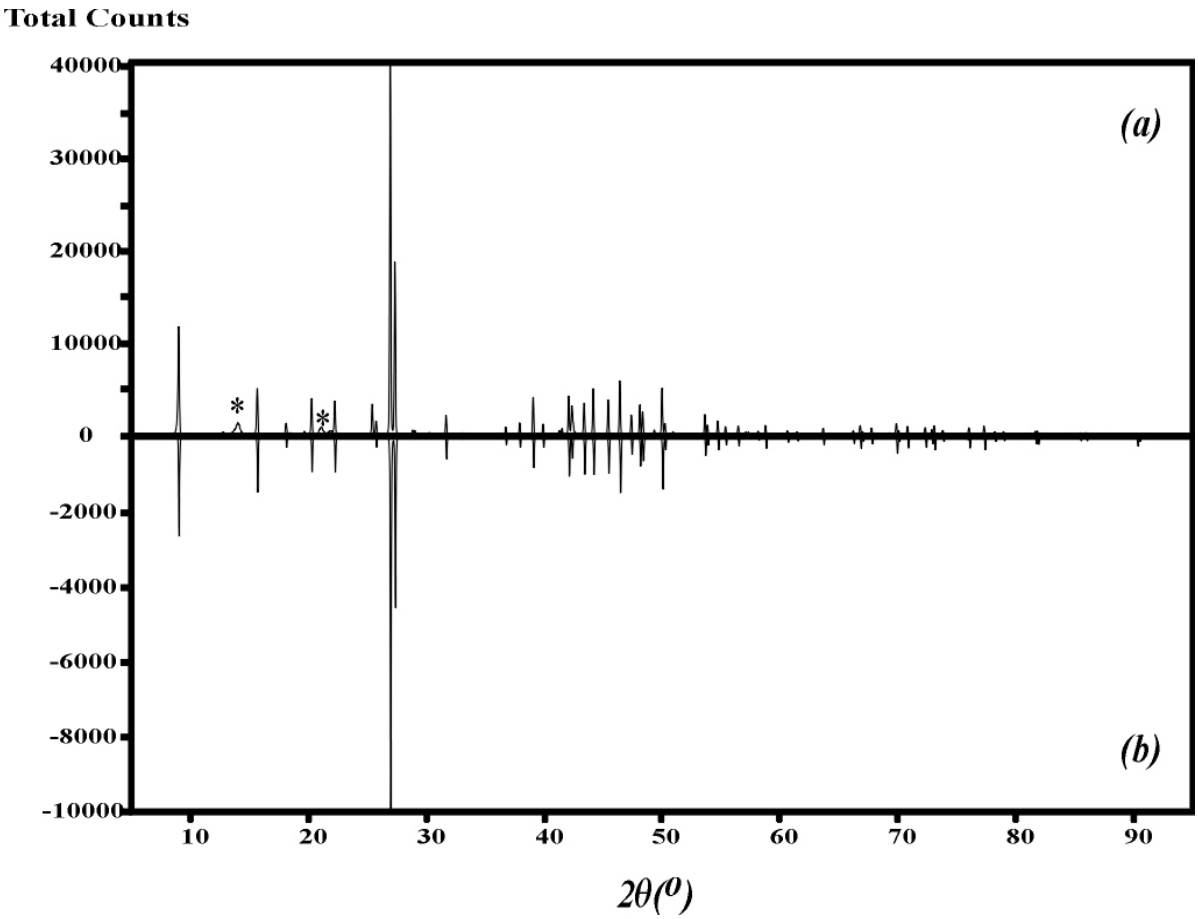

Fig. 3-2. The measured powder diffraction pattern of this clathrate system [(a) = measured pattern, (b) = theoretical pattern of Zizpse6144].

From refinement results of the powder diffraction patterns, all the newly synthesized crystalline compounds were able to be classified into the presumed non-centrosymmetric space group $F\bar{4}3c$ (No.219) within the estimated standard deviations (see **Appendix Table 1**). The [Zn-Se] hosts containing [P-Se] guest molecule were intensively investigated from the lowest stoichiometric limit-ratio of stable guest Se/P = 0 for tetrahedral P_4 inclusion to the ratio of Se/P = 1 for P_4Se_4 inclusion. The refined lattice constants which were varied by the initial compositions for synthesis of new crystalline compounds were summarized as following **Fig. 3-2**, especially with respect to a function of component Q/Zn (where Q = S and Se) ratio with lattice constant.

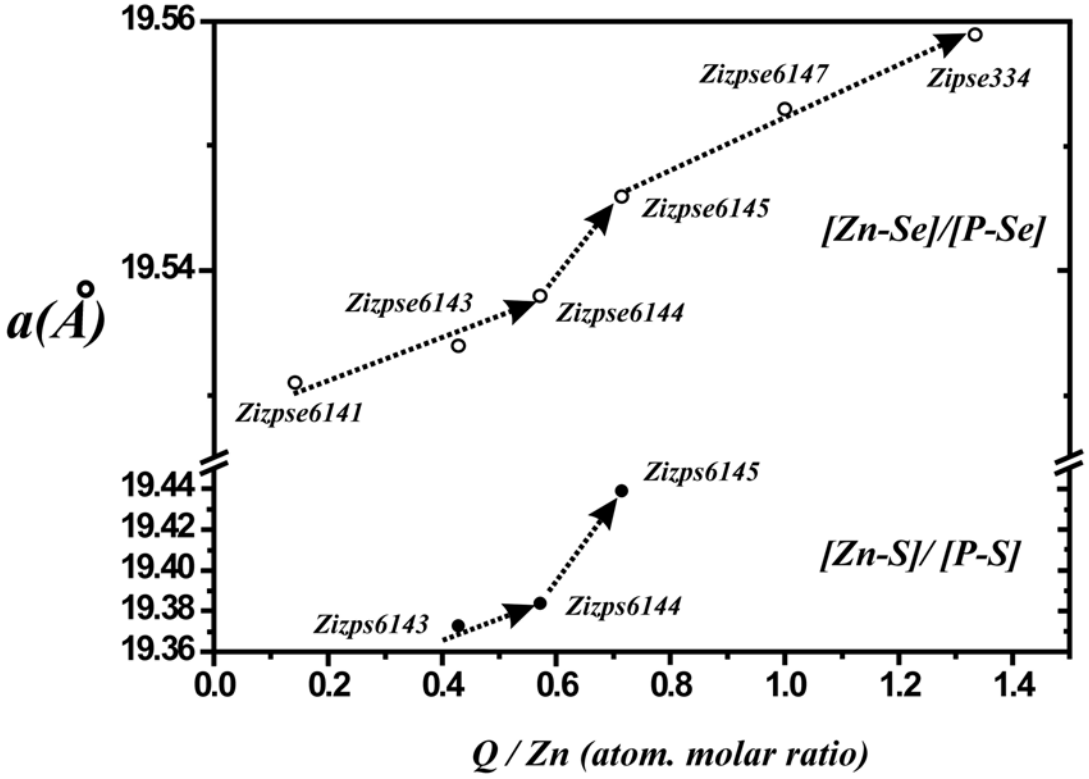

Fig. 3-2. The lattice constants vs. Q/Zn atomic molar ratio (x-axis : initial atomic component ratio of Q/Zn, where Q = S and Se and Zizasse6144 a = 19.602 Å is not showed here due to out of range) ($\sigma = \pm 0.001$ Å).

This **Fig. 3-2** indicates following points,

(i) the tendencies of the lattice constant of [Zn-Q] host lattice were closely related with the initial component Q (where Q = S, Se) amount. Especially,

(ii) the correlation between the initial component Q/Zn ratio and the variation of lattice constant was monitored due to the inclusion possibility of various stable [P-Q] cage molecules with a multiple occupancy which was believed as a main reason of lattice constant variation. A main reason why the lattice constant showed a slight variation can be considerable with respect to a comparison of the crystallographic molecular sizes of P_4Se_x was ignored and with respect to the theoretical simulation including the molecule geometry for inclusion occupancy.

But both approaches were postponed, since the exact bond lengths of α-P_4Se_4 have not been reported yet. As a result, the lattice constants of both [Zn-Se] host based compounds and [Zn-S] host based compound were slightly developed between Q/Zn = 0.57 (4/7) (for P_4Q_3) and 0.71 (5/7) (for P_4Q_4). Therefore, it was essential to synthesis and characterize the crystalline compounds, whether the newly synthesized crystalline compounds have a single molecule occupancy, i.e., [Zn-Q]/[P_4Q_3] or [Zn-Q]/[P_4Q_4] crystalline compound or not.

(iii) the crystalline compound Zizpse6147 was prepared for the purpose of both (1) a synthesis which have a single occupancy with [P_4Se_4] guest molecule and (2) the reaction dependency of P amount, which is comparable with the case of crystalline compound Zipse334. Conclusively speaking, both crystalline compounds Zizpse6144 and Zipse334 showed almost same lattice constant, *a* = 19.553(20) and 19.559(20) Å, respectively. Also the initial component Se/Zn ratios showed almost same, Se/Zn = 1 (7/7 for Zizpse6147) and 1.333 (4/3 for Zipse334) [see down the case (a)], respectively. However, with respect to a term of solute/solvent (where ZnI_2+Zn = solute and P+Se = solvent), the developed tendency of lattice constant showed quite different with one by presumed ZnI_2 solvent or P solvent, i.e., the initial component P or ZnI_2 amount and the formation of crystalline compound showed very low mutual correlation. To the contrary to this, the case (b) indicates another aspect of non-aqueous solvent with glassy phosphorus chalcogenides. This approach is based on a similarity of structural formation between silicate formation through oxolation (where oxolation is a condensation reaction in which an oxo bridge, - O -, is formed between two metal centers) and this neutral clathrate formation. Namely, in silicate formation the final product contains oxygen atoms which are induced from aqueous solvent media. Therefore, the main purpose of this approach by solute/solvent ratio is to give a correlation between the formation of silicate and the formation of this system. For simplicity, in this clathrate system the host lattice always contains one atomic molar chalcogen compared with one phosporus chalcogenide guest molecule in unit cell. But we have to consider about unreacted components in closed ampoule also.

Therefore, the ratio can be traced by initial composition. Probably both the ratio from initial composition vs. lattice constant and the ratio from various characterizations vs. lattice constant might be same.

case (a)

$$\frac{n(ZnI_2)+n(Se)}{n(P)}=\frac{7}{3}=2.333 \qquad \text{for Zipse334}$$

$$\frac{n(ZnI_2)+n(Zn)+n(Se)}{n(P)}=\frac{14}{4}=3.5 \qquad \text{for Zizpse6147}$$

case (b)

$$\frac{n(ZnI_2)+1}{n(P)+n(Se)-1}=\frac{3+1}{3+4-1}=0.67 \qquad \text{for Zipse334}$$

$$\frac{n(ZnI_2)+n(Zn)+1}{n(P)+n(Se)-1}=\frac{6+1+1}{4+7-1}=0.8 \qquad \text{for Zizpse6147}$$

The solute/solvent ratio by case (b) can be deduced as 2, 1.33, 1.14, 1, 0.8 and 0.67 for Zizpse6141, Zizpse6143, Zizpse6144, Zizpse6145, Zizpse6147 and Zipse334, respectively, and can be depicted with lattice constant variation as following **Fig. 3-3**.

As a results, (1) under the consideration about solute/solvent ratio, the P can be regarded as a non-aqueous solvent by a little correlation between stoichiometric amount of P with lattice constant variation which is comparable with case (b), (2) the case (b) indicates a better correlation than case (a), (3) the increment of stoichiometric (P+Se) amount leads to almost linear increment of lattice constant, and therefore, (4) the higher order [P-Se] guest molecules for instance P_4Se_4 and P_4Se_6 are able to be substituted by the increment of stoichiometric (P+Se) amount with similar ratio. Conclusively, [Zn-Se]/[P-Se] crystalline compounds might be formed through an equilibrium of ZnI_2 - chalcogen condensation reaction ($4ZnI_4^{2-} + Q \leftrightarrow QZn_4I_{12} + 2I_2$) on the glassy phase P_xQ_y (reaction medium).

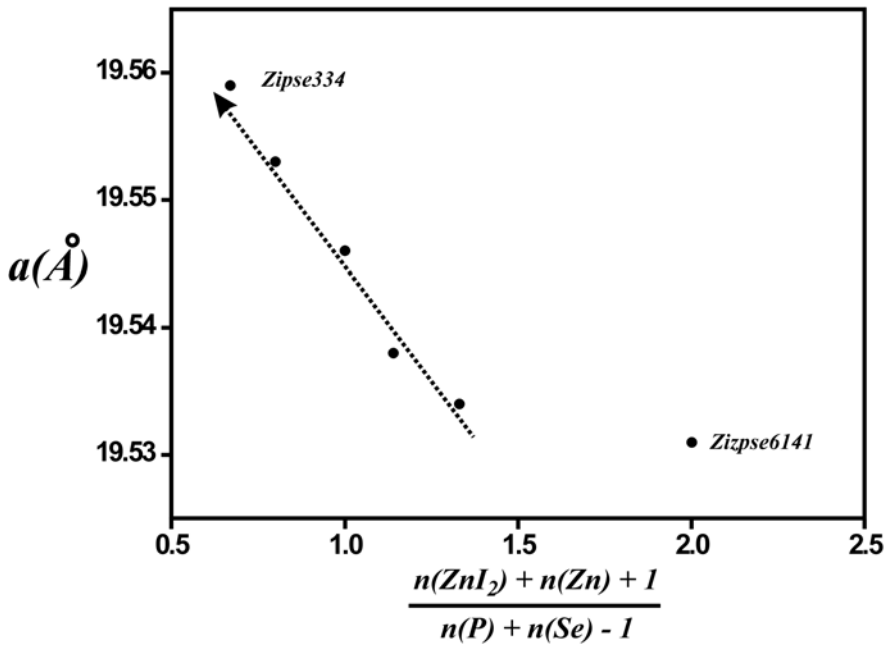

Fig. 3-3. The solute/solvent ratio with respect to (P+Se) non-aqueous solvent.

(iv) reminding the triangle phase diagram (see **Fig. 1.5**) compared [Zn-Se]/[P-Se] clathrate system with reported sodalite and boracites, above consideration leads us to a synthetic utilization using ZnI_2, P and Se quasi-ternary system based on following **Table 3-1**.

Table 3-1. The comparison of mole fraction between boracite, sodalite and [Zn-Se]/[P-Se] clathrate system.

compounds	x_M [1]	x_T	x_X	M[2]	T	X
[Zn-Se]/[P-Se][3]	0.39 ~ 0.50	0.22 ~ 0.29	0.21 ~ 0.39	1	0.6	0.6 ~ 0.7
Boracite ($M_3T_7X_{13}$)	0.13	0.30	0.57	1	2.3	4.4
Sodalite ($M_8X_2[TO_2]_{12}$)	0.36	0.55	0.09	1	1.5	0.25

1. x_M indicates the mole fraction of metal, M = Zn for all, T = B for boracite and sodalite, T = P for clathrate and X = O for boracite, X = Se for sodalite and clathrate.
2. atomic molar ratio based on M (metal) = 1.
3. clathrates ; Zizpse6143, Zizpse6144, Zizpse6145, Zizpse6147.

Table 3-1 is able to be summarized by a triangle phase diagram and shown in **Fig. 3-4**.

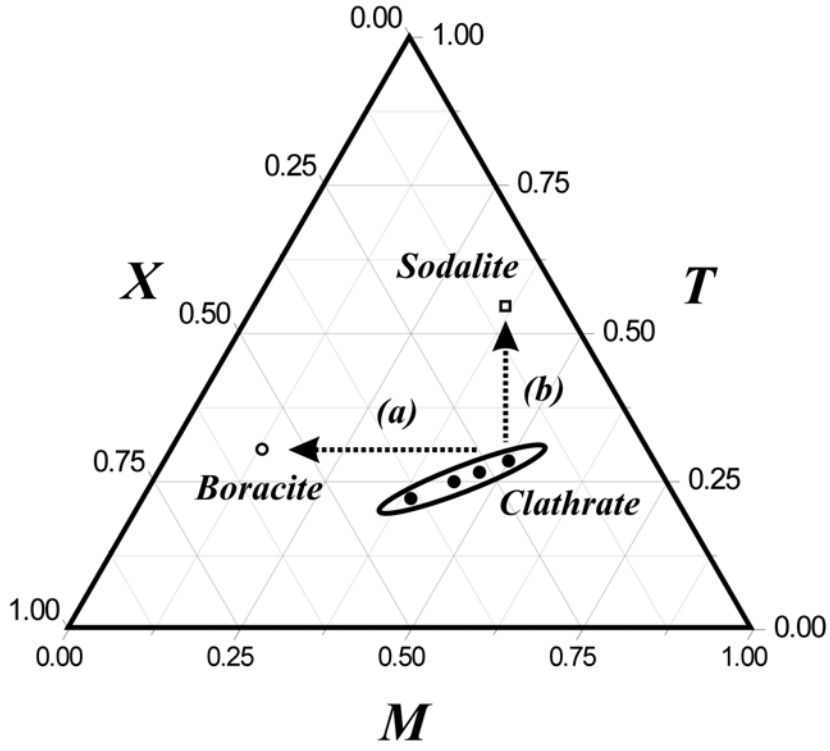

Fig. 3-4. The triangle phase diagram compared with sodalite, boracite and [Zn-Q]/[Pn-Q] clathrate (Where M = Zn, X = O and T = B for boracites $Zn_3B_7O_{13}$, M = Zn, X = Se and T = B for sodalite $Zn_8Se_2B_{12}O_{24}$ and M = Zn, X = Se and T = P, As for clathrates Zizpse6147, Zizpse6145, Zizpse6144 and Zizpse6143 from left one in oblate).

Conclusively speaking, the single phase [Zn-Q]/[Pn-Q] clathrate system were formed at a wide range of initial M, T and X composition. Therefore, varying the composition in the stage of designing new crystalline compounds and using the thermal control in the stage of synthesis, it is accessible into the analogues of boracite or sodalite family through the approaches by **(a)** and **(b)** in **Fig. 3-4**. The structural comparison of [Zn-Q]/[Pn-Q] clathrate with boracite and sodalite will be discussed in the **Section 3-2**.

3. 2. Single crystal measurements

As discussed in the former section and after the refinement result of single crystal measurement of Zipse344 crystalline compound, all the powder diffraction patterns of newly synthesized compounds were able to be indexed into both non-centrosymmetric space group $F\bar{4}3c$ and centrosymmetric space group $Fm\bar{3}c$. Consequently, the crystal structure of [Zn-Q]/[Pn-Q] crystalline compounds were determined from single crystals of suitable sizes at temperatures, mainly 123 K and 293 K and especially 15 ~ 473 K for Zizpse6144 crystalline compound which was believed by the resulting characterization of ^{31}P MAS NMR that the guest molecule P_4Se_3 was embedded into [Zn-Se] host framework with a single occupancy. All the crystals were prepared with the same way of Zipse334 and mounted on an STOE IPDS single crystal diffractometer providing monochromatic Mo *Ka* radiation (λ = 0.71073 Å). For identification of strongly disordered guest molecule(s) with respect to the geometry and the orientation, the solid state ir/Raman and ^{31}P MAS NMR spectroscopy (for composition and geometry) and sequentially classic Rigid-body refinement technique (for orientation) were used.

Even with this enhanced accuracy, however, the refinement results from the single crystal measurement did not provide the exact solution for intercalated guest molecules. In this crystallographic section, we have to discuss about the detailed reasons of difficulties for identifications.

3. 2. 1. Structural interpretation of clathrate [Zn-Q]/[Pn-Q] system

The crystal structures were solved by direct methods with the program SHELXS97 and refined by using the program SHELXL97[67]. Refining the $F\bar{4}3c$ atomic model type resulted in a satisfactory convergence than the refining the $Fm\bar{3}c$ atomic model to the unit cell parameters listed in **Appendix Table 2b** for Zizps6144 crystalline compound, **Table 3b** for Zizpse6144 crystalline compound including low and high temperature modification and **Table 4b** for Zizasse6144 crystalline compound with R_1 (for all), wR_2 (for all) residuals of ~ 2.5 %, ~ 5 % in $F\bar{4}3c$ space group, those of ~ 4 %, 8 % in $Fm\bar{3}c$ space group, respectively.

From a crystallographical point of view, the following characteristics were able to be expected from the consideration of space group ambiguity, and were summarized at **Table 3-2 A** and **B**.

Table 3-2A. The comparison of refinement results of Zizpse6144 at 293 K in $F\bar{4}3c$ and $Fm\bar{3}c$ space groups.

	$F\bar{4}3c$					$Fm\bar{3}c$				
atom	Wyck.	occ.	*x*	*y*	*z*	Wyck.	occ.	*x*	*y*	*z*
host										
Se1	*8a*	1	0	0	0	*8b*	1	0	0	0
Zn1	*24d*	1	0	¼	0	*24c*	1	0	¼	0
Zn2	*32e*	0.39(1)	0.0717(2)	-0.0717(2)	0.0717(2)	*64g*	0.5	0.0722(1)	0.0722(1)	0.0722(1)
Zn3	*32e*	0.61(1)	0.0724(1)	0.0724(1)	0.0724(1)					
I1	*96h*	1	0.1134(0)	0.1784(0)	-0.0007(1)	*96i*	0.5	0.1134(0)	0.1784(0)	0
guest										
P1	*96h*	0.22(5)	0.169(2)	0.229(3)	0.191(2)	*48f*	0.02(2)	¼	¼	0.102(1)
P2	*96h*	0.45(7)	0.221(2)	0.246(3)	0.155(1)	*192j*	0.44(5)	0.217(4)	0.217(4)	0.165(2)
Se2	*32e*	0.37(5)	0.194(1)	0.194(1)	-0.194(1)	*64g*	0.05(6)	0.202(13)	0.202(13)	0.202(13)

Table 3-2B. The point symmetry in $F\bar{4}3c$ and $Fm\bar{3}c$ space groups.

	$F\bar{4}3c$			$Fm\bar{3}c$		
atom	*(x, y, z)*	Wyckoff	point symmetry	*(x, y, z)*	Wyckoff	point symmetry
host						
Se1	*(0, 0, 0)*	*8a*	2 3 .	*(0, 0, 0)*	*8a*	m $\bar{3}$.
Zn1	*(0, 0, ¼)*	*24d*	$\bar{4}$ . .	*(0, 0, ¼)*	*24c*	$\bar{4}$ m 2
Zn2&3	*(x, x, x)*	*32e*	. 3 .	*(x, x, x)*	*64g*	. 3 .
I1	*(x, y, z)*	*96h*	1	*(x, y, 0)*	*96i*	m . .
guest						
P1	*(x, y, z)*	*96h*	1	*(x, ¼, ¼)*	*48f*	4 . .
P2				*(x, y, z)*	*196j*	1
Se2	*(x, x, x)*	*32e*	. 3 .	*(x, x, x)*	*64g*	. 3 .

(i) the Se1 and the Zn1 positions are identical and are fully occupied in both structural models. In the $F\bar{4}3c$ space group, the two distinct atomic positions; *8a* (0, 0, 0) and *8b* (¼, ¼, ¼), i.e., in both positions, the point symmetry (2 3 .), are belong to the centering problem which was able to be examined from the reflex condition. As justification of the centered cell, however, the *hkl* data with *h*, *k*, *l* = 2*n* + 1 were extraordinarily weak.

(ii) the Zn2 and Zn3 (*32e*) position in $F\bar{4}3c$ space group corresponds to Zn2 (*64g*) in $Fm\bar{3}c$ space group with an enhanced multiplicity due to the almost similar atomic coordinate of Zn2 and Zn3 ; (*x*, *x*, *x*) *x* = ~ 0.072.

(iii) both the atomic coordinate of I1 (*96h*) in $F\bar{4}3c$ atomic model and one of I1 (*96i*) in $Fm\bar{3}c$ atomic model are quite similar due to the convergence of *z* in I1 (*96h*) into 0 ; (*x*, *y*, ~0). Therefore, 4 × I1 atom are able to be located on the every planes in $Fm\bar{3}c$ atomic model due to the operation of mirror plane; (m . .).

(iv) the most significant contribution to refining residuals is based on the Se2. The Se2 occupancy in $Fm\bar{3}c$ atomic model showed a quite huge discrepancy with one in $Fm\bar{3}c$ atomic model. Therefore,

Consequently, the structural interpretation will be presented by the Wyckoff positioning procedure from higher symmetry, and divided into [Zn-Q] host lattice which composes of

two definite structural unit; an icosahedral analogue A unit and tetrahedral B unit, and [Pn-Q] guest molecule, since all the atoms consisting of host lattice were well fixed within estimated standard deviation of thermal location parameters, though the guest molecule showed a disordered manners, even at 15 K. Also, the system will be compared with a selected synthetic alkaliiodoindate, boracite and sodalite due to the mutual structural resemblance (see **Table 3-1**). This approach has some advantages for interpretation of clathrate [Zn-Q]/[Pn-Q] system.

A geometrical point of view, considering an octahedron which can be corresponded to 6 × Zn2 (*24d*) atom position in $F\bar{4}3c$ space group, an regular icosahedron which can be constructed by 12 × I1 (*96h*) atom position in clathrate [Zn-Q]/[Pn-Q] system is able to be defined by dividing the octahedron's edges into 'Golden ratio 1 : 1.618' segments[91]. The centers of the faces of an icosahedron comprise the vertices of a cube due to the polyhedron duality. This leads to the beautiful cube compound and is the basis for Jessen's orthogonal icosahedron (see **Fig. 3-5A**). This cube in clathrate [Zn-Q]/[Pn-Q] system was constructed by Q1 (*8a*) – Zn2 or Zn3 $(32e)_4$ double tetrahedra. Consequently, the highest symmetric position *8a* in $F\bar{4}3c$ space group was owned the center of symmetry jointly by a huge octahedron, an icosahedron and a cube.

The regularity or ideality of icosahedral analogues in clathrate [Zn-Q]/[Pn-Q] system is exactly pursuable by tracing atomic coordinates of I1 (*96h*) as a lowest symmetrical position in $F\bar{4}3c$ space group, i.e., by a suitable rotation, the polyhedron vertices of an octahedron of given side length ; $\sqrt{2}\phi$ can be placed at $(0, \pm\phi, 0)$, $(0, 0, \pm\phi)$ and $(\pm\phi, 0, 0)$ (where ϕ is the golden ratio), and consequently in the octahedron, the vertices of an icosahedron of given side length 2ϕ - 2 can be placed at $[\pm 1, \pm(\phi-1), 0]$, $[\pm 1, 0, \pm(\phi-1)]$ and $[\pm(\phi-1), \pm 1\ 0]$ [91]. These points divide the polyhedron edges of an octahedron into segments with lengths in the ratio ϕ -1 : 1. Also, this approach is comparable with respect to both (1) physical properties, including a structural transition, of clathrate [Zn-Q]/[Pn-Q] crystalline compounds and (2) a synthetic utilization of A, B units by means of a comparison with other chemical equivalents.

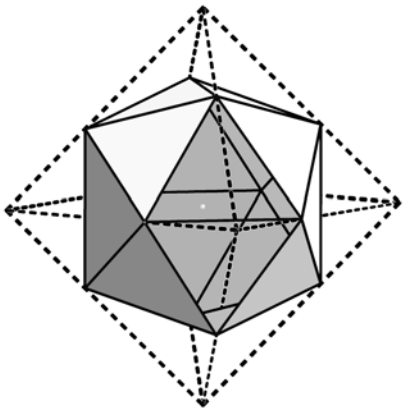

a regular icoahedron within the octahedron ;
K-I_{12} in $KInI_4$

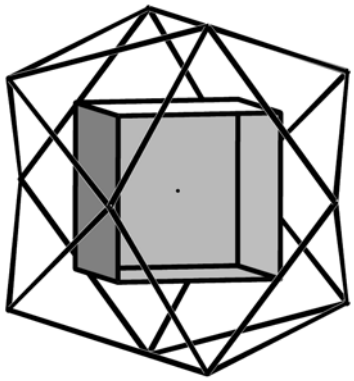

a cube within the Jessen's icosahedron ;
S-Cu_8-S_{12} in $[Cu_8Sb_3S_{13}]/[Fe(NH_3)_6]$

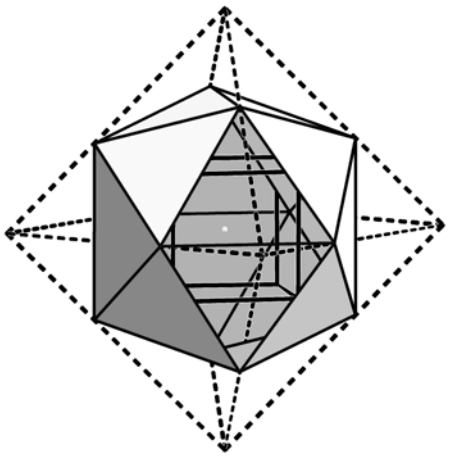

a octahedral, icosahedral and cubic environment of clathrate [Zn-Q]/[Pn-Q] system

Fig. 3-5A. The polyhedral environment of clathrate [Zn-Q]/[Pn-Q] system.

In addition, the structural presentation will be based on the measured results with $[(ZnI_2)_6(ZnQ)]/[P_4Q_3]$ (where Q = S and Se) crystalline compounds, [Zn-S]/[P-S] and [Zn-Se]/[P-Se], at room temperature for the convenience of comparison with other data, since the intercalated chalcogenide molecule was identified as a single-occupied P_4Q_3 molecule (cf. **Section 4.**) with acceptable major purity by solid state NMR technique and in the range of its time scale.

3. 2. 2. 1. Host lattice/Q1 (*8a*) – Zn2 or Zn3 (*32e*) – I1 (*96h*) (= A) unit

3. 2. 2. 1. 1. The icosahedral analogues

The structural interpretation of Q1 (*8a*) – Zn3 or Zn4 (*32e*) – I1 (*96h*) (= A) unit in host lattice of [Zn-Q]/[Pn-Q] will be presented by following procedure,

(i) the host lattice in clathrate [Zn-Q]/[Pn-Q] system composes of two definite polyhedral units ; an icosahedral analogue Q – Zn_4 – I_{12} (= A) structural unit and a tetrahedral ZnI_4 (= B) structural unit as a manner of ReO_3 structural type ; AB_3. (see **Fig. 3-5B**),

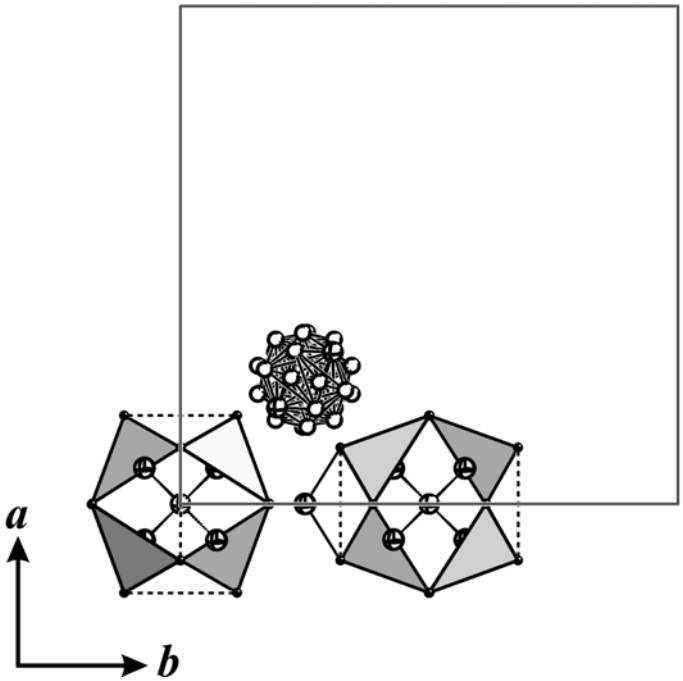

Fig. 3-5B. The Q – Zn_4 – I_{12} (= A) structural unit in clathrate [Zn-Q]/[Pn-Q] system (where A-B-A' array along *b*).

(ii) with respect to space group $F\bar{4}3c$, two structural analogues, alkaliiodoindate $KInI_4$ and boracite $Mg_3B_7O_{13}Cl$, were selected and compared with crystal chemical isotypes, clathrate $[(ZnI_2)_6(ZnSe)]/[P_4Se_3]$ and clathrate $[(ZnI_2)_6(ZnS)]/[P_4S_3]$ (see **Table 3-3**),

Table 3-3. The comparison of atomic coordinates with selected structural analogues.

atom	*Wyckoff*	*x*	*y*	*z*	*occupancy*	$U_{eq.}$
clathrate $[(ZnI_2)_6(ZnSe)]/[P_4Se_3]$			$F\bar{4}3c$ (Z = 8), a = 19.518(2) Å			
Se1	*8a*	0	0	0	1	0.0199(3)
Zn2	*32e*	0.0717(2)	-0.0717(2)	0.0717(2)	0.39(1)	0.0332(16)
Zn3	*32e*	0.0724(1)	0.0724(1)	0.0724(1)	0.61(1)	0.0205(8)
I1	*96h*	0.1134(0)	0.1784(0)	-0.0007(1)	1	0.0316(2)
clathrate $[(ZnI_2)_6(ZnS)]/[P_4S_3]$			$F\bar{4}3c$ (Z = 8), a = 19.386(2) Å			
S1	*8a*	0	0	0	1	0.0230(0)
Zn2	*32e*	0.0705(2)	-0.0705(2)	0.0705(2)	0.56(1)	0.0310(0)
Zn3	*32e*	0.0687(2)	0.0687(2)	0.0687(2)	0.44(1)	0.0234(0)
I1	*96h*	0.1135(2)	0.1771(1)	-0.0004(1)	1	0.0342(2)
alkaliiodoindate $KInI_4$			$F\bar{4}3c$ (Z = 24), a = 19.908(2) Å			
K1	*8a*	0	0	0	1	0.1461(0)
I1	*96h*	0.1126(0)	0.9979(0)	0.1746(0)	1	0.0793(0)
boracite $Mg_3B_7O_{13}Cl$			$F\bar{4}3c$ (Z = 8), a = 12.100(2) Å			
O1	*8a*	0	0	0	1	
B2	*32e*	0.0850(0)	0.0850(0)	0.0850(0)	1	-
O2	*96h*	0.0210(0)	0.0980(0)	0.1800(0)	1	

Where x, y and z are x/a, y/b and z/c, respectively, and $U_{eq.} = (U_{11} + U_{22} + U_{33})/3$

(iii) in all the structural analogues including clathrate, the main atoms for instance Se1 (and S1) and I1 in clathrate, O1 and O2 in boracite and K1 and I1 in alkaliiodoindate for composing of an icosahedral analogue are fully occupied. Therefore,

(iv) at first, the size of icosahedral analogues should be compared. For the detailed tetrahedral positions for instance Zn2 and Zn3 in clathrate, B2 in boracite will be discussed with other structural analogues for instance Se-Zn_4 in sodalite and with functional analogues Ge-Ge_4 in Ge_6Cl_{16} crystalline compound.

(v) For simplicity, the structural interpretation will be discussed under the definition of dimension for an icosahedron (see **Fig. 3-6**). In the definition of **(a)** in **Fig. 3-6**, the radius R1 in one of the two staggered pentagons indicates a edge length of planar polyhedra of Zn2 or Zn3 (*32e*) – I1 (*96h*)$_3$ structural unit in clathrate [Zn-Q]/[Pn-Q] system which corresponds with B2 (*32e*) – O2 (*96h*)$_3$ structural unit in boracite and in alkaliiodoindate R1 and R3 are not distinguishable due to the absence of equivalent atom position. The second radius R2, a length of shared edge with Zn2 (*24d*) – I1 (*96h*)$_4$ tetrahedral unit in clathrate [Zn-Q]/[Pn-Q] system, corresponds with B1 (*24d*) – O2 (*96h*)$_4$ tetrahedral unit in boracite and with In1 (*24d*) – I1 (*96h*)$_4$ in alkaliiodoindate. The third radius R3, a length of non-bonded I1 (*96h*) – I1 (*96h*) in clathrate [Zn-Q]/[Pn-Q] system, corresponds with non-bonded O2 (*96h*) – O2 (*96h*) in boracite and with undistingishable I1 (*96h*) – I1 (*96h*) in alkaliiodoindate. This caused that all the icosahedral analogues, in clathrate, boracite and alkaliiodoindate, were slightly deviated from the dimension of regular icosahedron.

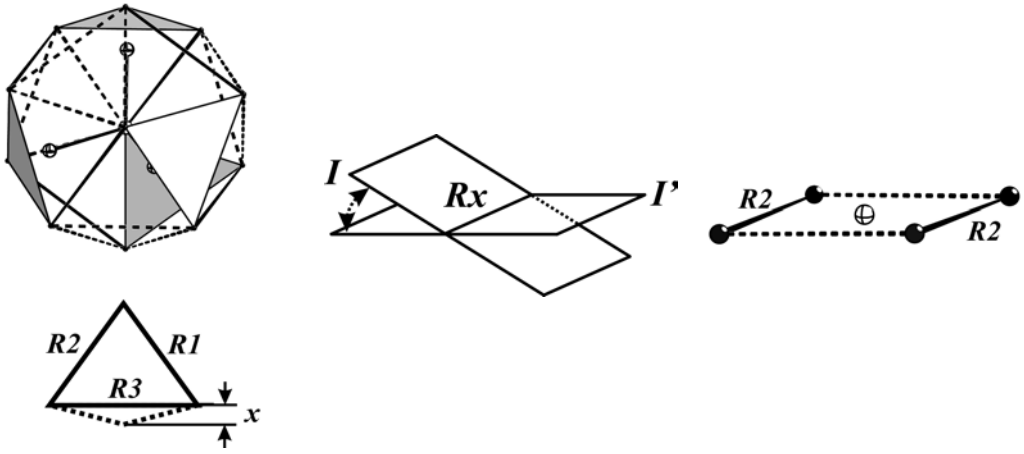

(a) length R1, R2 and R3 (b) dihedral angle (I-Rx-I' torsion angle) (c) planarity

Fig. 3-6. The definition of dimension of icosahedral analogues for comparison with the isotype structures [(a) above ; dotted line indicates non-bonded I-I, solid line an edge of ZnI_4 tetrahedra and the triangles indicate front opened ZnI_3 polyhedra, (b) dihedral angle in icosahedral analogues with I-Rx (x = 1, 2 and 3)-I' torsion angle and (c) planarity with R2-R2' torsion angle].

(vi) the defined dihedral angle [see **(b)** in **Fig. 3-6**] is comparable with a value of regular icosahedron, 138.19^{o}.

(vii) the planarity of oxygen, the deformation of oxygen plane varies with the metal ion and the halogen atoms present in the boracites. The deviation from planarity was introduced in form of a parameter ε and already discussed in former chapter. In addition to the planarity, the torsion angle R2 – R2 [see **(c)** in **Fig. 3-6**] is considerable with respect to a regular icosahedron.

Reminding to the atomic coordinates of Q1 (*8a*) – Zn2 or Zn3 (*32e*) – I1 (*96h*) (= A) structural unit in clathrate [Zn-Q]/[Pn-Q] system, the special atomic position *8a* ; Q1 (0, 0, 0) in space group $F\bar{4}3c$ was owned the center of symmetry jointly by both an icosahedral analogue 12 × I1 (*96h*) and a cube which is constructed by the approximately half-occupied two tetrahedra ; 4 × Zn2 and 4 × Zn3 (*32e*) ($x, \pm x, x$) (symmetry ; . 3 .) with $x \approx 0.072$ as an alternative manner. The refinement results from the single crystal mesurements of clathrate [Zn-Q]/[P_4Q_3] (where Q = S and Se) indicated that the Q – Zn bond lengths in two distinct tetrahedra are quite similar due to an inversion twinning. To the contrary to half-occupied tetrahedra in clathrate, the only one fully-occupied tetrahedra was presented in boracite system; B2 (*32e*) and there is no occupied tetrahedral position in the A structural unit of alkaliiodoindate $KInI_4$ due to 12 coordinated K^+. The characteristics of a cube in clathrate will be discussed in the end of this section. The composition of icosahedral analogues, the I1 (*96h*) atomic position in clathrate [Zn-Q]/[Pn-Q] system, was fully occupied and the correspondents in structural analogues, O2 (*96h*) in boracite and I1 (*96h*) in Alkaliiodoindate, also. The atoms on vertices of icosahedral analogues in clathrate [Zn-Q]/[Pn-Q] system were better fixed than alkaliiodoindate due to the discrepancy of mutual displacement parameter. The thermal displacement parameter data of boracite has not been reported.

Under the definition of **Fig. 3-6**, the dimensional properties of iscosahedral analogues were evaluated as following **Table 3-4A** and by means of temperature dependent single crystal

measurements, the dimensional properties of the icosahedral A unit in clathrate [Zn-Se]/[P_4Se_3] are summarized as **Table 3-4B**.

Table 3-4A. The dimensional properties of icosahedral A unit at 293 K in structural analogues.

		clathrate		boracite	alkaliiodoindate
		[Zn-Se]/[P_4Se_3]	[Zn-S]/[P_4S_3]	$Mg_3B_7O_{13}Cl$	$KInI_4$
length (Å) I-I	R1	4.33(1) for Zn2 4.30(1) for Zn3	4.28(1) for Zn3 4.25(1) for Zn2	2.36(1)	4.26(1)
	R2	4.43	4.40(1)	2.43(1)	4.48(1)
	R3	4.30(1) for Zn2 4.33(1) for Zn3	4.25(1) for Zn3 4.28(1) for Zn2	3.00(1)	4.37(1)
dihedral angle (°) I-R-I'	D1	137.8(1) for Zn2 137.6(1) for Zn3	137.7(1) for Zn3 137.5(1) for Zn2	137.8(1)	137.2(1)
	D2	140.0(1)	140.5(1)	140.9(1)	140.9(1)
	D3	137.6(1) for Zn2 137.8(1) for Zn3	137.5(1) for Zn3 137.7(1) for Zn2	144.7(1)	137.8(1)
planarity (°) R2-R2		0.7(1)	0.4(1)	24.0(1)	2.1(1)

Table 3-4B. The dimensional properties of icosahedral A unit at 123, 173, 293, 393 and 423 K in Zizpse6144 by temperature dependent X-ray measurements.

		123K	173K	293K	393K	423K	$\frac{dy}{dT}$
length (Å) I-I	R1	4.289(5)	4.291(5)	4.300(5)	4.306(5)	4.308(5)	6.3
		4.323(5)	4.324(5)	4.334(5)	4.337(5)	4.350(5)	9.0
	R2	4.442(5)	4.437(5)	4.428(5)	4.419(5)	4.416(5)	-8.7
	R3	4.323(5)	4.324(5)	4.334(5)	4.337(5)	4.350(5)	-
		4.289(5)	4.291(5)	4.300(5)	4.306(5)	4.308(5)	-
dihedral angle (°) I-R-I'	D1	137.5(2)	137.6(2)	137.4(2)	137.7(2)	137.7(2)	6.3
		137.7(2)	137.8(2)	137.8(2)	137.9(2)	138.0(2)	8.0
	D2	140.4(2)	140.3(2)	140.0(2)	139.8(2)	139.6(2)	27.7
	D3	137.7(2)	137.8(2)	137.8(2)	137.9(2)	138.0(2)	-
		137.5(2)	137.6(2)	137.4(2)	137.7(2)	137.7(2)	-
planarity (°) R2-R2		0.7(2)	0.7(2)	0.7(2)	0.6(2)	0.8(2)	5.7

dy/dT ; y is an angle or a length and T is temperature in K and $d(length)/dT \times 10^{-5}$ and $d(angle)/dT \times 10^{-4}$.

As a result, the evaluated data indicate that the icosahedral analogue A in clathrate [Zn-Q]/[Pn-Q] has the best regularity or the best ideality of icosahedra compared with other structural analogues.

(i) the dihedral angle of regular icosahedron, 138.19^{o}, is well matched in all the structural analogues within the deviation of ~ 1^{o}. The dihedral angle (D2) showed relatively higher values than others, i.e., the icosahedral analogues are slightly compressed by one edge of Zn1 (*24d*) bridging tetrahedron, i.e., along the Zn1 (*24d*) direction, which is believed that the relative huge icosahedral A unit than tetrahedral B unit is able to be easily deformed. Contrary to this, in boracite the icosahedral analogue showed a strong deformation on the direction of non-bonded O2-O2 due to the octahedral Mg/Cl environments.

(ii) a regular icosahedron should have 20 equivalent equilateral triangle faces. The edge length of triangles in the icosahedral analogues of every structures showed ~

4.35 , ~ 4.31, ~ 2.58 and ~ 4.37 Å in clathrate [Zn-Se]/[P-Se] system, clathrate [Zn-S]/[P-S] system, boracite system and alkaliiodoindate, respectively.

(iii) an ideal planarity of 6 × rectangles in a regular icosahedron, 0^o, is able to evaluate the regularity of an icosahedra and at same time, to evaluate the 3-dimensional location of the tetrahedra unit (= B) also. Consequently, the A-B-A' unit in clathrate [Zn-Q]/[P-Q] system is better located along the axes as a manner of (m . .), (. m .) and (. . m) than the one in alkaliiodoindate and boracites.

(iv) How does the Q – Zn_4 – I_{12} structural unit in clathrate [Zn-Q]/[P_4Q_3] system reserve the thermal energy which is transferred from the environments ? Conclusively speaking, the temperature dependent X-ray measurements in a wide range of temperature (15 – 473 K) of [Zn-Se]/[P_4Se_3] crystalline compound, Zizpse6144, showed no evidence of a phase transition. The dimensional properties of an icosahedral analogue in [Zn-Se]/[P_4Se_3] crystalline compound ; Zizpse6144 as a representative of clathrate [Zn-Q]/[Pn-Q] system were examined by temperature dependent single crystal measurement at the temperatures of 123, 173, 293, 373, and 423 K (the cases of 15, 223 and 473 K were disregarded due to an uncertainty) and which were mainly compared with the dimensional properties of icosahedral analogue in alkaliiodoindate $KInI_4$ and the cases of boracite were disregarded, since they are out of range. The **(a)** and **(b)** in **Fig. 3-7** indicate that the lengths of the triangle, R1, R2 and R3, and dihedral angles, D1 (I-R1-I), D2 (I-R2-I) and D3 (I-R3-I), linearly approach the ideal values, R1 = R2 = R3 and D1 = D2 = D3 = 138.19^o for a regular dihedral angle with increasing temperature. The most significant reduction in dimensional properties is that the slightly deformed R2 and D2 are converged to an ideal value by the increment of temperature ($dy/dT = -8.7\times10^{-5}$ Å/K and -27.7×10^{-4} °/K, respectively) compared with R1 and R3 or D1 and D3. This reduction is comparable with the case of planarity, i.e., R2 – R2 torsion angle variation, $dy/dT = -5.7\times10^{-4}$ °/K, which is believed as a deviation of angle deformation and with bond length deviation (0.2 % error bar); $dy/dT = 1.7\times10^{-5}$ Å/K. As a result, the icosahedral analogue, a structural A unit in clathrate [Zn-Se]/[P_4Se_3] system, is slightly deformed in room temperature or

below and linearly approaches to the condition of a regular icosahedron in proportion to the increment of temperature with respect to I – I distance and dihedral angle. This result indicates that (1) the Q – Zn_4 – I_{12} structural unit might have a regular form around its temperature of synthesis, 923 K, (2) the positions of I_{12} which are composed of the icosahedral analogue are quite well fixed and showed a very stable manner, (3) the approach to a regular icosahedra, R1 = R2 = R3 and D1 = D2 = D3 = 138.19^{o} for a regular dihedral angle leads to a constant volume of icosahedral analogue.

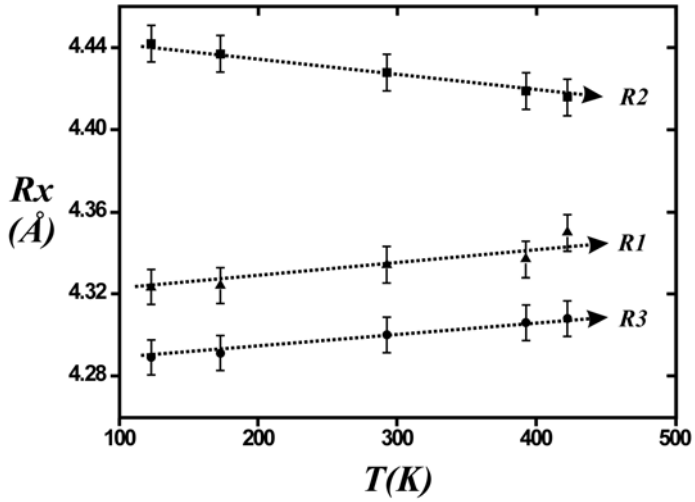

(a) variation of R1, R2 and R3 by temperature modification

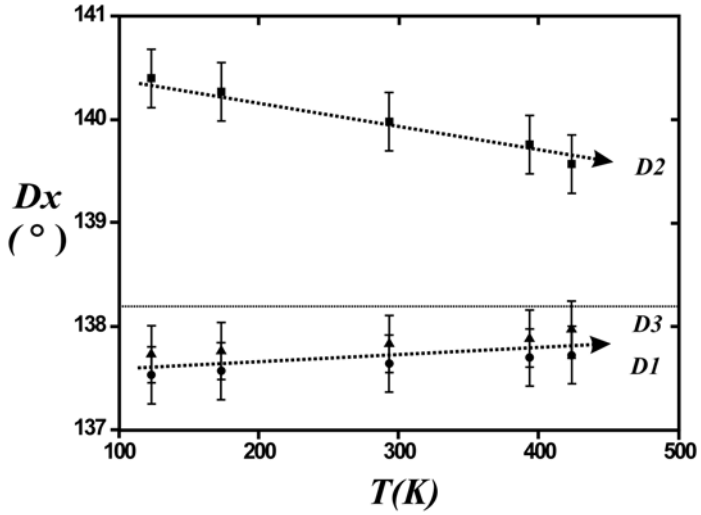

(b) variation of D1, D2 and D3 by temperature modification

Fig. 3-7. The temperature dependent variation of icosahdral analogue in [Zn-Se]/[P_4Se_3] system (with 0.2 % error bar ; down – horizontal line indicates an ideal dihedral angle of icosahedra ; 138.19 °).

(v) the extrapolated values from the possible pairs are 1149.3 and 859.0 K for R1-R2 and R2-R3, and 1013.9 and 932.1 K for D1-D2 and D2-D3, respectively. The icosahedra in alkaliiodoindate $KInI_4$ showed a relative high deformation is comparable to the icosahedral analogue of clathrate [Zn-Q]/[P_4Q_3] based on two reasons (1) relative bigger tetrahedral InI_4 (= B) unit than ZnI_4 unit and (2) the ambiguous dynamic properties of guest (K_2) molecule than P_4Q_3.

Table 3-5. The linear relationship of dimensional properties as a function of temperature.

	linear fit	R (regression value)
length ; R1, R2 and R3		
R1 (Å)	$= 4.28052 + 6.5045\times10^{-5}T(K)$	0.998
R2 (Å)	$= 4.45179 - 8.39751\times10^{-5}T(K)$	0.998
R3 (Å)	$= 4.31024 + 8.08162\times10^{-5}T(K)$	0.929

dihedral angle ; D1, D2 and D3		
D1 (°)	$= 137.45937 + 6.16555 \times 10^{-4} T(K)$	0.999
D2 (°)	$= 140.73079 + 0.00261 \times 10^{-4} T(K)$	0.993
D3 (°)	$= 137.62839 + 7.18469 \times 10^{-4} T(K)$	0.962

As a conclusion, the specific characteristics of structural unit A as an analogue of icosahedron can be summarized as follows,

(i) the dimensional properties of icosahedral analogue A unit in clathrate [Zn-Q]/[P_4Q_3] were compared with the structural analogues like alkaliiodoindate $KInI_4$ and boracite $Mg_3B_7O_{13}Cl$ at room temperature with respect to the regularity of the icosahedron.

(ii) the icosahedral analogue, the Q – Zn_4 – I_{12} structural unit, might have a regular form around its temperature of synthesis, 923 K.

(iii) the positions of I_{12} which are composed of the icosahedral analogue are quite well fixed and showed a very stable manner.

(iv) the approach to a regular icosahedra, R1 = R2 = R3 and D1 = D2 = D3 = 138.19^{o} for a regular dihedral angle leads to a constant volume of the icosahedral analogue over the wide range of temperature, which will be discussed on the section of thermodynamic property of clathrate [Zn-Q]/[Pn-Q] system.

(v) according to the evaluation by means of comparison of dimensional properties, clathrate [Zn-Q]/[P-Q] system showed a quite close resemblance with a regular icosahedron which was believed by the reasons, (1) a cube within Jessen's icosahedra, i.e., the 8 × equilateral triangles of icosahedral analogue in clathrate are well supported by double tetrahedra Zn2 $(32e)_4$ and Zn3 $(32e)_4$ and (2) the dynamic properties of guest molecule in cavity structure prevent the deformation of rather sparse icosahedral analogue.

3. 2. 2. 1. 2. Q1 (*8a*) – Zn2 or Zn3 (*32e*) unit in the icosahedral analogue

The centers of the faces of an icosahedron comprise the vertices of a cube due to the polyhedron duality. This leads to a beautiful cube and is the basis for Jessen's orthogonal icosahedron. This cube in clathrate [Zn-Q]/[Pn-Q] system was constructed by Q1 (*8a*) – Zn2 or Zn3 $(32e)_4$ double tetrahedra.

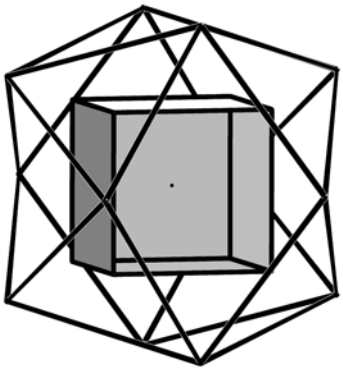

A cube within the Jessen's icosahedron

Fig. 3-8. The cube environment of clathrate [Zn-Q]/[Pn-Q] system.

Double tetrahedral interstitial sites of Q1 (*8a*) are coordinated and surrounded by two different kinds of Zn2 (*32e*) and Zn3 (*32e*) tetrahedra which is very similar case with polyatomic anions like SO_4^{2-} or PO_4^{3-} exhibit dynamic rotational disorder in the high-temperature modifications[91]. The neopentyl-like skeletons have been find out metal-halides or metal-chalcogenide system for instance O-$[BO_3]_4$ unit in $Mg_6B_{14}O_{26}Cl_2$ boracite system and Ge-$[GeCl_3]_4$ unit in Ge_6Cl_{16} or Si-$[SiCl_3]_4$ unit in Si_6Cl_{16} polymetalhalide system, especially in the $F\bar{4}3c$ structural model and Se-$[ZnO_3]_4$ unit in $Zn_8Se_2(BO_2)_{12}$ sodalite system, especially in the $I\bar{4}3m$ structural model (see **Fig. 3-9**). The atom position Q1 (where Q1 = S1 and Se1 for clathrate, O1 for boracite and Ge1 for polymetalhalide) (*8a*) (site symmetry 2 3 .) in the $F\bar{4}3c$ structural model of **(a)**, **(b)** and **(d)** in **Fig. 3-9** corresponds to Se1 (*2a*) (site symmetry $\bar{4}$ 3 m) in the $I\bar{4}3m$ structural model, but body-centered, and the atom position M (where M = Zn2 and Zn3 for clathrate, O2 for boracite and Ge3 for

polymetalhalide) (*32e*) (site symmetry . 3 .) corresponds to Zn1 (*8c*) (site symmetry . 3 m) in the $I\bar{4}3m$ structural model.

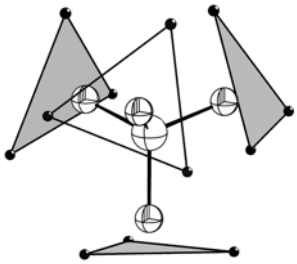

(a) Se-$[ZnI_3]_4$ in [Zn-Se]/[P-Se] clathrate system

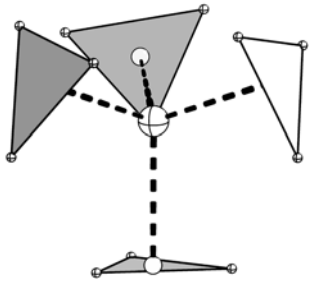

(b) O-$[BO_3]_4$ in $Mg_6B_{14}O_{26}Cl_2$ boracite system

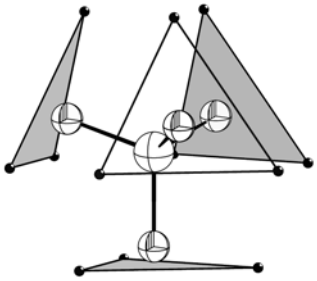

(c) Se-$[ZnO_3]_4$ in $Zn_8Se_2(BO_2)_{12}$ sodalite system

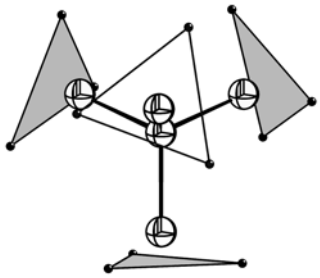

(d) Ge-$[GeCl_3]_4$ in Ge_6Cl_{16} polymetalhalide

Fig. 3-9. The tetrahedral environments of Q1 atom [(a) : cross = S1 or SE1 (*8a*) , octand = Zn2 or Zn3 (*32e*) and black = I1 (*96h*), (b) : cross = O1 (*8b*), open = B2 (*32e*) and black = O2 (*96h*)[67], (c) : cross = Se (*2a*), octand = Zn1 (*8c*) and black = O1 (*24g*) and (d) : octand = Ge2 (*8b*) and Ge3 (*32e*), black = Cl2 (*96h*) (a), (b) and (d) in $F\bar{4}3c$ structural model, and (c) in $I\bar{4}3m$ structural model].

The structural interpretation of Q1 (*8a*) – Zn3 or Zn4 (*32e*) unit in host lattice of [Zn-Q]/[Pn-Q] will be presented by following procedure,

(i) for simplicity, the structural interpretation will be discussed under a definition of dimension for one tetrahedron in Q1 (*8a*) – Zn2 (or Zn3) $(32e)_4$ unit (see **Fig. 3-10**).

(ii) a bond length (Å), AT1 [see **(a)** in **Fig. 3-10**], of Q1 (*8a*) – Zn2 or Zn3 (*32e*) fragment is able to be directly compared with other functional analogues for instance bond length Se (*2a*) – Zn (*8c*) in solalite $Zn_8Se_2(BO_2)_{12}$, O1 (*8a*) --- B2

(*32e*) in boracite $Mg_3B_7O_{13}Cl$ and Ge2 (*8b*) – G3 (*32e*) in polymetalhalide Ge_6Cl_{16}. The bond length (Å) and angle (°), AT2 and AA1 [see **(b)** in **Fig. 3-10**], of Q1 – Zn2 (or Zn3) – I1 fragment are comparable with the bond length and bond angle in ZnI_2 crystalline compounds and with those in B unit also. In addition, the torsion angle (°), AD1 [see **(c)** in **Fig.3-10**], of Zn (*32e*) – Q1 (*8a*) – Zn' (*32e*) – I 1 (*96h*) unit is able to indicate an elasticity of lattice deformation which is comparable with AD2 of Zn (*32e*) – Q1 (*8a*) – I1 (*96h*) – Zn' (*32e*) with respect to stable location of Se – Zn_4 tetrahedron in icosahedral analogue.

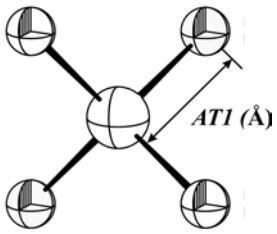

(a) bond length (AT1) ;
Q1 – Zn (Å)

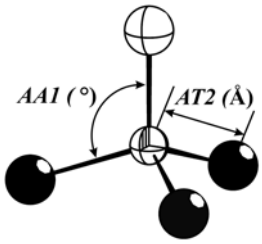

(b) bond length (AT2) and angle (AA1) ;
Zn – I (Å) and
Q1 – Zn – I (°)

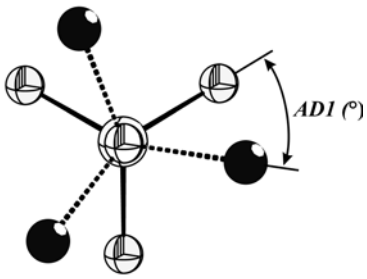

(c) torsion angle (AD1) ;
Zn – Q1 – Zn' – I (°)

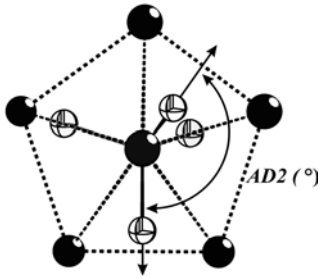

(d) torsion angle (AD2) ;
Zn – Q1 - I – Zn' (°)

Fig. 3-10. The definition of dimension for Q1-Zn_4 unit (cross = Q, octant = Zn, black = I).

Comparing the dimensional properties of Q1 – Zn_4 unit in clathrate [Zn-Q]/[P_4Q_3] system with the equivalent units in other structures at 293 K under the definition of structural fragment in **Fig. 3-10**, the summarized results are shown in **Table 3-5A**, and the results from temperature dependent single crystal measurements are followed as **Table 3-5B**.

Table 3-5A. The dimensional properties of Q1-Zn units at 293 K in functional analogues.

		clathrate		boracite	metalhalide	sodalite
		[Zn-Se]/[P_4Se_3]	[Zn-S]/[P_4S_3]	$Mg_3B_7O_{13}Cl$	Ge_6Cl_{16}	$Zn_8Se_2(BO_2)_{12}$
bond length (Å) Q1-Zn	AT1	2.45(1) for Zn2 2.42(1) for Zn3	2.31(1) for Zn3 2.37(1) for Zn2	1.78(1)	2.42(1)	2.37(1)
bond angle (°) Q1-Zn-I1	AA1	108.9(1) for Zn2 109.0(1) for Zn3	109.9(1) for Zn3 110.9(1) for Zn2	102.7(1)	110.2(1)	114.4(1)
bond length (Å) Zn-I	AT2	2.65(1) for Zn2 2.62(1) for Zn3	2.64(1) for Zn3 2.61(1) for Zn2	1.40(1)	2.12(1)	1.97(1)
torsion angle (°) Zn-Q1-Zn'-I	AD1	39.0(1) for Zn2 38.8(1) for Zn3	39.3(1) for Zn3 39.2(1) for Zn2	29.0(1)	38.7(1)	0.0
torsion angle (°) Zn-Q1 -I-Zn'	AD2	142.9(1) for Zn2 143.1(1) for Zn3	142.7(1) for Zn3 142.8(1) for Zn2	152.4(1)	107.8(1)	180.0

Table 3-5B. The dimensional properties of Q1-Zn units at 123, 173, 293, 393 and 423 K in Zizpse6144 by temperature dependent X-ray measurement.

		123K	173K	293K	393K	423K	$\frac{dy}{dT}$
bond length (Å) Q1-Zn	AT1	2.439(5) 2.434(5)	2.441(5) 2.431(5)	2.448(5) 2.422(5)	2.461(5) 2.414(5)	2.478(5) 2.407(5)	13.0 -9.0
bond angle (°) Q1-Zn-I1	AA1	109.1(2) 108.7(2)	109.0(2) 108.8(2)	108.9(2) 109.0(2)	108.6(2) 109.1(2)	108.3(2) 109.2(2)	-24.3 17.7
bond length (Å) Zn-I	AT2	2.619(5) 2.635(5)	2.620(5) 2.637(5)	2.623(5) 2.645(5)	2.622(5) 2.650(5)	2.620(5) 2.660(5)	0.3 8.3
torsion angle (°) Zn-Q1-Zn'-I	AD1	39.1(2) 39.3(2)	39.0(2) 39.2(2)	38.8(2) 39.0(2)	38.7(2) 38.9(2)	38.5(2) 38.8(2)	-18.7 -17.0
torsion angle (°) Zn-Q1 -I-Zn'	AD2	142.9(2) 142.7(2)	142.9(2) 142.9(2)	142.9(2) 142.9(2)	143.2(2) 143.2(2)	143.4(2) 143.4(2)	16.0 23.0

dy/dT ; y is an angle or a length and T is temperature in K, d(length)/dT $\times 10^{-5}$ and d(angle)/dT $\times 10^{-4}$.

As the results from the examination of dimensional properties about Q1 – Zn structural fragment in Q – Zn_4 – I_{12} icosahedral analogue,

(i) the bond lengths, AT1, of Q1 – Zn2 and Q1 – Zn3 unit in clathrate [Zn-Q]/[P_4Q_3], especially the bond lengths of Se1 – Zn unit in clathrate [Zn-Se]/[P_4Se_3] system showed relative short lengths than the Zn – Se bond length of synthetic stilleite, 2.46 Å, in $F\bar{4}3m$ and those of hexagonal modification, 2.45 ~ 2.49 Å, in $P6_3mc$, but the bond lengths of S1 – Zn unit in clathrate [Zn-S]/[P_4S_3] system showed that one is longer and the other is shorter than both the Zn – S length in synthetic sphalerite $F\bar{4}3m$ and in synthetic wurtzite $P6_3mc$, 2.35 Å. In addition, the bond length, AT1, of Se – Zn unit in sodalite $Zn_8Se_2(BO_2)_{12}$ system exactly corresponds to the longer AT1 of S – Zn unit in clathrate [Zn-S]/[P_4S_3] system and Ge – Ge in Ge_6Cl_{16} system to the shorter Se – Zn in clathrate [Zn-Se]/[P_4Se_3] system which are quite questionable with respect to (1) the variation of bond length by packing condition and (2) the possibility of substitution Ge_5 with Se – Zn_4.

Table 3-6. The reported Zn-Q bond length from synthetic ZnQ (Q = S, Se) compounds.

	ZnSe		ZnS	
	stilleite	hexagonal	sphalerite	wurtzite
length Zn-Q (Å)	2.46(1)	2.49(1) 2.45(1)	2.35(1)	2.35(1) 2.34(1)
ref.	59	93	94	95
Zn-Q1 (Å) in clathrate	2.42(1) ~ 2.45(1)		2.31(1) ~ 2.37(1)	

(ii) the bond angle AA1 of Q1 – Zn2 (or Zn3) – I1 in clathrate [Zn-Q]/[P_4Q_3] system showed a quite good approximation with an ideal value of regular tetrahedron, 109.47^o, and the values are comparable with the bond angle AA1 of the O1 – B2 – O2 unit in boracite $Mg_3B_7O_{13}Cl$ system, in which the O1 atom is quite released from BO_3 planar triangle, since B2 atom is almost on the plane of O_3 triangle. To

the contrary, Zn1 atom in sodalite $Zn_8Se_2(BO_2)_{12}$ is rather compressed by 6 × BO_4 tetrahedra in the direction of Zn - Se.

(iii) The Zn – I bond lengths have been reported in three cases, one in $I4_1/acd$ [28], a second in $R\bar{3}m$ [96] and a third in $P\bar{3}c1$ [97]. Zn(II) cations showed 4 – , 6 – and 12 – coordination, respectively (see **Table 3-7**). The bond lengths, AT2, of Zn – I unit in clathrate [Zn-Q]/[P_4Q_3] system showed a good approximation with the Zn – I bond length in ZnI_2 tetragonal modification ($I4_1/acd$) which was believed as an adamantane-like structure, but 10 % longer than one from the computation results, i.e., than ~ 2.4 Å and thermochemical approach[98], which means the surrounded iodide atoms are highly polarized to the bonding direction in both case of Se and S based host lattice.

Table 3-7. The reported Zn-I bond length from ZnI_2 compounds.

	ZnI_2		
modification	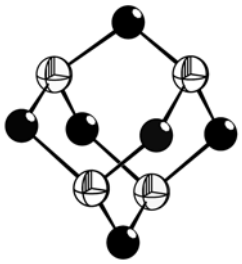	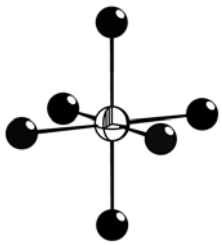	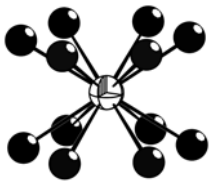
	tetragonal $I41/acd$	trigonal $R\bar{3}m$	trigonal $P\bar{3}c1$
length Zn-I (Å)	2.46(1) ~ 2.84(1)	3.03(1)	2.95(1)
ref.	28	96	97

(iv) finally, the torsion angle, AD1, of Zn – Q1 – Zn' – I unit in clathrate [Zn-Q]/[P_4Q_3] system showed quite huge discrepancy with an ideal value, 60^o. The ideal angle is regarded as the least hindered atom location in space. Contrary to this, the torsion angle, AD2, of Zn – Q1 – I – Zn' unit in clathrate [Zn-Q]/[P_4Q_3] system showed a good approximation with an ideal value, $\frac{360^o}{5} \times 2 = 144^o$,

within the angle deviation range of $\sim 1^{o}$. This means that it would seem that (1) it's very difficult for a tetrahedron to be located in an icosahedron as a manner of the least steric hinderance with I_{12} atoms on the icosahedral vertices and (2) the structural stability of the A unit in clathrate is compensatory supported by mutual structural ambiguities, i.e., one is an unstable location of tetrahedral Q1 – Zn_4 unit in icosahedral analogues and the other a sparse framework of rough octahedral cavity.

(v) the results of dimensional properties of Q – Zn_4 – I_{12} structural unit in clathrate [Zn-Se]/[P_4Se_3] system from the temperature dependent single crystal measurements were depicted as following **(a)**, **(b)**, **(c)**, **(d)** and **(e)** in **Fig. 3-12**.

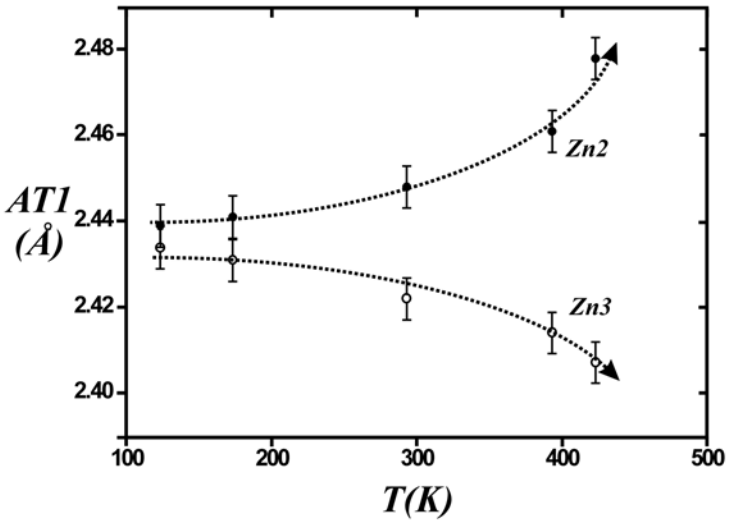

(a) variation of AT1 (Å)

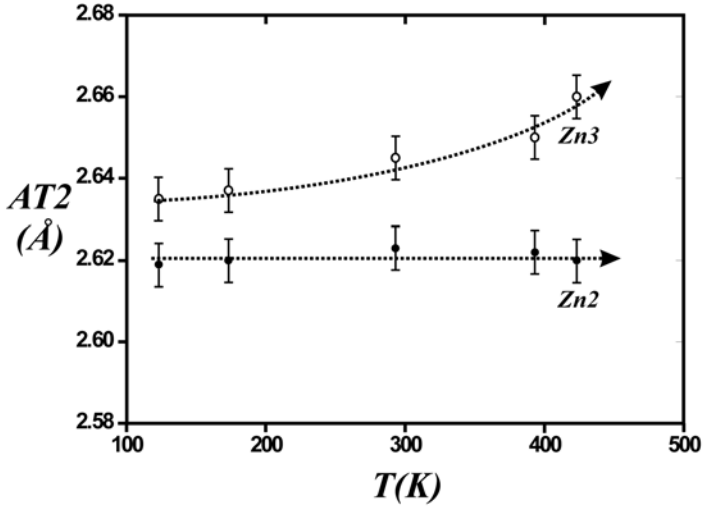

(b) variation of AT2 (Å)

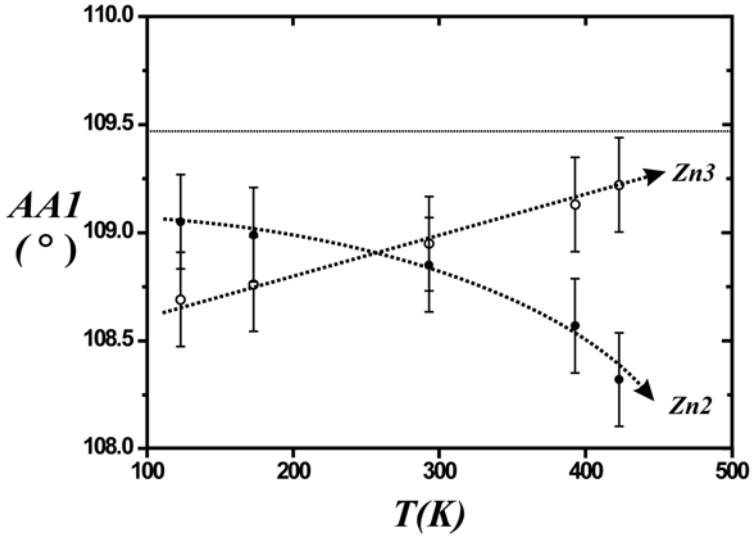

(c) variation of AA1 (°)

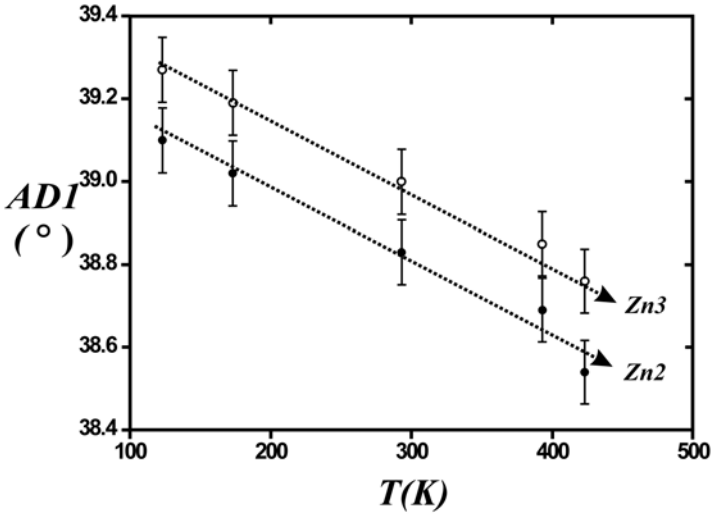

(d) variation of AD1 (°)

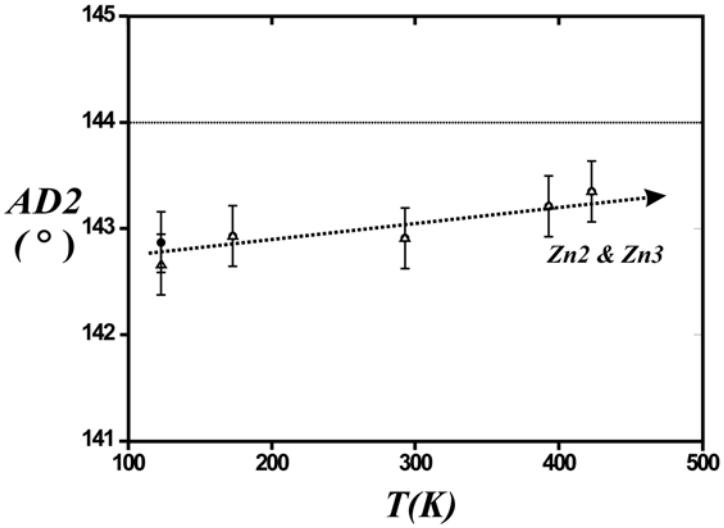

(e) variation of AD2 (°)

Fig. 3-11. The temperature dependent variation of Q-Zn_4 and Zn-I_3 units in [Zn-Se]/[P_4Se_3] system (with 0.2 % error bar ; (c) and (e) dotted line indicate a regular tetrahedral angle ; 109.47 ^{o} and a regular torsion angle of Q-Zn_4 tetrahedra in icosahedral analogue by I_{12} ; 144 ^{o}, respectively and the sum of occupancy with Zn2 and Zn3 is 1 ; Zn2 > Zn3).

(vi) according to the results from temperature dependent single crystal measurements and the I – I distance became close in proportion to temperature in order to approach to a regular icosahedron (see **Fig. 3-7**), it would seem that the variation of bond lengths, AT1, of Q – Zn unit is geared by the motion of intercalated guest molecule, since one of the bond lengths, AT1, i.e., one of Q – Zn2 unit is increased by the increasing temperature (linearly $dy/dT = 13.0\times10^{-5}$ Å/K) and this increment of bond length is exactly compensated by the angle decrement ($dy/dT = -24.3\times10^{-4}$ °/K) of Zn2 – I_3 tetrahedra and in addition, in spite of the decrement of tetrahedral angle, AA1, of Se – Zn2 – I unit, the bond length, AT2, of Zn2 – I unit is maintained ($dy/dT = 0.3\times10^{-5}$ Å/K which is believed actual deviation for bond length variation, ± 0.002 Å). Contrary to Zn2, the bond length, AT1, of Q – Zn3 unit is decreased by temperature ($dy/dT = -9.0\times10^{-5}$ Å/K) in spite of slight increment of the bond length, AT2, of Zn3 – I unit. Due to variation, the tetrahedral bond angle, AA1, of Se – Zn3 – I unit linearly approaches to the value of regular tetrahedron, 109.47^o ($dy/dT = 17.7\times10^{-4}$ °/K). The results, **(a)**, **(b)** and **(c)** in **Fig. 3-11**, are supported by **(d)** and **(e)**. The both motions by Zn2 and Zn3 (see **Fig. 3-12**) are governed by the stable formation of the icosahedral analogue, i.e., the two kinds of dihedral angles, AD1 and AD2, approach an ideal condition of regular icosahedron ($dy/dT \sim \pm 20\times10^{-4}$ °/K).

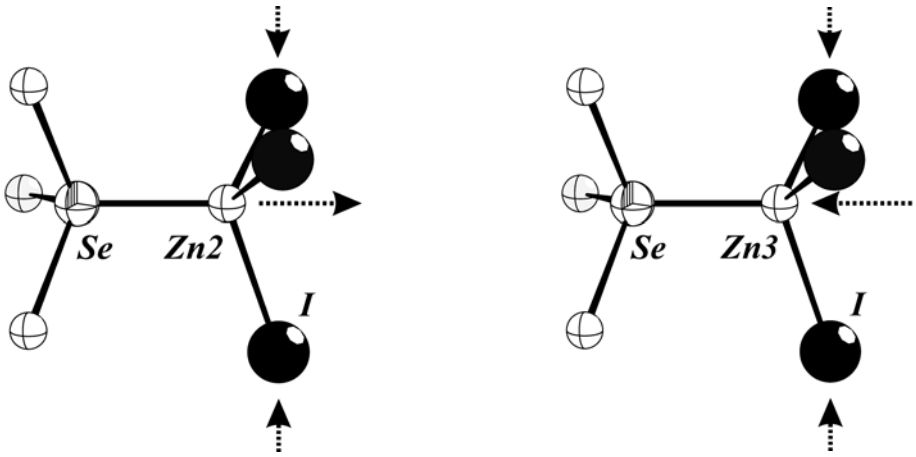

Fig. 3-12. The motion of 'flower bud' (the dotted arrow indicate the shifts by the increment of temperature).

(vii) the variations of bond lengths, AT1, of Q1 – Zn2 and Q1 – Zn3 units showed a notable aspect,

(a) the Q1 (*8a*) (site symmetry ; 2 3 .) atomic position is the most symmetric position in $F\bar{4}3c$ structure model. In addition, the equivalent isotropic displacement parameters of Q1, 0.0079(3) ~ 0.0334(4) Å^2 (123 ~ 423 K) for Se1 and 0.0152(8) ~ 0.0230(7) Å^2 (123 ~ 293 K) for S1, showed a very stable manner, i.e., a center of Q1 – Zn_4 tetrahedra is well fixed within the estimated standard deviation of thermal isotropic parameters.

(b) the sum of occupancies on Zn2 atom and Zn3 atom is almost 1, but the ratio varied from Zn2 : Zn3 = 0.63(1) : 0.37(1) (at 15 K) to 0.54(1) : 0.46(1) (at 423 K) in clathrate [Zn-Se]/[P_4Se_3] system.

Consequently, the two different kinds of tetrahedral distortion were able to be expected, as following **Fig. 3-13**.

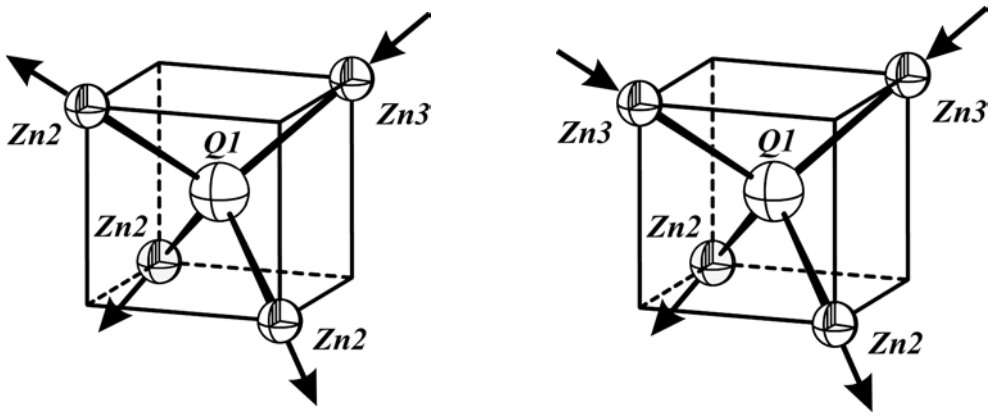

(a) distortion on C_3 axis (b) distortion on C_2 (S_4) axis

Fig. 3-13. The structural distortion of Q1 – Zn_4 tetrahedron.

Under the assumptions, (1) the translational motion of guest molecule is able to be disregarded at 15 K, (2) the C_{3v} symmetric axis of the guest molecule (P_4Q_3) exactly coincides with every C_3 axes, i.e., the guest molecule is on the most stable diagonal direction in the unit cell, the occupancy of Zn2 and Zn3 can be immediately calculated by means of term, [occupied positions / total position],

and then, 5/8 = 0.625 for Zn2 and 3/8 = 0.375 for Zn3. In addition, changing the orientation of guest molecule by increasing the temperature, i.e., recovering the translational energy of guest molecule(s) from environments, the guest molecule has a translational motion with D.O.F (degree of freedom) = 3 toward every face of the unit cell which leads the occupancy ratio of Zn2 : Zn3 to 0.5 : 0.5 [**(b)** in **Fig. 3-13** become predominant over the structure). This result from clathrate [Zn-Se]/[P_4Se_3] supported by (1) the variation of the equivalent isotropic displacement parameters by an increment of temperature, i.e., 0.0052(14) $Å^2$ (for Zn2) < 0.0140(3) $Å^2$ (for Zn3) at 15 K and 0.0435(20) $Å^2$ (for Zn2) ≈ 0.0390(30) $Å^2$ (for Zn3) at 423 K, and (2) the detection of distortions of tetrahedral symmetry by means of Raman spectroscopy in external region. The later will be discussed on the section of characterization by ir/Raman spectroscopy.

3. 2. 2. 2. Host lattice/Zn (*24d*) – I1 (*96h*) (= B) unit

No dimeric species have been detected by a mass spectrometric study in the vapor phase of Group 12 dihalides, i.e., ZnX_2 and CdX_2. Only HgX_2 dimers were identified by vibrational spectroscopy[99]. Consequently dimers of Zn and Cd dihalides have been revealed by computational study and suggested D_{2h}-symmetry structure with four equivalent bridging metal-halogen bonds[100]. Also, with very similar case of our study, the CuCl-based edge-sharing tetramer was reported[27].

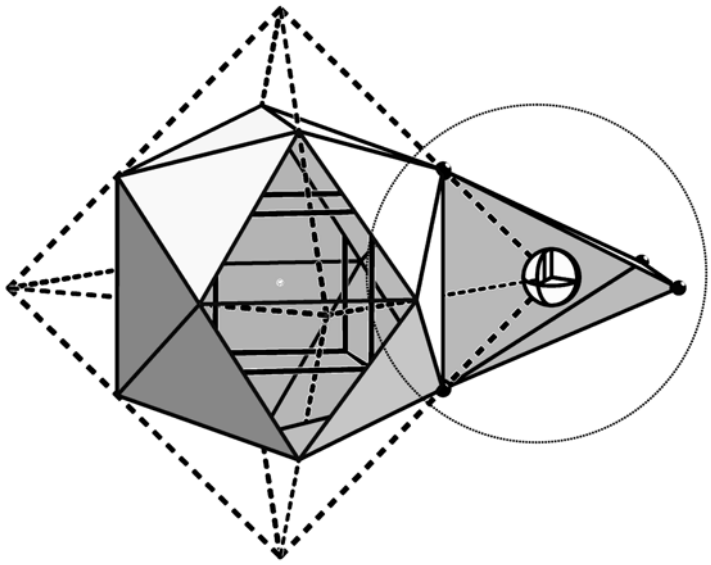

Fig. 3-14. The edge shared tetrahedron B unit in clathrate [Zn-Q]/[Pn-Q] system.

The Zn1 (*24d*) (site symmetry $\bar{4}$ . .) in the $F\bar{4}3c$ structural model is occupied on every vertex of a hypothetical octahedron. Consequently, the ZnI_4 tetrahedral unit (= B unit) in clathrate [Zn-Q]/[P_4Q_3] system shared one edge with every 6 edges of Q – Zn_4 – I_{12} icosahedral analogues (= A unit) as a bridging pattern (see **Fig. 3-14**). Zn1 atoms reside on a $\bar{4}$ symmetry site, and thus the bridging ZnI_4 tetrahedral unit (= B unit) have quite regular coordination and bonding. The orthogonal bridging pattern of the ZnI_4 tetrahedra, as viewed parallel to any of the cell axes, does not allow the necessary translational symmetry for a primitive cubic unit cell with 1/8 the volume.

The structural interpretation of tetrahedral B unit in host lattice of [Zn-Q]/[Pn-Q] will be presented by following procedure,

(i) for the purpose of comparison with other typical tetrahedral cations for instance In^{3+} in $KInI_4$, Tl^{3+} in $KTlBr_4$ or Ge^{4+} in Ge_6Cl_{16}, and in addition, recently $Sb(V)S_4$ tetrahedra in Werner type host / guest clathrate – $[Cu_8Sb(V)_3S_{13}]$ (-3) / $[Fe(NH_3)_6]$ (+3) crystalline compound reported, the definition of dimension for tetrahedral B unit is necessary as following **Fig. 3-15**.

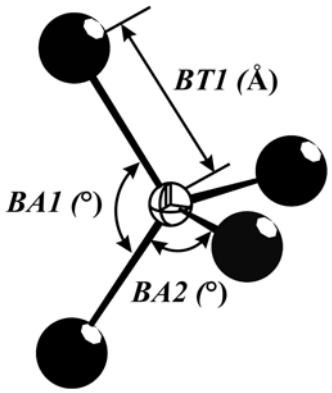

Fig. 3-15. The definition of dimension of tetrahedral unit (= B) for comparison with the structural analogues (horizontal direction, b).

(ii) a bond length (Å), BT1, of Zn1 (*24d*) – I1 (*96h*) unit is able to be directly compared with other tetrahedral fragments for instance bond length In1 (*24d*) – I1 (*96h*) in alkaliiodoindate $KInI_4$, B1 (*24d*) – O2 (*96h*) in boracite $Mg_3B_7O_{13}Cl$ and Ge1 (*8a*) – Cl1 (*32e*) in polymetalhalide Ge_6Cl_{16}. The bond angles (°), BA1 and BA2, of I1 – Zn1 – I1 and I1 – Zn1 – I1' units, respectively, are comparable with other tetrahedral units from typical molecular metal halides.

(iii) the results of dimensional properties from temperature dependent single crystal measurements provide an information about the thermal deformation of bridging tetrahedron ZnI_4 and a correlation between A and B structural unit.

(iv) In both S- and Se-based clathrate system, only B unit on *24d – 96h* atomic position is constant. Therefore, the approach in the synthetic point of view is essential to substitute ZnI_4 tetrahedron with other tetrahedral analogues.

According to above definition of dimension, the typical molecular metal iodide tetrahedra from ICSD were compared with B unit in clathrate [Zn-Q]/[P_4Q_3] system at room temperature as following **Table 3-8A** and the temperature dependent single crystal measurements as **Table 3-8B**.

Table 3-8A. The dimensional properties of ZnI_4 tetrahedron (= B unit) at 293 K in structural analogues.

		*$[ZnI_4]^{2-}$ in [Zn-Se]/ $[P_4Se_3]$	$[ZnI_4]^{2-}$ in [Zn-S]/ $[P_4S_3]$	$[InI_4]^-$ in $KInI_4$	$[BO_4]^{5-}$ in $Mg_3B_7O_{13}Cl$	$[SbS_4]^{3-}$ in $[Cu_8Sb_3S_{13}]$/ $[Fe(NH_3)_6]$	$GeCl_4$ in Ge_6Cl_6
length (Å) Zn2-I1	BT1	2.62(1)	2.62(1)	2.70(1)	1.48(1)	2.35(1)	2.08(1)
bond angle (°) I1-Zn-I1	BA1	115.5(1)	114.6(1)	112.4(1)	110.1(1)	113.1(1)	109.5(1)
bond angle (°) I1-Zn-I1'	BA2	106.6(1)	110.9(1)	108.0(1)	109.1(1)	107.7(1)	

*where the definition of dimensional properties are quoted from **Fig. 3-16**, and the case of BO_4 and SbS_4 tetrahedra follows a general meaning of tetrahedron.

Table 3-8B. The dimensional properties of B unit at 123, 173, 293, 393 and 423 K in Zizpse6144 by temperature dependent X-ray measurements.

		123K	173K	293K	393K	423K	$\frac{dy}{dT}$
length (Å) Zn2-I1	BT1	2.617(1)	2.617(1)	2.618(1)	2.619(1)	2.621(1)	1.3
bond angle (°) I1-Zn-I1	BA1	116.1(2)	115.9(2)	115.5(2)	115.1(2)	114.8(2)	-44.3
bond angle (°) I1-Zn-I1'	BA2	106.2(2)	106.3(2)	106.6(2)	106.7(2)	106.9(2)	21.0

dy/dT ; y is an angle or a length and T is temperature in K, d(length)/dT $\times 10^{-5}$ and d(angle)/dT $\times 10^{-4}$.

As the results from the examination of dimensional properties about ZnI_4 tetrahedral unit (= B unit) in clathrate [Zn-Q]/[P_4Q_3] system compared with the structural and functional analogues,

(i) the bond lengths ; BT1 of Zn1 – I1 unit showed same length in both S- and Se-based clathrate system, but bond angles ; BA1 and BA2 showed slight discrepancy from regular tetrahedron, 109.47^o (see **Table 3-8A**). Rather notable is the bond angle, BA1, in clathrate [Zn-S]/[P_4S_3] system. It is 114.6(1)^o at room temperature, which is almost the same value as the angle, BA1, in clathrate [Zn-Se]/[P_4Se_3] system, 114.8(2)^o at 423 K (see **Table 3-8B**). The angle, BA1, directly depends on the I – I distances of the icosahedral analogue A unit due to A-B-A' orthogonal bridging pattern.

(ii) with respect to the bond angles, BA1 and BA2, of ZnI_4 tetrahedron, BA1 showed obtuser angles, 110 ~ 116^o, in all the structural and functional analogues. Contrary to this, BA2 is acuter being 106 ~ 109^o except BA2 in the clathrate [Zn-S]/[P_4S_3] system (see **Table 3-8A**). As results, the tetrahedral B unit in clathrate [Zn-S]/[P_4S_3] system is rather expanded along every axis at room temperature than the B units in analogues of clathrate [Zn-Se]/[P_4Se_3] system for instance InI_4 in KIn_3I_{12}/K_2, BO_4 in $Mg_3B_7O_{13}Cl$ and SbS_4 in $[Cu_8Sb_3S_{13}]/[Fe(NH_3)_6]$.

(iii) according to the results from temperature dependent single crystal measurements, obtuser angle BA1 became to acuter ($dy/dT = -44.3\times10^{-4}$ °/K) and acuter BA2 to obtuser ($dy/dT = 21.0\times10^{-4}$ °/K), but the bond length BT1 is almost constant ($dy/dT = 1.3\times10^{-5}$ Å/K) in wide range of temperature (300 K) (see **Table 3-8B** and **Fig. 3-16**, **3-17**). This angle variation of B unit is believed as a main reason for variation of lattice constant as a function of temperature in clathrate [Zn-Q]/[Pn-Q] system. Consequently, the Zn1 position (the hypothetical vertices of a octahedron) at room temperature or lower rather approached to the icosahedral analogue A unit, and then approached to an ideal icosa-octahedral position by increasing the temperature [see **(b)** in **Fig. 3-17**].

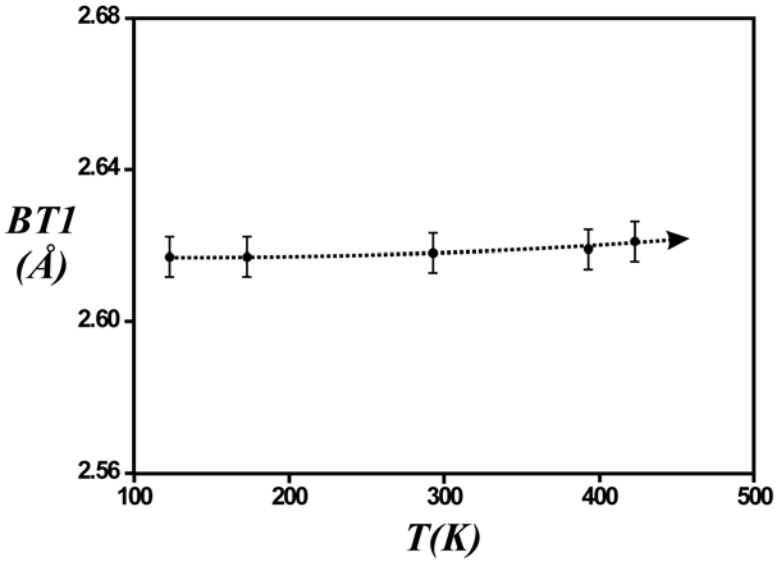

(a) bond length BT1

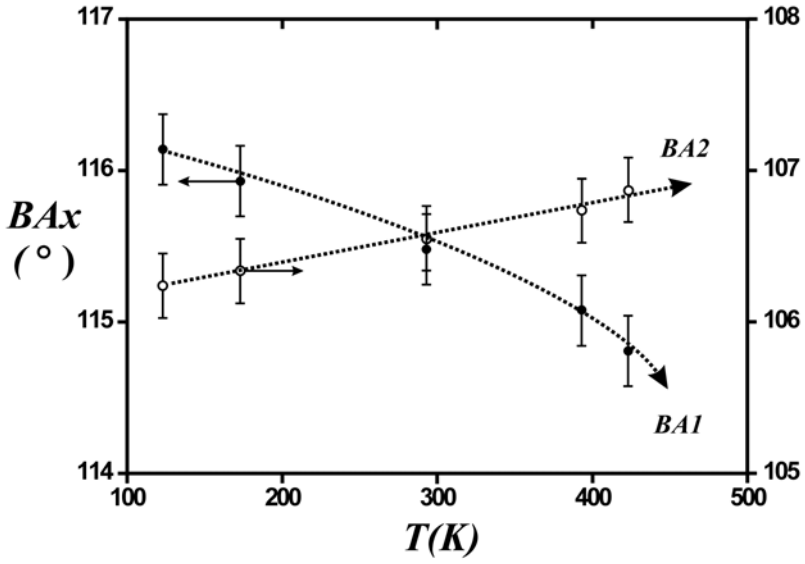

(b) bond angle BA1 and BA2

Fig. 3-16. The temperature dependent X-ray measurements of tetrahedron ZnI_4 (= B) unit in clathrate [Zn-Se]/[P_4Se_3] system.

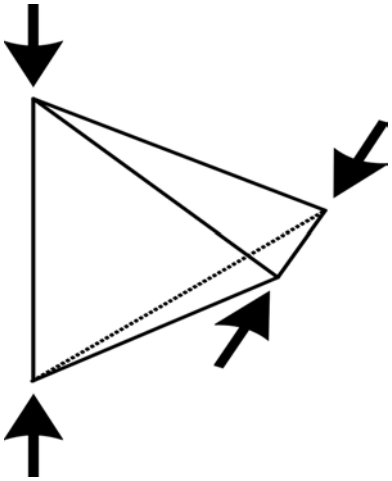

(a) angle distortion of Zn1 (*24d*) – I1 (*96h*)$_4$ tetrahedron

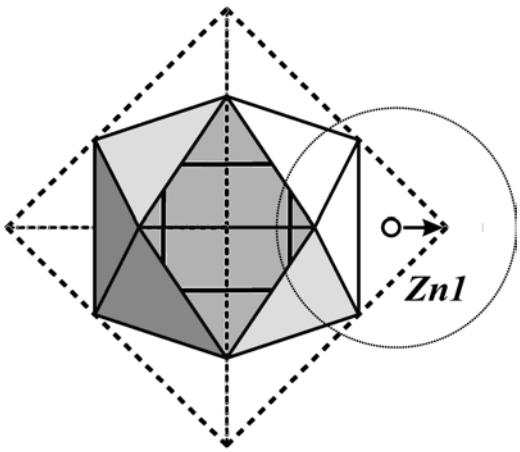

(b) Zn1 approach to an ideal octahedron-icosahedron

Fig. 3-17. The distortion of tetrahedron B unit by temperature dependent X-ray measurements.

(iv) the approach of Zn1 atom to an ideal octa-icosahedral position is able to be traced by some linked results, (1) the icosahedral analogue A unit in clathrate [Zn-Se]/[P_4Se_3] system approach to a regular shape with increasing the temperature, i.e., R1 = R2 = R3 for equilateral I – I distance and D1 = D2 = D3 = 138.19^o for a dihedral angle of a regular icosahedron, (2) a bond length, BT1, of Zn1 – I1 unit in tetrahedral B unit is almost constant over wide range of temperature. Therefore,

a structural correlation between icosahedral A unit and tetrahedral B unit by the golden ratio segment of octahedron is also quite questionable (see **Fig. 3-18**).

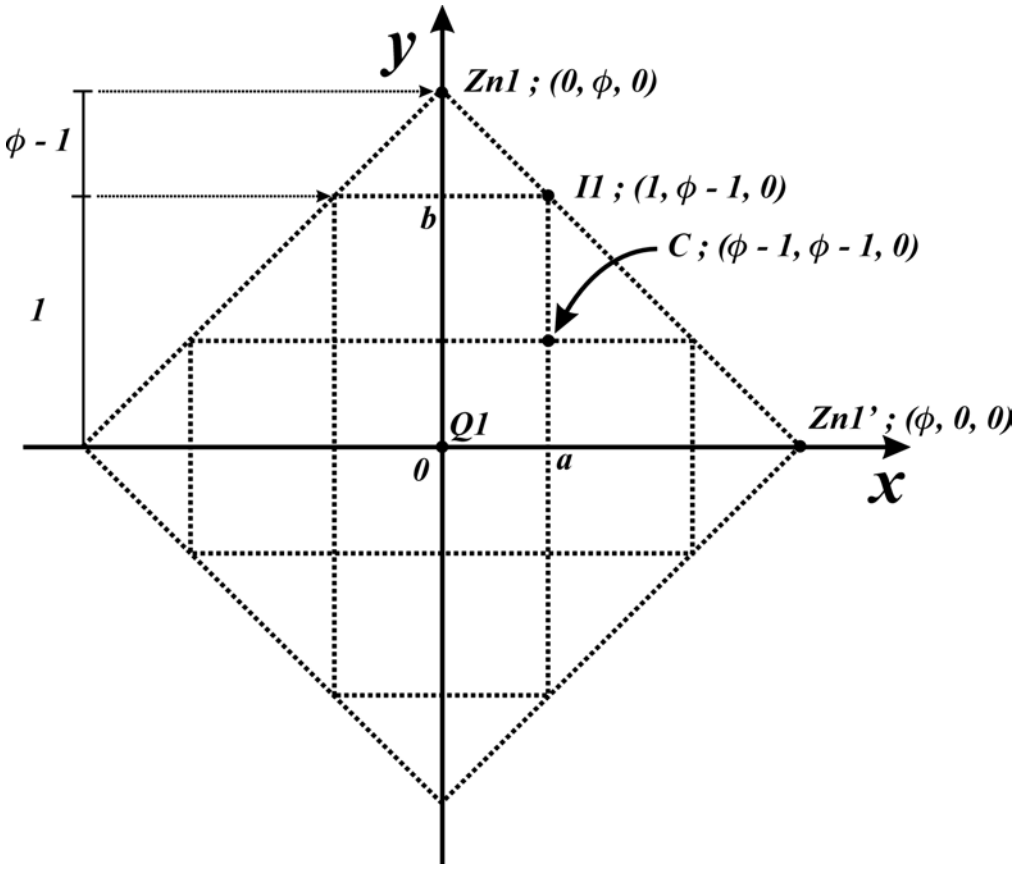

Fig. 3-18. The golden ratio segment of an octahedron into an icosahedron (2-D projection; where ϕ is the golden ratio).

For both the distances, Zn1 – I1 and Zn1' – I1, the following relationship is allowed with respect to the golden ratio (see **Fig. 3-18**). The crystallographical I1 atomic position, (*a*, *b*, ~0) (where $a < b$), which is a representative of 12 positions of the icosahedral vertices, in $F\bar{4}3c$ structural model is immediately convertible into (a/b, 1, 0) = (ϕ, 1, 0). Consequently, the atomic positions, I (*96h*) and Zn1 (*24d*) in clathrate [Zn-Q]/[P_4Q_3], can be described by the golden ratio segments, (1) with respect to structural A unit by the I atomic position and (2) with respect to the structural B unit by Zn – I bond length.

$$\phi = \frac{1}{\phi - 1} = \frac{\overline{Zn1 - I1'}}{\overline{Zn1 - I1}} = \frac{a}{b} \approx 1.618 \qquad (11)$$

In accordance with a definition [above Eq.(11)] about the golden ratio segments in clathrate [Zn-Q]/[P_4Q_3] system, the variation of I (*96h*) position and bond lengths, M (*24d*) – X (*96h*) and M (*24d*) – X'(*96h*) by temperature dependent variation with respect to the golden ratio, ϕ, is summarized in **Table 3-9** and depicted in **Fig. 3-19 (a)** and **(b)**.

Table 3-9. The variation of I (*96h*) position and bond lengths, M (*24d*) – X (*96h*) and M (*24d*) – X'(*96h*) by temperature dependent X-Ray measurements with respect to the golden ratio, ϕ.

temp.(K)	*a*/*x*	*b*/*y*	*c*/*z*	ϕ1	M1-I (Å)	M1-I' (Å)	ϕ2
[Zn-Se]/[P_4Se_3]							
123	0.1144(1)	0.1787(1)	-0.0007(1)	1.563(1)	2.617(1)	4.357(2)	1.665(1)
173	0.1141(1)	0.1786(1)	-0.0007(1)	1.566(1)	2.617(1)	4.364(2)	1.668(1)
293	0.1134(1)	0.1784(1)	-0.0007(1)	1.573(1)	2.618(1)	4.385(2)	1.675(1)
373	0.1129(1)	0.1782(1)	-0.0006(1)	1.578(1)	2.619(1)	4.400(2)	1.680(1)
423	0.1125(1)	0.1781(1)	-0.0008(1)	1.583(1)	2.621(1)	4.415(2)	1.685(1)
[Zn-S]/[P_4S_3]							
123	0.1144(1)	0.1774(1)	-0.0002(1)	1.550(1)	2.614(1)	4.307(2)	1.648(1)
293	0.1771(1)	0.1135(1)	-0.0004(1)	1.561(1)	2.615(1)	4.335(2)	1.658(1)
$KInI_4$							
293	0.1126(1)	0.1746(1)	-0.0021(1)	1.55(1)	2.70(1)	4.42(1)	1.64(1)
$KTlBr_4$							
293	0.1128(1)	0.1723(1)	0.0091(1)	1.53(1)	2.55(1)	4.09(1)	1.61(1)
[$Cu_8S_{13}Sb_3$]/[$Fe(NH_3)_6$]							
293	0.1102(1)	0.1771(1)	0.0040(1)	1.61(1)	2.35(1)	4.02(1)	1.71(1)

ϕ1 = *a*/*b*, ϕ2 = M-X'/M-X where M = Zn for [Zn-Q]/[P_4Q_3], In for $KInI_4$, Tl for $KTlBr_4$, Sb for [$Cu_8S_{13}Sb_3$]/[$Fe(NH_3)_6$], and X = I for [Zn-Q]/[P_4Q_3] and $KInI_4$, Br for $KTlBr_4$, and S for [$Cu_8S_{13}Sb_3$]/[$Fe(NH_3)_6$].

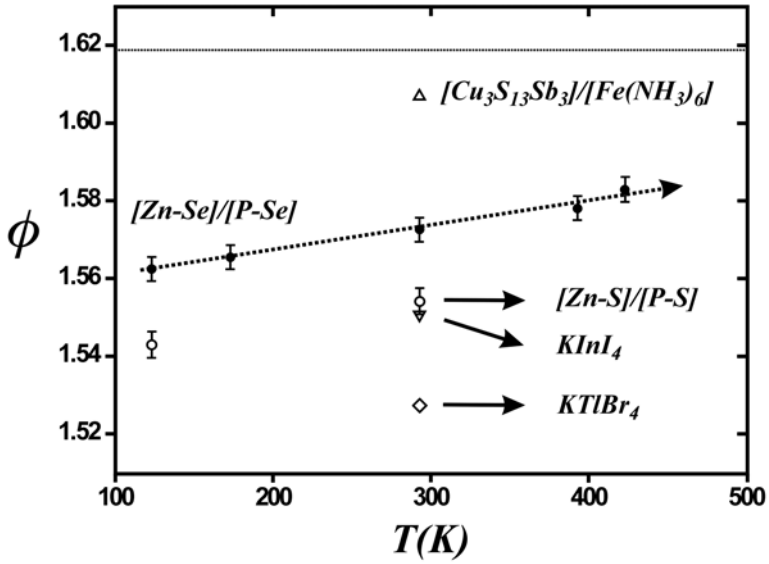

(a) variation of I1 (*96h*) position

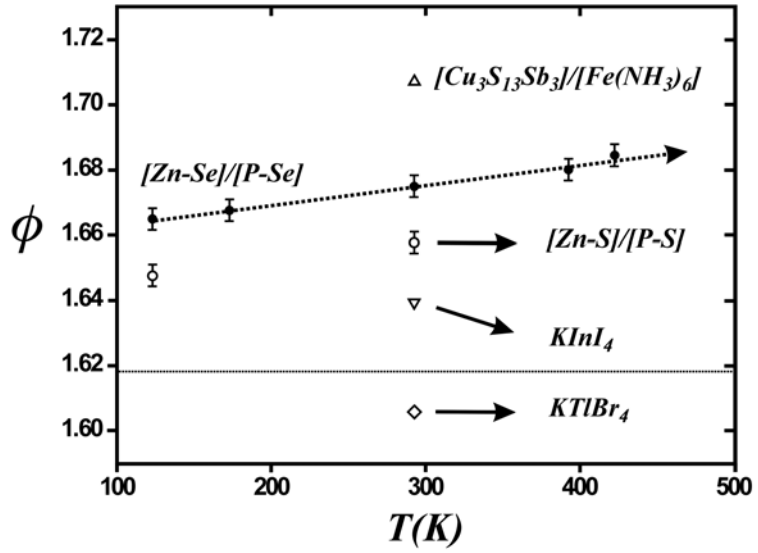

(b) variation of bond lengths, M (*24d*) – X (*96h*) and M (*24d*) – X'(*96h*)

Fig. 3-19. The comparison of golden ratio segments in clathrate [Zn-Q]/[P_4Q_3] system with other structural analogues with respect to the golden ratio, ϕ.

As the results under the assumptions, the icosahedral analogues in all the structural analogues showed the regularity over the wide range of temperature. Therefore,

a. the evaluated result, **Fig. 3-19**, indicates that (1) substituting on *8a* position for instance Se in [Zn-Se]/[P_4Se_3] with S in [Zn-S]/[P_4S_3] and constant on *24d* position for instance Zn1 in [Zn-Q]/[P_4Q_3], i.e., when the size of A unit becomes smaller constant size of B unit, the A unit slightly approaches to a disordered condition, but B unit approaches to a slightly more regular shape which is supported by the case of $KTlBr_4$, (2) when the size of the B unit becomes bigger constant size of the A unit for instance from [Zn-Se]/[P_4Se_3] to $KInI_4$ due to the size similarity of mutual A structural unit, also the A unit slightly approaches to a disordered shape, but B unit approaches to slightly a regular shape.
b. according to this evaluation, a structural formation of [$Cu_8S_{13}Sb_3$]/[$Fe(NH_3)_6$] analogue by a substitution of S by Se for structural A unit is geometrically unfavorable, but by a substitution of Sb by As for structural B unit should be geometrically favorable in the strong acidic condition. The problem of charge balance, +3 for intercalated guest molecule, however, is still remaining.
c. the appoach to the boracite family using ZnI_2, P and Q (Q = S, Se), if any, only allowed at very high temperature, around 1300 K due to the allowed extrapolation to a regular shape of A unit (see **Table 3-8A**).
d. the polymetal halides like Ge_6Cl_{16} and Si_6Cl_{16} which showed a different atomic distribution of A and B unit in $F\bar{4}3c$ space group with A and B unit of clathrate [Zn-Q]/[Pn-Q] system, i.e., the icosahedral analogue A unit occupies on the *8b* and tetrahedral B unit on *8a*. Therefore, the approach to a clathrate analogue using carbon group halides, if any, leads to two problems, (1) the edge-sharing possibility of very regular carbon group tetrahedral B unit with an icosahedral analogue A, and (2) the charge balance between host and guest.

3. 2. 2. 3. Host lattice/ I1 (*96h*) position

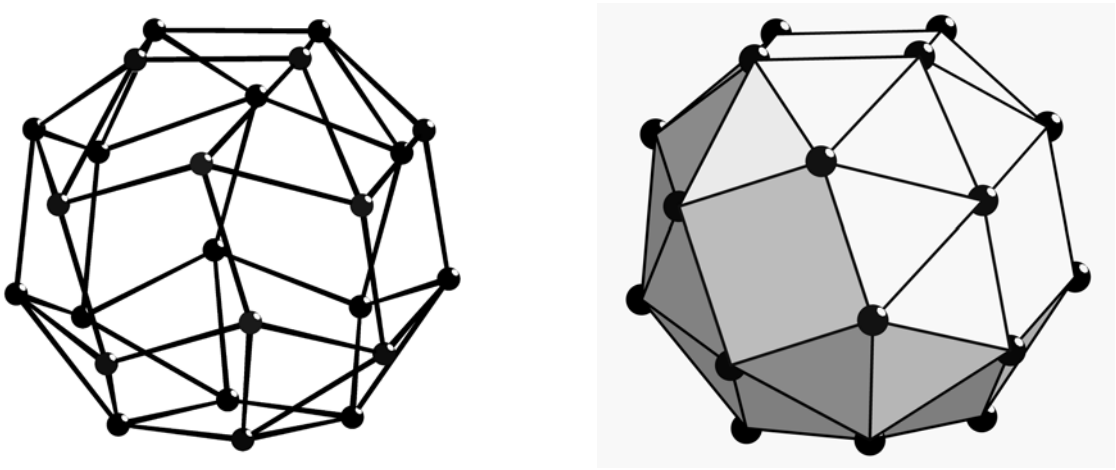

Fig. 3-20. I1 (*96h*) in clathrate [Zn-Q]/[P_4Q_3] system with respect to cavity (left) and snub cube ($3^4.4$) interpretation of I_{24} (right).

The atomic coordinates of I1 (*96h*) in $F\bar{4}3c$ space group and one of I1 (*96i*) in $Fm\bar{3}c$ space group are quite similar due to the convergence of z in I1 (*96h*) into 0, (x, y, ~0). Therefore, 4 × I1 atoms on rectangle face sharing snub cube (see **Fig. 3-20**) are located on the every rectangle plane in $Fm\bar{3}c$ space group also due to the operation of mirror plane, (m . .). The cavity structure in clathrate [Zn-Q]/[P-Q] system can be considered as the rectangle face sharing 8 snub cubes centering an icosahedron (see **Fig 3-20**). Therefore, the discussion about a snub cube is very important for whole structure interpretation.

As discussed in former section, the icosahedral analogues, A unit in clathrate [Zn-Q]/[P_4Q_3] system, showed quite similar with a shape of regular icosahedron with respect to the segments by a golden ratio, ϕ. The orthogonal pattern, A-B-A' of icosahedral analogues [see **(a)** in **Fig. 3-21**], however, leads that both edges in triangle and rectangle faces of hypothetical cuboctahedron be divided into segments with lengths in the ratio ϕ -1 : 1 [see **(b)**, **(c)** and **(d)** in **Fig. 3-21**].

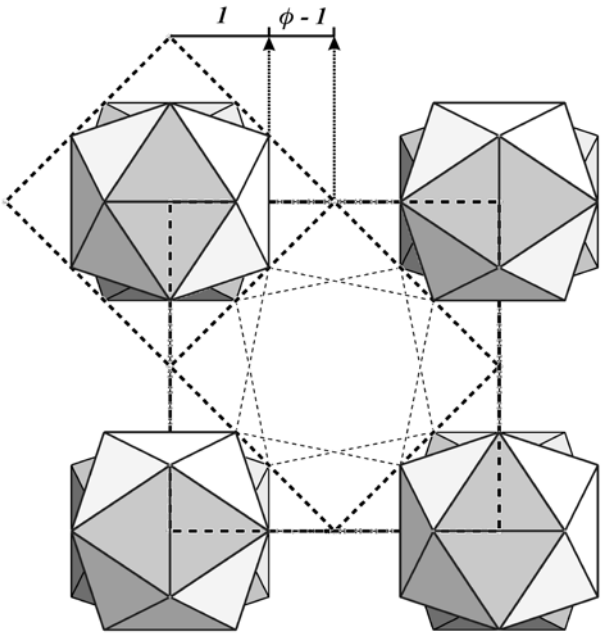

(a) the hypothetical Zn1 octahedra (dashed line) and A-B-A' alternating icosahedra (shadowed polyhedra)

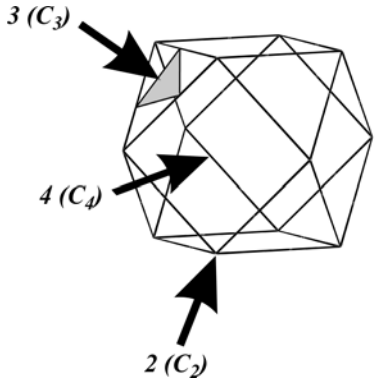

(b) the edge shared hypothetical cuboctahedra with Zn1 octahedra

(where a shadowed triangle indicates one face Zn – I_3 face)

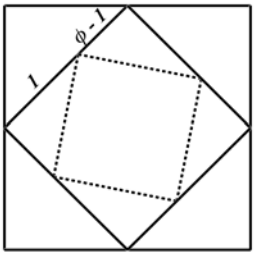

(c) the golden ratio segment into a triangle edge of cuboctahedra

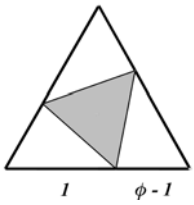

(d) the golen ratio segment into a rectangle edge of cuboctahedra

Fig. 3-21. The cuboctahedral interpretation of cavity structure.

In the $Fm\bar{3}c$ space group, if any, *8a* position (site symmetry ; m $\bar{3}$.) is occupied by Q1 atom and *96i* position (site symmetry ; m . .) by I1 which allows the element of point group symmetry of an icosahedra, I (or I_h), including an inversion center. Consequently, the center of cavity structure should have a site symmetry of *8b* position; (4 3 2) [see **(b)** in **Fig. 3-21** and **Fig. 3-22**], but the cavity structure has only a 4-fold rotation axis (site symmetry; 4 . .) with respect to a main axis [see **(a)** in **Fig. 3-22**]. Instead of that, a coupled symmetry operation is allowed along the 3-fold rotation axis with 2-fold rotation axis (site symmetry; 2 3 .), which is well matched with an identical site symmetry of *8a* or *8b* in the $F\bar{4}3c$ structural model. More precisely, in the $F\bar{4}3c$ structural model, a unified Zn2 (*64g*) position is divided into two distinguishable Zn2 (*32e*) and Zn3 (*32e*) positions, and no symmetry element is allowed for I1 position except an identical operation, 1. As a result, the $F\bar{4}3c$ space group is assigned as a the highest symmetry for clathrate [Zn-Q]/[P_4Q_3] system, even with consideration about which the guest molecule is excluded.

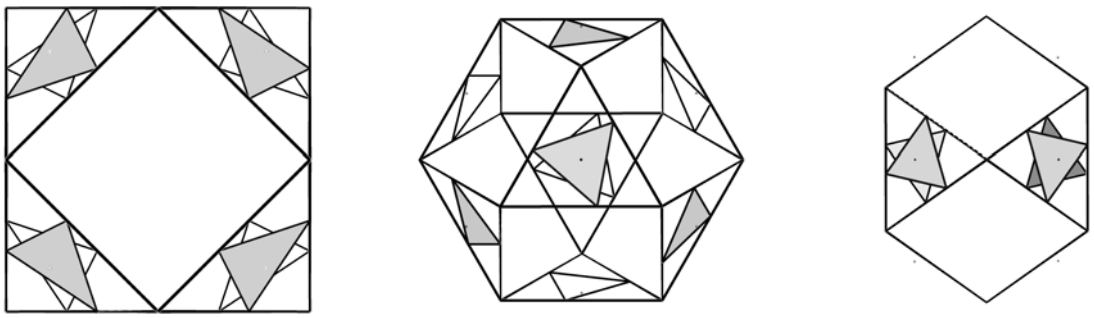

(a) 4 (C_4) rotation axis (b) 3 (C_3) rotation axis (b) 2 (C_2) rotation axis

Fig. 3-22. The symmetry elements in cavity structure.

Conclusively speaking, the I_{24} cavity structure was constructed by the staggered (along 3 and 4 fold rotation axes) Golden ratio segment of every triangle and rectangle faces of regular cuboctahedron. Therefore, a regular cuboctahedron was transformed into a snub cube. However, the I1 (*96h*) position in $F\bar{4}3c$ space group has no notable symmery element with respec to a cavity structure. Fortunately, an inner shape of cavity structure (see **Fig. 3-20**) is quite spherical due to the staggered golden ratio segments along every 3 and 4 fold axes. The

first approximation about a dynamic property of intercalated guest molecule will be discussed in the **Section 6**.

In the $I\bar{4}3m$ structural model for sodalite $Zn_8Se_2[BO_2]_{12}$, boron occupies the (1/4 , 1/2, 0) special positions (site symmetry ; 4 . .) and as a result, the boron atoms are represented by vertices of the truncated octahedral cage and are connected *via* bridging oxygens [see **(a)** in **Fig. 3-23**] and Se is located in the center of the cavity, surrounded by four Zn cations in a tetrahedral arrangement. The Zn cations are directed towards alternating 6-ring faces. This relationship between B and Zn in sodalite $Zn_8Se_2[BO_2]_{12}$ coincides with between I and Zn in clathrate [Zn-Q]/[P_4Q_3] system. This is belong to the coordination of I and Zn also. And the cationic unit $[SeZn_4]^{6+}$ is identical in both crystalline systems. The P(V) based-cubooctahedra in nitrido-sodalite $Zn_8Q_2(P_2N_4)_6$ (where Q = S, Se) in where P(V) atoms are connected by bridging N atoms which are directly linked by a cationic unit were already reported as the isotypes of sodalite $Zn_8Se_2[BO_2]_{12}$. The one edge length, N – N unit of Zn – N_3 polyhedra is 3.22 Å for $Zn_8Se_2(P_2N_4)_6$ system which is comparable with one, I – I unit, of Zn – I_3 polyhedra, 4.30 Å. This comparison is quite questionable with respect that $ZnBr_2$ or $ZnCl_2$ based composition with P and Se leads to sodalite analogue framework. Instead of sodalite, in boracite system the boron based cage showed a huge tetrahedral environment, i.e., a highly ordered cuboctahedral cage [see **(b)** in **Fig. 3-23**]. In the cavity structural point of view, the cage by I_{24} in clathrate (see **Fig. 3-20**) contains both the specific characteristics in sodalite and boracite [see **(a)** and **(b)** in **Fig. 3-23**].

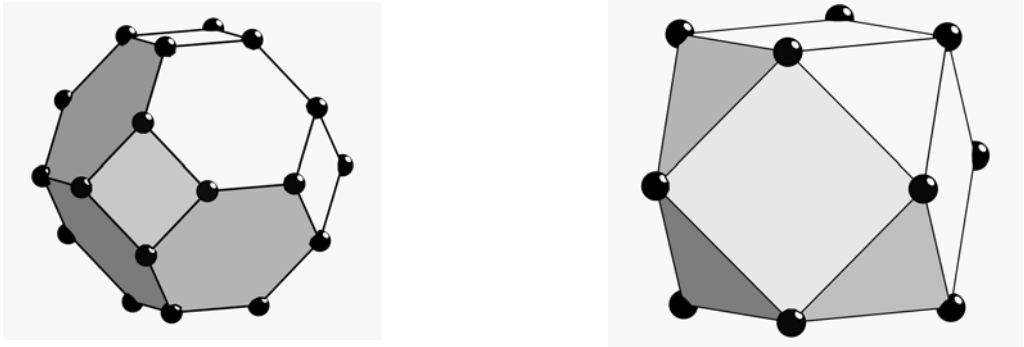

(a) truncated octahedron (4.6^2) of B_{24} in sodalite

(b) cuboctahedron (3.4.3.4) of B_{12} in boracite

Fig. 3-23. The comparison of a truncated octahedron in soldalite with a cuboctahedron boracite.

3. 2. 3. Guest molecule/ *32e*, *48g* and *96h* positions

All the crystallographic positions which are occupied by guest molecule showed a under-occupied status, and consequently the intercalated molecule(s) shows a highly disordered manner like a shape of 'football' (see **Fig. 3-24**) for instance the anisotropic displacement parameter for Se1 (*8a* in host lattice) is 0.02(0) Å^2 and for Se2 (*32e* in cavity) is 0.26(3) Å^2 at 293 K. As a conclusion, the exact dimensional properties of intercalated P_4Q_x molecule(s) could not be determined and even at 15K, by means of X-ray diffraction. The shortest distance, I1 - P1, is 4.00(1), I1 – Se2, 4.12(1) Å at 293 K for clathrate [Zn-Se]/[P_4Se_3] system, and I1 - P1 is 4.14(1) and I1 – S2 is 4.15(1) Å at 293 K for clathrate [Zn-S]/[P_4S_3] system. Therefore, no ordinary chemical bond exists between host lattice and guest molecule.
Therefore, the characterization of intercalated molecule(s) mainly depended on the solid state ^{31}P NMR spectroscopy and the molecule(s) were identified as P_4Q_x (where Q = S or Se and x = 3 and / or 4) cage molecule(s), especially the atom Q of guest molecule always coincides with the atom Q1 in special position of host lattice. In both models, $F\bar{4}3c$ and $Fm\bar{3}c$, the local site symmetries do not satisfy the symmetries of the phosphorus chalcogenide molecules for instance α-P_4Se_3 with C_{3v} symmetry and /or α-P_4Se_4 with D_{2d} symmetry.

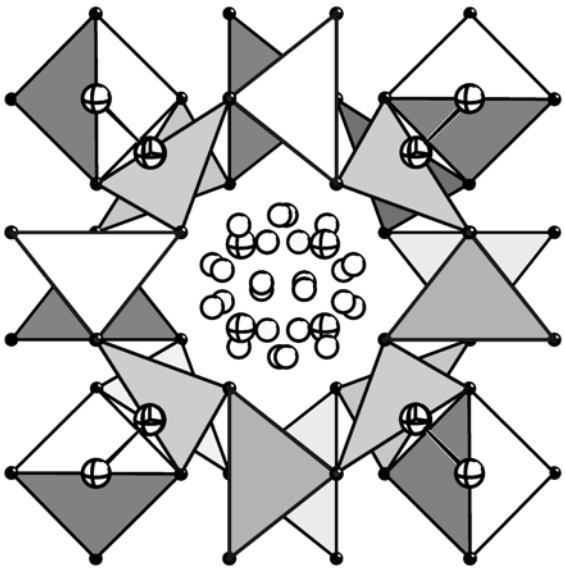

Fig. 3-24. The guest molecule in cavity structure.

In the crystallographic point of view, a point group symmetry, C_{3v} represents as an ideal pyramid with 3-fold-mirror plane (3 m) and D_{2h} as an ideal prism or planar object with an inversion center (m m m). Therefore, in order to describe such conformers, *a*-P_4Q_x (x = 3, 4), by means of crystallographic crystal systems, at least trigonal symmetry for P_4Q_3 and orthorhombic symmetry for P_4Q_4 are needed. However, the orthorhombic system were found (*Pnma* No. 62) for P_4Q_3 and the monoclinic system (*C*12/*c*1 No. 15) for α-P_4S_4 (the crystallographic data of Se conformer α-P_4Se_4 has not been reported yet)[101], because (1) such globular molecules are slightly deformed in the lattice of molecular crystal due to the weakly oriented intramolecular van der Waals forces and (2) the shapes of P_4Q_x molecules not allow the packing by an ideal pyramid or prism object. In spite of such a discrepancy between real molecule(s) and reported model molecule(s), the classical 'rigid-body refinement' (after this RB refinement) was adopted performed by following points;

(i) the clathrate [Zn-Se]/[P_4Se_3] system was examined in a wide range of temperature,

(ii) the RB refinement is limited on clathrate [Zn-Se]/[P_4Se_3] system using a model, α-P_4Se_3 which was reported by Rollo *et al.*, since only two cases of model were reported without temperature modification,

(iii) the mixed refinement using models, α-P_4Se_3 and α-P_4Se_4, was disregarded due to the lack of crystallographic data regarding conformer, α-P_4Se_4.

The results from RB refinement with clathrate [Zn-Se]/[P_4Se_3] system are quite complicate to project with 3-dimensional perspectives [see **(a)** in **Fig. 3-25**], since the intercalated chalcogenides consist of 7- or 8-membered atoms. For the convenience, only the refined locations of pivot atom (apical P atom) of globular P_4Se_3 molecule are focused to discuss. Therefore, it will be useful to project the results in 2-dimensions (*x*-*y*) instead of 3-dimensions. As a consequence, the other atom positions are automatically fixed at the counter side of pivot atom.

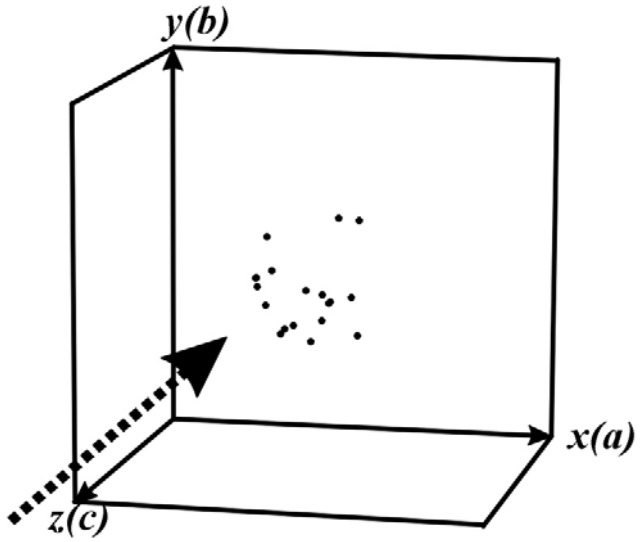

(a) 3-dimensional views

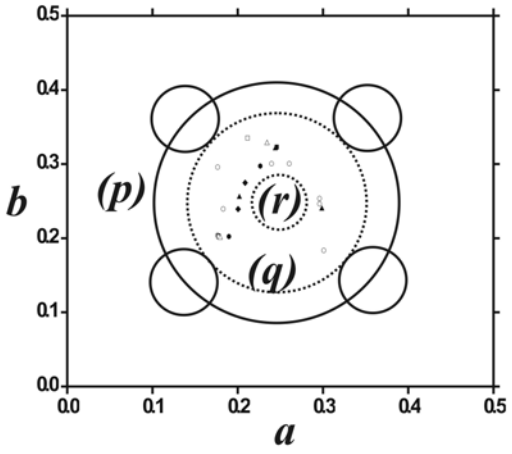

(b) 2-dimensional projection

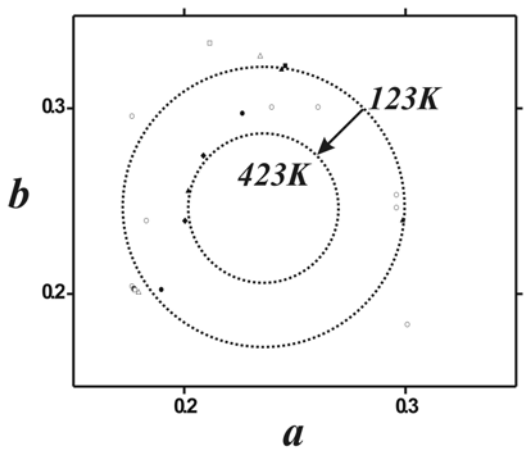

(c) 2-dimensional projection enlarged part of the circle (q) and (r)

Fig. 3-25. The RB refinement results with clathrate [Zn-Se]/[P_4Se_3] system with a model, α-P_4Se_3 [the circle (p), (q) and (r) see following text].

As the results, following points were discussed,

(i) the distribution of pivot atoms (apical P in P_4Se_3) shows a quite spherical tendency.

(ii) the solid circle, **(p)** in **Fig. 35 (a)**, indicates the average atom location of iodine atoms, since the coordinates of I1 (*96h*) were varied in a range of 0.1 ~ 0.2, (0.5 - 0.1) ~ (0.5 - 0.2) (*a* and *b*). the dotted circle, **(q)** in **Fig. 3-25 (a)**, indicates the distribution of refined apical P atoms of model guest molecule. The dotted circles in **Fig. 3-25 (c)** show a quite interesting aspect of guest molecule with respect to a dynamic property of guest molecule, i.e., the intra-molecular force between guest molecules not allows a mutual approach towards a middle of rectangle face of the snub cube.

(iii) **Fig. 3-25 (c)** is the enlarged part of circle **(p)** and **(q)** in **Fig. 3-25 (b)**. In accordance with increasing the temperature, the tendency of molecule approach toward the rectangle faces of snub cube shows that the average circle became smaller due to the increment of translational energy. It's a quite rough approximation, but well matched with common physical senses, i.e., a translational D.O.F (degree of freedom) of a particle motion in space should have 3 (see **Fig. 3-26**).

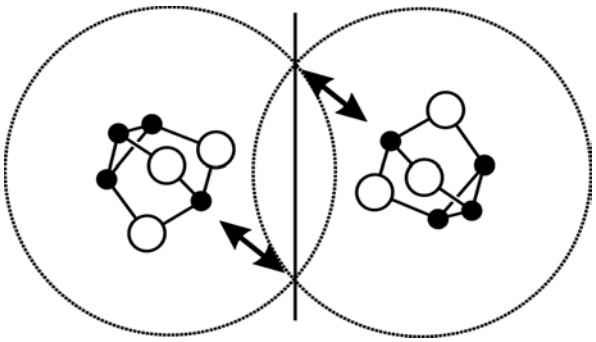

Fig. 3-26. The intra-molecular interference model of guest molecule.

(iv) a displacement trace from the refinement results is based on the difference between C_m and C_s [where C_m = center of mass, C_s = center of symmetry (*8b* in $F\bar{4}3c$)], since the most stable position of guest molecule might be fixed at *8b*, with respect to a center of mass at any given temperature, i.e., both center of mass and center of symmetry might be the same due to the force balance in cavity

structure. Therefore, if there is any contribution of motion (translation, rotation and vibration), the center of mass, C_m can be immediately reflected by the thermal motion of guest molecule. And the actual displacement of guest molecule (d_{eff}) in the cavity is defined as following Eq.(12),

$$d_{eff} = 2 \times |C_m - C_s|$$

$$|C_m - C_s| = \left| \sqrt{(x_{cm} - x_s)^2 + (y_{cm} - y_s)^2 + (z_{cm} - z_s)^2} \right| \quad (12)$$

(v) the effective displacements (d_{eff}) of guest molecule are depicted with function of temperature as following **Fig. 3-27**. The tendency of (a) in **Fig. 3-27** indicates that the effective displacements increase with temperature. The displacements, 0.3 ~ 0.5 Å, are huge quantities as compared with the isotropic displacement parameters. The whole tendency exhibits a quite good approximation with its physical concept, even though the RB refinement provides very low resolution with respect to the thermal parameters.

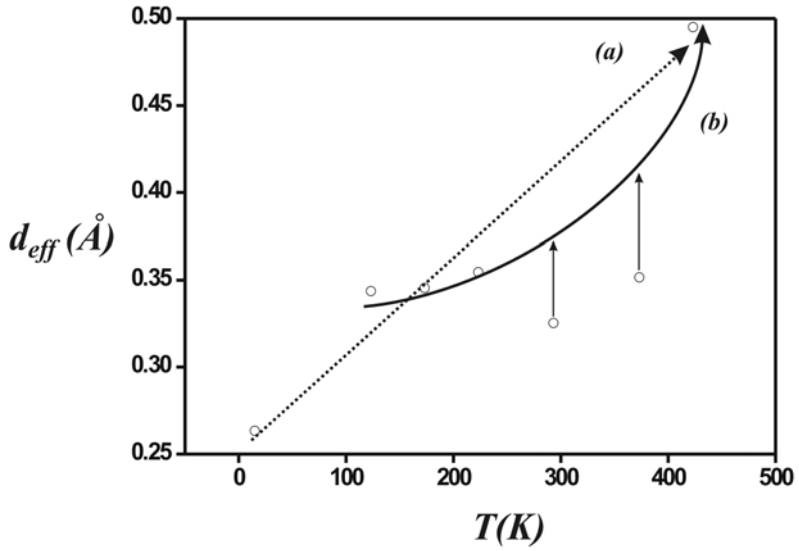

Fig. 3-27. The molecule displacement with function of temperature [(a) indicate a linear tendency and (b) resulted distance from Rigid body refinement].

4. The characterization by solid state MAS ^{31}P NMR spectroscopy

The ^{31}P NMR spectroscopy with respect to the generality concerning multiple and single bonds was deeply investigated and discussed by J. R. Van Wazer[102,103] in '50s. They suggested that the relationship between chemical shift and the various substituted atoms or radicals by using orthophosphoric acid as a reference, actually it is very rough approximation, but useful for initial stage of investigation (see **Fig 4-1**).

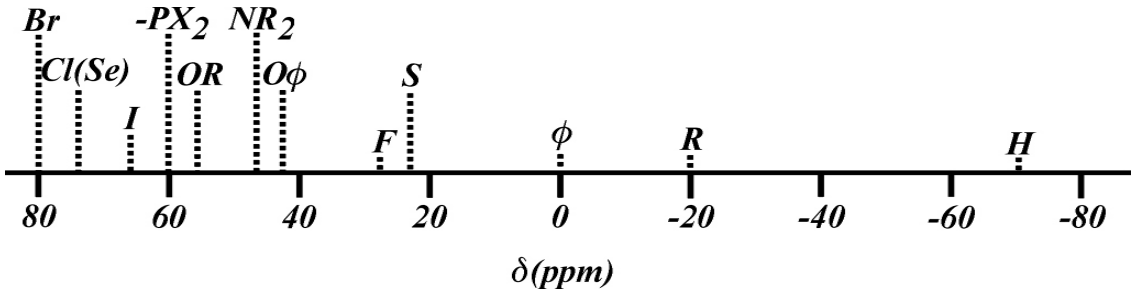

Fig. 4-1. The generalized resonance shift contribution of ^{31}P for various substituents (the chemical shifts are constructed by modern term; down field negative).

According to their reports, the chemical shifts for P_4 tetrahedral unit assigned to -450 ppm, P_3 (from P_4S_3) unit to -120 ppm and P-Se unit to +73 ppm, which was essential to consider about the characterization of [P-Q] guest molecule(s) in [Zn-Q]/[P-Q] clathrate system.
For more precious and refined characterization of such cage-type guest molecule(s) regarding the unidentified [P-Q] structural unit by means of X-ray tools,

(i) a powerful technique that avoids structural anisotropy factors in binary phosphorus chalcogenide system P_xSe_{1-x}, i.e., solid-state NMR spectroscopy including fast magic-angle-spinning (MAS), cross polarization (CP) and recently two-dimensional technique has been well developed by H. Eckert, *et al.*[12, 71] in collaboration with our work group[72].

(ii) from former crystallographic consideration about $[(ZnI_2)_6(ZnQ)]/[Pn_4Q_x]$ (Pn = P, As ; Q = S, Se) system, the disordered chalcogenide molecules were embedded into host framework, also observed no reasonable chemical bond between host

$[(ZnI_2)_6(ZnQ)]$ lattice and guest molecule $[Pn_4Q_x]$ by means of crystallographic tools.

(iii) with respect to a solvent/solute point of view, we were able to approach to the identification of disordered chalcogenide molecules. Solid state MAS ^{31}P NMR spectra resemble ^{31}P NMR spectra known from solution chemistry. This means the host lattice, actually mutually compensatory with [P-Q] guest molecule(s), provides a highly ordered environment for guest molecule(s) so that the anisotropic dipolar interferences are able to be minimized in the range of NMR time scale, which leads to sharp resonance.

(iv) the structure of [As-Se] guest molecule in Zizasse6144 crystalline compound which is supposed to be a [Zn-Se]/[As-Se] clathrate system, derived single crystal measurements is still unclear due to the difficulty of As (I = 3/2) NMR measurements. This nucleus can only be detected in a very symmetrical environment due to the large quadrupole moment of ^{75}As.[104] The first tetrahedrally coordinated arsenic halogen compounds characterized by ^{75}As NMR spectroscopy were the $AsCl_4^+$ and the $AsBr_4^+$ cations recently published by Schrobilgen *et al.*[105].

As the results, quite simple spectra were obtained for all measured [Zn-Q]/[P-Q] crystalline compounds and the following points for the interpretation of spectra have to be considered,

(i) the measured chemical shifts were compared with well reported data of binary P-Q (where Q = S, Se) compounds which have been performed in both the solid state and solution phase. Consequently,

(ii) the difference or resemblence between the chemical shifts in the solid state measurement and the solution phase measurement was discussed with respect to the following points,

(a) the area integral of measured peaks provides a useful information about both, the composition of intercalated molecule with a single occupancy in the host lattice and the rough composition ratio of intercalated molecule(s) with different structures.

(b) the chemical environments of intercalated molecule(s) play a main role for a dipolar spin coupling mechanism. Therefore, the chemical shifts can be immediately reflected by varying the nature of environment and the temperature. This will be discussed in next section.

(c) the center of spherical snub cube provides an isotropic nature to the intercalated guest molecule(s) which is able to compensate the procedure of magic angle spinning technique for ^{31}P MAS NMR spectroscopy. Consequently, the single crystal static ^{31}P NMR spectroscopy with respect well identically separated guest molecule(s) should be accessible for an ongoing research.

(iii) one of the P-Se binary conformers, the intercalated α-P_4Se_4 molecule, which has been seldom characterized by means of crystallographic tools, ir/Raman spectroscopy and ^{31}P NMR spectroscopy was identified by analyzing the measured chemical shifts from the crystalline compound Zipse334 and Zizpse6147 compared with Zizpse6144. The later showed solely intercalated P_4Se_3 molecule in host lattice.

4. 1. P_4S_3 molecule in Zizps6144

The following **Fig. 4-2** presents a ^{31}P MAS NMR spectrum of Zizps6144 crystalline compound which was interpreted by a sequential procedure,

(i) the area integral of measured peaks for rough information about the composition of intercalated molecule(s) due to relative strong main peaks compared with spinning side bands,

(ii) the comparison of measured chemical shifts with well reported data concerning P-S binary cage molecule(s),

(iii) the evaluation of chemical / physical environment effects to the chemical shifts of intercalated molecule(s),

(iv) the rough estimation of molecular geometry in host lattice through above consideration.

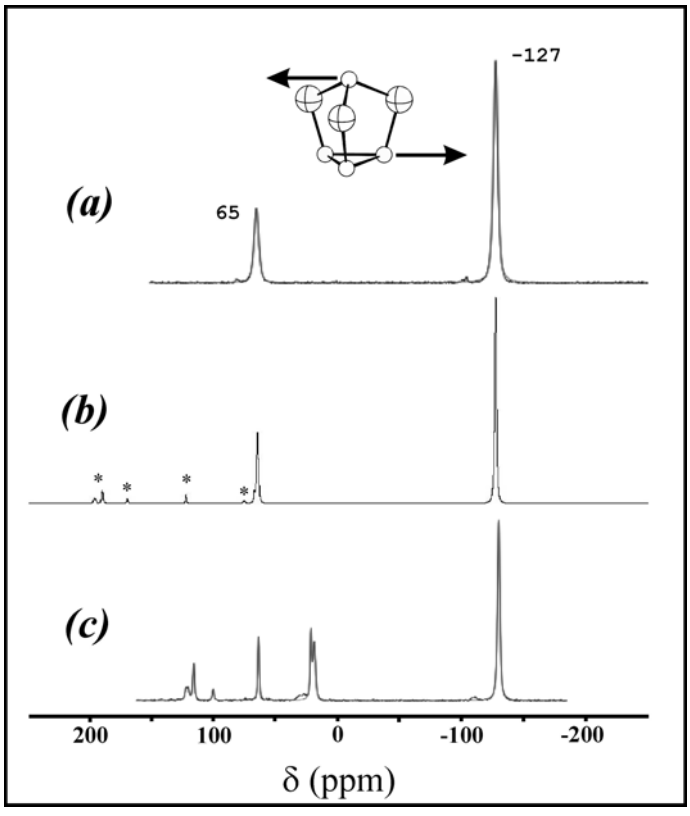

Fig. 4-2. ^{31}P-MAS-NMR spectra of $[(ZnI_2)_6(ZnS)]/[P_4S_x]$ [* indicate the spinning side bands and (a), (b) and (c) is related to Zizps6143, Zizps6144 and Zizps6145, respectively).

The chemical shift for the apical P (which is actually quartet due to the magnetic quantum number of S, $I = 3/2$) is centered at 65.4 ppm and the one for the basal P (doublet) at -129.9 ppm, which were compared with the results by other [see **(b)** in **Fig. 4-2** and **Table 4-1**, the spectra, **(a)** and **(c)**, were recently measured]. According to the comparison, the spectrum shows that the α-P_4S_3 molecule relatively well embedded into the [Zn-S] host lattice, also the asterisks indicate spinning side bands, and one of these bands may indicate the α-P_4S_4 molecule (G. Sheldrick *et al.*[106] reported the chemical shift 89.4 ppm from external P_4O_6 with respect of CS_2 solution). The ratio of area integrals from the downfield shift is 22.7 % : 77.3 % and is able to be elucidated as a ratio of 23 : 26 ≈ 1 : 1 = *n*[P-S_3] : *n*[P_3-S_3] with respect to the equivalent species. The P_4S_3 molecule has been widely investigated in the field of P NMR spectroscopy due to the stability of binary P-S cage molecules in various solvents. This will be discussed in the following section.

Table 4-1. The comparison of reported chemical shifts from ^{31}P-NMR spectra of P_4S_3 molecular crystalline compounds with Zizps6144.

	chemical shift [ppm]									
δ_B	-121	-100 ~ -135	-124.5 (1.5)	-87.9 (1.5)	-73.2 (1.5)	-70.8 (1.5)	-113 (5)	-103 (10)	-87 (16)	-126.9
δ_A	68	62 ~ 79	112.3 (1.5)	100.1 (1.5)	95.2 (1.5)	70.8 (1.5)	72 (5)	72	89 (8)	65.4
J_{AB} [Hz]	71	-	-	-	-	-	70 (3)	-	-	-
temp. (K)	293	293	309	327	333	351	293	293	293	293
phase	SS [1]	VS [2]	S [3]	S	S	S	α [4]	β [4]	β [4]	α [5]
Refs.	107	108	109	109	109	109	110	110	110	this work

1. SS = Saturated solution in CS_2/Benzol-d_6, simulated by PANIC from Bruker (0.2 Hz/pt).
2. VS = various 23 solvents, 36.45 MHz.
3. S = 10mg of P_4S_3 were dissolved in 250 mg of EBBA (see **Fig. 4-6**)
4. α = alpha, β = beta indicate solid phase; MAS (magic angle spinning) solid state-NMR spectra at 121.65 and 121.46 MHz with variable spinning speeds (5.0 ~ 14.0 kHz).

5. α = alpha indicates solid phase; MAS (magic angle spinning) solid state-NMR spectra at 162.01 MHz (spinning speed = 25 kHz).
6. All the chemical shift data are related to 85 % H_3PO_4 (downfield shifts positive).

Conclusively speaking,

(i) the ratio of area integrals with respect to the apical P vs. basal P atoms showed a strong evidence of intercalated P_4S_3 molecule in Zizps6144 crystalline compound.

(ii) all the results (see **Fig. 4-3**) have *a good approximation to solution measurements, but not to the solid state measurements*. It means that the P_4S_3 molecule with respect to solute manner were well embedded into the [Zn-S] host lattice with respect to solvent manner in solution chemistry. Consequently, this clathrate [Zn-S]/[P-S] system resembles a solution behavior.

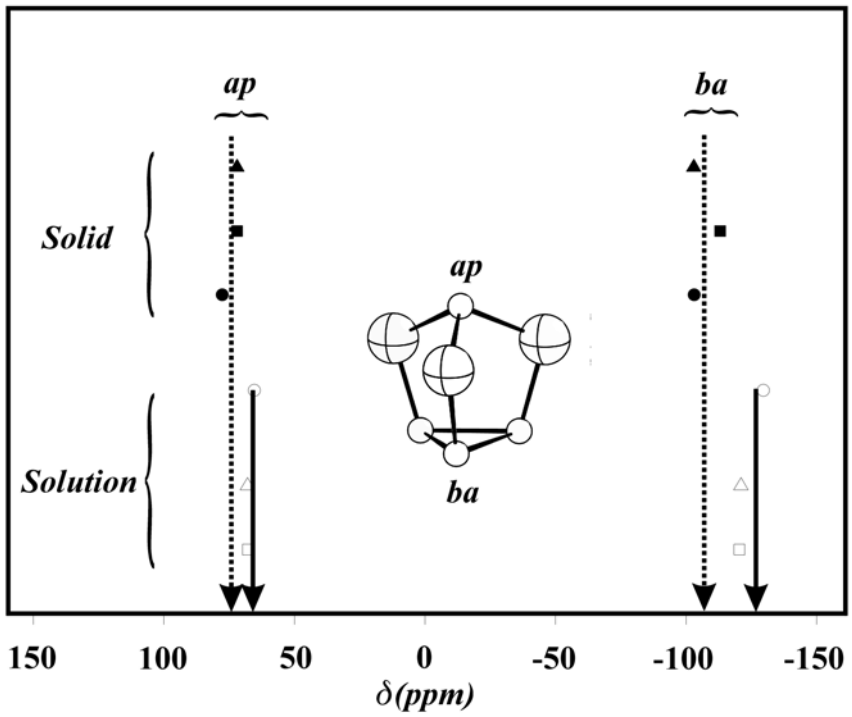

Fig. 4-3. The direct comparison of chemical shifts between the solid state measurements and solution phase measurements (dotted allows indicate the results from solid ^{31}P NMR spectra and solid allows indicate the result from solution ^{31}P NMR spectra comparable with this work ; δ_A = 65.4 and δ_B = -126.9 ppm).

(iii) as concluded in the crystallographic section, the intercalated guest molecule(s) have no ordinary chemical bond with its environment, i.e., with the host lattice.

(iv) consequently the guest molecule is solvated into host framework, just like a solute-solvent relationship in solution chemistry.

(v) as an ongoing research, the solute/solvent approach leads us to a possibility for detecting such a species with single crystal static ^{31}P NMR measurement. This could also solve the dynamic properties of guest molecule for instance tracing the line widths of measured spectra as a function of temperature.

4. 1. 1. The chemical shift dependency on the solvents and the concentration of P_4S_3

The next two sections present the comparisons of the measured results of [Zn-S]/[P-S] crystalline compound by means of solid state ^{31}P MAS NMR measurement with the reported data from solution NMR measurements. Specially the two different kinds of experiments were reported by

(i) G. Heckmann and E. Fluck[108] with respect to *the chemical shift dependency on the solvents and the concentration*, and

(ii) N. Zumbulyadis, *et al.*[109] with respect to *the chemical shift dependency on the temperature in a fixed solvent.*

Both reports are quite useful to understand a correlation between the environment of intercalated guest molecule(s). The host lattice or a similar solvent and the guest molecule including the mutual molecular forces and own molecular geometry.

The spectra of P_4S_3 which was measured in various organic solvents are summarized and compared with the spectrum of Zizps6144 in **Fig. 4-4**.

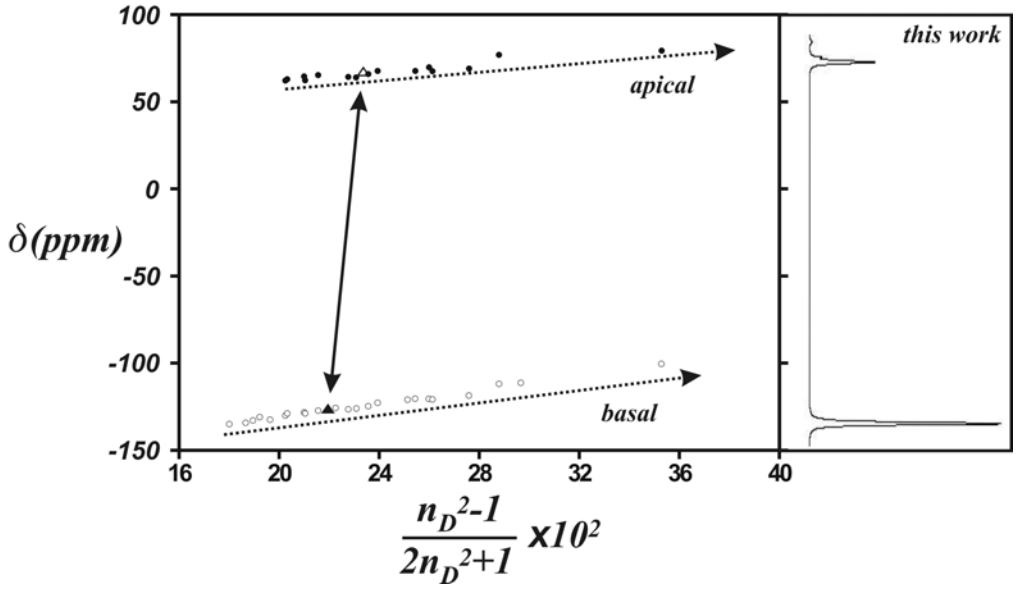

Fig. 4-4. The chemical shift dependency in various chemical solvents (figure is reconstructed by the modern term 1 ppm = 36.45 Hz, downfield shifts positive and open, solid triangle indicates chemical shift of apical P, basal P, respectively, by this work).

The measured chemical shifts show a very good linear relationship with the reflective index term (n_D) with respect to both, doublet (basal P) and quartet (apical P) splitting. The centered chemical shifts vary with the same tendency, keeping a difference ($|\delta_B - \delta_A|$) between chemical shift by apical P and by basal P. Also with small deviation the difference is reduced by the increment of solvent concentration (see **Fig. 4-5**), i.e., by the increment of the London dispersion force of molecule, since the London force relates closely to van der Waals force. Heckmann and Fluck assumed the contribution of London force between molecule and solvent to total chemical shift macroscopically as following Eq.(13),

$$\delta_n \propto \frac{n_D^2 - 1}{2n_D^2 + 1} \tag{13}$$

where δ_n is the contribution of London force between the solvent and molecule to total chemical shift, and n_D is the reflective index of the solvent, i.e., the x increment [the increment of right term of Eq. (13)] expresses the increased London force. The dipole moment contribution of host lattice to the guest molecule(s) can be expressed by the relationship of solvent to solute. As a results, the chemical shift by basal P is centered between $OPCl_3$ and $CH_3(CH_2)_{10}CH_2I$ and the one of the apical P is centered between PCl_3 and Thiophen. Also the chemical shift variation with solvent concentration shows almost same values, i.e., -2 ppm changed by the increment of concentration, but the tendency is clear, decreasing with respect to $|\delta_B - \delta_A|$ (see **Fig. 4-5**).

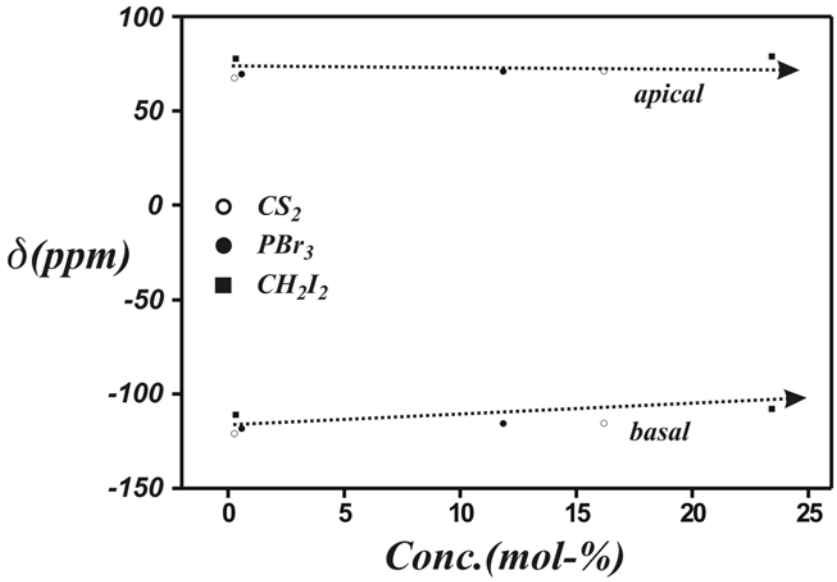

Fig. 4-5. The chemical shift dependency of P resonances as a function of P_4S_3 concentration.

4. 1. 2. The chemical shift dependency of P_4S_3 on the temperature in a fixed solvent

Also with the P_4S_3 molecule, a very interesting experiment was performed by N. Zumbulyadis *et al.*[109], who used the nematic solvent EBBA (*p*-ethoxybenzylidene-*p'*-n-butyl-aniline) (see **Fig. 4-6**) in order to determine the shielding anisotropies during temperature variation. Consequently, this is in order to confirm coupling constant J_{pp} between the apical and basal phosphorus atoms, since to study the AX_3 system, like P_4S_3 and P_4Se_3, in the nematic phase provide also a convenient means to determine the sign of the scalar coupling constant J_{AX}.

Fig. 4-6. The molecular structure of liquid crystal EBBA.

The main advantage of using such a nematic solvent is to make a regular solution which provides a well ordered displacement or environment for solute molecule. The summarized result of temperature dependent NMR measurement with fixed solvent is as following **Fig. 4-7**.

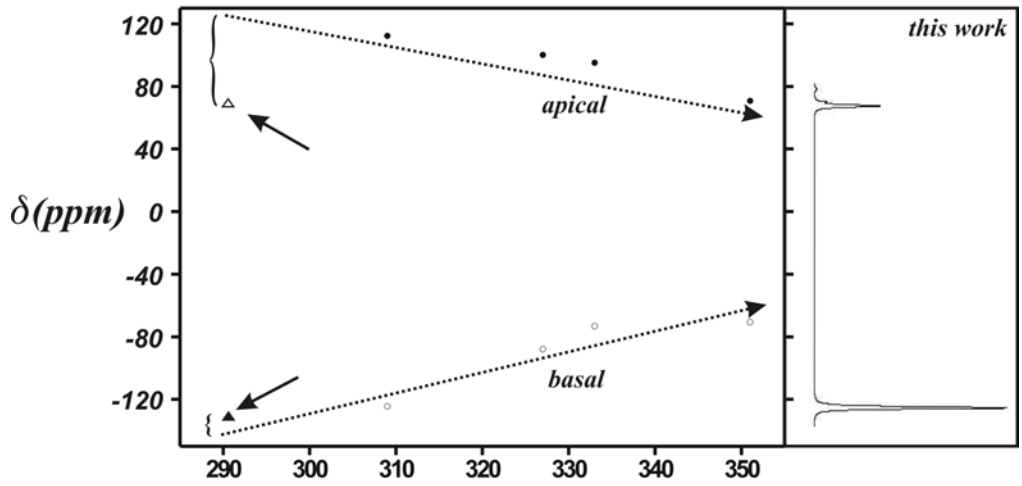

Fig. 4-7. The chemical shift dependency of P_4S_3 in EBBA with temperature variation (the allowed triangle indicate this work).

According to N. Zumbulyadis *et al.*, the dipolar coupling constants are given by

$$D_{ba-ba} = \left(\frac{\hbar}{4\pi}\right)\frac{\gamma_P^2 S}{r_{ba-ba}^3} \tag{14}$$

$$D_{ap-ba} = \left(\frac{\hbar}{4\pi}\right)\frac{\gamma_P^2 S P_2 \cos\theta}{r_{ap-ba}^3} \tag{15}$$

where θ is the angle between C_3 axis of P_4S_3 and r_{XY} (XY = apical P atom-basal P atom or basal P atom-basal P atom). They deduced the general relationship of splittings, i.e., apical and basal splitting respectively, using the spin hamiltonian, as follows,

$$\Delta\nu_{ap-ba} = 2D_{ap-ba} + J_{ap-ba} \tag{20}$$

$$\Delta\nu_{ba-ba} = 3D_{ba-ba} \tag{21}$$

Therefore, we can compare the results of above two different cases, i.e., the chemical shift dependency on various solvents and on temperature, with our result from solid state ^{31}P MAS NMR measurement of Zizps6144 with included P_4S_3.

(i) the chemical shift of basal P is a predominant term to decide the dipole moment contribution of solvents to dissolved molecules. It means that the direct bonded basal P-P is rather less affected by changing environments than the non-direct bonded apical P---P (see **Fig. 4-4** and **Fig. 4-7**).

(ii) according to measured results from Zizps6144 crystalline compound, the chemical shift of basal P unit in P_4S_3 molecule (in Zizps6144 crystalline compound) is centered between the chemical shift data of $OPCl_3$ solvent system and one of $CH_3(CH_2)_{10}CH_2I$ solvent system. The chemical shift of apical P unit in P_4S_3 molecule (Zizps6144 crystalline compound) between one of PCl_3 and one of Thiophen solvent system (see **Fig. 4-4**).

(iii) the environment of P_4S_3 guest molecule in Zizps6144 crystalline compound should have a quite low reflective index compared with normal various solvents. It means that [Zn-S] host - [P_4S_3] guest system exhibits a very dilute concentration of P_4S_3, since **Fig. 4-4** indicates that the chemical shift by basal P is quite lower than one by normal solvents, and since the **Fig. 4-5** indicates that an increased concentration of solvent (closer distance between molecules) provides a slightly narrower difference ($|\delta_B - \delta_A|$). And the chemical shift by apical P has a direct dependency on the molecule geometry, i.e., the vertical elongation or equatorial expansion. Actually the geometry of basal P is almost fixed at any given condition, only the temperature effect is able to change such a geometry. Therefore, at any fixed temperature, the dipolar coupling of basal P is not significantly changed by different solvents (see **Fig. 4-4**). Comparing measured results in a nematic solvent EBBA at room temperature with [Zn-S] host, the chemical shifts of basal P are almost the same, but those by the apical P are quite distinguishable (see **Fig. 4-7**).

(iv) the nematic solvent EBBA provides a more elongated environment for geometry of P_4S_3 molecule than [Zn-S] host, since according to a temperature dependent

measurement, especially at high temperature, both chemical shifts by apical P and basal P unit approach to an isotropic chemical shift. It means that with increasing temperature the P_4S_3 molecule approaches a spherical geometry in nematic solvent EBBA, even at 351 K (78 ^oC) (see **Fig. 4-7**).

(v) the interaction of 'normal' (completely isotropic) liquids with dissolved P_4S_3 is comparably small and therefore, P_4S_3 molecules are quite undistorted. A liquid is not structured, but a nematic phase and also the phase of [Zn-S] host are structured. The normal solvents provide the best spherical environments for P_4S_3 molecule. The order of spherical environments are 'the normal solvents < Zn-S host < EBBA', and the 23 normal solvents which are investigated by G. Heckmann and E. Fluck showed almost same tendencies. The increment of solvent concentration provides more spherical environments for solute P_4S_3 molecule. Conclusively speaking, the reason why more spherical environments is provided by using 23 normal solvents is probably based on the molecule dynamics in solution, i.e., the smaller or lighter solvent molecules transfer those own energy to relative static solute P_4S_3 molecule through the molecular collision. To the contrary to this, a structured solvent like EBBA or [Zn-S] host framework is so static that the interface between solvent and solute is able to be mainly maintained by the motions of solute molecule including translation, rotation and vibration.

4. 2. P_4Se_x (x = 3, 4) molecules in Zipse334 and Zizpse6147

As mentioned, solid state ^{31}P NMR spectroscopy is a quite powerful tool to identify crystallographically disordered chalcogenide molecule(s) at least with respect to a qualitative identification. The main difficulty for the interpretation of measured spectra, however, is a lack of related experimental data by both solid state and solution phase NMR measurement concerning α-P_4Se_4 as a conformer of binary P-Se cage molecules. Instead of that, the measured P NMR data with P_4Se_3 in both, solid state and solution have been well reported. The interpretation of the spectra of [Zn-Se]/[P_4Se_x] is based on the measured data for P_4Se_3. Finally a remaining peak is interpreted as one for α-P_4Se_4 conformer.

The following **Fig. 4-8** presents the measured ^{31}P MAS NMR spectra by Zizpse6144, Zipse334 and Zizpse6147 crystalline compounds which were interpreted by the same in the case of Zizps6144,

(i) the area integral of measured peaks for rough information about the composition of intercalated molecule(s) due to relative strong main peaks.

(ii) the comparison of measured chemical shifts with well reported data concerning P-Se binary cage molecule(s),

(iii) the evaluation of chemical / physical environment effects to the chemical shifts of intercalated molecule(s),

(iv) the rough estimation of molecular geometry in [Zn-S]/[P-Se] by the considerations described in **Section 4.1**.

The spectrum **(a)** in **Fig. 4-8** shows an ideal spectrum of P_4Se_3, i.e., the two separated peaks impose that Zizpse6144 has two different kinds of P atom with a rough area integral ratio 1 : 3 (area integrals with %; 8 % : 23 % : 70 %). That means that the Zizpse6144 crystalline compound was well formed with the [Zn-Se] host and the [P_4Se_3] guest as the only guest molecule. The more dramatic aspects of molecule substitution are the followed spectra. Both spectra **(b)** and **(c)** in **Fig. 4-8** impose that there are additional guest molecules present. The **(b)** and **(c)** in **Fig. 4-8** indicate the spectra of Zipse334 and Zizpse6147, respectively. The area integrals showed the ratio of components roughly. For instance, in the case of spectrum

(b) in **Fig. 4-8**, the ratio of integrals for the signals at 90, 35, and -120 ppm is 1 : 3 : 9. The second and third peak indicate P_4Se_3 analogues to spectrum **(a)** in **Fig. 4-8**. The peak ratio shows very good approximation with an ideal value, 1 : 3. The ratio between the first and the second signal indicates the ratio between the 2 equivalents [P_2-$(Se_{1/2})_4$ fragment] of α-P_4Se_4 and apical P-Se_3 unit in P_4Se_3.

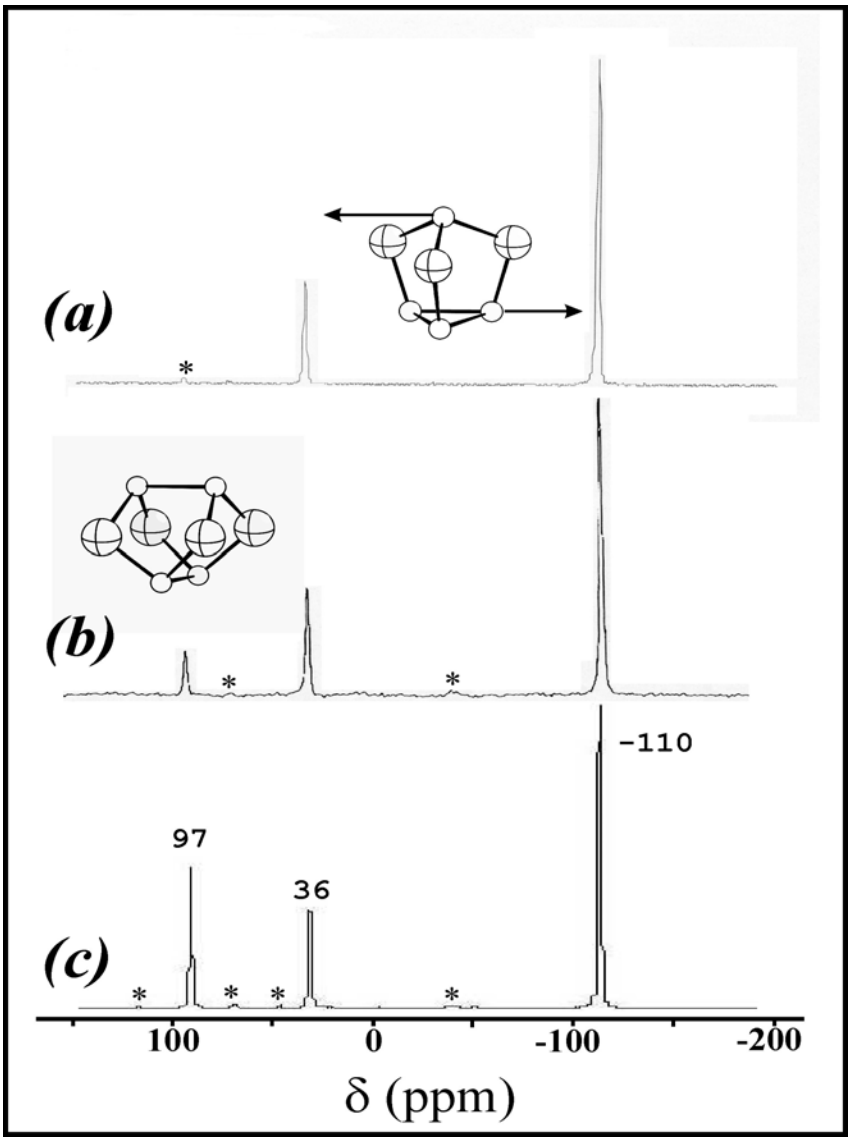

Fig. 4-8. ^{31}P-MAS-NMR spectra of [$(ZnI_2)_6(ZnSe)$]/[α-P_4Se_x] [* indicate the spinning side bands and (a), (b) and (c) is related to Zizpse6144, Zipse334 and Zizpse6147, respectively).

The ratio of integrals between peak *a* and peak *b* can be expressed by the term, $\frac{\Delta_a}{n_a} : \frac{\Delta_b}{n_b}$, where Δ_X is an integral of peak X and n_X is a number of equivalents for each molecule, respectively . Therefore the ratio can be roughly elucidated as 1 : 6 : 6 = *n*[P_2-($Se_{1/2}$)$_4$] : *n*[P-Se_3] : *n*[P_3-Se_3] with respect to equivalent species. The ratio of second and third one is clear, i.e., P-Se_3 unit (one equivalent in P_4Se_3 molecule) and P_3-Se_3 unit (three equivalents in P_4Se_3 molecule). With respect to this sense, the one cavity among 7 cavities in Zipse334 crystal system is occupied by α-P_4Se_4. Also in the case of spectrum **(c)** in **Fig. 4-8**, the ratio of integrals from the downfield shift is 24 % : 20 % : 56 %, and it follows 12 : 20 : 19 with equivalents, about 2 : 3 : 3. This means that two cavities occupied with α-P_4Se_4 molecule among 5 cavities in Zizpse6147. Actually the cavity occupancy of α-P_4Se_4 is not under control with synthetic utilities. We may suggest that the two molecules have almost same molecular energy level and the molecules are not able to be separated by means of thermally controlled reaction. It were believed that the α-P_4Se_4 have a meta-stability against P_4Se_3 molecule.

In parallel with an approach of area integral, the results from solid state measurement by H. Eckert *et al.* and one by others follow as **Table 4-2** which were compared with the measurement results from [Zn-Se]/[P-Se] crystalline compounds.

Table 4-2. The comparison of reported chemical shifts from ^{31}P-NMR spectra of P_4Q_x molecular crystalline compounds with Zizpse6147.

	chemical shift [ppm]							
	P_4Se_3						P_4Se_4	
δ_B	-106(d)[1]	-106	-106(d)	-64	-77	-110	-85	δ_{iso}
δ_A	38(q)	36	37(q)	68/87/90	63	36.2	59/127	96.6(s)
J_{AB} [Hz]	-	72	72			73.1		
temp. (K)	RT	RT	RT	RT		RT	RT	RT
phase	SS [2]	SS [3]	-	α [4]	α [4]	α [4]	α [5]	α [5]
Refs.	111	107	12	12	12	this work	12	this work

1. multiplicity: s = singlet, d = doublet, q = quartet.
2. Saturated solution in CS_2 operating at 24.3 Mc.
3. Saturated solution in CS_2/Benzol-d_6, simulated by PANIC from Bruker (0.2 Hz/pt).
4. α = alpha, β = beta indicate solid phase; MAS (magic angle spinning) solid state-NMR spectra at 121.65 and 121.46 MHz with variable spinning speeds (5.0 ~ 14.0 kHz).
5. α = alpha indicates P_4Se_4 conformer; MAS (magic angle spinning) solid state-NMR spectra at 162.01 MHz with the spinning speeds (25 kHz).
6. All the chemical shift data are related to 85 % H_3PO_4 (downfield shifts positive).

According to a recent experiment by Eckert *et al.*[112], the functional units in both, α-P_4Se_3 and α-P_4Se_4 were identified by measuring ^{31}P MAS NMR spectra of binary P-Se glasses as a function of x in P_xSe_{1-x} system. They observed two peaks which are probably originated by the structural skeletons, i.e., both of ethylene-like species $P_2(Se_{1/2})_4$, quasi-tetrahedral species $Se = P(Se_{1/2})_3$ and pyramidal species $P(Se_{1/2})_3$ with varying concentration range as $0.1 < x < 0.4$. To add to this, in the concentration range $x > 0.47$, ideally $x = 0.5$ for P_4Se_4 molecular, they confirmed the existence of ethylene-like species $P_2(Se_{1/2})_4$ of which the peaks was centered at around 100 ppm. Those notable evidences match with our data in terms of functional group approach, i.e., the concept of ethylene-like species $P_2(Se_{1/2})_4$, quasi-tetrahedral species $Se = P(Se_{1/2})_3$ and pyramidal species $P(Se_{1/2})_3$. For simplicity, we can

assume that α-P_4Se_4 consists of two ethylene-like species $P_2(Se_{1/2})_4$, and α-P_4Se_3 of pyramidal species $P(Se_{1/2})_3$ and basal P_3 species, actually three identical Se-P_3 units. We can exclude the possibility of existence of the quasi-tetrahedral species Se = $P(Se_{1/2})_3$ in our compounds, since no peak around 0 ppm was observed. This is also well supported by Raman scattering explanation. As a conclusion from our NMR spectra and above senses, the most up-field-shifted peak at -110 ppm can be assigned to the basal P_3 species, and consequently the signal at 36 ppm to pyramidal species $P(Se_{1/2})_3$, i.e., apical P. Finally the 97 ppm signal shows two identical ethylene-like species $P_2(Se_{1/2})_4$ as an isotropic chemical shift δ_{iso}. The confirmed single ^{31}P NMR peak (δ_{iso} = 89.4 ppm) in iso-type structure α-P_4S_4 are reported by G. M. Sheldrick *et al.*[106]. The dependency on Se concentration was confirmed by our experiments, which shows good approximation with the chemical shifts from solution NMR measurements[107,111], and some additional trials, **(b)** in **Fig. 4-8** (ZnI_2/P/Se = 3/3/4) and **(c)** in **Fig. 4-8** (ZnI_2/Zn/P/Se = 6/1/4/7), showed more P_4Se_4 guests in accordance with Se rich condition. The solid state NMR spectra indicate very dramatic aspect of a tendency of multiple guest substitution into [Zn-Se] host framework, but the chemical shifts are quite well differently centered compared with already reported solid state data of iso-type molecules (see **Fig. 4-8**).

The P NMR spectra of saturated solutions of P_4Se_3, was reported firstly by K. Irgolic *et al.*[111]. A linear relationship between chemical shift and an angle increment was revealed by R. Blachnik[107]. The characteristic data of an angle increment, which were based on solid crystals, but the P NMR measurements were accompanied in a saturated solution with fixed solvent system CS_2/benzol-d_6, are still quite arguable (closed circle in **Fig. 4-9**), since the crystallographic data of such chalcogenide molecules are no more matched in solution, i.e., the geometry of the molecule can be immediately affected by the solvent. Actually, the angle increment affects the chemical shift as a manner of $\cos^2\theta$. The angle increment in such cage structures is so small that Blachnik was able to make an approximation with the obtained data to a linear relationship **(b)** in **Fig. 4-9**. Namely, in such a short angle range, we are able to approximate the term of $\cos^2\theta$ **(a)** in **Fig 4-9** to a linear relationship **(b)** in **Fig. 4-9**. Even with this linear approximation (open circle in **Fig. 4-9**), however, it was not possible to determine the exact bond length and bond angle of guest molecule.

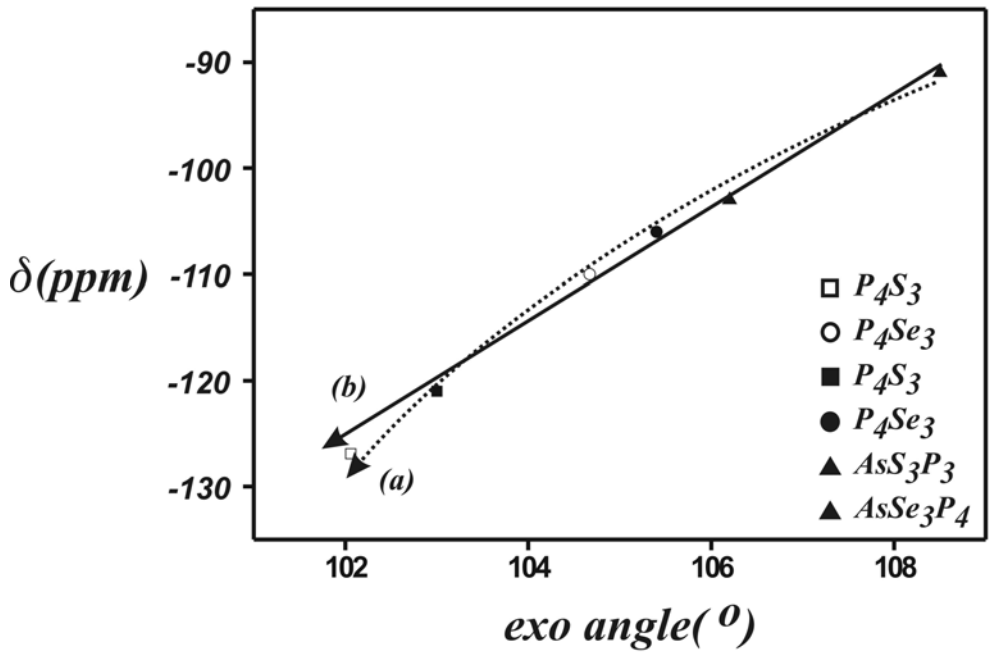

Fig. 4-9. The relationship between exo angle (P_{ba}-P'_{ba}-Q) and P chemical shift [regarding (a) and (b), see text].

By means of the Blachnik' concept, i.e., under a linear relationship between chemical shift and an angle increment, especially P_4Se_3 molecule in [Zn-Se] host lattice, the exo-angle of basal P_3-Se could be immediately calculated as 104.67° (105.40° from crystallographic data), which indicates that P_4Se_3 molecule is pressed along the equatorial direction of Se_3 unit and is elongated along the vertical direction of apical P-basal P_3 unit by surrounded iodine atoms (*96h*). With this evidence, we might suggest that the intermolecular P-P distance are quite relaxed so that the measured spectroscopic data, both of mass domain and distance domain, accurately fit the case of high temperature structure determination for instance in the case of Zizpse6144 crystalline compound, the comparison of measured data by ir/Raman spectroscopy (actually a mass domain spectroscopy) with well reported data shows a similarity with high temperature measurements.

Conclusively speaking,

(i) the ratio of area integral with respect to apical P unit against basal P unit showed the evidence of intercalated binary P-Se molecule as follows (host framework with Z = 8) and especially Zizpse6144 showed a single occupancy with P_4Se_3 molecule,

Table 4-3. The guest occupancy on cavities.

comp.	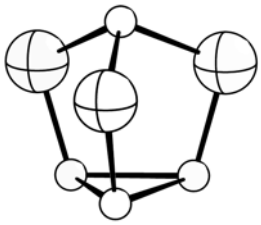 P_4Se_3	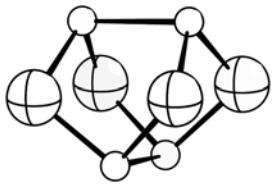 α-P_4Se_4
Zizpse6144	~ 8.0(5)	~ 0
Zipse334	~ 6.6(5)	~ 1.4(5)
Zizpse6147	~ 2.9(5)	~ 5.1(5)

(ii) all the measured results have *a good approximation with the solution measurements, not the solid state measurements*. Consequently, this clathrate system showed a solution behavior as the analogues S containing system (see **Fig. 4-10**).

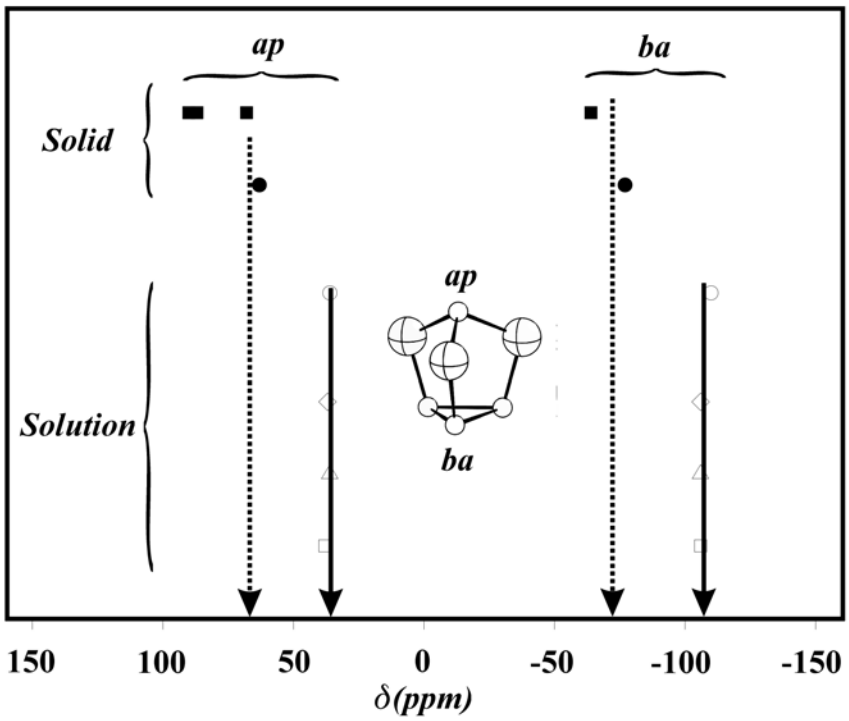

Fig. 4-10. The direct comparison of chemical shifts between the solid state measurements and solution phase measurements (dotted allows indicate the results from solid ^{31}P NMR spectra and solid allows indicate the result from solution ^{31}P NMR spectra comparable with this work ; δ_A = 36.2 and δ_B = -110 ppm for P_4Se_3 and δ_{iso} = -96.6 ppm for α-P_4Se_4).

(iii) as concluded in crystallographic section, the intercalated guest molecule(s) have no ordinary chemical bond with the environment, i.e., with [Zn-Se] host lattice. Consequently, the guest molecule(s) are regarded to be the host framework, just like a solute-solvent relationship in solution chemistry.

(iv) from the consideration of a linear relationship between chemical shift and a P_{ba}-P_{ba}-Se_{eq} angle increment, the molecular geometry of P_4Se_3 might be elongated along the vertical direction and compressed along equatorial direction by the host lattice as following **Fig. 4-11**. Such a structural deformation can be due to (1) Coulombic interaction between the positive partial charge(s) of P atoms, the negative partial charge(s) of Se atoms and the negative partial charge(s) of iodine

atoms and (2) an undetectable dynamic property of guest molecule by Doppler-broadening independent MAS NMR technique, i.e., only detectable average location of moving or vibrating guest molecule(s) in cavity due to NMR time scale. Therefore, if any, such a dynamic property of guest molecule should be confirmed by X-ray tools or ir/Raman spectroscopy.

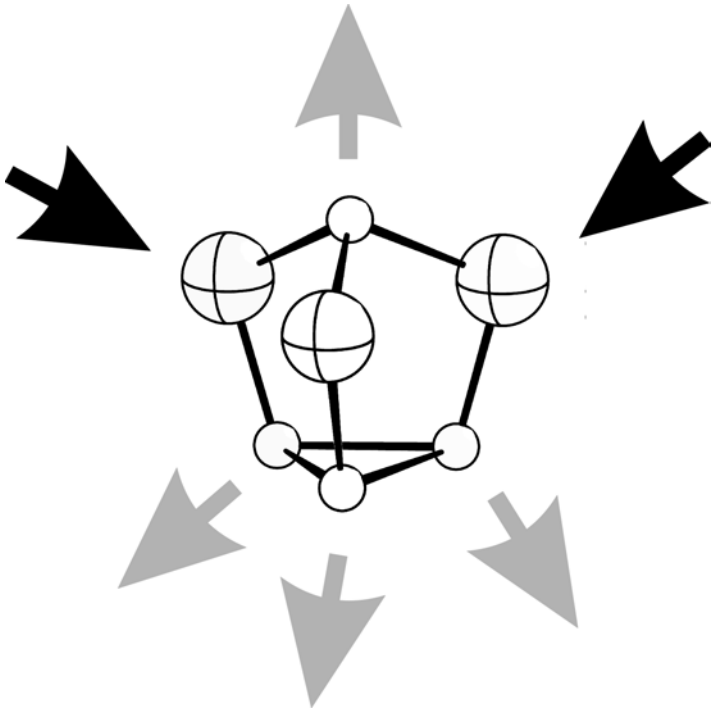

Fig. 4-11. The elongated molecule model by NMR measurement.

5. The characterization by FT- ir / Raman spectroscopy

In this section, we present the evidence of phosphorous chalcogenides by the analysis of vibrational spectroscopy. The Raman scattering modes of host lattice are well separated, since it has quite ionic characteristics, i.e., the host lattice, and the guest(s) have quite different covalent characteristics. The 3-dimensional open framework behaves like a solvent against solute, i.e., host framework against guest molecules. As we discussed in section of P NMR measurement, the static single crystal NMR measurement was suggested for detecting such a molecule under the concept of solution. The FT-Raman scattering method also provides same concept, since the detector in Raman scattering method usually is located on 90^{o} or back scattering from incident beam. In addition, the conventional method are adopting a solid suspension Nujol method, but statistically superior scattering beam can be detectable, even in such dispersed condition, since the successive filtering process in recent method provides to separate the desired Raman scattering transition from the all possible transitions, i.e., the filtering of undesirable Rayleigh scatterings. In this sense, we can evaluate the exact vibrational assignments within long-range ordering, also the structural anisotropic conditions can be minimized. Following this reason, the measured vibration and scattering frequencies of disordered chalcogenide molecule showed almost no overtones and almost no interference mutually, which can be almost perfect separated from lattice modes. This means the crystal vibrations including chalcogenide molecule are compensatory each other between host lattice and guest molecule. First of all, we need to separate the acoustic modes from total spectra, since we already discussed in the crystallographic section that the intercalated molecule showed the motion of translation in the cavity with D.O.F (degree of freedom) = 1 (x, y and z respectively). Also it is helpful to understand the vibration assignments of guest molecules.

5. 1. The acoustic modes from host / guest interaction

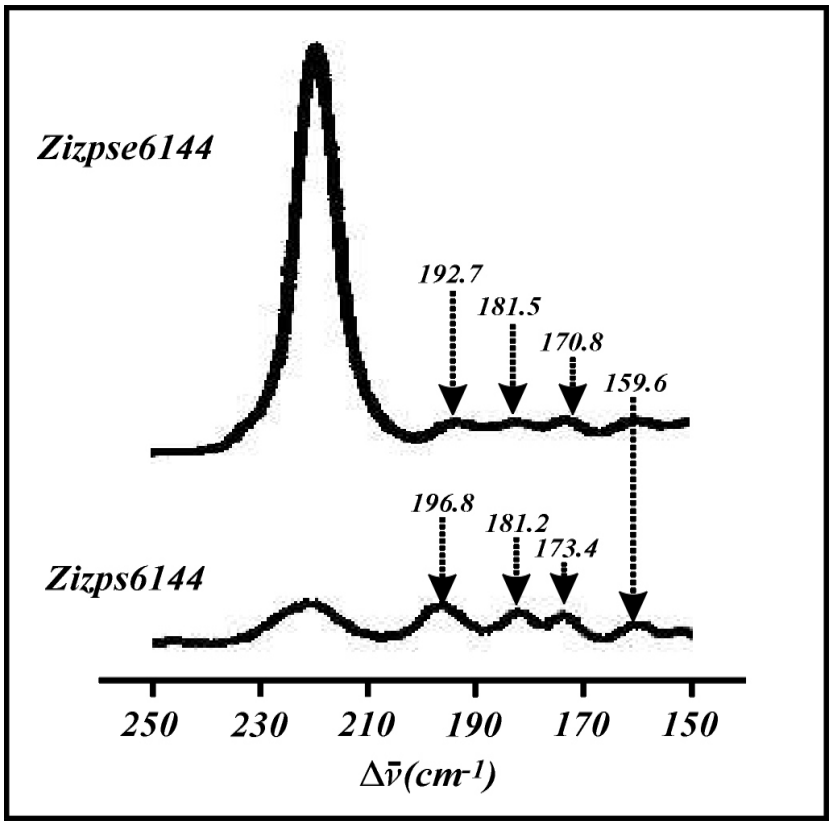

Fig. 5-1. Acoustic modes from Raman scattering spectra by referred compounds.

Actually those successive frequencies in the spectra (see **Fig. 5-1**) of Zizpse6144 showed same tendencies with 11 cm^{-1} difference in every interval from 150 cm^{-1} to 200 cm^{-1}, and in the spectra of zizps6144, 13 cm^{-1} differences in every interval. The both values of frequency differences, 11 cm^{-1} and 13 cm^{-1}, are more than in the case[113] of ZnI_4^{2-}-$ZnBr_4^{2-}$, 8 cm^{-1}, and less than ZnI_4^{2-}-$ZnCl_4^{2-}$, 18 cm^{-1}. The notable aspect is that the initial scattering values of those successive frequencies in the both host lattices, [Zn-Se] and [Zn-S], have almost same value, 159.6 cm^{-1}.

For simplicity, let us make several assumptions about those frequencies,

(i) those frequencies are due to the interactions between the guest molecule and the host lattice.

(ii) the libration motion of molecule is restricted as one-dimensional motion containing the molecular oscillation and quasi-rotation, as we discussed in crystallographic section.

(iii) the apical part of molecule interacts with *three iodine atoms* of the Se(S)-Zn-I_3 host lattice species. Therefore the same initiated frequency can be assigned as P---I_3 interaction (denoted as 'ap-I') at 159.6 cm^{-1} and the frequencies from both [Zn-Se] host lattice and [Zn-S] host lattice should be same.

(iv) the interaction force (with respect to Hook's law) of ap-I is weaker than basal part of molecule ; P_3---I_x interaction, i.e., the actual distance ; ap-I > basal unit of molecule-I_x.

(v) the force constants of both k_{ap-I} and k_{ba-I} are almost same.

These assumptions are summarized as following **Fig. 5-2**.

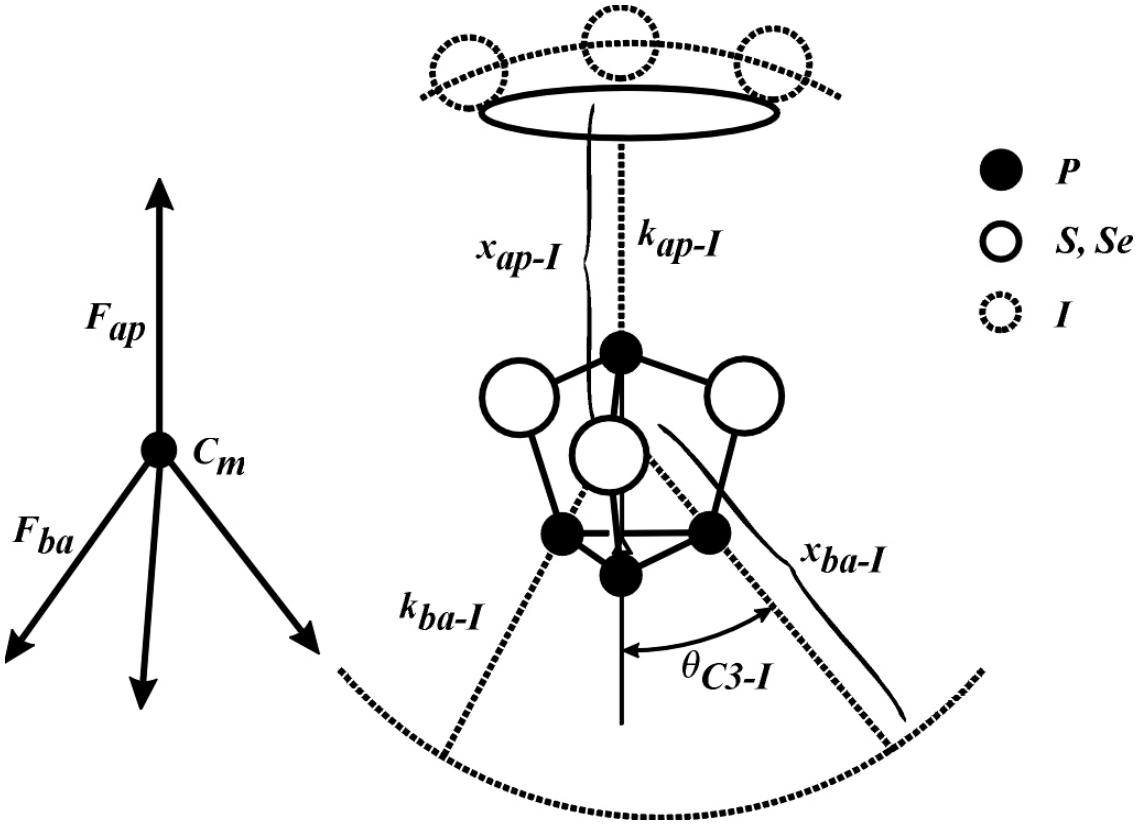

Fig. 5-2. The force balance of P_4Q_3 molecule in the cavity.

Now consider about the successive frequencies with respect to general vibration relationship Eq.(16).

$$\bar{v} = \frac{1}{2\pi c}\sqrt{\frac{k}{\mu}} \ , \tag{16}$$

where $\bar{v}$ is wave-number of considered peak, c is the speed of light, k is force constant and μ is a reduced mass of considered system. Adopting Eq. (16) to this system, then

$$\left(\frac{\bar{v}_{ap-I}}{\bar{v}_{ba-I}}\right)^2 = \left(\frac{k_{ap-I}}{k_{ba-I}}\right)\left(\frac{\mu_{ba-I}}{\mu_{ap-I}}\right) \tag{17}$$

From the assumption (v), we can deduce the Eq. (17) as following Eq.(18), then

$$\left(\frac{\bar{v}_{ap-I}}{\bar{v}_{ba-I}}\right)^2 \approx \left(\frac{\mu_{ba-I}}{\mu_{ap-I}}\right) \tag{18}$$

Table 5-1. The change of reduced mass ratios due to the acoustic modes.

compounds	1	2	3
Zizpse6144	$\left(\frac{\mu_{ba-I}}{\mu_{ap-I}}\right)=\left(\frac{159.6}{170.8}\right)^2=\frac{2.6}{3}$	$\left(\frac{\mu_{ba-I}}{\mu_{ap-I}}\right)=\left(\frac{159.6}{181.5}\right)^2=\frac{2.3}{3}$	$\left(\frac{\mu_{ba-I}}{\mu_{ap-I}}\right)=\left(\frac{159.6}{192.7}\right)^2=\frac{2.1}{3}$
Zizps6144	$\left(\frac{\mu_{ba-I}}{\mu_{ap-I}}\right)=\left(\frac{159.6}{173.4}\right)^2=\frac{2.5}{3}$	$\left(\frac{\mu_{ba-I}}{\mu_{ap-I}}\right)=\left(\frac{159.6}{181.2}\right)^2=\frac{2.3}{3}$	$\left(\frac{\mu_{ba-I}}{\mu_{ap-I}}\right)=\left(\frac{159.6}{196.8}\right)^2=\frac{2.0}{3}$

Above calculation indicates that the apical atom interacts with 3 iodine atoms, as we already assumed in (iii), and the individual basal atom interacts with 2.6, 2.3 and 2 iodine atoms respectively, i.e., if we follow the assumption (ii), the motion of guest molecule is

immediately reflected to the change of polarization of iodine atoms with manner of collaborated interference. Also the ratio 1 : 1 is possible, i.e., one iodine atom interacts with one phosphorous atoms individually, but such interaction is too weak to detect, i.e., if the part of apical phosphorus approaches to iodine atoms, the maximum interaction is with 3 iodine atoms, and if it is far away from iodine atoms the minimum interaction can occur. Anyway, the final case of above calculations can be explained by the result of rigid-body refinement of Zizpse6144 at 293 K, which can be also comparable with room temperature Raman scattering measurement (see **Fig. 5-3**).

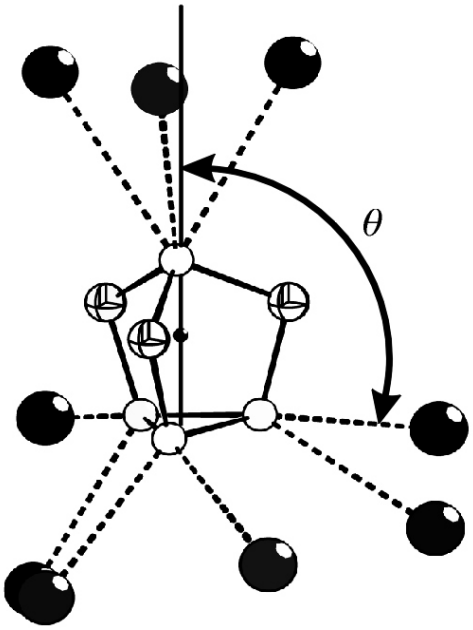

Fig. 5-3. The rigid-body refinement of Zizpse6144 at 293 K (The distances between basal P atoms and I atoms, 3.92 ~ 4.12 Å, and the average angle θ , 127 °).

The whole frequencies are relatively weak but quit distinguishable, which supports the assumption (ii), i.e., the quite regular oscillating motion of guest molecule, and it is well detectable in the range of 150 ~ 250 cm^{-1} with an enhanced Raman scattering resolution. Finally the above **Fig. 5-3** indicates that the molecule itself is located in the cavity with same force constants; $k_{ap-I} = k_{ba-I}$, as the assumption (v), since the angles θ have almost same

values, 120 ° except one, 150.41 °. Considering the inaccuracy of refinement, it is not so serious value.

Conclusively speaking, those stepwise degenerated frequencies are originated by the non-symmetrical interactions, i.e., the volumetric polarization between the Se (or S) - Zn - I_3 pseudo-tetrahedral unit, especially I_3 unit and the atomic part of chalcogenide molecules, i.e., those frequencies contain the forbidden transition of ν_5 (A_2) mode which is inactive in both ir and Raman. The initiated frequency, 159.6 cm^{-1}, from the successive series, shows very high value, comparing with ZnI_3Br^{2-} [this is similar unit with Se (or S) - Zn - I_3 unit with respect of atomic mass], 130 cm^{-1} (ν_1), and ZnI_3Cl^{2-}, 140 cm^{-1} (ν_1). This means that first frequency is constructed by the interaction between the I_3 unit and apical P atom or one Se (or S) atom of Se (or $S)_3$ unit in very dilute concentration. It is quit distinguishable from the symmetric vibration of Se (or S) - Zn - I_3 unit. This suggestion is supported by which the successive frequencies is continued on the ν_4 (A_1) mode of chalcogenide molecule. As we pointed out in the section of crystallographic consideration, we suggested those successive frequencies as the libration motions of chalcogenide molecule in the environments of the iodine atoms (*96h*). This evidence provides us that the polarization of chalcogenide molecule is constructed by a physical interaction so that the symmetric vibrations can be restricted, but such a change of bonding polarity can be detected. Comparing with solution Raman measurement, the chalcogenide molecule is quite released from the halide atoms of host lattice, and the enhanced D.O.F (degree of freedom) of intercalated molecule may be detected by the rotation-vibration Raman spectroscopy in a far ir region.

5. 2. The normal mode analysis for Pn_4Q_x (Pn = P, As ; Q = S, Se ; x = 3, 4) molecules

For simplicity, these Pn (Pn = P, As)-based cluster molecules are revealed in terms of point symmetry from the character table, i.e., those are analyzed by normal modes of vibration based on the degree of freedom.

At first, the vibrational spectrum of Pn_4Q_3 (C_{3v} symmetry) (see **Fig. 5-4**) consist of a total of ten fundamental frequencies, i.e., four symmetrical A_1 frequencies, one A_2 frequencies and five doubly degenerate class E frequencies and summarized the reported the fundamental mode investigations of Pn_4Q_3 (C_{3v} symmetry) are shown in **Appendix Table 6a ~ 7b**.

Table 5-2. Analysis for the normal modes of vibration (Pn = P, As; Q = S, Se).

molecule	point sym.	total DOF[1] (3n)	trans.[2] DOF	rot.[3] DOF	vib.[4] DOF (3n-6)	trans.-rot.[5] Fund. Modes	vib. Fund. Modes
α-Pn_4Q_3	C_{3v}	21	3	3	15	A_1 , A_2 2E	$4A_1$ (IR,R)[6] A_2 5E (IR,R)
α-Pn_4Q_4	D_{2d}	24	3	3	18	A_2 B_2 2E	$3A_1$ (R) $2A_2$ $2B_1$ (R) $3B_2$ (IR, R) 4E (IR, R)

1. DOF = degree of freedom, n = number of atom.
2. Trans. = translation.
3. Rot. = rotation.
4. Vib. = vibration.
5. Trans.-Rot. = translation + rotation.
6. IR = Infrared active, R = Raman active.

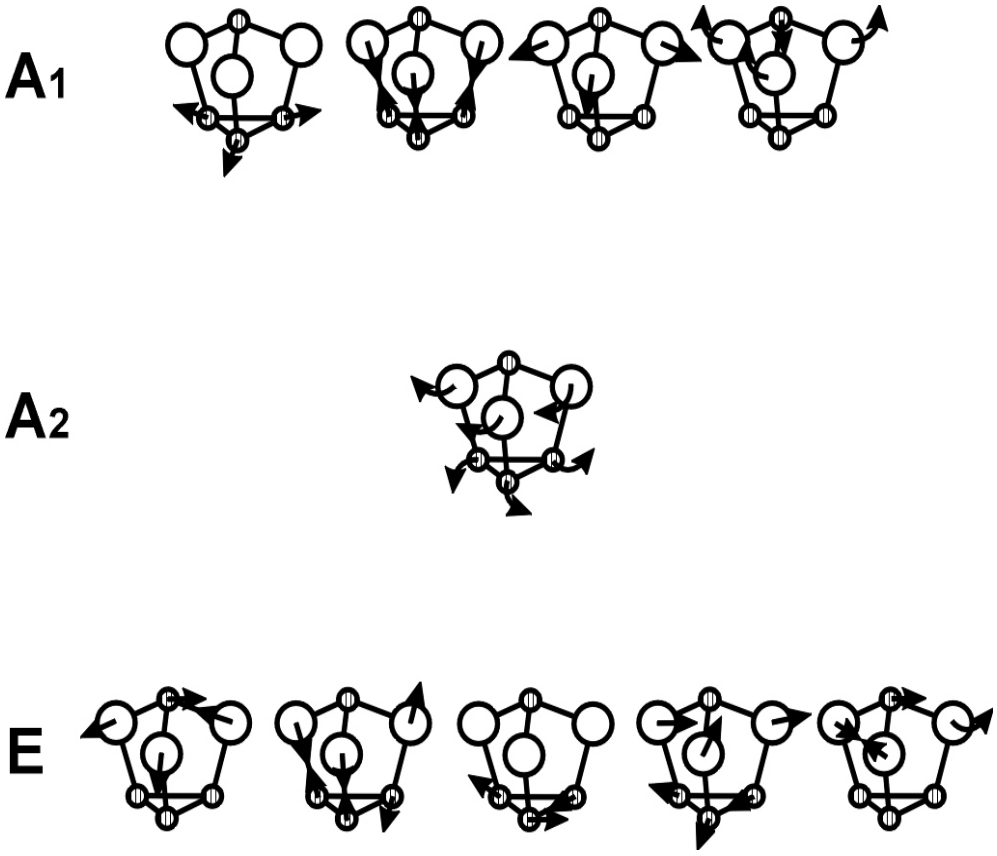

Fig. 5-4. Normal mode analysis of Pn_4Q_3 (Pn = P, As; Q = S, Se) molecules[70].

5. 2. 1. α-P_4Se_3 (C_{3v}) in Zipse6144, Zipse334 and Zizpse6147

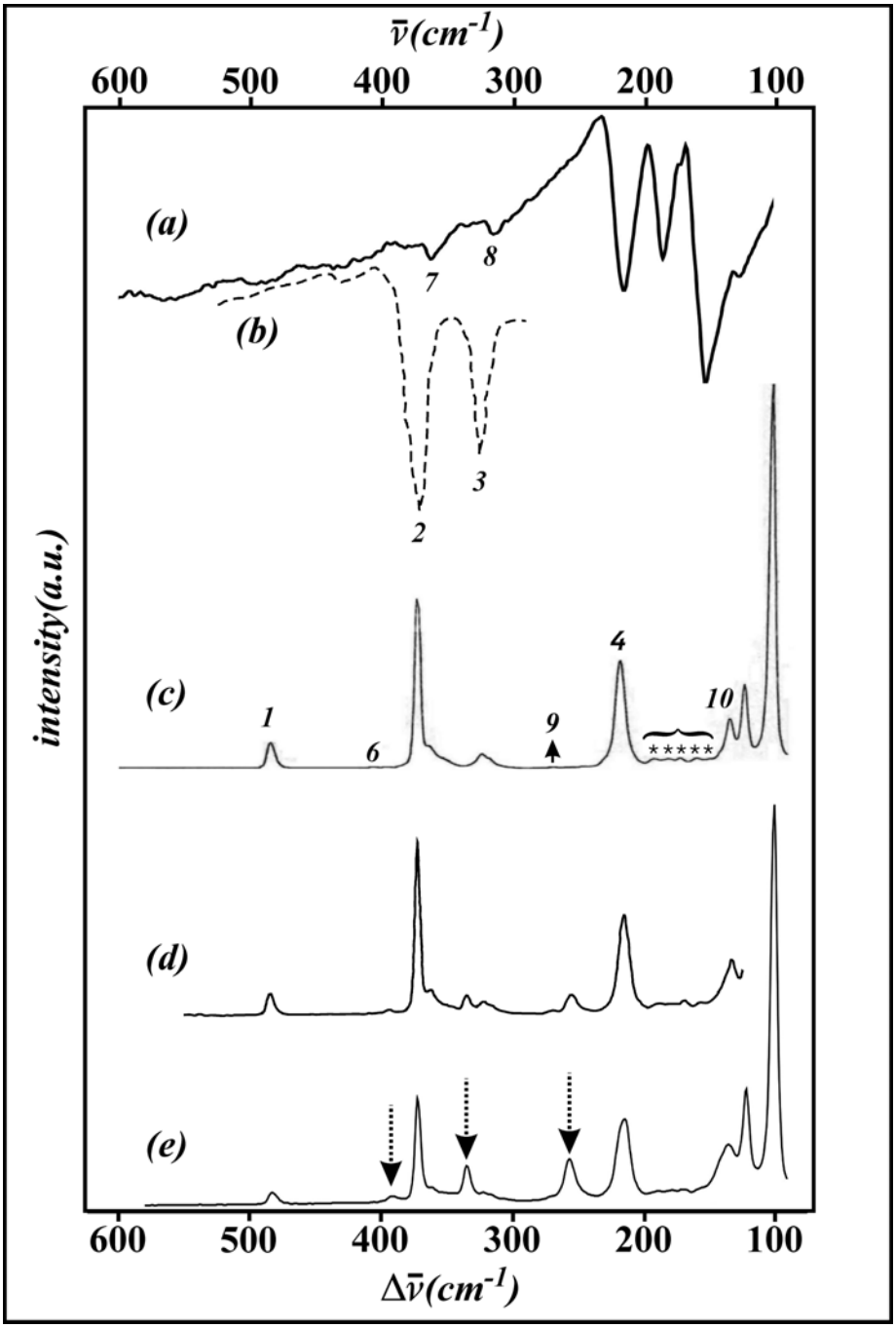

Fig. 5-5. FT-ir/Raman spectra of $[(ZnI_2)_6(ZnSe)]/[\alpha\text{-}P_4Se_x]$ [(a) = ir (Zizpse6144), (b) = ir by Bues et al.[70], (c) Raman (Zizpse6144), (d) Raman (Zipse334) and (e) Raman (Zizpse6147), the numbers indicate normal mode frequencies, downward allows indicate the developed frequencies and the asterisks indicates the acoustic modes].

In above **Fig. 5-5 (a)**, **(b)** and **(c)** indicate a direct comparison with the results of W. Bues *et al.*[70], i.e., in case of **(a)** and **(c)**, Zizpse6144 (25 °C, ir) and α-P_4Se_3 (25 °C, ir) by W. Bues *et al.,* respectively, and also **(c)** indicates Zizpse6144 (25 °C ; Raman). All the numbers were abbreviated in the sense of those frequencies as the normal mode analysis. Tentatively, the acoustic modes of chalcogenide molecule are represented by asterisks. Both the spectra (d) and the spectra **(e)** which are measured from the Se-rich crystals can be abbreviated as the Zipse334 **(d)** and Zizpse6147 **(e)** respectively.

All the results from our work match with temperature modification results of W. Bues, *et al.* within the range of root mean square, R^2 = 0.995 ~ 0.998, especially well matched with high-temperature modification, and best matched linearity with theoretically simulated harmonic assignments by Schulz *et al.*[115], R^2 = 0.999. But we guess there is a problem for the scaling factor in the harmonic approximation method with B3LYP/6-31G (d, p) base set and also assignments. All reported results are summarized at two different figures (see **Fig 5-6**, **Appendix Table 6a** and **6b**), and all the measured results, adapting various techniques, i.e., the saturated solution method with various solvents and the solid state suspension methods, showed very small deviations in all the ranges of wave numbers. Contrary to that, the theoretically calculated results showed huge versatility, i.e., the compared frequencies showed very big deviation. But the assignments of normal modes which depend on the polarization technique are quite different, i.e., all the symmetrical modes can be polarized and the other degenerated modes are not. Even though such a good linearity between this work and the others showed, it very difficult to weigh the energy contribution of molecular vibration without exact assignments of D.O.F (degree of freedom). Therefore, in the following section, we allow the pages for summary such arguments concerning the cluster molecules.

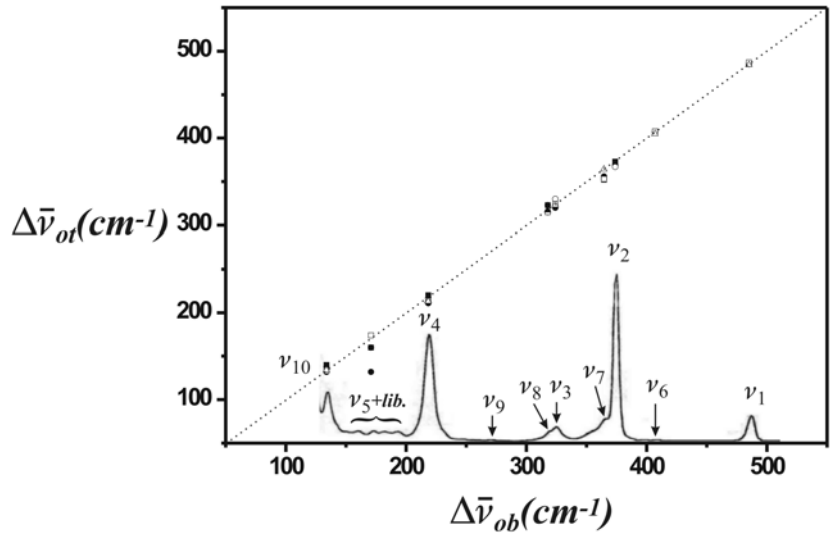

(data : solid circle, open circle and solid rectangle = ref. 70, open rectangle = ref. 132 and open triangle = ref. 21, also see **Appendix Table 6a**)

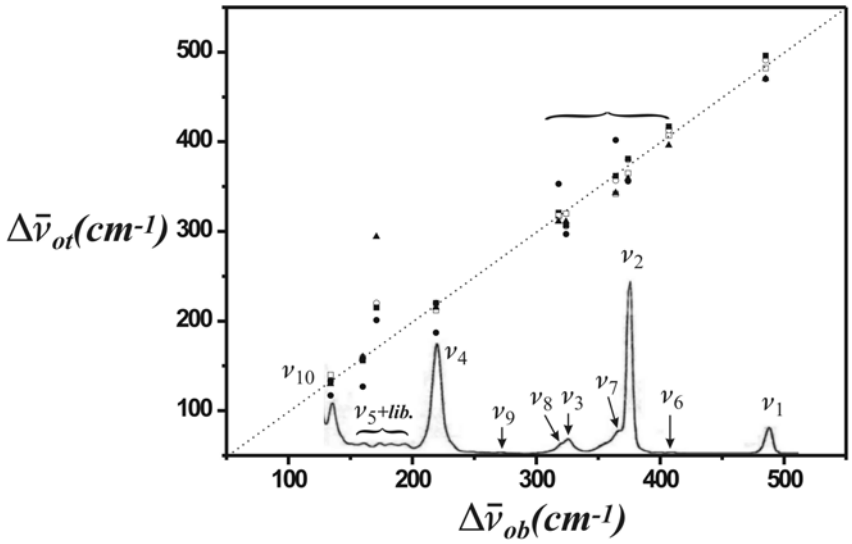

(data : solid circle = ref. 121, open circle and solid rectangle = ref. 117, open rectangle = ref. 134, and solid triangle = ref. 21, also see **Appendix Table 6b**)

Fig. 5-6. P_4Se_3 - The data comparison between Raman scattering spectra by others (*y-axis*) and this work (*x-axis*) (above = measured, down = calculated and the horizontal crammer indicate the uncertain frequencies).

For the least ambiguity about the various vibrational assignments for the normal modes of P_4Se_3 or such analogues, there were so many disputes worldwide. At least, however, we need to induce the confluence about the vibrational motions of symmetrical A_1 and A_2 frequencies, since all the measured Raman scattering data showed almost same tendencies except the doubly degenerated mode ν_9 (E) (see above **Fig. 5-6**). According to the theoretically calculated Raman spectra, the authors urged that the forbidden frequency of ν_5 (A_2) mode can be assigned within the wide range of 130 ~ 170 cm^{-1}, in which contained the ν_9 (E) or ν_{10} (E) frequencies. The theoretically induced frequencies concerning such kinds of cluster molecule, however, have so much ambiguities in the main two range of spectra (see **Fig. 5-6** down), i.e., both the frequencies which are within 150 ~ 250 cm^{-1} and within 300 ~ 400 cm^{-1} are hardly distinguishable due to the similar molecular vibration energy level. In detail, we guess there is no argument with respect to ν_1, ν_2, ν_3, and ν_4 symmetric fundamental modes, all the Raman and infrared active modes. The first ν_1 can be regarded as one of the triple-degenerated modes in P_4 (T_2). Regarding hypothetical Se_3 species which has two degenerated point-group symmetries, D_{3h} and C_{2v}, it's also helpful to consider the assignments of ν_2, ν_7 and ν_3, ν_8 mode respectively, since two kinds of these frequencies showed almost same values in both of experimental and theoretical consideration.

According to the theoretical calculation of Se_3 species with B3LYP/6-311+G (2df) method indicates some different tendencies into the symmetrical stretching with D_{3h} as 334 cm^{-1} and symmetric stretching with C_{2v} as 319 cm^{-1}, respectively, which both results showed very good approximation with our measured frequencies, 324 cm^{-1} and 317 cm^{-1}. The frequencies of ν_3 and ν_4 can be considered as the symmetric stretching and symmetric angle deformation of Se_3 species, which are spontaneously accompanied with angle deformations of basal and apical phosphor atoms. Those symmetric modes ν_2 and ν_3, which are measured with the inelastic neutron scattering experiments, are also well supported by Elliot *et al.*[116]. Actually, ν_5 (A_2) normal mode frequency, twisting mode, is both Raman and ir inactive. This frequency was interesting for chemical theoreticians. They have pointed out the range of this calculated frequency, as 130 ~ 170 cm^{-1}. But from our spectral data, this frequency is initiated of 150 cm^{-1} which can be regard as the changing of polarity by means of torsion-initiation.

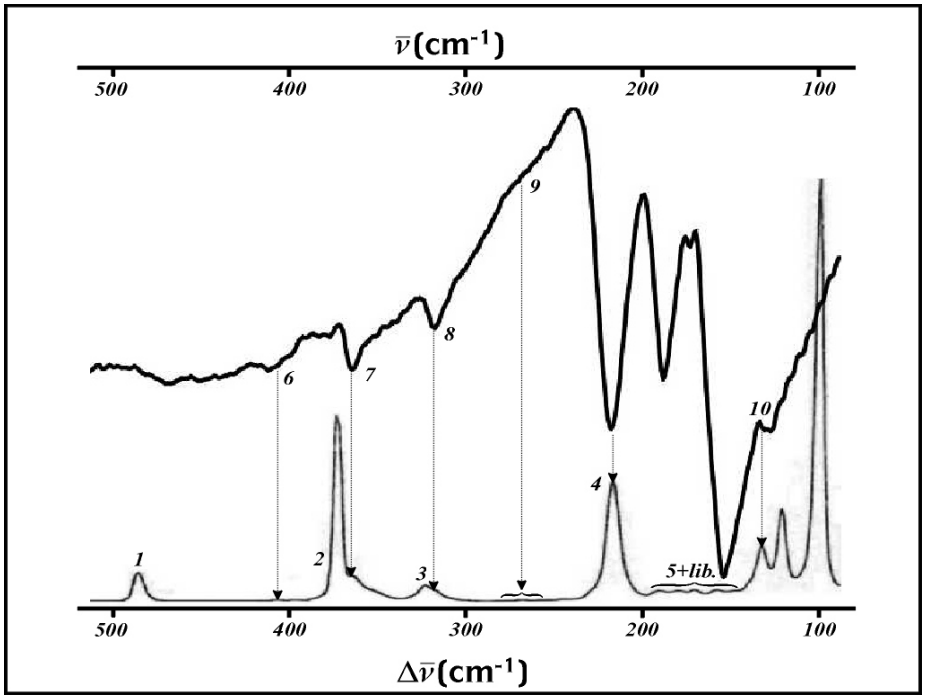

Fig. 5-7. Direct comparison between ir and Raman spectrum of Zizpse6144.

Above **Fig. 5-7** indicates the direct comparison between ir and Raman spectra and the notable aspect of this comparison is symmetric stretching modes ν_1, ν_2 and ν_3 are highly restricted by lattice environment, i.e., by its potential field, but symmetric angle deformation mode ν_4 is quite detectable including doubly degenerated E modes.

With respect to this conclusion, the α-P_4Se_3 molecule in the lattice is slightly distorted and twisted so that the measured frequencies could be matched with results of C_{2v} approximation. A. Sergi *et al.*[117] reported the spectral density of the A_1 normal modes of isolated P_4Se_3, which were calculated with Car-Parrinello molecular dynamics simulation, represented the order of such symmetric vibrational intensities, as the sequence of ν_4, ν_3, ν_2 and ν_1. Contrary, the direct powder Raman measurements of phosphorus selenide glasses showed some diverse tendencies in accordance with various synthetic routes. Such a structural diversity in the molecular crystal, so called van der Waals crystal, is explained by the concept of zero-dimensional glasses[14].

5. 2. 2. α-P_4S_3 (C_{3v}) in Zizps6144

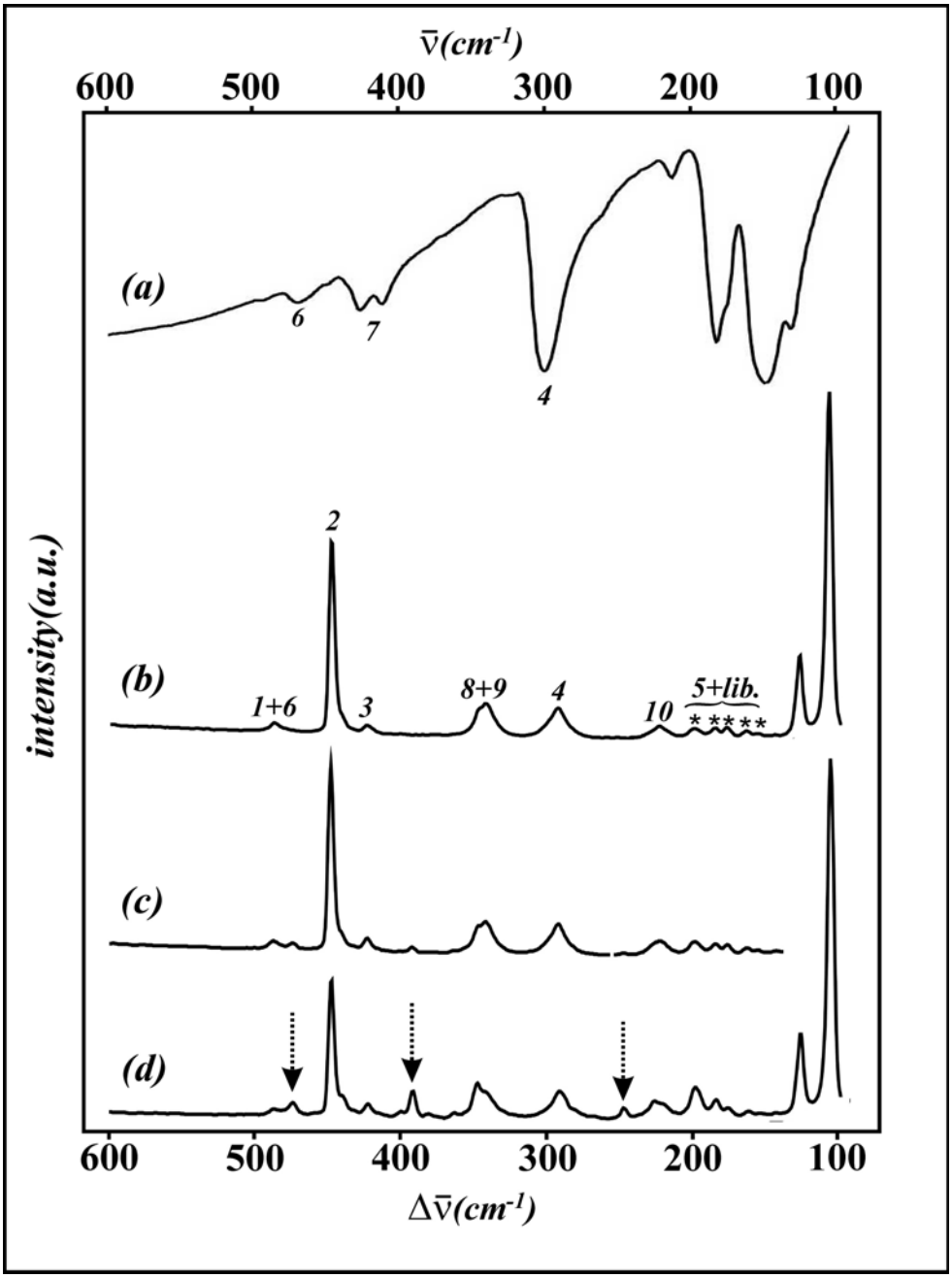

Fig. 5-8. FT-ir/Raman spectra of $[(ZnI_2)_6(ZnS)]/[\alpha\text{-}P_4S_3]$ [(a) = ir (Zizps6144), (b) = Raman (Zizpse6143), (c) Raman (Zizpse6144) and (d) Raman (Zizps6145), the numbers indicate normal mode frequencies, downward allows indicate the developed frequencies and the asterisks indicates the acoustic modes].

The above scattering spectra (see **Fig. 5-8**) are obtained from the [Zn-S]/[P-S] crystalline compounds at room temperature from suspensions in Nujol. All the numbers are abbreviated in the sense of those frequencies as the normal mode analysis by W. Bues *et al.*[70] (some parts modified) and especially tentative acoustic modes of chalcogenide molecule is represented by asterisks. In case of P_4Se_3, the reported vibration spectra were quite clear in both the measured data and the theoretically calculated data, since the decomposed redundant motions of P-Se bonding are quite distinguishable compared with P-S bonding, i.e., all the P-S-P symmetric stretch or asymmetric stretch, P-S-P bend and P-S-P wag motions (P-P stretch is same as for P_4Se_3) are so similar that even with theoretical tools it is very difficult to divide into individual normal modes due to almost same atom weights. These difficulties caused wide arguments worldwide. In two different tables (see **Appendix Table 7a** and **7b**), such arguments are summarized and compared with this work and other assignments.

The most serious problem is the ν_4 (A_1) mode which is centered at 290 cm^{-1} in our spectra, which is tentatively assigned. This mode was recently assigned as symmetric bending ν_4 (A_1) by W. Bues, *et al.*[70] who urged that the frequency was polarized, using the polarization measurement. However, H. Gerding *et al.*[118] and M. Gardner[119] assigned it as doubly degenerated ν_8 (E), and M. Gardner urged that this frequency was 'clearly' depolarized. Also, three different results did not provide the ν_6 (E) frequencies, since both the symmetric stretching ν_1 (A_1) and asymmetric stretching ν_6 (E) are almost similar and continuously converted from one to the other. Let us cross over whole data including the theoretical calculations at this stage. Recently, reasonable calculated frequencies of normal modes of P_4S_3 were reported by J. O. Jensen *et al.*[120], who used the Gaussian94 set of quantum chemistry codes at the Hartee-Fock (HF), second-order Moller-Plesset (MP2), and density functional theory (DFT), which can be meaningfully compared with former results by H. Gerding, *et al.*[118]. He performed the calculation with classical Wilson GF-Matrix and the deduced force constants of frequencies were factored with the empirical rules, Badger's and Gordy's rule, or by J. Brunvoll *et al.*[121] who performed the calculation with a modified Wilson GF-matrix method, i.e., the energy term of GF-matrix was modified, so called the PED (potential energy distribution) approach by the 'method of fragments'. They, however, felt

that there is a break-down of the theory when the PED is tentatively applied to cage-like molecule, since the discrepancy between the experimental evidences from W. Bues *et al.*[70] and theoretical calculations from J. Brunvoll *et al.*[121] did not meet a confluence. As a conclusion, the normal mode frequencies from our data are quite well matched with whole data both with calculated and measured, except the corresponding vibrational assignments, since in accordance with the adopted calculation methods, the results varied. We could show nobody's hand, since almost it looks like a catastrophe. The both cases agree that ν_1 and ν_6 frequencies can be detected within the range of 460 ~ 490 cm^{-1}, and the measured solid state result by H. Gerding *et al.*[118], the higher frequency which is centered at 486 cm^{-1} is depolarized and by W. Bues *et al.*[70] not. To add to this, all the calculated results indicate that two frequencies have almost identical value. It means that two frequencies are superimposed, as a result with polarization measurement, sometimes it may seem to be polarized and sometimes not. Since this frequency, however, which is based on the symmetric stretching of P-P unit will be located similar as the symmetric stretching of P_4Se_3. Therefore, the higher frequency at 486.7 cm^{-1} can be assigned as ν_1, and consequently 473.2 cm^{-1} as ν_6. The most intense frequency at 446.8 cm^{-1} can be no argued except the HF calculation by J. O. Jensen *et al.*[120] and assigned as ν_2. Also, the ν_3 and ν_7 frequencies are quite similar, as we discussed in the section of P_4Se_3 molecule and the calculated frequencies. The measured data provide ν_3 frequencies which are centered at 420 ± 3 cm^{-1} and all are polarized, in our spectra at 421.6 cm^{-1}. But in case of ν_7 frequency, nobody has detected it with any measurement tools. Only W. Bues *et al.*[70] reported this frequency with room temperature solid state measurement which was centered at 417 cm^{-1}, in our spectra at 416.5 cm^{-1} as a shoulder, but quite distinguishable. The ir spectrum also supports the evidence of splitting up between ν_3 and ν_7.
In this stage, we have to divide the remaining frequencies into the normal modes and libration modes, i.e., the translational modes, since the remaining frequencies, ν_4, ν_5, ν_8, ν_9 and ν_{10}, contain the acoustic modes of molecule. According to the 'factor group analysis' of W. Bues *et al.*[70], actually this analysis can provide qualitative meanings concerning widely distributed frequencies. Those frequencies can be distributed in polycrystalline state ; D_{2h}^{16}. Among them, the A_{1g}, B_{1g}, B_{2g} and B_{3g} are Raman active modes and later three can occur by molecule oscillation. The theoretical calculations can give us useful information about this

consideration, i.e., all the calculation tools suggested that the forbidden frequency ν_5 (Raman, ir inactive) can be centered in the range of 160 ~ 190 cm^{-1}. In our spectra, the successive frequencies are ranged as same manner. Is the forbidden frequency really detectable? If it is really detectable, it should be showed in limited circumstance, i.e., the factor group splitting in crystalline phase, in the very concentrated solution condition and so on. Contrary, in the gas phase or very dilute solution the molecule itself can diverse enough vibration energy into the circumstances with manner of increased D.O.F (degree of freedom). The notable evidences regarding above concept can be found out from the solution to the various measurement conditions. The frequency which is centered at 187 cm^{-1}, ν_4 from M. Gardner[119] and ν_{10} from W. Bues *et al.*[70], was detected only in the crystalline phase and more splitted into several series of frequencies in accordance with increasing temperature. To the contrary, in solution (H. Gerding *et al.*[118] and by M. Gardner[119]) and in gas phase (M. Gardner) it was not found. To add to this, the detected frequencies were sometimes polarized and sometimes depolarized. Regarding this frequencies, we suggest the estimation in following section.

Finally remaining frequencies are ν_8, ν_9 and ν_{10}. M. Gardner[119] assigned 142 cm^{-1} as ν_{10}, and it's quite good approximation with ν_{10} of P_4Se_3 at 132 cm^{-1}. If it's real, it is too weak to detect in our spectra (~ 1 % of ν_2), 141 cm^{-1}. Instead of that, we assign 221.8 cm^{-1} as ν_{10}, 345.3 cm^{-1} and 340.2 cm^{-1} as ν_8 and ν_9, respectively. As a result, we have to show W. Bues's hand, since he showed the figure in which is the evidence of 'clearly depolarized ν_4 mode'. With respect to ir spectra, the symmetrical stretching and bending motions are strongly restricted by the I *96h* environments.

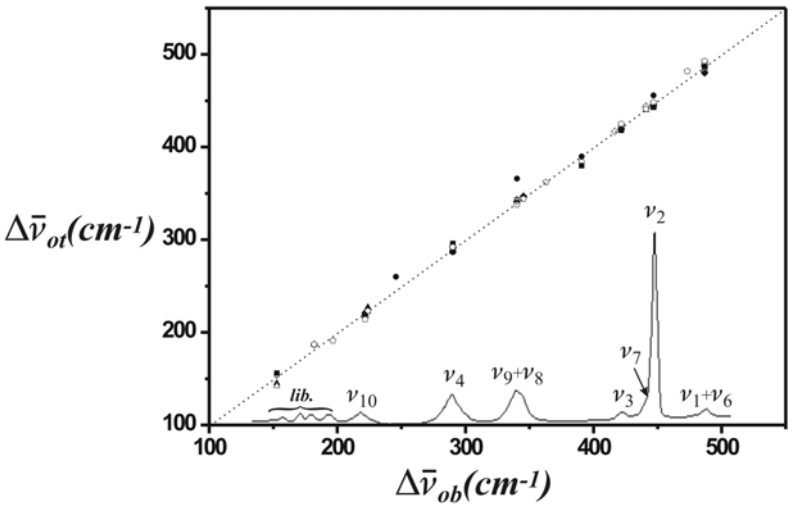

(data : solid circle, open circle and solid rectangle = ref. 118, open rectangle, solid triangle, open triangle and solid diamond = ref. 119 and open diamond, solid pentagon and open pentagon = ref. 70, also see **Appendix Table 7a**)

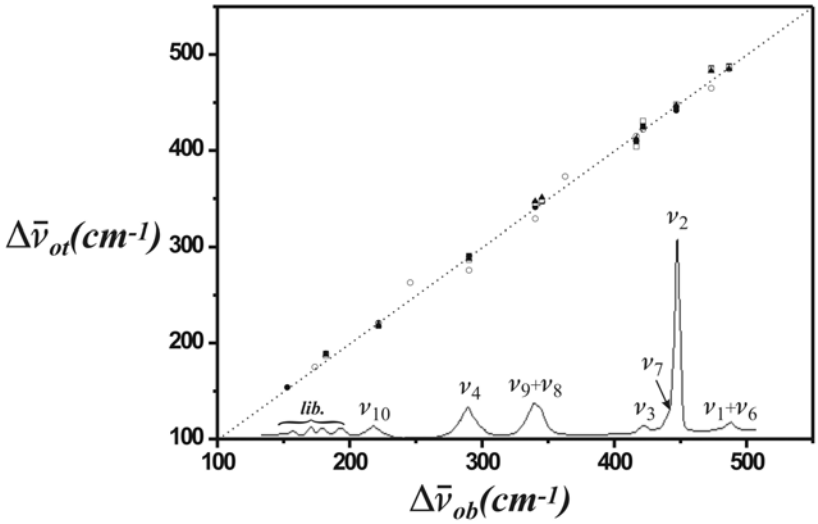

(data : solid circle = ref. 118, open circle = ref. 121, and solid rectangle, open rectangle and solid triangle = ref. 120, also see **Appendix Table 7b**)

Fig. 5-9. P_4S_3 - The data comparison between Raman scattering spectra by others (*y-axis*) and this work (*x-axis*) (above = measured, down = calculated).

In this stage, we have to consider about the difference between the ir and Raman scattering spectra (see **Fig. 5-10**).

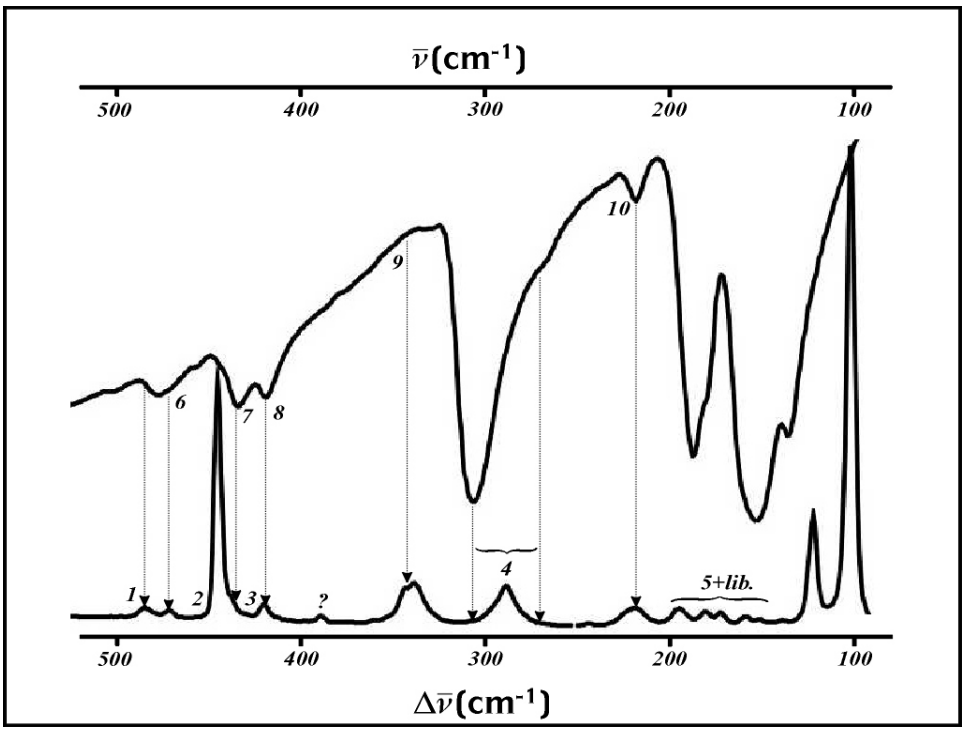

Fig. 5-10. Direct comparison between ir and Raman scattering spectrum of Zizps6144.

As a conclusion, some normal modes of intercalated chalcogenide molecules are very restricted by the interactions between the [Zn-S] host lattice and chalcogenide molecule. With our measurements, the symmetric stretching modes of this molecule, i.e., ν_1, ν_2 and ν_3 are not detectable with ir spectroscopy, to the contrary, the symmetric angle deformation ν_4 and the libration modes are well detectable in both ir and Raman spectra. Actually the degenerated E modes are hardly distinguishable, even the direct comparison between ir and Raman spectra. The ir spectra show beautiful splitting between ν_7 and ν_8, which is very similar case with these splitting of Zizpse6144, and the ν_9 mode also shows quite good splitting in Raman spectra, suggesting that it is also an E mode.

5. 2. 3. α-P_4Se_4 (D_{2d}) in Zipse6144, Zipse334 and Zizpse6147

The structural backbone has been rarely reported about such symmetric species P_4Se_4 (D_{2d})[13, 122], but recently the evidence of binary glassy P_4Se_4 backbone was given by means of Raman scattering[122] and ^{31}P NMR[12], even in such cases no evidence as provided for the isolated molecule. In the first vibrational analysis from Monteil *et al.*[13], they assigned at *exo*-P_4Se_4 which was based on the vibration frequency of P = Se, 473 ~ 577 cm^{-1}, and also J. D. Sarfati *et al.*[122] reported that α- and β-P_4Se_4 molecular units in the amorphous phase neither possess an infrared absorption in such region, suggesting that no terminal P = Se bonding is in this crystal system. According to the concept of zero-dimensional glasses, those show too narrow energy gap between P_4Se_4 and P_4Se_3 to divide into individual molecules, i.e., into the isolated P_4Se_4 and isolated P_4Se_3, respectively, during the synthesis. In those senses, by means of vibration spectroscopic tools, it is very difficult to assign the different molecular, P_4Se_4 and P_4Se_3, units with correct vibrational modes. Only the available approach to confirmation of α-P_4Se_4 with such tools, at least the symmetric vibrational modes of hypothetical species Se_4 (D_{4h}, D_{2h} and T point symmetry), actually the vibrational investigations about such Se_4^{2+} cationic species have been reported by J. Gillespie, *et al.*[123,124], can be detected from the spectra of α-P_4Se_4. However, not only in the spectrum analysis of such cationic species in both of the crystalline state $Se_4(SO_3F)_2$, $Se_4(HS_2O_7)_2$, $Se_4(SO_3F)_2$, and $Se_4(Sb_2F_{11})_2$, and those various solvent media, but also in the correlation method approach, but there are so many distinguishable ambiguities. Concerning such species, the theoretical vibration assignments were investigated by R. Steudel[125] who derived the Urey-Bradley Se-Se bond force constants from the crystallographic bonding lengths and the infrared and Raman spectra of Se_8. And such force constants difference between Se-Se bonding and α-P_4Se_4 bonding can be easily compensated by a bond length consideration with the term of force vector. Comparing our spectra, Steudel's consideration shows quite good approximation with all the range, especially Raman inactive modes, ν_4 (B_{2u}) and ν_5 (E_u). The notable frequency from our spectra is very broad and intense peak which is centered at 256 cm^{-1} with the range of 240 ~ 275 cm^{-1} [see **Fig. 5-5 (d)** and **(e)**]. With respect to this reason, we can assign some of the doubly degenerated modes 4E of α-P_4Se_4 molecule at such range. R. J. Gillespie *et al.*[124] suggested

the symmetrical degeneration of Se_4^{2+} species from the rectangle-planar D_{4h} (E_u) to diamond planar D_{2h} (B_{2u} and B_{3u}), since the theoretical frequencies of trans-$Te_2Se_2^{2+}$ species showed 253 cm^{-1} (B_{2u}) and 242 cm^{-1} (B_{3u}), respectively. To add to this, both 268 cm^{-1} (A_g) and 270 cm^{-1} (B_{1g}) showed almost same values. As a conclusion, the vibrational energy levels of α-P_4Se_4 (D_{2d}) molecule have very dense excitation tendency, so that it is too difficult to divide into the individual assignments, even with the theoretical means.

6. The thermodynamic consideration of $[(ZnI_2)_6(ZnSe)]/[\alpha\text{-}P_4Se_3]$ system

The I1 (*96h*) position in $F\bar{4}3c$ atomic model has no notable symmetric pattern. How can we approach to the solution for whole crystal structure with respect to (1) the orientation of guest molecule, (2) a dynamic property of intercalated molecule and (3) the interfacial correlation between the host lattice, [Zn-Q] and guest molecule, $[P_4Q_3]$? The confluence of above 3 respects can be regarded as an energy relationship between host lattice and guest molecule. As a first approximation, the model of 'a particle in a sphere' is essential for such a solution.

Therefore, the approach to a solution is allowed as following procedure,

(i) at first, the free volume element of cavity structure can be defined by a spherical nature of cavity structure,

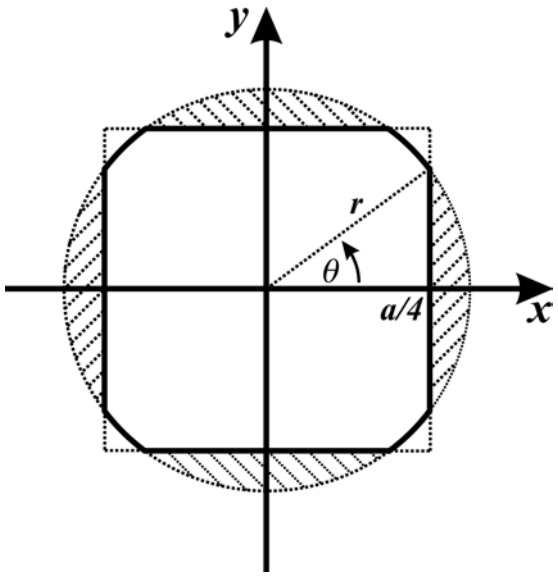

Fig. 6-1. The definition of cavity volume (where a = lattice constant with Z = 8, r = cavity radius and the shadowed section indicates the overlapped parts with adjacent cell).

(ii) a cavity radius, r_{cavity}, is derived from the length between *8b* position and I1 (*96h*) as an arithmetic average.

(iii) a cavity volume, V_{cavity}, is able to be calculated by the following relationship, where $b = a/4$ (a = lattice constant with Z = 8).

$$V_{cavity} = 2\pi r^3 \left[3\left(\frac{b}{r_{cavity}} \right) - \left(\frac{b}{r_{cavity}} \right)^3 - \frac{4}{3} \right] (\mathring{A})^3 \qquad (19)$$

With simple numerical calculation, under the assumptions (1) of a spherical form of cavity structure, and (2) that no phase transition is observed in clathrate [Zn-Q]/[P_4Q_3] system by means of temperature modification, and (3) of a single occupancy by P_4Q_3 (Q= S or Se) molecule with Z = 1, the pre-defined cavity radius (r_{cavity}) and cavity volume (V_{cavity}) can be derived from the lattice constant and the atomic coordinates of I1 (*96h*) as following **Table 6-1**.

Table 6-1. The calculated cavity volume from lattice constants and atom location parameters.

	temp. (K)	*a* (Å)	r_{cavity} (Å)	V_{cavity} (Å^3)
[Zn-Se] host	Zizpse6144			
	123	19.419(2)	5.694(1)	701.4(1)
	173	19.444(2)	5.704(1)	704.8(1)
	293	19.518(2)	5.733(1)	714.5(1)
	373	19.570(2)	5.755(1)	721.6(1)
	423	19.624(2)	5.775(1)	728.6(1)
	Zipse334			
	123	19.422(1)	5.697(1)	702.2(1)
	293	19.542(1)	5.743(1)	717.8(1)
	Ziasse6144			
	293	19.595(2)	5.765(1)	725.1(1)
[Zn-S] host	Zizps6144			
	123	19.290(2)	5.662(1)	688.8(1)
	293	19.386(2)	5.670(1)	701.2(1)

r = cavity radius and *a* = lattice constant in Å.

As the results from the examination for a correlation between host lattice and cavity structure,

(i) between the lattice volume, $V_{lattice}$ and the cavity volume, V_{cavity}, a quite good linear relationship was showed in **Fig. 6-2**,

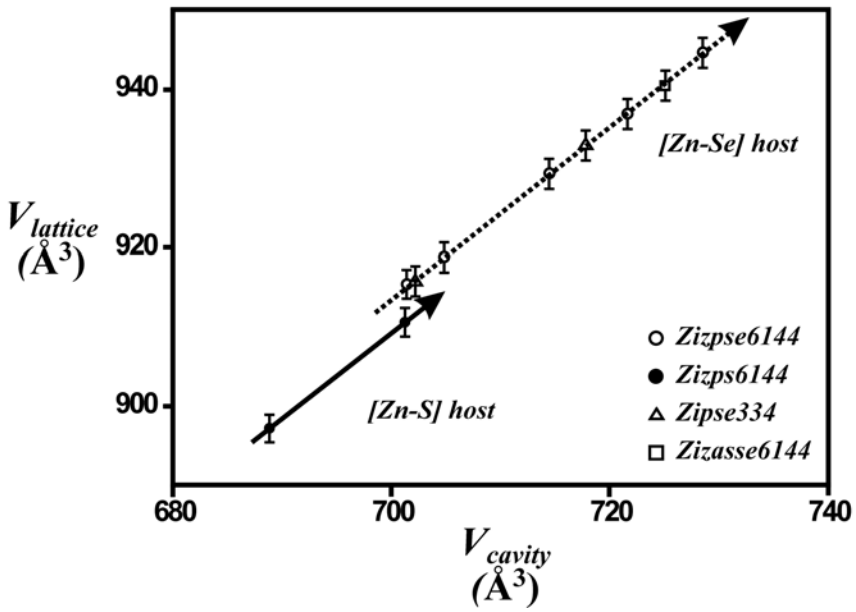

Fig. 6-2. A linear relationship between lattice volume ($V_{lattice}$) and cavity volume (V_{cavity}) [where Vlattice = a (Å)^3/8 and a = lattice constant with Z= 8].

The net volume element of host lattice depends directly on the cavity volume, V_{cavity}, over the wide range of temperature, 123 ~ 423 K. The limiting slope $(\frac{\Delta V_{lattice}}{\Delta V_{cavity}})$ is 1.09(1).

(ii) the tendencies of volume expansion for [Zn-Se] host lattice and [Zn-S] host lattice are extremely distinguishable with common physical sense, i.e., S atom should be smaller than Se.

(iii) for an interpretation of cavity volume expansion by means of temperature modification, 'a balloon model' can be suggested for a solution of lattice dynamics for instance a solution from a term of surface tension.

Within the accuracy of temperature dependent X-ray measurements concerning Zizpse6144 crystal (see **Fig. 6-3**), the effective volume (V) element of [Zn-Se] host lattice can be relatively well justified with a simplified physical concept upon the effective bonding radius of atom, which follows rather ambiguous and quite arguable effective cavity volume ($V_{eff.cavity}$) and the deduced cavity pressure (p) by intercalated molecule has a room for wide discussions about nature or for an advanced theoretical approach. But how can we make systematic approach from following sigmoid shaped temperature modification result to solution for understanding clathrate system?

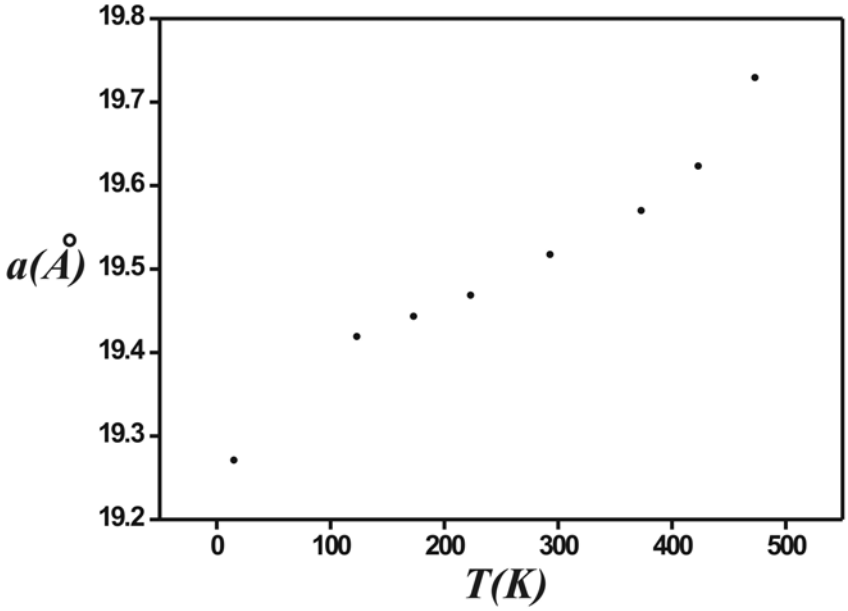

Fig. 6-3. The lattice constant variation by temperature dependent X-ray measurements of Zizpse6144.

Consequently with p, V, T and n data, I will allow the space with intensive numerical calculation for examining the thermodynamic aspect of this crystal system from a gas approximation to a liquid one in order to examine *the generalized thermodynamic relationship* for this clathrate system and others.

6. 1. The definition of isobaric coefficient of the thermal expansion

From the manipulating the thermodynamics first law, it gives Eq. (20),

$$dU = \left(\frac{\partial U}{\partial T}\right)_V dT + \left(\frac{\partial U}{\partial V}\right)_T dV \tag{20}$$

Above Eq. (20) divides through by dT, and then imposes the condition of constant pressure. It yields

$$\left(\frac{\partial U}{\partial T}\right)_p = C_V + \left(\frac{\partial U}{\partial V}\right)_T \left(\frac{\partial V}{\partial T}\right)_p \tag{21}$$

The thermal expansivity defined as Eq. (22),

$$\alpha = \frac{1}{V}\left(\frac{\partial V}{\partial T}\right)_p \tag{22}$$

i.e., as the rate of change of volume with temperature per unit volume. Introduction of this definition readily gives

$$\left(\frac{\partial U}{\partial T}\right)_p = C_V + \alpha V \left(\frac{\partial U}{\partial V}\right)_T \tag{23}$$

Eq. (23) is entirely general (so long as the system is closed and its composition constant). It expresses the dependence of the internal energy on the temperature at constant pressure in terms of the constant volume heat capacity, C_V, which can be measured in proper experiment, i.e., normally with vibrational spectroscopy in clathrate systems, the coefficient of expansion, α, which can be measured in X-ray techniques and the quantity $\left(\frac{\partial U}{\partial V}\right)_T$.

6. 1. 1. The thermal expansivity of $[(ZnI_2)_6(ZnSe)]/[\alpha\text{-}P_4Se_3]$ system

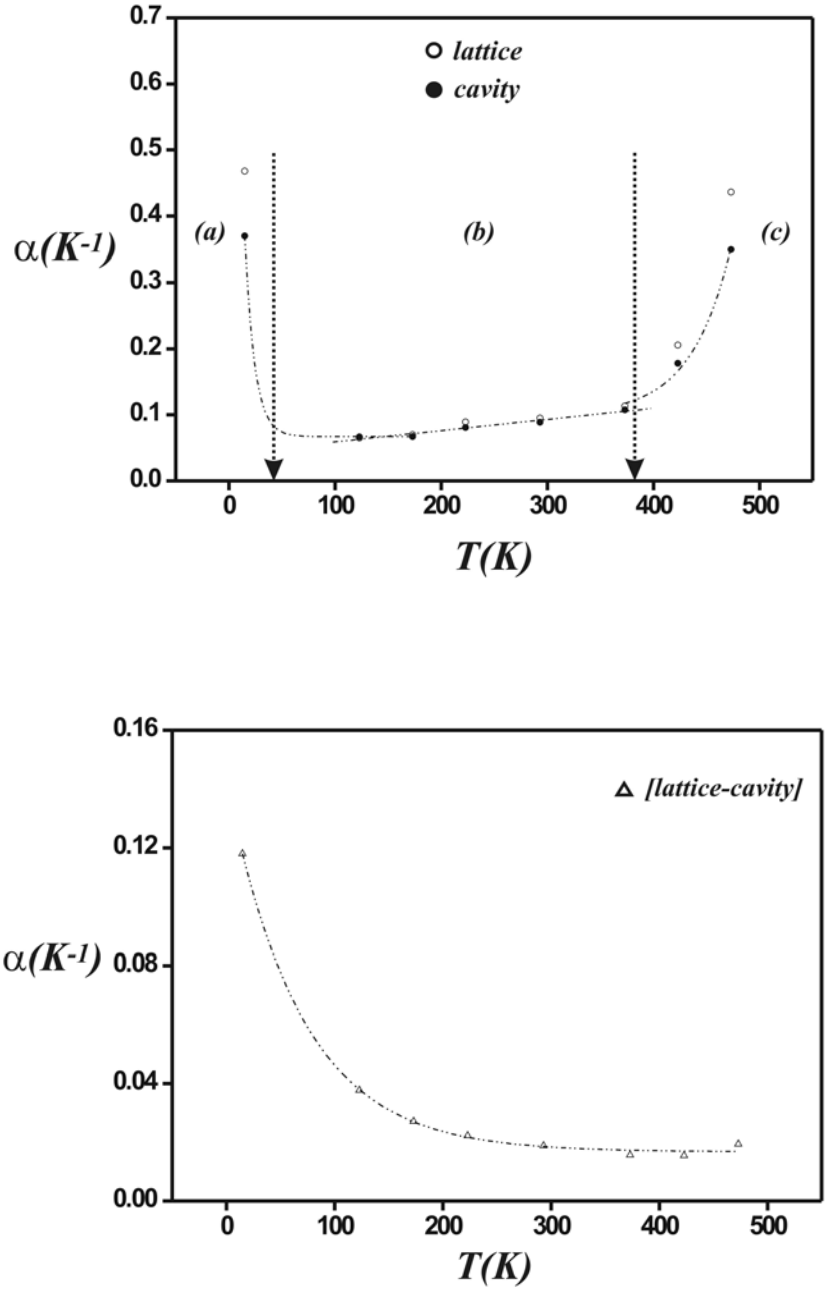

Fig. 6-4. The thermal expansivity of Zizpse6144 [down, pure Zn-Se based host lattice ; the region (a) indicate a compression limit of host lattice, the region (c) a expansion limit and region (b) regards as a linear elastic range of host lattice].

The thermal expansivities of both cavity volume variation and lattice volume variation show same tendency and both of data points are exactly superimposed in the range **(b)**, 100 ~ 400 K, which means that the lattice expansion directly depends on the motion of guest molecule above 100 K. The curve fitting result in the range **(c)** is well matched with various kinds of first order exponential growth model or distribution models, i.e., the best matched with Boltzmann distribution ($R^2 =$ 0.99992) above 293 K. It means that the guest vibrational energy contribution to host lattice becomes predominant at this temperature, i.e., from the thermodynamic relationship, αV gives the change of the volume when temperature is raised, and $\left(\frac{\partial U}{\partial V}\right)_T$ converts this change of volume into a change of internal energy. In this stage, we have to notice the vibrational contribution of guest molecule with increasing temperature, i.e., the C_V change with temperature. The range **(a)** is quite interesting for understanding the motion of guest molecule and the limitation of lattice compression in liquid He temperature, i.e., the lattice volume itself can be no more compressed by lowing the temperature. The curve fitting with three data (15 ~ 173 K) may be incorrect, but the tendency of exponential decay is sure to estimating the zero vibration and rotation of guest molecule around 30 K.

Conclusively speaking, regarding the clathrate research, some authors have traced the thermal expansivity with respect to either lattice constant variation or size of cavity variation. But form our evaluation, both results from lattice volume and cavity volume are not exactly the same [see **(a)** and **(c)** in **Fig. 6-4**]. This means that the characterization of clathrate system based on tracing thermal expansivity may lead to serious failures, at least when a rigid host is considered.

6. 1. 2. The temperature dependence of volume of [$(ZnI_2)_6(ZnSe)$]/[α-P_4Se_3] system

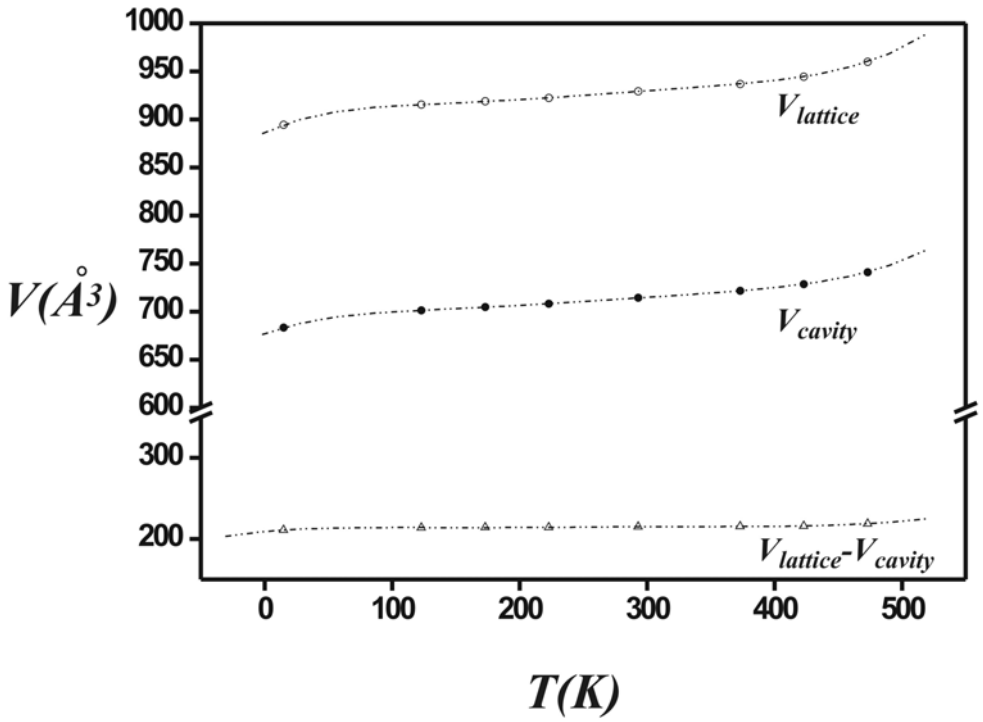

Fig. 6-4. The polynomial curve fitting of volume elements as a function of temperature of Zizpse6144.

The polynomial curve fitting results show a quit linear tendencies on both volume elements, lattice volume and cavity volume (see **Fig. 6-4**), since the contributions under quadratic term (T^2) are very small to whole curve fitting.

Table 6-2. The results of polynomial curve fittings of volume elements of Zizpse6144.

$V(T)(\overset{o}{A^3})$	polynomial curve fitting	R^2	σ
$V_{lattice}$	$886.44799 + 0.62588T - 0.00571T^2 + 2.77476\cdot10^{-5}T^3 - 6.58463\cdot10^{-8}T^4 + 6.9553\cdot10^{-11}T^5 - 2.06924\cdot10^{-14}T^6$	0.99996	0.33661
V_{cavity}	$677.16683 + 0.48501T - 0.00413T^2 + 1.94241\cdot10^{-5}T^3 - 4.45509\cdot10^{-8}T^4 + 4.48729\cdot10^{-11}T^5 - 1.14859\cdot10^{-14}T^6$	0.99996	0.29028
$V_{lattice-cavity}$	$209.28116 + 0.14087T - 0.00158T^2 + 8.32348\cdot10^{-6}T^3 - 2.12954\cdot10^{-8}T^4 + 2.46802\cdot10^{-11}T^5 - 9.20653\cdot10^{-15}T^6$	0.99994	0.04633

The curve fittings were carried out with (n-2) order in order to avoid the polynomial wiggle problems. Above results indicate following points,

(i) the volume increments of both the cell (host lattice + guest molecule), $V_{lattice}$ and the cavity, V_{cavity} showed same increasing tendency, but slightly deviated. Two increments have a linear relationship (see **Fig. 6-2**).

(ii) the volume increment of host lattice itself, $V_{lattice-cavity}$, i.e., a pure volume increment of [Zn-Se] host lattice shows almost the same value over the whole temperature range, i.e., almost no volume changed, only ~ 7 Å^3 increased over 15 ~ 473 K (only 3 % increment compared with volume of 0 K. It is almost a constant value). This result strongly supports '*a balloon model of host framework*' as I discussed in former crystallographic section, i.e., the volume increment of host lattice itself can be interpreted by the concept of surface tension and increment of surface area with respect to thermodynamic function of Helmholtz free energy (A)[126] or recently of thermal elasticity consideration based on Laplace-Young model[127].

(iii) regarding the clathrate research, the indicated results suggest that the research which are based on the increment of lattice parameter can lead to serious failure.

6. 2. The cavity pressure by guest molecule in $[(ZnI_2)_6(ZnSe)]/[\alpha\text{-}P_4Se_3]$ system

In crystallographic section, we discussed about

(i) the crystallographic views of $[(ZnI_2)_6(ZnQ)]/[Pn_4Q_x]$ (Pn = P, As ; Q = S, Se) crystal systems, and $[(ZnI_2)_6(ZnSe)]/[\alpha\text{-}P_4Se_3]$ system was intensively investigated from 15 to 473 K, which can provide exact information about the thermodynamic volume elements,

(ii) and results of RB refinements indicated the one-dimensional translation motion of intercalated guest molecule,

(iii) and some spectroscopic tools indicated the evidence of isolated free molecules in cavity volume of $[(ZnI_2)_6(ZnQ)]/[Pn_4Q_x]$ (Pn = P, As ; Q = S, Se) crystal system. Especially with solid state NMR technique, the molecules were identified.

Now we know the whole thermodynamic conditions for considering the molecule pressure in cavity volume. The final goal of research for this clathrate system is to obtain the thermodynamic properties, for example, U (internal energy), H (enthalpy) and its free energy (G or A) from the p (pressure), V (volume) and T (temperature) data, and those relationship. Also, the single occupancy provides us that the molar change of guest molecule in cavity is ignoble. The procedure including numerical calculations is limited on the hard-sphere model and also with hard-sphere potential. Those arguable assumptions can be open to discussions concerning the internal potential of cavity of this clathrate system, and concerning the consideration about the reaction conditions. I guess that this approach is really helpful to give an information for synthetic aspects of other material combinations and the intercalating possibilities of other guest molecules into cavity. The thermodynamic relationship and its stability between host lattice and guest molecule also will give a good information for closely examining other clathrate systems.

For simplicity, let us assume the following conditions,

(i) the guest molecule has a rigid-spherical form and the effective molecular volume, $V_{m.eff.} = \frac{4}{3}\pi\left(\frac{\sigma}{2} + r_{co.}\right)^3$ (Å^3) is defined as follows, where σ = molecule diameter and $r_{co.}$ = covalent radius of Pn atoms in Pn_4Q_3 molecule (see **Fig. 6-5**),

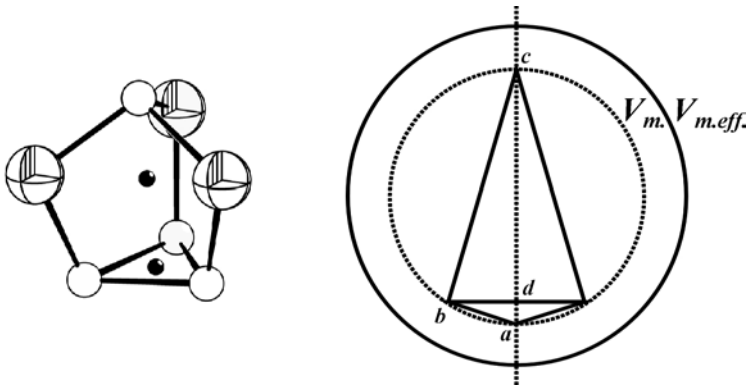

Fig. 6-5. The definition of effective P_4Se_3 molecular volume.

In case of P_4Se_3, $\theta_{cba} = \theta_{cab} = 68.02^o$ and $\overline{bc} = 3.429$ Å, therefore $\sigma = 3.697$ Å and $r_{co.} = 1.10$ Å.

(ii) the effective radius for cavity volume is defined as follows,

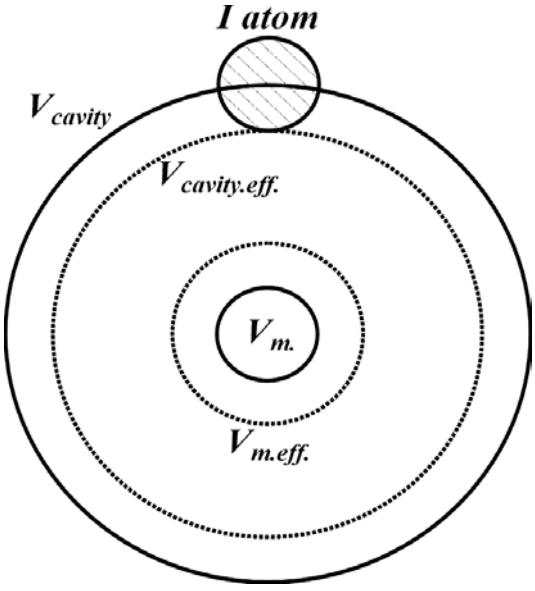

Fig. 6-6. The definition of effective cavity volume and free volume.

Due to the strong polarizability of iodine atoms, we can consider that the effective radius of iodine atoms confined on the van der Waals radius, i.e., 2.516 Å (I atoms, location parameter from crystallographic data at 15 K). The van der Waals radius was varied from 2.15 Å to 2.516 Å. The total relationship between the effective radius and the free volume of molecule is summarized as following Eq. (24), where V_f = free volume, r'_{cavity} = crystallographic cavity radius, r_{vdw} = van der Waals radius, b_0 = co-volume with respect to gas approximation,

$$V_f = \frac{4}{3}\pi\left(r'_{cavity} - r_{vdw}\right)^3 - \frac{4}{3}\pi\left(\frac{\sigma}{2} + r_{co.}\right)^3 \left(\text{Å}^3\right) \approx b_0 \tag{24}$$

(iii) the virial equation of state was adopted to calculate the thermodynamic properties, since it is quite well matched with not only gas approximation, with but also liquid approximation, as following Eq. (25)[126], and corresponding virial coefficients were line-fitted for calculation of other thermodynamic properties.

$$\begin{aligned} &\frac{pV}{k_B T} \\ &= 1 + \frac{B(T)}{V} + \frac{C(T)}{V^2} + \frac{D(T)}{V^3} + \frac{E(T)}{V^4} + \cdots \\ &= 1 + \frac{b_0}{V} + \frac{0.625{b_0}^2}{V^2} + \frac{0.2869{b_0}^3}{V^3} + \frac{0.115{b_0}^4}{V^4} + \cdots \end{aligned} \tag{25}$$

where $V = V_{cavity.eff.}$

With above assumptions, the pressure could be calculated as following **Fig. 6-7**.

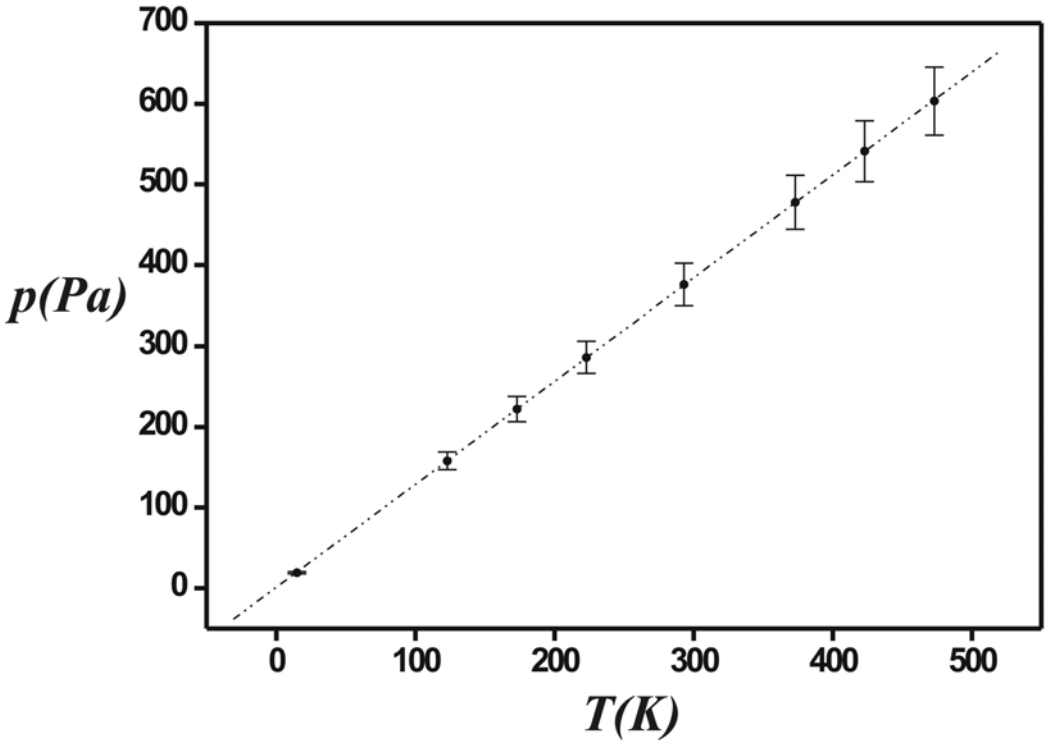

Fig. 6-7. The P_4Se_3 molecular pressure in the effective cavity volume with rigid-sphere model (with 7 % error bar and 2.15 Å < r_{vdw} < 2.516 Å).

The pressure increasing tendency shows a quite good linear approximation as $R^2 = 0.99999$ ($\sigma = 0.885$). And the D.O.F. (degree of freedom) shows good spherical approximation with ideal value 1.5 for translational molecular motion in decomposition temperature (which indicates the temperature for escaping molecule from lattice) as following **Fig. 6-8**.

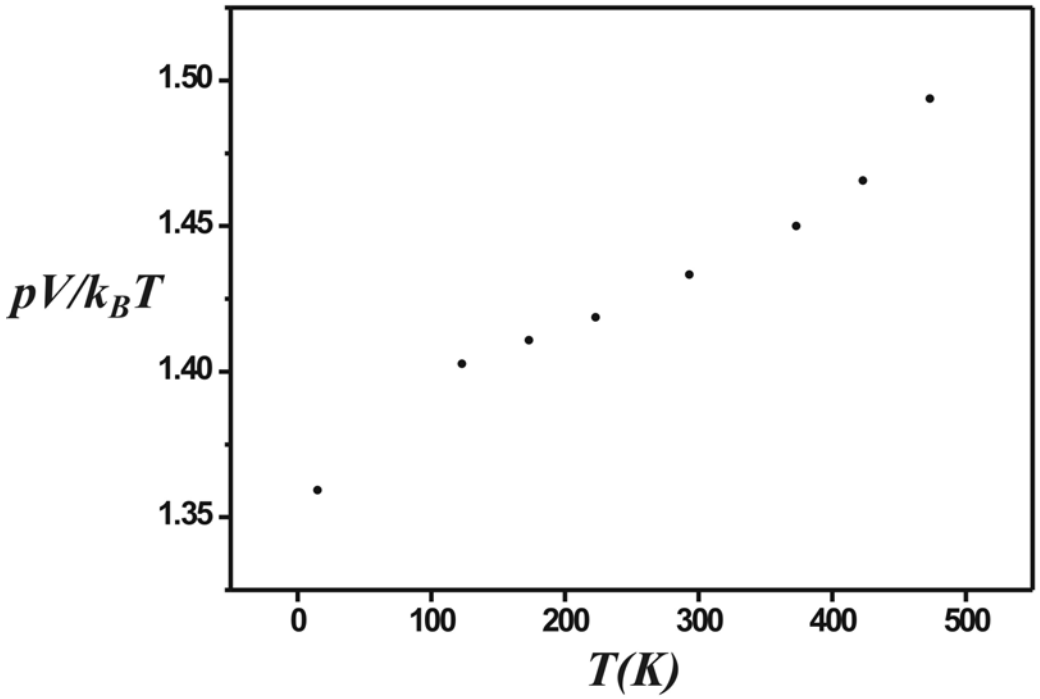

Fig. 6-8. The translational D.O.F. of P_4Se_3 molecule in cavity.

Above results from numerical calculations indicates notable points concerning this crystal system as follows,

(i) the pressure (*p/molecule*) increasing on temperature (*T*) shows an ideal gas behavior with the slope of $\frac{\Delta p}{\Delta T} = 1.186 \ \ (\sigma = 0.006)(Pa/K)$.

(ii) the pressure shows moderate value 353.5 *Pa* ($Pa = \frac{J}{m^3} = \frac{N}{m^2}$) at room temperature which is comparable with other inert gas calculation[126]. This indicates that the *pV*-work term of guest molecule may be converted into other generalized work term.

(iii) The compression factor ($z = \frac{pV}{k_B T}$) over the temperature shows the free translation motion, i.e., D.O.F. (degree of freedom) = 3 for free particle, at molecule escape temperature (473 K) from lattice potential.

6. 3. Other thermodynamic properties of [$(ZnI_2)_6$(ZnSe)]/[α-P_4Se_3] system from virial equation of state

As we mentioned in former section, the other thermodynamic properties of guest molecule can be elucidated from the final thermodynamic variable *p* (cavity pressure by guest molecule), and pre-defined volume (*V*) and temperature (*T*). Definitions for other thermodynamic properties are as follows[126],

(i) internal energy

$$\begin{aligned} & U - U(0) \\ & = -\int_V^\infty \left\{ T\left(\frac{\partial p}{\partial T}\right)_V - p \right\} dV \\ & = -RT\left\{ \frac{T}{V}\frac{dB}{dT} + \frac{T}{2V^2}\frac{dC}{dT} + \frac{T}{3V^3}\frac{dE}{dT} + \cdots\cdots \right\} \end{aligned} \tag{26}$$

(ii) enthalpy

$$\begin{aligned} & H - H(0) \\ & = pV - RT - \int_V^\infty \left\{ T\left(\frac{\partial p}{\partial T}\right)_V - p \right\} dV \\ & = -RT\left\{ \frac{1}{V}\left[B - T\frac{dB}{dT} \right] + \frac{1}{V^2}\left[C - \frac{1}{2}T\frac{dC}{dT} \right] + \frac{1}{V^3}\left[E - \frac{1}{3}T\frac{dE}{dT} \right] + \cdots\cdots \right\} \end{aligned} \tag{27}$$

(iii) entropy

$$\begin{aligned} & S - S(0) \\ & = -R\ln p + R\ln\frac{pV}{RT} - \int_V^\infty \left\{ \left(\frac{\partial p}{\partial T}\right)_V - \frac{R}{V} \right\} dV \\ & = -R\left\{ \ln p + \frac{T}{V}\frac{dB}{dT} + \frac{B^2}{2V^2} - \frac{C}{2V^2} + \frac{T}{2V^2}\frac{dC}{dT} + \cdots\cdots \right\} \end{aligned} \tag{28}$$

(iv) Gibbs free energy

$$G = H - TS \tag{29}$$

(v) Helmholtz free energy

$$A = U - TS \tag{30}$$

For numerical calculation, the virial coefficients are line-fitted with polynomial equations, as following **Table 6-3.** Regarding line fitting, I allowed the accuracy as T^6 term and left the figures of standard deviation as those own decimal point for any theoretical accessions.

Table 6-3. The polynomial curve fittings of virial coefficients.

virial coeff.	polynomial curve fitting	R^2	σ
B(T)	$42.81733 + 0.17874\mathrm{T} - 0.152\times10^{-2}\mathrm{T}^2 + 0.709429\times10^{-5}\mathrm{T}^3 - 0.161045\times10^{-7}\mathrm{T}^4 + 0.158425\times10^{-10}\mathrm{T}^5 - 0.365306\times10^{-14}\mathrm{T}^6$	0.99996	0.10839
C(T)	$1139.1285 + 10.26233\mathrm{T} - 0.08204\mathrm{T}^2 + 0.35378\times10^{-3}\mathrm{T}^3 - 0.663929\times10^{-6}\mathrm{T}^4 + 0.33539\times10^{-9}\mathrm{T}^5 + 0.267866\times10^{-12}\mathrm{T}^6$	0.99997	7.29076
D(T)	$22206.10261 + 315.48748\mathrm{T} - 2.24946\mathrm{T}^2 + 0.797\times10^{-2}\mathrm{T}^3 - 0.65125\times10^{-5}\mathrm{T}^4 - 0.198467\times10^{-7}\mathrm{T}^5 + 0.33002\times10^{-10}\mathrm{T}^6$	0.99997	263.94118
E(T)	$380540.96122 + 7151.82538\mathrm{T} - 39.41699\mathrm{T}^2 + 0.05698\mathrm{T}^3 + 0.436224\times10^{-3}\mathrm{T}^4 - 0.170302\times10^{-5}\mathrm{T}^5 + 0.176752\times10^{-8}\mathrm{T}^6$	0.99998	7168.53355

The results of numerical calculations are following **Table 6-4**.

Table 6-4. The summarized thermodynamic properties of P_4Se_3.

T(K)	U-U(0)(J/mol)	H-H(0)(J/mol)	S-S(0)(J/mol·K)	G-G(0)(J/mol)	A-A(0)(J/mol)
15	2.06	42.75	21.92	-286.10	-326.79
123	24.04	387.78	39.29	-4444.30	-4808.04
173	46.24	544.63	41.91	-6706.47	-7204.86
223	92.14	684.15	44.10	-9151.23	-9743.24
293	172.48	883.32	46.47	-12732.21	-13443.05
373	336.66	1058.80	48.66	-17093.08	-17815.22
423	728.49	909.31	50.40	-20407.84	-20588.66
473	1811.64	130.43	53.27	-25065.57	-23384.37

6. 4. Generalized thermodynamics on the imaginary surface between host lattice and guest molecule

For simplicity, we need following assumptions,

(i) the free volume of wandering for guest molecule is very small relative with the effective cavity volume,

(ii) the volume change of host lattice itself including the van der Waals radius is constant over all the whole temperature range, i.e., $dV_h = 0$, and also the pressure change constant, i.e., $dp_h = 0$,

(iii) the motion of guest molecule in the cavity is very limited, so consequently most of pV-work by guest molecule is converted into the surface tension energy on imaginary surface between host and guest, i.e., $p_g dV_g (= dV_{cavity.eff}) << \gamma d\alpha$,

(iv) on the imaginary internal surface between host lattice and guest molecule, the chemical potential correspond to each other.

(v) the intercalated cavity molecule has a single occupancy on its cavity and does not move into adjacent sites.

Consider a spherical interface between pure phase *h* (host) and *g* (guest). This interface is characterized by a surface tension γ expressed in terms of force per unit length. The interface is always a site of disturbance on an molecule scale, since the environment of molecules at interface is not regular as it is in the interior of the phase. As a result, to increase the area of an interface, work must be expended by the system (guest molecule). This generalized work was found to be given by

$dw = -\gamma d\alpha$ (work done by system)

From the thermodynamic first law,

$dU = dq - \gamma d\alpha$

and for a reversible process $dq = TdS$. If the work done by the system including pV-work ; totally *an effective work* ($w_{eff} = \gamma d\alpha + pdV$) is to increase the area of interface, $dw = -[\gamma d\alpha + pdV]$. At constant volume and pressure, $dH = dU$.

With above assumptions and in thermal equilibrium for the single occupancy in cavity, $d\mu_g = d\mu_h$ (the subscriptions g : guest molecule, h : host lattice and γ : surface tension, α : surface area)

For the chemical potential of host lattice with assumption (ii),

$$d\mu_h$$
$$= dG_h \approx dA_h$$

$$= dU_h - d(TS_h)$$

$$\begin{bmatrix} dw_h = +\gamma d\alpha \\ \therefore dV_h \approx 0 \end{bmatrix} \text{(work done on system)}$$

$$= -S_h dT + \gamma d\alpha$$

And for the chemical potential of guest molecule,

$$d\mu_g$$
$$= dG_g$$

$$= dH_g - d(TS_g)$$

$$\begin{bmatrix} dH_g = dU_g + d(p_g V_g) \\ = [TdS_g - \gamma d\alpha - p_g dV_g] + p_g dV_g + V_g dp_g \\ \therefore dp_g dV_g \approx 0 \\ dH_g = TdS_g - \gamma d\alpha + V_g dp_g \end{bmatrix} \text{(work done by system)}$$

$$= TdS_g - \gamma d\alpha + V_g dp_g - TdS_g - S_g dT$$
$$= -S_g dT - \gamma d\alpha + V_g dp_g$$

$$-S_h dT + \alpha d\gamma = -S_g dT - \gamma d\alpha + V_g dp_g$$
$$(S_h - S_g)dT = 2\gamma d\alpha - V_g dp_g \quad (31)$$

dp_g was constant over the temperature range from **Fig. 6-7**. Thus, above finally equation leads to following generalized form.

$$\left(S_h - S_g\right) = 2\gamma\left(\frac{d\alpha}{dT}\right) - const. \quad (32)$$

If the constant value, $V_g\left(\frac{dp_g}{dT}\right)$ is very small, the overall equation leads to following Eq. (33),

$$\left(S_h - S_g\right) \approx 2\gamma\left(\frac{d\alpha}{dT}\right) \quad (33)$$

Above thermodynamic relationship between host and guest is a general expression on clathrate system with following evidences,

(i) between the pV-work term which was calculated by gas approximation (see **Fig. 6-7**) and one which was calculated by the thermodynamic relationship $H - U = pV$ $(H_o = U_o)$ (see **Table 6-4**) has a huge discrepancy. So finally we can suggest the relationship as one word, $dG_g \rightarrow dA_h$.

(ii) the volume change of host lattice was not changed over the temperature range (see **Fig. 6-4**), and its pressure change is zero. It is well matched with former assumption (ii).

(iii) the infinitesimal change of pV-work by changing guest molecule on cavity or distributed over the cavity can be used for estimating the thermodynamic properties from chemical potential change. It is really arguable for theoretical chemists and means that fromer assumption (iii) is still alive and quite questionable.

(iv) among the final relationship, the surface tension term γ can be substituted by the lattice elastic constant at any given radius, i.e., the shear Lame constant with stress tensor approach.

6. 5. Free energy calculation from lattice elasticity in [$(ZnI_2)_6(ZnSe)$]/[α-P_4Se_3] system

Recently, the calculation method of the free energy of a particle in a cavity of radius r and the elastic energy required to create such a cavity using hard sphere f.c.c. cell model was reported by S. Pronk and D. Frenkel[128] as following Eq.(34) with respect to translational contribution of interstitial (3-D term) and surface tension contribution of interstitial (2-D term),

$$F(r) = -k_B T \ln\left[V_{free}\right] + 8\pi\mu r_o \left(r - r_o\right)^2 \qquad (34)$$

where free volume, $V_{free} = \left(\frac{4\pi}{3}\right)\left(r - \frac{\sigma}{2}\right)^3$ (where σ = diameter of rigid sphere), μ = shear Lame coefficient, $r_o = \left(\frac{\sqrt{2}}{2} - 0.5\right)a$ (where a = the nearest-neighbor distance) and r = radius of cavity, respectively. Also they used following assumptions for calculating point defects of hard-sphere crystal,

(i) a crystal contains one single vacancy and one can attempt a trial insertion in the Wigner-Seitz cell surrounding that vacancy. It means a single occupancy.

(ii) they introduce the grand canonical partition function of a perfect lattice, i.e., under the assumption of no point defect with a fixed number of particles.

(iii) the cavity has to be isotopic expanded.

(iv) the free energy is calculated by only the term of surface tension energy of an interstitial in cavity.

Comparing with our data and Eq. (34),

(i) with our temperature modification data, there is no information about the shear Lame constant in the relationship, $W = 8\pi\mu r_o \left(r - r_o\right)^2$.

(ii) by Brillouin spectroscopy the possibility to be measured the elastic constants of clathrate system, and the acoustic velocities of interstitial in clathrate hydrate were suggested[129].

(iii) in our thermodynamic consideration, we suggest that the free volume contribution to free energy change is almost zero under above assumption (ii) compared with surface contribution, therefore, the 3-D volumetric term (which can express with pV-work) from our data should have a linear relationship with 2-D surface tension energy term W by S. Pronk and D. Frenkel[128].

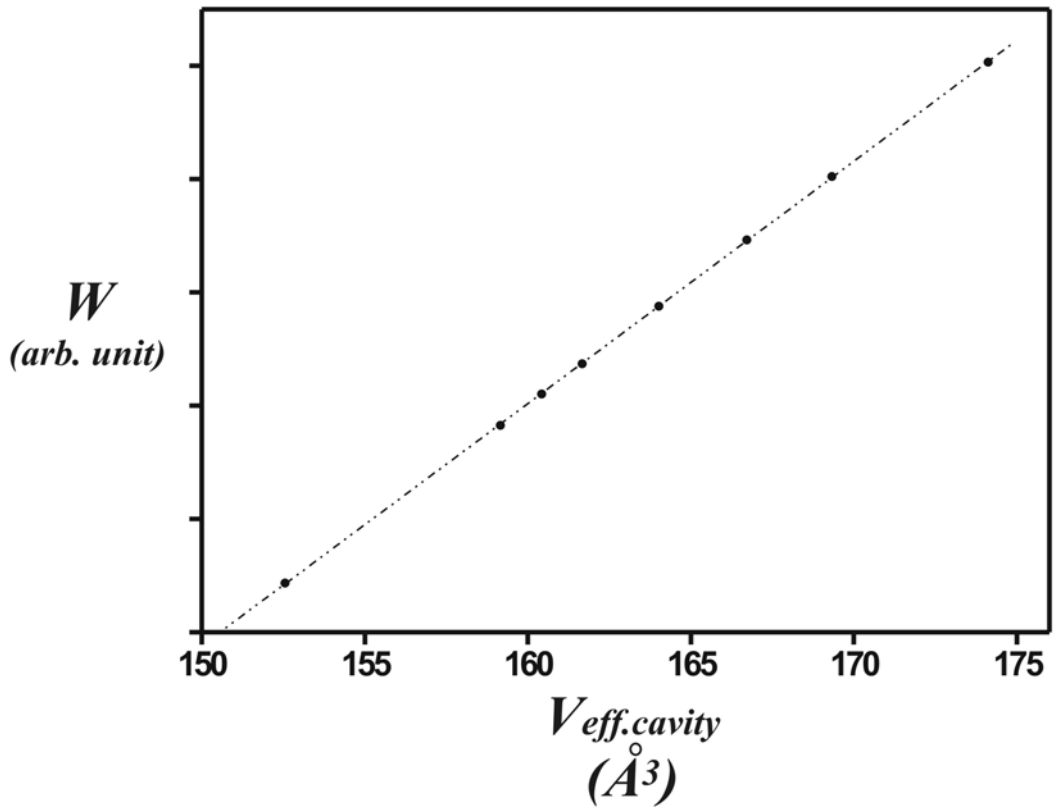

Fig. 6-9. The linear relationship between theoretical surface tension term W and experimental volumetric term.

Above linear relationship is line-fitted with $R^2 = 0.99998$ ($\sigma = 0.47417$).

As a conclusion,

(i) the zizpse6144 system has almost no point defect, i.e., it looks like a perfect lattice. This concept is well matched with the B. Moulton and M. J. Zaworotko's view[130], i.e., the clathrate systems need to *'avoid a vacuum'*.

(ii) for both theoretical and experimental way, this clathrate system should be investigated by the light scattering sources.

7. Summary

The host/guest clathrate systems - $[(ZnI_2)_6(ZnQ)]/[Pn_4Q_x]$ (Pn = P, As ; Q = S, Se) are obtained by one-step or two-step reaction of stoichiometric amounts of ZnI_2, Pn, and Q or varying Q, I amounts in evacuated silica ampoules. The compounds consist of monomeric α-Pn_4Q_3 and α-Pn_4Q_4 cage molecules which are separated by a cubic host lattice of $[(ZnI_2)_6(ZnQ)]$. This contains almost spherical cavities about 10 Å diameter. $[(ZnI_2)_6(ZnQ)]$ / $[Pn_4Q_x]$ crystallize in the cubic system, space group $F\bar{4}3c$ (No. 219) with Z = 8. Especially the lattice constants are slightly varied by initial Q rich condition. Pn_4Q_x molecules which have C_{3v} and D_{2d} point group symmetry respectively, are embedded into $[(ZnI_2)_6(ZnQ)]$ host 3D framework, are located on the center of LJD (Lennard-Jones-Devonshire) potential field in a disordered manners. Between host lattice and guest molecule no chemical bond is observed from the structural data. ^{31}P-MAS solid state NMR spectra show the component ratios of disordered chalcogenide molecules. Also, solid state FT-ir and FT-Raman spectra were measured and discussed.

For simplicity, we have to summarize the specific characteristics of this type of components.

(i) A concept for synthetic strategy using Cu halides which has been targeted for stabilization of neutral molecules or analogues was successfully expanded into that using ZnI_2.

(ii) The thermodynamic pre-calculation for quasi-binary metal halide – chalcogen (group 16 elements) system was helpful for adopting quasi-ternary metal halide – chalcogen – pnictogen systems.

(iii) The compounds were characterized by X-ray powder diffraction, single crystal measurements, solid state FT-ir/Raman and solid state MAS ^{31}P NMR spectroscopy.

(iv) All the X-ray powder diffraction showed same pattern and tentatively the space group $F\bar{4}3c$ (no. 219) was assigned. With this space group, the refined results showed a quite good linear relationship between the lattice constants from 19.38 to 19.60 Å and the initial endorsements of atomic molar ratio

Q/Zn (Q = S, Se). The increasing tendency stiffly jumped between the ratio Q/Zn = 0.57 (for Pn_4Q_3) and 0.71 (for Pn_4Q_4).

(v) The preliminary solutions of single crystal measurements indicated $m\bar{3}m$ as the Laue class. Either centro- or acentro symmetric assignment could not be distinguished. The exact atomic positions of intercalated molecules were not detectable. Even though, all the refinement values were optimal and especially, R_1 [$I > 2\sigma(I)$] showed an over- correct values of 0.016 - 0.024.

(vi) The elucidated structure with space group $F\bar{4}3c$ indicated all the structures as 'host / guest clathrate system' $[(ZnI_2)_6(ZnQ)]/[Pn_xQ_y]$ (Pn = P, As ; Q = S, Se) with Z = 8.

(vii) The results of MAS ^{31}P NMR spectroscopy concluded the intercalated guest molecules $[Pn_xQ_y]$ with qualitative as monomeric globular α-P_4Q_y (Q = S, Se ; y = 3, 4), but the measured data of chemical shift were quite different with data from solid state measurement, to the contrary, quite well matched data from solution measurements.

(viii) The results of RB refinements indicated that the intercalated guest molecule in confined cavity can be showed an 1-D translational motion ($E_T = \frac{1}{2}k_BT$), therefore the location for D.O.F. = 3 (for *x, y,* and *z,* respectively) were suggested and other energy contributions by guest molecule can be compensated with potential energy of its cavity environments in order to maintain the spherical shape of host lattice, and molecules never approach each other.

(ix) The temperature dependent X-ray measurements of $[(ZnI_2)_6(ZnSe)]/[\alpha$-$P_4Se_3]$ from 15 to 473 K showed no phase transition. Consequently, pure volume change rates of the $[(ZnI_2)_6(ZnSe)]$ host lattice are constant over whole the temperature range, showing 'an ideal balloon behavior'.

(x) The characterization of this clathrate system based on tracing thermal expansivity may lead to serious failure, since the values for the lattice and cavity were not exactly the same.

(xi) The virial expansion of cavity volume based on the rigid-sphere model of guest molecule provided rough information about internal pressure of guest molecule in the cavity and consequently related thermodynamic properties were derived. The results indicate that most of pV-work by guest molecule may be converted into $\gamma\alpha$-work (where γ = inter-surface tension and α = inter-surface area) of host lattice, i.e., most of the change of free Gibbs energy by guest molecule converted into the change of free Helmholtz energy for sustaning interface between guest molecule and host lattice.

(xii) Comparing statistical thermodynamic relationship with our temperature variation data, this clathrate system showed almost no point defect and this evidence is well matched with those refinement values of $[(ZnI_2)_6(ZnSe)]/[\alpha\text{-}P_4Se_3]$.

Based on above characteristics, we suggest the following points,

(i) The concept of formation of this clathrate system under thermodynamic consideration can be expanded to other metal halides based quarsi– ternary system, i.e., MX or MX_2 – Pn – Q (where Pn = group 15 and Q = group 16 elements). The reaction thermodynamics concerning this quasi– ternary system should be systematically evaluated with respect to constant volume reactor and its reaction kinetics.

(ii) Under the assumption of quasi binary treatment about quasi-ternary system MX_2 (or MX) – Pn – Q, the stiochiometric molar ratios for $\Delta_r G < 0$ (at 1000K) of reactions based on CdX_2, CuX and AgX were suggested as following relationships. And those evaluations may be helpful to expand this system into other metal halides or analogues.

$$\frac{n\ [\Delta_{diss.}G\ (MX - MX_2)]}{n\ [\Delta_{for.}G\ (MQ)]} = \frac{x}{y} \qquad \text{at 1000K}$$

comp.	M_2S	M_2Se	comp	MS	MSe
CuF	7.43	14.23	ZnF_2	3.26	3.85
$CuCl$	3.68	7.05	$ZnCl_2$	1.61	1.90
$CuBr$	3.37	6.46	$ZnBr_2$	1.30	1.54
CuI	1.53	2.94	ZnI_2	0.84	0.99
AgF	6.46	4.61	CdF_2	4.06	4.38
$AgCl$	3.20	2.29	$CdCl_2$	1.91	2.06
$AgBr$	2.77	1.97	$CdBr_2$	1.50	1.62
AgI	1.95	1.39	CdI_2	1.02	1.10

Since these compounds have been made with the range of x/y ratio from 0.84 (Zn-S sytem) to 0.99 (Zn-Se system), the cases based on Cu and Cd metal halides and AgI are quite questionable. The systems based on Br and Cl may lead $\Delta_r G < 0$ (at 1000 K) with additional metal amount compared with equi-molar condition. Most of metal florides showed a high thermodynamic obstacle to make analogues for this crystal system. Instead of that, the Q/metal ratios at 1000 K, however, indicate that with those ratios, this quasi ternary system is accessible to the analogues for boracite family. In a parallel with oxidation technique, also, the reduction routes of metal chalcogenide (MCh or M_2Ch) or metal halides using reductive elements (for instance group 13 and group 14 elements) or analogues should be considerable. Such a reduction technique also has been well developed in mining and semi-conductor industry.

(iii) The refinement method for various embedded guest molecules should be developed by proper modernized term, for instance the TLS (translation, libration and screw-rotation) tensor formalism of Schomaker and Trueblood[131] developed in the '60s which can be supported by program RESTRAIN (from CCP4 Program Suite).

(iv) Either by theoretical or by thermodynamical considerations, the physical properties of globular molecules should be established.

(v) The spectroscopic measurements should avoid the suspension methods. The measurements with single crystal are recommendable due to the solution-like behavior of these compounds, and for the identification of chalcogenide molecules, the polarity ir/Raman measurements are indispensable including far-ir region, and static single crystal measurements are also quite interesting.

(vi) The generalized thermodynamic relationship between host lattice and guest molecule was suggested as $(S_h - S_g)dT = 2\gamma d\alpha - V_g dp_g$. Under the isothermal condition ($dT = 0$), i.e., using pressure dependent X-ray measurement the lattice entropy can be elucidated and also the results are comparable with a lattice elasticity approach.

(vii) For detecting the motion of guest molecules and lattice elastic properties, a light scattering method like Brillouin spectroscopy is suggested.

(viii) This clathrate system provides a quite good source to research the energy relationship concerning heavy molecule dynamics, intercalation mechanism and reaction thermodynamics, since it showed almost no point defect and no phase transition was detected over the measured temperature range by conventional analysis tools.

8. Appendix

Table 1. Powder Diffraction Data at 293 K with Estimated Standard Deviations in Parentheses.

comp.	Zizps 6143	Zizps 6144	Zizps 6145	Zizpse 6141	Zizpse 6143	Zizpse 6144	Zizpse 6145	Zizpse 6147	Zizasse 6144
$\lambda(\AA)$	1.5406 (Cu-Kα)								
accepted peaks (*n*)	62	71	61	57	64	73	55	71	61
symmetry	Cubic F								
space group	$F\bar{4}3c$ (No. 219)								
cell param. a ($\AA$)	19.373 (1)	19.384 (0)	19.439 (0)	19.531 (0)	19.534 (0)	19.538 (0)	19.546 (0)	19.553 (0)	19.602 (0)
cell param. V($\AA^3$)	7270.6 (1)	7283.8 (1)	7245.6 (1)	7450.3 (2)	7453.4 (1)	7457.8 (2)	7467.9 (1)	7475.2 (1)	7531.4 (2)
single indexed lines (*n*)	62	71	64	57	64	73	55	71	61
FOM F(30)	541.7 (0.001, 37)	372.6 (0.002, 36)	433.5 (0.002, 37)	424.5 (0.002, 38)	363.6 (0.002, 37)	422.0 (0.002, 35)	303.6 (0.003, 38)	584.0 (0.001, 36)	392.6 (0.002, 36)
D	1.907	1.536	2.262	2.235	1.789	2.112	2.156	2.161	1.228

1. Measured by STOE Transmission X-ray diffraction system STADI P type[generator : 1.68kW, 2theta range : 0 ~ 90°, detector : linear PSD and measuring time : 24h] and refined by the STOE Powder Diffraction Software-*WinXPow* 1.08 packages.
2. FOM = Figure of Merit[de Wolff, *J. Appl. Crystallography* **1**(1968)108].
3. D = Durbin-Watson serial correlation (where δx_i and δx_{i-1} are the successive residuals in a series for $1.7 < D < 2.3$, with $n > 100$ distribution is random with 95% confidence interval.).

$$D = \frac{\sum_{i=2}^{n} (\delta x_i \cdot \delta x_{i-1})}{\sum_{i=2}^{n} (\delta x_i \cdot \delta x_i)}$$

Table 2a. X-Ray Crystallographic data for Zizps6144 at 123 and 293 K with Estimated Standard Deviations in Parentheses [section of measurement].

temp. (K)		123	293
crystal system		cubic	
space group		$F\bar{4}3c$ (no. 219)	
lattice parameters	a (Å)	19.290(2)	19.386(2)
	V (Å^3)	7177.9(1)	7285.6(1)
	Z	8	
$d_{calc.}$ (g/cm^3)		-	-
diffractometer		STOE IPDS	
λ (Å)		0.71073	
μ (mm^{-1})		15.330	15.104
scan range (θ)		$2.94 < \theta < 24.98$	$2.94 < \theta < 24.98$
measured reflections(n)		4938	10887

Table 2b. X-Ray Crystallographic data for Zizps6144 at 123 and 293 K with Estimated Standard Deviations in Parentheses [section of refinement].

temp. (K)	123	293
measured reflections (*n*)	4938	10887
unique reflections (R_{int})	531 (0.0268)	549 (0.0516)
used parameters (*n*)	43	37
wR_2 (for all)	0.0502	0.0432
R_1 (for all)	0.0221	0.0213
wR_2 [$I > 2\sigma(I)$]	0.0491	0.0423
R_1 [$I > 2\sigma(I)$]	0.0192	0.0184
S on *F*	1.168	1.054
residual density (*e.* $Å^{-3}$)	+0.73/-0.54	+0.46/-0.43

Table 2c. Position Parameters and Equivalent Isotropic Displacement Values (Å^2) for Zizps6144 at 123 and 293 K with Estimated Standard Deviations in Parentheses [Host Part].

temp. (K)	atom	Wyckoff	x	y	z	occup.	$U_{eq.}$
123	I1	*96h*	0.1144(2)	0.1774(2)	-0.0002(1)	1	0.0209(2)
	S1	*8a*	0	0	0	1	0.0152(8)
	Zn1	*24d*	0	¼	0	1	0.0187(3)
	Zn2	*32e*	0.0702(1)	-0.0702(1)	0.0702(1)	0.58(1)	0.0152(1)
	Zn3	*32e*	0.0695(2)	0.0695(2)	0.0695(2)	0.42(1)	0.0183(20)
293	I1	*96h*	0.1135(2)	0.1771(1)	-0.0004(1)	1	0.0342(2)
	S1	*8a*	0	0	0	1	0.0230(7)
	Zn1	*24d*	0	¼	0	1	0.0307(3)
	Zn2	*32e*	0.0705(2)	-0.0705(2)	0.0705(2)	0.56(1)	0.0310(20)
	Zn3	*32e*	0.0687(2)	0.0687(2)	0.0687(2)	0.44(1)	0.0230(30)

Table 2d. Position Parameters and Equivalent Isotropic Displacement Values (Å²) for Zizps6144 at 123 and 293 K with Estimated Standard Deviations in Parentheses [Guest Part].

temp. (K)	atom	Wyckoff	x	y	z	occup.	$U_{eq.}$
123	P1	*48g*	¼	¼	0.148(1)	0.26(8)	0.110(20)
	P2	*96h*	0.262(3)	0.297(2)	0.171(1)	0.34(4)	0.147(18)
	S2	*32e*	0.197(1)	-0.197(1)	0.197(1)	0.32(6)	0.081(18)
293	P1	*48g*	-	-	-	-	-
	P2	*96h*	0.264(2)	0.290(1)	0.170(1)	0.51(2)	0.235(19)
	S2	*32e*	0.197(1)	-0.197(1)	0.197(1)	0.31(7)	0.294(60)

Table 2e. Anisotropic Displacement Values (Å^2) for Zizps6144 at 123 and 293 K with Estimated Standard Deviations in Parentheses [Host Part].

temp. (K)	atom	U_{11}	U_{22}	U_{33}	U_{12}	U_{13}	U_{23}
123	I1	0.0179(2)	0.0166(2)	0.0281(2)	0.0005(1)	-0.0008(5)	-0.0048(5)
	S1	0.0152(8)	0.0152(8)	0.0152(8)	0	0	0
	Zn1	0.0207(4)	0.0145(5)	0.0207(4)	0	0	0
	Zn2	0.0152(13)	0.0152(13)	0.0152(13)	0.0019(12)	-0.0019(12)	0.0019(12)
	Zn3	0.0183(19)	0.0183(19)	0.0183(19)	0.0016(16)	0.0016(16)	0.0016(16)
293	I1	0.0292(2)	0.0267(2)	0.0465(2)	0.0013(1)	-0.0017(8)	-0.0042(7)
	S1	0.0230(7)	0.0230(7)	0.0230(7)	0	0	0
	Zn1	0.0339(3)	0.0245(5)	0.0339(3)	0	0	0
	Zn2	0.0310(20)	0.0310(20)	0.0310(20)	0.0010(16)	-0.0010(16)	0.0010(16)
	Zn3	0.0234(30)	0.0234(30)	0.0234(30)	-0.0009(17)	-0.0009(17)	-0.0009(17)

Table 2f. Anisotropic Displacement Values (Å^2) for Zizps6144 at 123 and 293 K with Estimated Standard Deviations in Parentheses [Guest Part].

temp. (K)	atom	U_{11}	U_{22}	U_{33}	U_{12}	U_{13}	U_{23}
123	P1	0.16(8)	0.12(8)	0.06(1)	0.03(5)	0	0
	P2	0.28(4)	0.11(4)	0.06(3)	0.05(3)	0.04(3)	0.05(4)
	S2	0.08(2)	0.08(2)	0.08(2)	0.02(1)	-0.02(1)	0.02(1)
293	P1	-	-	-	-	-	-
	P2	0.28(3)	0.26(3)	0.16(1)	0.11(3)	0.10(2)	0.15(2)
	S2	0.29(6)	0.29(6)	0.29(6)	0.15(3)	-0.15(3)	0.15(3)

Table 2g. Selected bond distance and angle for Zizps6144 at 123 and 293 K with Estimated Standard Deviations in Parentheses (Z = 1).

atom	bond length(Å) / angle(°)	
	123 K	293 K
S1 – Zn2	2.344(5)	2.367(7)
S1 – Zn3	2.321(7)	2.306(8)
Zn1 – I1	2.614(0)	2.615(0)
Zn2 – I1	2.614(2)	2.610(2)
Zn3 – I1	2.625(3)	2.640(3)
S1 – Zn2 – I1 S1 – Zn3 – I1	110.33(10) [110.69(14)]	109.94(15) [110.90(16)]
I1 – Zn1 – I1 I1' – Zn1 – I1'	106.68(1) [115.22(1)]	106.97(1) [114.60(1)]
Zn1 – I1 – Zn2 Zn1 – I1 – Zn3	98.55(3) [98.34(4)]	99.24(4) [98.72(4)]

Table 3a. X-Ray Crystallographic data for Zizpse6144 at 15, 123, 173, 223, 293, 373, 423, 473 K with Estimated Standard Deviations in Parentheses [section of measurement].

temp. (K)		15	123	173	223	293	373	423	473
crystal system		cubic							
space group		$F\bar{4}3c$ (no. 219)							
lattice param.	a ($Å$)	19.271(2)	19.417(2)	19.444(2)	19.469(2)	19.518(2)	19.570(2)	19.624(2)	19.729(2)
	V ($Å^3$)	7156.7(1)	7320.6(1)	7351.2(1)	7379.6(1)	7435.4(1)	7495.0(1)	7557.2(1)	7679.2(1)
	Z	8							
$d_{calc.}$ (g/cm^3)		4.493(1)	4.392(1)	4.374(1)	4.357(1)	4.325(1)	4.290(1)	4.255(1)	4.187(1)
diffractometer		-	STOE IPDS						
λ ($Å$)		0.71069	0.71069						
μ (mm^{-1})		18.991	18.775	18.703	18.631	18.491	18.344	18.193	17.904
scan range (θ)		$2.94 < \theta < 24.98$	$2.94 < \theta < 24.98$	$2.94 < \theta < 24.98$	$2.94 < \theta < 24.98$	$2.94 < \theta < 24.98$	$2.94 < \theta < 24.98$	$2.94 < \theta < 24.98$	$2.94 < \theta < 24.98$
measured reflections (n)		3628	7898	6434	5566	16738	7407	11746	1801

Table 3b. X-Ray Crystallographic data for Zizpse6144 at 15, 123, 173, 223, 293, 373, 423, 473 K with Estimated Standard Deviations in Parentheses [section of refinement].

temp. (K)	15	123	173	223	293	373	423	473
measured reflections (*n*)	3628	7898	6434	5566	16738	7407	11746	1801
unique reflections (R_{int})	545 (0.0451)	549 (0.0380)	557 (0.0388)	557 (0.0817)	565 (0.0480)	565 (0.0912)	568 (0.0463)	567 (0.1461)
used parameters (*n*)	43	47	47	47	46	46	46	51
wR_2 (for all)	0.0411	0.0420	0.0382	0.0549	0.0447	0.0578	0.0466	0.1552
R_1 (for all)	0.241	0.0194	0.0194	0.0277	0.0203	0.0275	0.0254	0.0953
wR_2 [$I > 2\sigma(I)$]	0.0404	0.0418	0.0378	0.0542	0.0440	0.0562	0.0444	0.1428
R_1 [$I > 2\sigma(I)$]	0.0218	0.0183	0.0177	0.0255	0.0187	0.0230	0.0184	0.0558
S on *F*	1.212	1.228	1.163	1.055	1.126	1.062	1.029	0.859
residual density($e.\ Å^{-3}$)	+0.50/ -0.64	+0.75/ -0.48	+0.77/ -0.56	+0.85/ -0.56	+0.82/ -0.37	+0.50/ -0.43	+0.48/ -0.51	+0.97/ -0.94

Table 3d. Position Parameters and Equivalent Isotropic Displacement Values (Å²) for Zizpse6144 at 15, 123, 173 and 223 K with Estimated Standard Deviations in Parentheses [Host Part].

temp. (K)	atom	Wyckoff	x	y	z	occup.	$U_{eq.}$
15	I1	*96h*	0.1151(0)	0.1790(0)	-0.0008(1)	1	0.0103(2)
	Se1	*8a*	0	0	0	1	0.0063(5)
	Zn1	*24d*	0	¼	0	1	0.0089(4)
	Zn2	*32e*	0.0728(2)	-0.0728(2)	0.0728(2)	0.64(1)	0.0052(14)
	Zn3	*32e*	0.0725(3)	0.0725(3)	0.0725(3)	0.37(1)	0.0140(3)
123	I1	*96h*	0.1144(1)	0.1787(1)	-0.0007(1)	1	0.0148(2)
	Se1	*8a*	0	0	0	1	0.0079(3)
	Zn1	*24d*	0	¼	0	1	0.0116(2)
	Zn2	*32e*	0.0725(1)	-0.0725(1)	0.0725(1)	0.60(1)	0.0028(7)
	Zn3	*32e*	0.0724(2)	0.0724(2)	0.0724(2)	0.40(1)	0.0245(15)
173	I1	*96h*	0.1141(1)	0.1786(0)	-0.0007(1)	1	0.0186(2)
	Se1	*8a*	0	0	0	1	0.0104(3)
	Zn1	*24d*	0	¼	0	1	0.0148(2)
	Zn2	*32e*	0.0725(1)	-0.0725(1)	0.0725(1)	0.58(1)	0.0065(8)
	Zn3	*32e*	0.0722(2)	0.0722(2)	0.0722(2)	0.43(1)	0.0273(16)
223	I1	*96h*	0.1138(0)	0.1785(0)	-0.0006(1)	1	0.0237(2)
	Se1	*8a*	0	0	0	1	0.0142(4)
	Zn1	*24d*	0	¼	0	1	0.0195(3)
	Zn2	*32e*	0.0722(1)	-0.0722(1)	0.0722(1)	0.59(1)	0.0112(10)
	Zn3	*32e*	0.0724(2)	0.0724(2)	0.0724(2)	0.43(1)	0.0306(19)

Table 3f. Position Parameters and Equivalent Isotropic Displacement Values (Å^2) for Zizpse6144 at 293, 373, 423 and 473 K with Estimated Standard Deviations in Parentheses [Host Part].

temp. (K)	atom	Wyckoff	x	y	z	occup.	$U_{eq.}$
293	I1	*96h*	0.1134(0)	0.1784(0)	-0.0007(1)	1	0.0316(2)
	Se1	*8a*	0	0	0	1	0.0199(3)
	Zn1	*24d*	0	¼	0	1	0.0270(3)
	Zn2	*32e*	0.0717(2)	-0.0717(2)	0.0717(2)	0.39(1)	0.0332(16)
	Zn3	*32e*	0.0724(1)	0.0724(1)	0.0724(1)	0.61(1)	0.0205(8)
373	I1	*96h*	0.1129(0)	0.1782(0)	-0.0007(1)	1	0.0431(2)
	Se1	*8a*	0	0	0	1	0.0277(4)
	Zn1	*24d*	0	¼	0	1	0.0380(3)
	Zn2	*32e*	0.0726(2)	-0.0726(2)	0.0726(2)	0.53(1)	0.0310(20)
	Zn3	*32e*	0.0712(2)	0.0712(2)	0.0712(2)	0.49(1)	0.0410(30)
423	I1	*96h*	0.1125(0)	0.1781(0)	-0.0008(1)	1	0.0522(2)
	Se1	*8a*	0	0	0	1	0.0334(4)
	Zn1	*24d*	0	¼	0	1	0.0463(3)
	Zn2	*32e*	0.0729(2)	-0.0729(2)	0.0729(2)	0.54(1)	0.0435(20)
	Zn3	*32e*	0.0708(2)	0.0708(2)	0.0708(2)	0.46(1)	0.0390(30)
473	I1	*96h*	0.1120(1)	0.1783(1)	0.0016(3)	0.88(1)	0.0820(5)
	I2	*96h*	0.1134(5)	0.1781(5)	-0.0037(6)	0.12(1)	0.1110(30)
	Se1	*8a*	0	0	0	1	0.0560(10)
	Zn1a	*24d*	0	¼	0	0.90(1)	0.0655(11)
	Zn1b	*48f*	0	0.1128(18)	0	0.10(1)	0.390(90)
	Zn1c	*48f*	0	0.2000(40)	0	0.14(2)	0.320(60)
	Zn2	*32e*	0.0706(2)	-0.0706(2)	0.0706(2)	0.42(1)	0.0550(30)
	Zn3	*32e*	0.0724(3)	0.0724(3)	0.0724(3)	0.55(1)	0.0760(30)

Table 3g. Position Parameters and Equivalent Isotropic Displacement Values (Å²) for Zizpse6144 at 15, 123, 223, 293, 373, 423 and 473 K with Estimated Standard Deviations in Parentheses [Guest Part].

temp. (K)	atom	Wyckoff	x	y	z	occup.	$U_{eq.}$
15	P1	*48g*	¼	¼	0.146(2)	0.21(5)	0.05(2)
	P2	*96h*	0.271(3)	0.213(2)	0.163(1)	0.64(3)	0.30(2)
	Se2	*32e*	0.191(0)	0.191(0)	0.191(0)	0.28(2)	0.04(4)
123	P1	*96h*	0.190(4)	0.207(2)	0.184(3)	0.32(3)	0.16(2)
	P2	*96h*	0.218(2)	0.255(2)	0.154(1)	0.51(4)	0.17(2)
	Se2	*32e*	0.193(1)	0.193(1)	-0.193(1)	0.19(4)	0.16(4)
173	P1	*96h*	0.194(4)	0.209(2)	0.181(3)	0.33(4)	0.16(2)
	P2	*96h*	0.217(2)	0.256(2)	0.155(1)	0.47(5)	0.16(2)
	Se2	*32e*	0.193(1)	0.193(1)	-0.193(1)	0.16(5)	0.19(6)
223	P1	*96h*	0.193(5)	0.214(3)	0.181(5)	0.35(6)	0.15(4)
	P2	*96h*	0.218(4)	0.260(3)	0.155(1)	0.47(8)	0.17(3)
	Se2	*32e*	0.191(1)	0.191(1)	-0.191(1)	0.16(6)	0.17(9)
293	P1	*96h*	0.169(2)	0.229(3)	0.191(2)	0.22(5)	0.13(2)
	P2	*96h*	0.221(2)	0.246(3)	0.155(1)	0.45(7)	0.17(3)
	Se2	*32e*	0.194(1)	0.194(1)	-0.194(1)	0.37(5)	0.26(3)
373	P1	*96h*	0.173(3)	0.232(2)	0.203(2)	0.68(5)	0.30(3)
	P2	*96h*	0.213(5)	0.270(3)	0.152(2)	0.12(5)	0.18(5)
	Se2	*32e*	0.192(1)	0.192(1)	-0.192(1)	0.17(5)	0.28(8)
423	P1	*96h*	0.171(2)	0.229(2)	0.209(2)	0.55(8)	0.25(3)
	P2	*96h*	0.205(4)	0.259(4)	0.157(3)	0.21(9)	0.31(5)
	Se2	*32e*	0.193(1)	0.193(1)	-0.193(1)	0.21(6)	0.34(9)
473	P1	*96h*	0.215(1)	0.165(1)	-0.229(2)	1	0.99(3)

Table 3h. Anisotropic Displacement Values (Å²) for Zizpse6144 at 15, 123, 173 and 223 K with Estimated Standard Deviations in Parentheses [Host Part].

temp. (K)	atom	U_{11}	U_{22}	U_{33}	U_{12}	U_{13}	U_{23}
15	I1	0.0081(3)	0.0069(3)	0.0160(3)	-0.0003(2)	-0.0009(7)	-0.0031(8)
	Se1	0.0060(5)	0.0060(5)	0.0060(5)	0	0	0
	Zn1	0.0104(6)	0.0059(9)	0.0104(6)	0	0	0
	Zn2	0.0052(14)	0.0052(14)	0.0052(14)	-0.0003(15)	0.0003(15)	-0.0003(15)
	Zn3	0.0140(0)	0.0140(0)	0.0140(0)	-0.0040(30)	-0.0040(30)	-0.0040(30)
123	I1	0.0110(2)	0.0097(2)	0.0238(2)	0.0004(1)	-0.0012(4)	-0.0052(4)
	Se1	0.0079(3)	0.0079(3)	0.0079(3)	0	0	0
	Zn1	0.0135(3)	0.0078(5)	0.0135(3)	0	0	0
	Zn2	0.0028(1)	0.0028(1)	0.0028(1)	-0.0010(8)	0.0010(8)	-0.0010(8)
	Zn3	0.0245(2)	0.0245(2)	0.0245(2)	-0.0025(19)	-0.0025(19)	-0.0025(19)
173	I1	0.0142(2)	0.0127(2)	0.0289(2)	0.0007(1)	-0.0018(4)	-0.0047(5)
	Se1	0.0104(3)	0.0104(3)	0.0104(3)	0	0	0
	Zn1	0.0170(3)	0.0105(5)	0.0170(3)	0	0	0
	Zn2	0.0065(8)	0.0065(8)	0.0065(8)	-0.0003(9)	0.0003(9)	-0.0003(9)
	Zn3	0.0273(16)	0.0273(16)	0.0273(16)	-0.0005(20)	-0.0005(20)	-0.0005(20)
223	I1	0.0187(3)	0.0169(3)	0.0354(3)	0.0011(1)	-0.0018(5)	-0.0036(7)
	Se1	0.0142(4)	0.0142(4)	0.0142(4)	0	0	0
	Zn1	0.0221(4)	0.0144(7)	0.0221(4)	0	0	0
	Zn2	0.0112(10)	0.0112(10)	0.0112(10)	-0.0004(13)	0.0004(13)	-0.0004(13)
	Zn3	0.0306(19)	0.0306(19)	0.0306(19)	-0.0000(30)	-0.0000(30)	-0.0000(30)

Table 3i. Anisotropic Displacement Values (Å²) for Zizpse6144 Parentheses at 293, 373, 423 and 473 K with Estimated Standard Deviations in [Host Part].

temp. (K)	atom	U_{11}	U_{22}	U_{33}	U_{12}	U_{13}	U_{23}
293	I1	0.0259(2)	0.0236(2)	0.0453(2)	0.0014(1)	0.0035(4)	0.0051(5)
	Se1	0.0199(3)	0.0199(3)	0.0199(3)	0	0	0
	Zn1	0.0301(4)	0.0206(6)	0.0301(4)	0	0	0
	Zn2	0.0332(16)	0.0332(16)	0.0332(16)	-0.0004(20)	0.0004(20)	-0.0004(20)
	Zn3	0.0205(8)	0.0205(8)	0.0205(8)	-0.0000(10)	0.0000(10)	-0.0000(10)
373	I1	0.0362(3)	0.0332(3)	0.0599(3)	0.0018(2)	-0.0035(8)	-0.0056(8)
	Se1	0.0277(4)	0.0277(4)	0.0277(4)	0	0	0
	Zn1	0.0427(5)	0.0288(8)	0.0427(5)	0	0	0
	Zn2	0.0310(20)	0.0310(20)	0.0310(20)	-0.0026(17)	0.0026(17)	-0.0026(17)
	Zn3	0.0419(30)	0.0419(30)	0.0419(30)	-0.0022(20)	-0.0022(20)	-0.0022(20)
423	I1	0.0442(3)	0.0407(2)	0.0720(3)	0.0025(1)	-0.0050(8)	-0.0059(8)
	Se1	0.0334(4)	0.0334(4)	0.0334(4)	0	0	0
	Zn1	0.0515(5)	0.0358(7)	0.0515(5)	0	0	0
	Zn2	0.0435(20)	0.0435(20)	0.0435(20)	-0.0038(16)	0.0038(16)	-0.0038(16)
	Zn3	0.0410(30)	0.0410(30)	0.0410(30)	-0.0035(16)	-0.0035(16)	-0.0035(16)
473	I1	0.0704(8)	0.0632(7)	0.1122(12)	-0.0069(6)	0.0100(20)	0.0140(20)
	I2	0.1330(60)	0.1400(60)	0.0610(50)	0.1300(50)	-0.0770(50)	-0.0830(50)
	Se1	0.0560(10)	0.0560(10)	0.0560(10)	0	0	0
	Zn1a	0.0734(15)	0.0500(20)	0.0734(15)	0	0	0
	Zn1b	0.130(40)	0.023(18)	1.00(30)	0	0.10(30)	0
	Zn1c	0.150(40)	0.27(8)	0.52(16)	0	-0.06(15)	0
	Zn2	0.0549(30)	0.0549(30)	0.0549(30)	0.0103(20)	-0.0103(20)	0.0103(20)
	Zn3	0.0755(30)	0.0755(30)	0.0755(30)	0.0100(30)	0.0100(30)	0.0100(30)

Table 3j. Anisotropic Displacement Values (Å²) for Zizpse6144 at 15, 123, 173, 223, 293, 373, 423 and 473 K with Estimated Standard Deviations in Parentheses [Guest Part].

temp. (K)	atom	U_{11}	U_{22}	U_{33}	U_{12}	U_{13}	U_{23}
15	P1	0.00(2)	0.11(4)	0.04(1)	0.05(2)	0	0
	P2	0.63(7)	0.18(3)	0.10(2)	-0.02(3)	0.13(2)	-0.12(2)
	Se2	0.04(5)	0.04(5)	0.04(5)	-0.02(2)	-0.02(2)	-0.02(2)
123	P1	0.23(4)	0.12(2)	0.12(3)	-0.05(2)	-0.16(3)	0.05(2)
	P2	0.29(3)	0.14(2)	0.07(1)	0.05(3)	-0.13(1)	-0.03(2)
	Se2	0.16(4)	0.16(4)	0.16(4)	0.07(2)	0.07(2)	-0.07(2)
173	P1	0.24(5)	0.12(3)	0.11(2)	-0.03(2)	-0.14(3)	0.02(2)
	P2	0.29(3)	0.15(3)	0.06(1)	0.06(3)	-0.12(2)	-0.02(2)
	Se2	0.19(6)	0.19(6)	0.19(6)	-0.09(3)	0.09(3)	0.09(3)
223	P1	0.16(4)	0.15(5)	0.15(4)	-0.04(3)	-0.13(3)	0.00(4)
	P2	0.30(5)	0.13(4)	0.07(1)	0.04(4)	-0.11(2)	-0.00(2)
	Se2	0.17(9)	0.17(9)	0.17(9)	-0.07(4)	0.07(4)	0.07(4)
293	P1	0.10(3)	0.23(3)	0.06(2)	-0.09(2)	-0.06(2)	0.01(2)
	P2	0.15(3)	0.25(6)	0.09(1)	-0.01(2)	-0.09(2)	0.04(2)
	Se2	0.26(3)	0.26(3)	0.26(3)	0.10(2)	0.10(2)	-0.10(2)
373	P1	0.21(2)	0.28(4)	0.40(5)	-0.13(4)	-0.24(3)	0.14(4)
	P2	0.42(12)	0.09(3)	0.04(3)	0.13(5)	-0.18(4)	-0.04(2)
	Se2	0.28(9)	0.28(9)	0.28(9)	-0.13(5)	0.13(5)	0.13(5)
423	P1	0.19(3)	0.25(3)	0.31(6)	-0.06(3)	-0.19(4)	0.08(3)
	P2	0.47(9)	0.33(7)	0.13(3)	0.26(7)	-0.26(7)	-0.17(4)
	Se2	0.34(9)	0.34(9)	0.34(9)	-0.15(4)	0.15(4)	0.15(4)
473	P1	0.35(2)	0.21(1)	0.71(6)	-0.19(1)	0.04(3)	0.08(3)

Table 3k. Selected bond distance and angle for Zizpse6144 at 15, 123, 173 and 223 K with Estimated Standard Deviations in Parentheses (Z = 1).

atom	bond length(Å) / angle(°)			
	15 K	123 K	173 K	223 K
Se1 – Zn2	2.429(5)	2.439(3)	2.441(3)	2.436(4)
Se1 – Zn3	2.419(9)	2.434(5)	2.431(6)	2.441(7)
Zn1 – I1	2.607(1)	2.617(0)	2.617(0)	2.617(0)
Zn2 – I1	2.605(2)	2.620(1)	2.620(1)	2.624(1)
Zn3 – I1	2.623(3)	2.635(2)	2.637(2)	2.634(2)
Se1 – Zn2 – I1 Se1 – Zn3 – I1	109.10(11) [108.30(18)]	109.05(6) [108.69(10)]	108.99(7) [108.76(12)]	109.05(8) [108.57(14)]
I1 – Zn1 – I1 I1' – Zn1 – I1'	105.99(1) [116.69(2)]	106.24(1) [116.14(1)]	106.34(1) [115.93(1)]	106.43(1) [115.74(2)]
Zn1 – I1 – Zn2 Zn1 – I1 – Zn3	98.54(4) [98.10(5)]	98.95(2) [98.58(3)]	99.12(2) [98.73(3)]	99.23(3) [98.95(4)]

Table 3l. Selected bond distance and angle for Zizpse6144 at 293, 373, 423 and 473 K with Estimated Standard Deviations in Parentheses (Z = 1).

atom	bond length(Å) / angle(°)			
	293 K	373 K	423 K	473 K
Se1 – Zn2	2.448(3)	2.461(7)	2.473(8)	2.465(11)
Se1 – Zn3	2.422(5)	2.414(9)	2.410(8)	2.428(8)
Zn1 – I1	2.618(0)	2.619(1)	2.621(1)	2.627(1)
Zn2 – I1	2.623(1)	2.622(2)	2.621(3)	2.639(5)
Zn3 – I1	2.645(2)	2.650(3)	2.659(3)	2.670(4)
Se1 – Zn2 – I1 Se1 – Zn3 – I1	108.85(7) [108.95(11)]	108.57(16) [109.13(18)]	108.43(18) [109.14(18)]	108.80(26) [108.91(18)]
I1 – Zn1 – I1 I1' – Zn1 – I1'	106.55(1) [115.48(1)]	106.74(1) [115.08(2)]	106.87(1) [114.81(2)]	106.97(2) [114.59(5)]
Zn1 – I1 – Zn2 Zn1 – I1 – Zn3	99.52(2) [99.04(3)]	99.87(4) [99.31(5)]	100.22(5) [99.44(5)]	100.41(9) [99.72(9)]

Table 4a. X-Ray Crystallographic data for Zipse334 at 123 and 293 K with Estimated Standard Deviations in Parentheses [section of measurement].

temp. (K)		123	293
crystal system		cubic	
space group		$F\bar{4}3c$ (no. 219)	
lattice parameters	a (Å)	19.422(2)	19.542(2)
	V (Å^3)	7326.3(1)	7462.9(1)
	Z	8	
$d_{calc.}$ (g/cm^3)		-	-
diffractometer		STOE IPDS	
λ (Å)		0.71069	
μ (mm^{-1})		19.015	18.667
scan range (θ)		$2.94 < \theta < 24.98$	$2.94 < \theta < 24.98$
measured reflections (n)		12326	15144

Table 4b. X-Ray Crystallographic data for Zipse334 at 123 and 293 K with Estimated Standard Deviations in Parentheses [section of refinement].

temp. (K)	123	293
measured reflections (*n*)	12326	15144
unique reflections (R_{int})	549 (0.0563)	565 (0.0371)
used parameters (*n*)	46	46
wR_2 (for all)	0.0383	0.0375
R_1 (for all)	0.0196	0.0172
wR_2 [$I > 2\sigma(I)$]	0.0378	0.0372
R_1 [$I > 2\sigma(I)$]	0.0175	0.0164
S on *F*	1.024	1.129
residual density ($e.\ Å^{-3}$)	+0.53/-0.57	+0.43/-0.39

Table 4c. Position Parameters and Equivalent Isotropic Displacement Values (Å²) for Zipse334 at 123 and 293 K with Estimated Standard Deviations in Parentheses [Host Part].

temp. (K)	atom	Wyckoff	x	y	z	occup.	$U_{eq.}$
123	I1	*96h*	0.1141(0)	0.1787(0)	-0.0004(1)	1	0.0222(2)
	Se1	*8a*	0	0	0	1	0.0141(3)
	Zn1	*24d*	0	¼	0	1	0.0185(2)
	Zn2	*32e*	0.0721(1)	-0.0721(1)	0.0721(1)	0.61(1)	0.0167(10)
	Zn3	*32e*	0.0727(2)	0.0727(2)	0.0727(2)	0.39(1)	0.0167(17)
293	I1	*96h*	0.1132(0)	0.1783(0)	-0.0008(0)	1	0.0349(2)
	Se1	*8a*	0	0	0	1	0.0226(3)
	Zn1	*24d*	0	¼	0	1	0.0298(2)
	Zn2	*32e*	0.0721(1)	-0.0721(1)	0.0721(1)	0.64(1)	0.0244(7)
	Zn3	*32e*	0.0719(2)	0.0719(2)	0.0719(2)	0.36(1)	0.0328(14)

Table 4d. Position Parameters and Equivalent Isotropic Displacement Values (Å²) for Zipse334 at 123 and 293 K with Estimated Standard Deviations in Parentheses [Guest Part].

temp.(K)	atom	Wyckoff	x	y	z	occup.	$U_{eq.}$
123	P1	*96h*	0.212(2)	0.199(2)	0.167(1)	0.35(3)	0.103(11)
	P2	*96h*	0.219(1)	0.251(2)	0.152(1)	0.49(5)	0.141(14)
	Se2	*32e*	0.195(1)	0.195(1)	-0.195(1)	0.27(5)	0.209(40)
293	P1	*96h*	0.196(4)	0.219(4)	0.172(4)	0.43(8)	0.200(40)
	P2	*96h*	0.219(4)	0.260(2)	0.152(1)	0.44(9)	0.178(30)
	Se2	*32e*	0.193(1)	0.193(1)	-0.193(1)	0.18(5)	0.222(60)

Table 4f. Anisotropic Displacement Values (Å²) for Zipse334 at 123 and 293 K with Estimated Standard Deviations in Parentheses [Host Part].

temp. (K)	atom	U_{11}	U_{22}	U_{33}	U_{12}	U_{13}	U_{23}
123	I1	0.0181(2)	0.0164(2)	0.0320(2)	0.0004(1)	-0.0028(5)	-0.0008(7)
	Se1	0.0141(3)	0.0141(3)	0.0141(3)	0	0	0
	Zn1	0.0206(3)	0.0143(5)	0.0206(3)	0	0	0
	Zn2	0.0167(10)	0.0167(10)	0.0167(10)	-0.0018(1)	0.0018(1)	-0.0018(1)
	Zn3	0.0167(17)	0.0167(17)	0.0167(17)	-0.0034(19)	-0.0034(19)	-0.0034(19)
293	I1	0.0290(2)	0.0266(2)	0.0492(2)	0.0016(1)	-0.0028(4)	-0.0066(4)
	Se1	0.0226(3)	0.0226(3)	0.0226(3)	0	0	0
	Zn1	0.0328(3)	0.0238(5)	0.0328(3)	0	0	0
	Zn2	0.0244(7)	0.0244(7)	0.0244(7)	0.0001(8)	-0.0001(8)	0.0001(8)
	Zn3	0.0328(14)	0.0328(14)	0.0328(14)	0.0017(17)	0.0017(17)	0.0017(17)

Table 4g. Anisotropic Displacement Values (Å²) for Zipse334 at 123 and 293 K with Estimated Standard Deviations in Parentheses [Guest Part].

temp. (K)	atom	U_{11}	U_{22}	U_{33}	U_{12}	U_{13}	U_{23}
123	P1	0.11(4)	0.10(2)	0.10(1)	0.00(2)	-0.07(2)	-0.05(2)
	P2	0.23(2)	0.11(3)	0.08(1)	-0.00(3)	-0.11(1)	-0.02(2)
	Se2	0.21(4)	0.21(4)	0.21(4)	-0.06(2)	0.06(2)	0.06(2)
293	P1	0.22(6)	0.21(6)	0.18(4)	-0.01(4)	-0.15(5)	-0.04(4)
	P2	0.31(7)	0.13(3)	0.09(1)	0.01(2)	-0.10(2)	0.02(2)
	Se2	0.22(6)	0.22(6)	0.22(6)	-0.08(3)	0.08(3)	0.08(3)

Table 4h. Selected bond distance and angle for Zipse334 at 123 and 293 K with Estimated Standard Deviations in Parentheses (Z = 1).

atom	bond length(Å) / angle(°)	
	123K	293K
Se1 – Zn2	2.426(4)	2.442(3)
Se1 – Zn3	2.445(5)	2.435(5)
Zn1 – I1	2.614(0)	2.619(0)
Zn2 – I1	2.624(1)	2.625(1)
Zn3 – I1	2.627(2)	2.644(2)
Se1 – Zn2 – I1 Se1 – Zn3 – I1	109.17(9) [108.49(12)]	109.02(6) [108.65(11)]
I1 – Zn1 – I1 I1' – Zn1 – I1'	106.32(1) [115.99(1)]	106.64(1) [115.29(1)]
Zn1 – I1 – Zn2 Zn1 – I1 – Zn3	98.97(3) [98.84(3)]	99.65(2) [99.20(3)]

Table 5a. X-Ray Crystallographic data for Zizasse6144 at 293 K with Estimated Standard Deviations in Parentheses [section of measurement].

temp. (K)	293
crystal system	cubic
space group	$F\bar{4}3c$ (no. 219)
lattice parameters a ($\AA$)	19.592(2)
lattice parameters V ($\AA^3$)	7523.8(1)
Z	8
$d_{calc.}(g/cm^3)$	-
Diffractometer	STOE IPDS
λ ($\AA$)	0.71069
μ (mm^{-1})	21.596
scan range (θ)	$2.94 < \theta < 24.98$
measured reflections (n)	17358

Table 5b. X-Ray Crystallographic data for Zizasse6144 at 293 K with Estimated Standard Deviations in Parentheses [section of refinement].

temp. (K)	293
measured reflections (*n*)	17358
unique reflections (R_{int})	567 (0.2450)
used parameters (*n*)	37
wR_2 (for all)	0.1372
R_1 (for all)	0.0629
wR_2 [$I > 2\sigma(I)$]	0.1364
R_1[$I > 2\sigma(I)$]	0.0620
S on *F*	1.213
residual density ($e.\ Å^{-3}$)	+1.35/-1.10

Table 5c. Position Parameters and Equivalent Isotropic Displacement Values (Å²) for Zizasse6144 at 293 K with Estimated Standard Deviations in Parentheses [Host Part].

temp. (K)	atom	Wyckoff	x	y	z	occup.	$U_{eq.}$
293	I1	*96h*	0.1125(1)	0.1781(1)	0.0016(1)	1	0.0378(6)
	Se1	*8a*	0	0	0	1	0.0243(12)
	Zn1	*24d*	0	¼	0	1	0.0323(9)
	Zn2	*32e*	0.0697(4)	-0.0697(4)	0.0697(4)	0.50(2)	0.0601(50)
	Zn3	*32e*	0.0729(2)	0.0729(2)	0.0729(2)	0.54(2)	0.0131(20)

Table 5d. Position Parameters and Equivalent Isotropic Displacement Values (Å²) for Zizasse6144 at 293 K with Estimated Standard Deviations in Parentheses [Guest Part].

temp. (K)	atom	Wyckoff	x	y	z	occup.	$U_{eq.}$
293	As1	*96h*	0.215(2)	0.226(2)	0.159(1)	0.50(2)	0.278(19)
	Se2	*32e*	0.191(1)	-0.191(1)	0.191(1)	0.28(5)	0.182(50)

Table 5e. Anisotropic Displacement Values (Å²) for Zizasse6144 at 293 K with Estimated Standard Deviations in Parentheses [Host Part].

temp. (K)	atom	U_{11}	U_{22}	U_{33}	U_{12}	U_{13}	U_{23}
293	I1	0.0316(7)	0.0286(7)	0.0532(9)	0.0017(4)	0.0019(11)	0.0113(10)
	Se1	0.0243(12)	0.0243(12)	0.0243(12)	0	0	0
	Zn1	0.0353(14)	0.0261(20)	0.0353(14)	0	0	0
	Zn2	0.0601(50)	0.0601(50)	0.0601(50)	0.0047(40)	-0.0047(40)	0.0047(40)
	Zn3	0.0131(20)	0.0131(20)	0.0131(20)	-0.0012(18)	-0.0012(18)	-0.0012(18)

Table 5f. Anisotropic Displacement Values (Å²) for Zizasse6144 at 293 K with Estimated Standard Deviations in Parentheses [Guest Part].

temp. (K)	atom	U_{11}	U_{22}	U_{33}	U_{12}	U_{13}	U_{23}
293	As1	0.38(7)	0.32(6)	0.14(1)	-0.02(2)	-0.17(3)	-0.06(2)
	Se2	0.18(5)	0.18(5)	0.18(5)	0.08(2)	-0.08(2)	0.08(2)

Table 5g. Selected bond distance and angle for Zizasse6144 at 293 K with Estimated Standard Deviations in Parentheses (Z = 1).

atom	bond length(Å) / angle(°)
Se1 – Zn2	2.367(13)
Se1 – Zn3	2.474(7)
Zn1 – I1	2.617(1)
Zn2 – I1	2.677(5)
Zn3 – I1	2.609(3)
Se1 – Zn2 – I1 Se1 – Zn3 – I1	109.73(28) [108.59(16)]
I1 – Zn1 – I1 I1' – Zn1 – I1'	106.84(2) [114.87(5)]
Zn1 – I1 – Zn2 Zn1 – I1 – Zn3	99.03(8) [100.41(6)]

Table 6a. The comparison of reported experimental frequency of P_4Se_3 with Zizpse6144.

assign	$\Delta\bar{\nu}$ (cm^{-1})						
$\nu_1(A_1)$	485 m[1]	486 m	486 m(p)[2]	487	483~486	484 (12)[6]	485 (14)[7]
$\nu_2(A_1)$	360vs 369ms	367 vs	373 s(p)	365	~372	364 (100,br)	374 (100)
$\nu_3(A_1)$	320 m	330 m	323 mw(p)	324	324~326	323 (14)	324 (10)
$\nu_4(A_1)$	207s 211sh	217 s	220 s(p)	214	213~218	213 (43)	219 (60)
$\nu_5(A_2)$ + lib.	-	160 w	160 sh(dp)	174	-	-	193/182 171/160 145
$\nu_6(E)$	404 w	407 w	-	408	~405	405 (4)	407 (2)
$\nu_7(E)$	344sh 356sh	353 sh	352 sh(dp)	353	-	364 (100,br)	364 (15, sh) 353
$\nu_8(E)$	315 mw	323 sh	323 mw(p)?	315	316~318	-	318 (7)
$\nu_9(E)$	-	-	-	-	-	-	271 (2)
$\nu_{10}(E)$	132 m	138 ms	140 m(dp)	133	132~137	134 (19)	134 (25)
temp.[3](K)	293	363	673	RT	RT	RT	RT
phase	α[4]	β[4]	*g*[4]	*g*[4]	-	-	α
ref.	70	70	70	132	133	21	this work

1. s = strong, m = medium, w = weak, v = very, sh = shoulder.
2. p = polarized, dp = depolarized.
3. RT = room temperature.
4. $\alpha = \alpha$-P_4Se_3, $\beta = \beta$-P_4Se_3 indicate the solid phase of considered molecule, *g* = glassy phase.
5. in parenthesis intensities in km mol^{-1}.
6. in parenthesis intensities in %.
7. All the data of frequencies are reconstructed by a sense of ref. 70.

Table 6b. The comparison of reported calculated frequency of P_4Se_3 with Zizpse6144.

assign.	$\Delta\bar{\nu}$ (cm^{-1})					
$\nu_1(A_1)$	470	491	496	~482	470 (0)[2]	485 (14)[3]
$\nu_2(A_1)$	356	380	381	~353/~357/ ~365	359 (1)	374 (100)
$\nu_3(A_1)$	297	306	307	~320	311 (1)	324 (10)
$\nu_4(A_1)$	187	220	220	~208 ~212	215 (0)	219 (60)
$\nu_5(A_2)$	127	160	156	-	160 (0)	193/182/171/ 160/145
$\nu_6(E)$	415	413	417	~407	396 (1)	407 (2)
$\nu_7(E)$	402	357	362	~342	343 (10)	364(15, sh)/ 353
$\nu_8(E)$	353	316	321	~318	311 (1)	318 (7)
$\nu_9(E)$	201	220	215	-	294 (6)?	271 (2)
$\nu_{10}(E)$	117	133	133	~130	130 (0)	134 (25)
Method[1]	PED	MD	MD	A.i.	DFT	S
Refs.	121	117	117	134	21	this work

1. S = solid-state(crystal powder) method with Nujol mulls, PED = calculation with potential energy distribution, MD = molecular dynamics calculation by term of Car-Parrinello, A.i. = Ab initio calculation, DFT = Gaussian 94[P with 6-31G(d,p) basis set, Se with quasi-relativistic pseudo-potentials(ECP28MWB), the computation was carried out at the DFT level using the B3LYP].
2. in parenthesis intensities in km mol^{-1}.
3. in parenthesis intensities in %.
4. All the data of frequencies are reconstructed by a sense of ref. 70.

Table 7a. The comparison of reported experimental frequency of P_4S_3 with Zizps6144.

assign.	$\Delta\bar{\nu}$ (cm^{-1})										
$\nu_1(A_1)$	487(7)	492	486 (dp)	484 (?)	490 w(?)	489 m	483 w(?)	480 w(?)	493m	489 m	487 ms[1](p)
$\nu_2(A_1)$	447(100)[5] 441sh(18)	456	442 (p^2)	443 (p)	444 vs(p)	443 vs	440 vs(p)	446 vs(p)	448ms 441vs	444 vs	444 vs(p)
$\nu_3(A_1)$	422(11)	-	420 (?)	418 (p)	423 w(p)	422 m	420 w(p)	420 w(p)	429w 425w	423 m	419 sh(p)
$\nu_4(A_1)$	291(18)	260	290 (p)	290 (?)	291 m(dp)	288 m	287 m(dp)	292 m(dp)	292ms 287ms	287 s	287 ms(p)
$\nu_5(A_2)$ + *lib.*	197 ~141	-	154 (?)	156 (dp)	-	187 w 145 vw	187 vw(?) 142 vw(dp)	-	191vw 187vw 183vw	187 vw	187 vvw(dp)
$\nu_6(E)$	473(6)	-	-	-	-	-	-	-	482w	-	
$\nu_7(E)$	417(8)	-	-	-	-	-	-	-	-	417 sh	-
$\nu_8(E)$	345(17)	336	-	-	-	347 s	339 m(dp)	347 m(dp)	344	-	-
$\nu_9(E)$	340(19)	-	341 (dp)	343 (dp)	343 m(dp)	343 s	-	-	338	342 s-vs	340 s(dp)
$\nu_{10}(E)$	224(10) 222(10)	-	221 (dp)	223 (dp)	223 w(dp)	227m 221m	218 w(dp)	221 w(dp)	223m 214vw	217 m	219 m(dp)
temp.[3](K)	RT	RT	RT	RT	RT	RT	523	823	77	293	453
phase[5]	α	*SS*	α	*M*	*SS*	*a*	*g*	*Gas*	α	α	β
Refs.	this work	118	118	118	119	119	119	119	70	70	70

1. s = strong, m = medium, w = weak, v = very, sh = shoulder.
2. p = polarized, dp = depolarized.
3. RT = room temperature.
4. $\alpha = \alpha$-P_4S_3, $\beta = \beta$-P_4S_3, *g* = glassy phase, SS = saturated solution and M = molten compound, Gas = gas phase.
5. in parenthesis intensities in %.
6. All the data of frequencies are reconstructed by a sense of ref. 70.

Table 7b. The comparison of reported calculated frequency of P_4S_3 with Zizps6144.

assign.	$\Delta\bar{\nu}$ (cm^{-1})					
$\nu_1(A_1)$	487(7)	442	485	488	487	485
$\nu_2(A_1)$	447(100)[3] 441sh(18)	420	-	444	448	447
$\nu_3(A_1)$	422(11)	290	422	426	431	424
$\nu_4(A_1)$	291(18)	87	276	291	287	288
$\nu_5(A_2)$ + lib.	197~141	-	-	189	187	188
$\nu_6(E)$	473(6)	486	465	486	485	483
$\nu_7(E)$	417(8)	384	415	410	404	412
$\nu_8(E)$	345(17)	341		347	348	351
$\nu_9(E)$	340(19)	221	329	345	345	347
$\nu_{10}(E)$	224(10) 222(10)	154	175	218	220	219
method[1]	S[2]	GF	PED	HF	MP	DFT
Refs.	this work	118	121	120	120	120

1. GF ; GF matrix method, PED ; potential energy distribution, HF ; HF/6-31G(with Gaussian 94 set), MP ; MP2/6-31G(with Gaussian94 set), DFT ; DFT/B3LYP/6-31G(with Gaussian94 set).
2. S = solid-state(crystal powder) method with Nujol.
3. in parenthesis intensities in %.
4. All the data of frequencies are reconstructed by a sense of ref. 70.

9. References

1. H.D. Lutz, A. Pfitzner, *Z. Naturforsch.* **B44**(1989)1047.
2. A. Pfitzner, *Chem. Eur. J.* **6**(11)(2000)1891.
3. M. H. Möller, W. Jeitschko, *J. Sol. Stat. Chem.* **65**(1986)187.
4. A. Pfitzner, E. Freudenthaler, *Angew. Chem. Int. Ed. Eng.* **34**(1995)1647.
5. A. Pfitzner, E. Freudenthaler, *Z. Naturforsch.* **B52**(1997)199.
6. A. Pfitzner, S. Zimmerer, *Angew. Chem. Int. Ed. Eng.* **36**(1997)982.
7. A. Pfitzner, *Inorg. Chem.* **37**(1998)5164.
8. E. Freudenthaler, Ph. D. thesis, Universität Siegen, 1997.
9. E. Freudenthaler, A. Pfitzner, *Solid State Ionics* **101-103**(1997)1053.
10. M. Ruck, *Z. anorg. allg. Chem.* **620**(1994)1832.
11. A. Pfitzner, S. Reiser, *Inorg. Chem.* **38**(1999)2451.
12. H. Eckert, and D. Lathrop, *J. Phys. Chem.* **93**(1989)7895.
13. Y. Monteil and H. Vincent, *Z. anorg. allg. Chem.* **416**(1975)181.
14. G. M. Lister and R. Jones, *J. Phys. Condens. Matter.* **1**(1989)6039.
15. A. Pfitzner, S. Reiser, H.-J. Deiseroth, *Z. anorg. allg. Chem.* **625**(1999)2196.
16. V. Manriquez, W. Hoenle, H. G. von Schnering, *Z. anorg. allg. Chem.* **539**(1986)95.
17. (a) M. E. Jason, T. Ngo and S. Rahman, *Inorg. Chem.* **36**(1997)2633. (b) J. Wachter, *Angew. Chem. Int. Ed.* **37**(1998)750.
18. (a) T. Chattopadhyay, E. Gmelin, H. G. v. Schnering, *J. Phys. Chem. Solids* **43**(1982)925. (b) H. L. Clever, E. F. Westrum, Jr., A. W. Cordes, *J. Phys. Chem.* **69**(1965)1214. (c) R. Blachnik, U. Wickel, *Thermochim. Acta* **81**(1984)185. (d) L. Operti, G. A. Vaglio, M. Peruzzini, P. Stoppioni, *Inorganica Chim. Acta* **96**(1985)43.
19. (a) M. D. Vaira, M. Peruzzini, P. Stoppioni, *J. Organometall. Chem.* **258**(1983)373. (b) K. Neininger, H. W. Rotter, G. Thiele, *Z. anorg. allg. Chem.* **622**(1996)1814.
20. H. Nowottnick, K. Stumpf, R. Blachnik, H. Reuter, *Z. anorg. allg. Chem.* **625**(1999)693.
21. C. Aubauer, T. M. Klapötke, and A. Schulz, *J. Mol. Model.* **6**(2000)76.
22. E.Guidoboni, I. de los Rios, A.Ienco, L. Marvelli, C.Mealli, A. Romerosa, R. Rossi, M. Peruzzini, *Inorg. Chem.* **41**(4)(2002)659.

23. H.D. Lutz, A. Pfitzner, W. Schmidt, E. Riedel, D. Prick, *Z. Naturforsch.* **A44**(1989)756.
24. A. Pfitzner, J. K. Cockcroft, I. Solinas, H.D. Lutz, *Z. anorg. allg. Chem.* **619**(1993)993.
25. E. Riedel, D. Prick, A. Pfitzner, H. D. Lutz, *Z. anorg. allg. Chem.* **619**(1993)901.
26. H. D. Lutz, Z. Zhang, A. Pfitzner, *Solid State Ionics* **62**(1993)1.
27. J. R. D. DeBord, Y. Lu, C. J. Warren, R. C. Haushalter and J. Zubieta, *Chem. Commun.* **15**(1997)1365.
28. P. H. Fourcroy, D. Carre, J. Rivet, *Acta Crystallogr.* **B34**(1978)3160.
29. S. Yamaguchi, *Scientific Papers of the Institute of Physical and Chemical Research* **39**(1942)357.
30. J. D. Martin, A. M. Dattelbaum, T. A. Thornton, R. M. Sullivan, J. Yang, and M. T. Peachey, *Chem. Mater.* **10**(1998)2699.
31. A. Grzechnik, S. Stϕlen, E. Bakken, T. Grande, and M. Mezouar, *J. Sol. Stat. Chem.* **150**(2000)121.
32. E. G. Tulsky, J. R. Long, *Chem. Mater.* **13**(2001)1149.
33. J. Goodyear, S. A. D. Ali, G. A. Steigmann, *Acta Crystallogr.* **B27**(1971)1672.
34. F. Rodi, D. Babel, *Z. Anorg. Allg. Chem.* **336**(1965)17.
35. D. Babel, M. Otto, *Z. Naturforsch.* **B44**(1989)715 and D. Babel, W. Rüdorf, R. Tschöpp, *Z. anorg. allg. Chem.* **347**(1966)282.
36. B. H. W. S. de Jong, P. G. G. Slaats, H. T. J. Super, N. Veldman, A. L. Spek, *J. Non-Cryst. Solids* **176**(1994)164 and H. Völlenkle, A. Wittmann, *Monatsh. Chem.* **99**(1968)251.
37. D. Tranqui, R. D. Shannon, H. Y. Chen, S. Iijima, W. H. Baur, *Acta Crystallogr.* **B35**(1979)2479 and H. Vincent, G. Perrault, *Bull. Soc. Fr. Mineral. Cristallogr.* **94**(1971)551.
38. L. Leduc, A. Perrin, M. Sergent, *Acta Crystallogr.* **C39**(1983)1503.
39. J. R. Long, A. S. Williamson, R. H. Holm, *Angew. Chem., Int. Ed. Engl.* **34**(1995)226.
40. J. R. Long, L. S. Mc Carty, R. H. Holm, *J. Am. Chem. Soc.* **118**(1996)4603.
41. K. Machida, G. Adachi, N. Yasuoka, N. Kasai, J. Shiokawa, *Inorg. Chem.* **19**(1980)3807.
42. (a) R. J. Nelmes, F. R. Thornley, *J. Physics* **C7**(1974)3855. (b) W. J. Becker, G. Will, *Z. Kristallogr.* **131**(1970)139. (c) G. Berset, W. Depmeier, R. Boutellier, H. Schmid, *Acta Crystallogr.* **C41**(1985)1694. (d) F. Kubel, *Ferroelectrics* **160**(1994)61. (e) O. Crottaz, F. Kubel, H. Schmid, *J. Sol. Stat. Chem.* **120**(1995)60.

43. W. Jeitschko, T. A. Bither, P. E. Bierstedt, *Acta Crystallogr.* **B33**(1977)2767.
44. M. Vlasse, A. Levasseur, P. Hagenmuller, *Sol. Stat. Ion.* **2**(1981)33.
45. D. M. Schubert, F. Alam, M. Z. Visi, C. B. Knobler, *Chem. Mater.* **15**(2003)866.
46. G. Corbel, E. Suard, J. Emery, M. Leblanc, *J. Alloys Compd.* **305**(2000)49.
47. R. J. Nelmes, *J. Phys.* **C7**(1974)3840.
48. R. B. Heslop, K. Jones, *Inorganic Chemistry – A Guide to Advanced Study*, Elsevier Scientific Publishing Co., New York, 1976.
49. T. C. Waddington (Ed.), *Non-Aqueous Solvent System*, Academic Press, London, 1971.
50. J. D. Corbett, S. V. Winbush, F. C. Albers, *J. Am. Chem. Soc.* **79**(1957)3020.
51. L. E. Topol, A. L. Laudis, *J. Am. Chem. Soc.* **82**(1960)6291.
52. G. Hevesy, E. Löwenstein, *Z. anorg. allg. Chem.* **187**(1930)266.
53. H. Schlundt, *J. Phys. Chem.* **8**(1904)122.
54. (a) I. Krossing, *J. Chem. Soc., Dalton Trans.* (2002)500. (b) I. Krossing, L. Wüllen, *Chem. Eur. J.* **8**(2002)700. (c) I. Krossing, *J. Am. Chem. Soc.* **123**(2001)4603.
55. (a) D. R. Stull, H. Prophet, JANAF Thermochemical Tables (2nd Ed.), National Breau of Standards, Washington, 1971. (b) W. M. Latimer, '*The oxidation states of the elements and their potentials in aqueous solution* (2 Ed.)', Prentice-Hall, 1952. (c) B. Meyer, *Chem. Rev.* **76**(1976)367.
56. (a) A. Nasar and M. Shamsuddin, *Thermochimica Acta* **205**(1992)157, and R. C. Sharma, Y. A. Chang, *J. Cryst. Growth* **88**(1988)193 (for ZnS, ZnSe and ZnTe). (b) A. Nasar and M. Shamsuddin, *Thermochimica Acta* **197**(1992)373 (for CdS). (c) A. Nasar and M. Shamsuddin, *J. Less. Metal.* **158**(1990)131 (for CdSe). And also in K. C. Mills, *Thermodynamic data for inorganic sulphides, selenides and tellurides*, Butterworths (London), 1974.
57. L. L. Quill (Ed.), *The chemistry and metallurgy of miscellaneous materials – Thermodynamics*, McGraw-Hill Book Company, 1950 and also in L. Brewer, G. R. Somayajulu and E. Brackett, *Chem. Rev.* **63**(2)(193)111.
58. M. E. Schlesinger, *Chem. Rev.* **102**(2002)4267

59. (a) P. D. Lao and Yile Guo, G. G. Siu, S. C. Shen, *Phys. Rev.* **B48**(1993)11701. (b) C. Yeh, Z. W. Lu, S. Froyen, A. Zunger, *Phys. Rev.* **B46**(1992)10086. (c) B. K. Agrawal, P. S. Yadav, S. Agrawal, *Phys. Rev.* **B50**(1994)14881.
60. K. T. Jacob, *Thermochimica Acta* **15**(1)(1976)79.
61. R. Blachnik, A. Hoppe, *Z. anorg. allg. Chem.* **457**(1979)91.
62. P. –E. Werner, *J. Appl. Cryst.* **9**(1976)216.
63. J. W. Vissor, *J. Appl. Cryst.* **2**(1969)89.
64. D. Louer, M. Louer, *J. Appl. Cryst.* **5**(1972)271 and A. Boultif, D. Louer, *ibid.* **24**(1991)987.
65. P. M. de Wolff, *J. Appl. Cryst.* **1**(1968)108.
66. R. A. Young, The Rietveld Method, Oxford University Press, London, 1993.
67. G. M. Sheldrick, SHELX-97, Program package for crystal structure solution and refinement, Universität Göttingen, Germany, 1997.
68. L. J. Farrugia, *J. Appl. Cryst.* **32**(1999)837.
69. H. D. Flack, *Acta Crystallogr.* **A39**(1983)876.
70. W. Bues, M. Somer and W. Brockner, *Z. Naturforsch.* **35b**(1980)1063.
71. H. Eckert, G. Brunklaus, M. Micoulaut, D. G. Georgiev, M. Mitova, and P. Boolchand, *Phys. Rev.* **B64**(2001)134204.
72. A. Pfitzner, H. Eckert, S. Reiser, G. Brunklaus, J. H. Hong, J. C. C. Chan, *Chem. Eur. J.* **8**(2002)4228.
73. U. Müller, Inorganic Structural Chemistry, John Wiley & Sons, Chichester, 1999.
74. R. Burnus, G. Meyer, *Z. anorg. allg. Chem.* **602**(1991)31.
75. G. L. Schimek, J. W. Kolis, G. J. Long, *Chem. Mater.* **9**(1997)2776.
76. I. R. Beattie, P. J. Jones, G. Reid, M. Webster, *Inorg. Chem.* **37**(1998)6032.
77. K. L. Moran, T. E. Gier, W. T. A. Harrison, G. D. Stucky, H. Eckert, K. Eichele, R. E. Wasylishen, *J. Am. Chem. Soc.* **115**(1993)10553.
78. (a) J. Glaser, *Acta Chem. Scand.* **A34**(1980)157. (b) H. W. Rotter, G. Thiele, *Z. Naturforsch.* **B37**(1982)995.
79. H. Schmid, *J. Phys. Chem. Solid* **26**(1965)973.

80. Z. H. Wang, D. Y. Geng, D. Li, Z. D. Zhang, Y. P. Wang, J.-M. Liu, *J. Alloys Comp.* **329**(2001)278.
81. D. Li, Z. J. Xu, Z. H. Wang, D. Y. Geng, J. S. Zhang, Z. D. Zhang, G. L. Yuan and J. -M. Liu *J. Alloys Comp.* **351**(2003)235.
82. G. Corbel, E. Suard, J. Voiron, M. Leblanc, *J. Mag. Mater.* **234**(2001)423.
83. A. Schmidt, R. Glaum, *Inorg. Chem.* **36**(1997)4883.
84. A. Schmidt, R. Glaum, J. Beck, *J. Sol. Stat. Chem.* **127**(1996)331.
85. D. Taylor, *Contrib. Mineral Petrol.* **16**(1967)172.
86. I. Hassan, H. D. Grundy, *Acta Crystallogr.* **B40**(1984)6.
87. M. O'Keeffe, B. G. Hyde, *Crystal Structures – I. Patterns and Symmetry*, Mineralogical Society of America, Washington, D.C., 1996.
88. (a) H. G. von Schnering, H. Menke, *Angew. Chem.* **84**(1972)30. (b) H. Menke, H. G. von Schnering, *Z. Anorg. Allg. Chem.* **395**(1973)223.
89. M. M. Shatruk, K. A. Kovnir, A. V. Shevelkov, I. A. Presniakov, B. A. Popovkin, *Inorg. Chem.* **38**(1999)3455.
90. B. D. Cullity, *Element of X-ray Diffraction (2nd Ed.)*, Addison-Wesley Publishing Company, 1978.
91. (a) D. Wells, *The Penguin Dictionary of Curious and Interesting Geometry*, Penguin Press, London, 1991. (b) H. S. M. Coxeter, P. Du Val, H. T. Flather, J. F. Petrie, *The Fifty-Nine Icosahedra*, Tarquin Publications, Stradbroke, 1999. (c) W. H. Beyer, *CRC Standard Mathematical Table (28 th Ed.)*, CRC Press, Boca Raton, 1987.
92. D. Wilmer, K. Funke, M. Witschas, R. D. Banhatti, M. Jansen, G. Korus, J. Fitter, R. E. Lechner, *Physica* **B266**(1999)60.
93. I. V. Korneeva, *Kristallografiya* **6**(1961)630.
94. E. A. Jumpertz, *Z. Elektrochem.* **59**(1955)419.
95. E. H. Kisi, M. M. Elcombe, *Acta Crystallogr.* **C45**(1989)1867.
96. Z. G. Pinsker, L. I. Tatarinova, V. A. Novikova, *Zhurnal Fizicheskoi Khimii* **20**(1946)1401.
97. S. Yamaguchi, *Scientific Papers of the Institute of Physical and Chemical Research (Japan)* **39**(1942)357.

98. (a) M. Hargittai, *Chem. Rev.* **100**(2000)2233. (b) H. D. B. Jenkins, H. K. Roobottom, J. Passmore, L. Glasser, *Inorg. Chem.* **38**(1999)3609.

99. A. Givan, A. Loewenschuss, *J. Chem. Phys.* **72**(1980)3809.

100. M. Kaupp, H. G. von Schnering, *Inorg. Chem.* **33**(1994)4718.

101. (a) T. K.Chattopadhyay, W. May, H. G. von Schnering, G. S. Pawley, *Z. Kristallogr.* **165**(1983)47. (b) Y. C. Leung, J. Waser, S. van Houten, A. Vos, G. A: Wiegers, E. H. Wiebenga, *Acta Cryst.* **10**(1957)574. (c) T. K. Chattopadhyey, W. May, H. G. v. Schnering, G. S. Pawley, *Z. Kristallogr.* **165**(1983)47 (for P_4S_3) (d) A. Vos, E. Keulen, *Acta Crystallogr.* **12**(1059)323. (for P_4Se_3) (e) P. C. Minshall, G. M. Sheldrick, *Acta Crystallogr.* **B34**(1978)1326. (f) J. R. Rollo, G. R. Burns, W. T. Robin, J. H. Clark, H. Dawes, M. B. Hursthouse, *Inorg. Chem.* **29**(1990)2889 (for α- P_4S_4)

102. J. R. Van Wazer, *J. Am. Chem. Soc.* **78**(22)(1956)5709.

103. J. R. Van Wazer, C. F. Callis, J. N. Shoolery, and R. C. Jones, *J. Am. Chem. Soc.* **78**(1956)5715.

104. (a) G.Baliman, P. S. Pregosin, *J. Magn. Reson.* **26**(1977)283. (b) C. Brevard, P. Granger, *Handbook of High-Resolution Multinuclear NMR*, Wiley, New York, 1981. (c) H. P. A. Mercier, J. C. P. Sanders, G. J. Schrobilgen, *J. Am. Chem. Soc.* **116**(1994)2921. (d) M. F. A. Dove, J. C. P. Sanders, E. L. Jones, M. J. Parkin, *J. Chem. Soc., Chem. Commun.* (1984)1578.

105. M. Gerken, P. Kolb, A. Wegner, H. P. A. Mercier, H. Borrmann, D. A. Dixon, G. J. Schrobilgen, *Inorg. Chem.* **39**(2000)2813.

106. A. M. Griffin, P. C. Minshall, and G. M. Sheldrick, *J. Chem. Soc. Chem. Comm.* (1976)809.

107. B. Blachnik, U. Wickel, and P. Schmitt, *Z. Naturforsch.* **39b**(1984)1135. also in R. K. Harris, P. J. Wilkes, P. T. Wood, J. D. Woollins, *J. Chem. Soc. Dalton Trans.* (1989)809.

108. G. Heckmann, E. Fluck, *Z. Naturforsch.* **26b**(1971)982.

109. N. Zumbulyadis, B. P. Dailey, *Chem. Phys. Lett.* **26**(2)(1974)273.

110. E. R. Andrew, W. S. Hinshaw and A. Jasinski, *Chem. Phys. Lett.* **24**(3)(1974)399.

111. K. Ingolic, R. A. Zingaro, M. Kudchadker, *Inorg. Chem.* **4**(10)(1965)1421.

112. H. Eckert, G. Brunklaus, M. Micoulaut, D. G. Georgiev, M. Mitova, and P. Boolchand, *Phys. Rev.* **B64**(2001)134204.
113. M. Delawaulle, *Bull. Soc. Chim. France* (1955)1294.
114. W. Bues, M. Somer, W. Brockner, *Z. Naturforsch.* **35b**(1980)1063.
115. C. Aubauer, T. M. Klapötke, A. Schulz, *J. Mol. Model.* **6**(2000)76.
116. D. J. Verrall and S. R. Elliott, *Phys. Rev. Lett.* **61**(1988)974.
117. A. Sergi, M. Ferrario, F. Buda, I. R. McDonald, *Chem. Phys. Lett.* **259**(1996)301.
118. H. Gerding, J. W. Maarsen, P. CHR. Nobel, *Recueil* **76**(1957)757.
119. M. Gardner, *J. Chem. Soc. Dalton* (1973)1740.
120. J. O. Jensen, D. Zeroka, A. Banerjee, *J. Mol. Struct.* **505**(2000)31.
121. (a) J. Brunvoll, B. N. Cyvin, S. J. Cyvin, *Z. Naturforsch.* **37a**(1982)342. (b) S. J. Cyvin, B. N. Cyvin, M. Somer, W. Brockner, *ibid.* **36a**(1981)774. (c) W. Brockner M. Somer, B. N. Cyvin, S. J. Cyvin, *ibid.* **36a**(1980)846 (for calculated thermodynamic properties of P_4Se_3). (d) S. J. Cyvin, J. Brunvoll, B. N. Cyvin, M. Somer, W. Brockner, *ibid.* **35a**(1980)1062 (for calculated thermodynamic properties of P_4S_3).
122. J. D. Sarfati, G. R. Burns, K. R. Morgan, *J. Non-Cryst. Sol.* **188**(1995)93.
123. R. J. Gillespie and G. P. Pez, *Inorg. Chem.* **8**(1969)1229.
124. R. J. Gillespie and R. C. Burns, *Inorg. Chem.* **21**(1982)3877.
125. R. Steudel, *Z. Naturforsch.* **30a**(1975)1481.
126. J. O. Hirtschfelder, C. F. Curtiss and R. B. Bird, *Molecular Theory of Gases and Liquids*, John Wiley & Sons, Inc., 1967.
127. H. Schüring, R. Stannarius, C. Tolksdorf, and R. Zentel, *Macromolecules* **34**(2001)3962.
128. S. Pronk and D. Frenkel, *J. Phys. Chem.* **B105**(2001)6722.
129. (a) H. Kiefte, M. J. Clouter, and R. E. Gagnon, *J. Phys. Chem.* **89**(1985)3103. (b) P. H. Gammon, H. Kiefte, and M. J. Clouter, *J. Phys. Chem.* **87**(1983)4025. (c) C. A. Tulk, H. Kiefte, and M. J. Clouter, R. E. Gagnon, *J. Phys. Chem.* **B101**(1997)6154.
130. B. Moulton and M. J. Zaworotko, *Chem. Rev.* **101**(6)(2001)1629.
131. V. Schomaker and K.N. Trueblood, *Acta Cryst.* **B24**(1968)63.
132. R. T. Phillips, D. Wolverson, M. S. Burdis, and Y. Fang, *Phys. Rev. Lett.* **63**(1989)2574.
133. G. R. Burns, J. R. Rollo, and R. J. H. Clark, *Inorg. Chem.* **25**(1986)1145.

134. G. M. Lister and R. Jones, *J. Phys. Condens. Matter.* **1**(1989)6039.

ERKLÄRUNG

Hiermit versichere ich, dass ich die vorliegende Arbeit selbst verfasst und nur die angegebenen Quellen und Hilfsmittel verwendet habe.

Regensburg, 14. Jan 2004

Jung Hoon Hong